

For Library

NRL Report 7871

Radiation from Sources Moving in a Warm Magnetoplasma

DENNIS JOHN BAKER

*Electromagnetic Propagation Branch
Communications Sciences Division*

PLEASE RETURN THIS COPY TO:

NAVAL RESEARCH LABORATORY

WASHINGTON, D.C. 20375

ATTN: CODE 2628

Because of our limited supply you are requested to return this copy as soon as it has served your purposes so that it may be made available to others for reference use. Your cooperation will be appreciated.

NDW-NRL-5070/2616 (1-84)

April 10, 1975



NAVAL RESEARCH LABORATORY
Washington, D.C.

Approved for public release; distribution unlimited.

SECURITY CLASSIFICATION OF THIS PAGE (When Data Entered)

REPORT DOCUMENTATION PAGE		READ INSTRUCTIONS BEFORE COMPLETING FORM
1. REPORT NUMBER NRL Report 7871	2. GOVT ACCESSION NO.	3. RECIPIENT'S CATALOG NUMBER
4. TITLE (and Subtitle) RADIATION FROM SOURCES MOVING IN A WARM MAGNETOPLASMA		5. TYPE OF REPORT & PERIOD COVERED This is a final report on one phase of the problem.
		6. PERFORMING ORG. REPORT NUMBER
7. AUTHOR(s) Dennis John Baker		8. CONTRACT OR GRANT NUMBER(s)
9. PERFORMING ORGANIZATION NAME AND ADDRESS Naval Research Laboratory Washington, D.C. 20375		10. PROGRAM ELEMENT, PROJECT, TASK AREA & WORK UNIT NUMBERS NRL Problem R07-30 Project RF 21-222-401-4360
11. CONTROLLING OFFICE NAME AND ADDRESS Department of the Navy Office of Naval Research Arlington, Virginia 22217		12. REPORT DATE April 10, 1975
		13. NUMBER OF PAGES 228
14. MONITORING AGENCY NAME & ADDRESS (If different from Controlling Office)		15. SECURITY CLASS. (of this report) Unclassified
		15a. DECLASSIFICATION/DOWNGRADING SCHEDULE
16. DISTRIBUTION STATEMENT (of this Report) Approved for public release; distribution unlimited.		
17. DISTRIBUTION STATEMENT (of the abstract entered in Block 20, if different from Report)		
18. SUPPLEMENTARY NOTES		
19. KEY WORDS (Continue on reverse side if necessary and identify by block number) Antenna Magnetosphere Beam Plasma Cerenkov Ionosphere Magnetoplasma		
20. ABSTRACT (Continue on reverse side if necessary and identify by block number) The power lost through radiation by an electric charge as it spirals in a homogeneous magneto- plasma is calculated. Coherent Cerenkov radiation from a group of charges is studied by assuming the charges radiate as a single macroscopic ellipsoid of revolution having a uniform volume charge density. The total power radiated by such a macroscopic source is shown to be finite even in those cases where the refractive index is unbounded. The power radiated by electric dipole and loop an- tennas oriented with their axes along the magnetic field of an anisotropic plasma and moving paral- lel to this field are given in the form of integrals which are easily evaluated numerically. <p style="text-align: right;">(Continued)</p>		

DD FORM 1473
1 JAN 73

EDITION OF 1 NOV 65 IS OBSOLETE
S/N 0102-014-6601

i

SECURITY CLASSIFICATION OF THIS PAGE (When Data Entered)

20. Abstract (Continued)

Mathematical models of the plasma dielectric tensor are derived using kinetic theory in addition to using the so-called hydrodynamic and full adiabatic theories (our Model H and A, respectively) with allowances made for the finite temperatures of both ions and electrons.

Numerical results obtained using Models A and H are compared. For example, Model A predicts that in some cases a large fraction of the power radiated by a moving point charge source at frequencies near the upper hybrid resonance is in the form of thermal mode excitation. However, this "high energy" thermal mode is missing from results obtained for the same source charge using Model H.

The radiation from the moving electric dipole antenna is shown to be a combination of ordinary dipole radiation and Cerenkov radiation. Both the electric dipole and loop antennas excite a band of frequencies when they are moving. Expressions for use in computing the power radiated by these antenna at the various Doppler shifted frequencies is given.

Finally, some potential applications of the theory are described as well as suggestions for extending the present theory.

ACKNOWLEDGMENTS

The preparation of a list of acknowledgments is, indeed, one of the most pleasant aspects of writing a thesis. Most enjoyable is the opportunity it affords me to thank people who must have felt unappreciated at times, especially my parents. The sacrifices they endured and the never complaining manner in which these were made helped me through many difficult times. I am grateful also to Dr. Charles Pelzer for his good example, and to Mr. Lee Ives for encouraging me through his frequent expressions of interest in my work. Dr. Gerhard Blass has been an inspiration to me of what a scientist and teacher should be. To Mr. Loren Bearce I am appreciative for introducing me to both Plasma Physics and Professor Herschel Weil. It has been a pleasure to do research work under Prof. Weil's guidance, and I thank him for his patience. I am indebted to the Naval Research Laboratory for providing me with a research grant, and to the many people there who have helped me these past few years, especially Mr. Plumer Leiphart. Finally, I wish to thank my dear wife for her marathon typing of this thesis, and for being with me when I needed her most.

TABLE OF CONTENTS

	Page
DEDICATION.....	ii
ACKNOWLEDGMENTS.....	iii
LIST OF TABLES	vi
LIST OF ILLUSTRATIONS	vii
LIST OF APPENDICES	xvi
SELECT LIST OF NOMENCLATURE	xviii
CHAPTER	
I. INTRODUCTION.....	1
Charged Particle Radiation in Plasmas Antennas Radiating in the Ionosphere	
II. GOVERNING EQUATIONS-HYDRODYNAMIC APPROACH..	6
Moments of the Boltzmann Equation Continuity Equation Momentum Transport Equation Transport Equation for Kinetic Pressure "Wave Equation" Linearization and Transformation	
III. GOVERNING EQUATIONS-KINETIC APPROACH	21
IV. DERIVATION OF DIELECTRIC TENSOR	32
Model H Model K Model A Derivation of Model A From Moment Equations Derivation of Model A From Kinetic Theory	
V. RADIATIVE POWER LOSS.....	50
Source Currents and Their Fourier Transforms	

		Page
	Current Density for a Spiraling Point Charge	
	Current Density for an Extended Charge	
	Current Density for an Electric Dipole Antenna	
	Current Density for a Loop Antenna	
	Power Loss Formulas	
	Power Radiated by Point Charge	
	Power Radiated by Extended Charge Source	
	Power Radiated by Electric Dipole Antenna	
	Power Radiated by Loop Antenna	
	Reversible and Irreversible Power	
VI.	NUMERICAL RESULTS	77
	Results Using Model H	
	Results Using Model A	
VII.	POTENTIAL APPLICATIONS OF THEORY	96
	Noise Generation in the Ionosphere	
	Antennas in the Ionosphere	
VIII.	CONCLUSIONS	105
APPENDIX		
	A. Polarized-Wave (PW) Space	110
	B. Basic Magnetoionic Theory	119
	C. Adjoint Matrix	133
	D. Evaluation of Selected Integrals	138
	E. Special Case	146
	F. The Emission Equation	150
	G. Refractive Index Diagrams	161
	H. Relevant Formulas, Definitions, and Physical Constants..	192
	LIST OF REFERENCES	199

LIST OF TABLES

TABLE		Page
1	VALUES OF X_c CORRESPONDING TO PRINCIPAL RESONANCES ^e AND CUTOFFS FOR THE OPERATING LINE $R^2 = 0.4$	78
2	PRINCIPAL CUTOFFS AND RESONANCES FOR A COLD PLASMA.....	124
3	NAMES OF PRINCIPAL CUTOFFS AND RESONANCES.....	127
4	PHASE VELOCITY AND REFRACTIVE INDEX SURFACES FOR VARIOUS REGIONS OF THE CMA DIAGRAM.....	129
5	SUMMARY OF SIGNIFICANCE OF POSITIVE AND NEGATIVE HARMONICS FOR SPIRALING CHARGED PARTICLES	155

LIST OF ILLUSTRATIONS

Figure		Page
1	Sketch of geometry of charged ellipsoid. The ellipsoid is fixed relative to its center of mass.	53
2	Sketch of the "operating line" $R^2 = 0.4$ superimposed on the CMA Diagram.	77
3	Power spectral density for a non-spiraling electron	79
4	The contribution to the total power spectral density due to Cerenkov radiation from a spiraling charge.	80
5	Contribution to the total power spectral density for a spiraling electron due to normal Doppler emission at the harmonic $p = -1$	81
6	Contribution to the total power spectral density for a spiraling electron due to anomalous Doppler emission at the harmonic $p = 1$	82
7	Phase velocity directions of the various waves excited by Cerenkov radiation.	83
8	Phase velocity directions of the various waves excited by normal Doppler emission at the harmonic $p = -1$	83
9	Phase velocity directions of the various waves excited by anomalous Doppler emission at the harmonic $p = 1$	84
10	The direction of energy propagation associated with the various waves excited by Cerenkov radiation. Negative angles indicate oppositely directed radial components of the phase and group velocity vectors.	85
11	The direction of energy propagation associated with the various waves excited by normal Doppler emission at the harmonic $p = -1$. Negative angles indicate oppositely directed radial components of the phase and group velocity vectors	86

12	The direction of energy propagation associated with the various waves excited by anomalous Doppler emission at the harmonic $p = 1$. Negative angles indicate oppositely directed radial components of the phase and group velocity vectors.....	87
13	Comparison of the power spectral densities for a) a point charge source, b) a spherical source of radius 10 cm and uniform density N_b , and c) a spherical source of radius 1 m and with a uniform number density N_b	89
14	Power spectral density at high frequencies for Cerenkov radiation from a non-spiraling electron obtained using Model A. Dashed lines indicate regions where model is not valid	92
15	Power spectral density at high frequencies for Cerenkov radiation from a spiraling electron obtained using Model A. Dashed lines indicate regions where model is not valid	93
16	High frequency spectrum of phase velocity directions excited by Cerenkov emissions obtained using Model A. Dashed lines indicate regions where model is not valid	94
17	High frequency spectrum of group velocity directions excited by Cerenkov emissions obtained using Model A. Dashed lines indicate regions where model is not valid	95
18	"Direct" path from L to R	96
19	Whistler path from L to R	96
20	Graph of principal cutoffs and resonances for high frequencies.....	126
21	Graph of principal cutoffs and resonances for $X_e \geq 1$ and $Y_e^2 \geq 1$	127

22	Geometrical relation between direction of the group velocity and the refractive index surface	130
23	Integration path for the integral (D.2)	138
24	Geometry for obtaining the emission equation via Doppler effects	151
25	The three topologically distinct refractive index surfaces which exist in a cold collisionless magneto-plasma. The external magnetic field is in the vertical direction. A radial from the origin to the surface represents the magnitude of the refractive index in the radial direction	156
26	Typical shape for a closed refractive index surface with the critical index n_{ZC1} indicated.....	157
27	Typical refractive index surface for modes which are evanescent in the direction of the magnetic field	158
28	Typical refractive index surface for modes which are evanescent in directions perpendicular to the magnetic field	159
29	Cold plasma refractive index surfaces for frequencies above the upper hybrid resonance. Curves are labeled according to values of X_e with $R^2 = 0.4$	162
30	Cold plasma refractive index surfaces for frequencies between the upper hybrid resonance and the electron plasma frequency. Curves are labeled according to values of X_e with $R^2 = 0.4$	163
31	Cold plasma refractive index surfaces for frequencies between the electron plasma frequency and the ion cyclotron cutoff frequency. Curves are labeled by values of X_e with $R^2 = 0.4$	164
32	Cold plasma refractive index curves for frequencies between the electron gyro-resonance and the lower hybrid resonance. Curves are labeled by values of X_e with $R^2 = 0.4$	165

33	Cold plasma refractive index surfaces for frequencies between the lower hybrid resonance and the ion gyro-resonance. Curves are labeled by values of X_e with $R^2 = 0.4$	166
34	Cold plasma refractive index surfaces for a frequency below the ion gyro-resonance. Curves are labeled by values of X_e with $R^2 = 0.4$	167
35	Refractive index surfaces obtained with Model H (first order in temperature) for frequencies above the upper hybrid resonance. (Expanded scale shown). Curves are labeled according to values of X_e with $R^2 = 0.4$...	172
36	Refractive index surfaces obtained with Model H (first order in temperature) for frequencies above the upper hybrid resonance. (Compressed scale shown). Curves are labeled according to values of X_e with $R^2 = 0.4$	172
37	Refractive index surfaces obtained with Model H (first order in temperature) for frequencies between the UHR and the plasma cutoff. (Expanded scale shown). Curves are labeled according to values of X_e with $R^2 = 0.4$	173
38	Refractive index surfaces obtained with Model H (first order in temperature) for frequencies between the UHR and the plasma cutoff. (Compressed scale shown). Curves are labeled according to values of X_e with $R^2 = 0.4$	173
39	Refractive index surfaces obtained with Model H (first order in temperature) for frequencies between the plasma cutoff and the ion cyclotron cutoff. Curves are labeled according to values of X_e with $R^2 = 0.4$	174

40	Refractive index surfaces obtained with Model H (first order in temperature) for the higher frequency portion of the band between the electron gyro-resonance and the LHR. Curves are labeled according to the value of X_e with $R^2 = 0.4$	175
41	Refractive index surface obtained with Model H (first order in temperature) for a frequency in the lower frequency portion of the band between the electron gyro-resonance and the LHR. (Expanded scale shown). The curve is labeled according to the value of X_e with $R^2 = 0.4$	176
42	Refractive index surfaces obtained with Model H (first order in temperature) for a frequency in the lower frequency portion of the band between the electron gyro-resonance and the LHR. (Compressed scale shown). The curves are labeled according to the value of X_e with $R^2 = 0.4$	176
43	Refractive index surfaces obtained with Model H (first order in temperature) for frequencies between the LHR and the ion gyro-resonance. (Expanded scale shown). Curves are labeled according to values of X_e with $R^2 = 0.4$	177
44	Refractive index surfaces obtained with Model H (first order in temperature) for frequencies between the LHR and the ion gyro-resonance. (Compressed scale shown). Curves are labeled according to values of X_e with $R^2 = 0.4$	177
45	Refractive index surfaces obtained with Model H (first order in temperature) for a frequency below the ion gyro-resonance. (Expanded scale shown). Curves are labeled according to values of X_e with $R^2 = 0.4$	178

46	Refractive index surfaces obtained with Model H (first order in temperature) for a frequency below the ion gyro-resonance. (Compressed scale shown). Curves are labeled according to values of X_e with $R^2 = 0.4$	178
47	Refractive index surfaces obtained with Model A for frequencies above $X_e = 0.625$. (Expanded scale shown). Curves are labeled according to values of X_e with $R^2 = 0.4$	181
48	Refractive index surfaces obtained with Model A for frequencies above $X_e = 0.625$. (Compressed scale shown). Curves are labeled according to values of X_e with $R^2 = 0.4$	181
49	Refractive index surfaces obtained with Model A for frequencies between $X_e = 0.625$ and the upper hybrid resonance. (Expanded scale shown). Curves are labeled according to values of X_e with $R^2 = 0.4$	182
50	Refractive index surfaces obtained with Model A for frequencies between $X_e = 0.625$ and the upper hybrid resonance. (Compressed scale shown). Curves are labeled according to values of X_e with $R^2 = 0.4$	182
51	Refractive index surfaces obtained with Model A for the higher frequency portion of the band between the UHR and the plasma cutoff. (Expanded scale shown). Curves are labeled according to values of X_e with $R^2 = 0.4$	183

52	Refractive index surfaces obtained with Model A for the higher frequency portion of the band between the UHR and the plasma cutoff. (Compressed scale shown). Curves are labeled according to values of X_e with $R^2 = 0.4$	183
53	Refractive index surfaces obtained with Model A for the lower frequency portion of the band between the UHR and the plasma cutoff. (Expanded scale shown). Curves are labeled according to values of X_e with $R^2 = 0.4$	184
54	Refractive index surfaces obtained with Model A for the lower frequency portion of the band between the UHR and the plasma cutoff. (Compressed scale shown). Curves are labeled according to values of X_e with $R^2 = 0.4$	184
55	Refractive index surfaces obtained with Model A for frequencies between the plasma cutoff and the ion cyclotron cutoff. (Expanded scale shown). Curves are labeled according to values of X_e with $R^2 = 0.4$	185
56	Refractive index surfaces obtained with Model A for frequencies between the plasma cutoff and the ion cyclotron cutoff. (Compressed scale shown). Curves are labeled according to values of X_e with $R^2 = 0.4$	185
57	Refractive index surfaces obtained with Model A for frequencies between the ion cyclotron cutoff and the electron gyro-resonance. Curves are labeled according to values of X_e with $R^2 = 0.4$	186

58	Refractive index surfaces obtained with Model A for frequencies just below the electron gyro-resonance. (Expanded scale shown). Curves are labeled according to values of X_e with $R^2 = 0.4$	187
59	Refractive index surfaces obtained with Model A for frequencies just below the electron gyro-resonance. (Compressed scale shown). Curves are labeled according to values of X_e with $R^2 = 0.4$	187
60	Refractive index surface obtained with Model A for the higher frequency portion of the band between the LHR and the electron gyro-resonance. (Expanded scale shown). Curve is labeled according to value of X_e with $R^2 = 0.4$	188
61	Refractive index surface obtained with Model A for the higher frequency portion of the band between the LHR and the electron gyro-resonance. (Compressed scale shown). Curve is labeled according to value of X_e with $R^2 = 0.4$	188
62	Refractive index surface obtained with Model A for the lower frequency portion of the band between the LHR and the electron gyro-resonance. (Expanded scale shown). Curve is labeled according to value of X_e with $R^2 = 0.4$	189
63	Refractive index surface obtained with Model A for the lower frequency portion of the band between the LHR and the electron gyro-resonance. (Compressed scale shown). Curve is labeled according to value of X_e with $R^2 = 0.4$	189

64	Refractive index surfaces obtained with Model A for frequencies between the LHR and the ion gyro-resonance. Curves are labeled according to values of X_e with $R^2 = 0.4$	190
65	Refractive index surfaces obtained with Model A for a frequency below the ion gyro-resonance. (Expanded scale shown). Curves are labeled according to values of X_e with $R^2 = 0.4$	191
66	Refractive index surface obtained with Model A for a frequency below the ion gyro-resonance. (Compressed scale shown). Curve is labeled according to value of X_e with $R^2 = 0.4$	191

LIST OF APPENDICES

APPENDIX	Page
<p>A POLARIZED-WAVE (P-W) SPACE.....</p> <p style="padding-left: 40px;">Diagonalizing the Matrix for ($\hat{e}_z \cdot x$) Transformations Between Cartesian and "Polarized-Wave" Spaces Vector and Tensor Algebra in P-W Space Vector Analysis in P-W Space</p>	110
<p>B BASIC MAGNETO-IONIC THEORY</p> <p style="padding-left: 40px;">Dispersion Relation Cold Plasma Dielectric Tensor Cold Plasma Dispersion Relation CMA Diagram Ray Direction in Anisotropic Plasmas</p>	119
<p>C ADJOINT MATRIX</p> <p style="padding-left: 40px;">The Adjoint Matrix for Model H The Adjoint Matrix for Model A</p>	133
<p>D EVALUATION OF SELECTED INTEGRALS</p> <p style="padding-left: 40px;">A Useful Integral Integrals Related to Weber's Second Exponential Integral Integrals Related to the "Plasma Dispersion Function"</p>	138
<p>E SPECIAL CASE</p>	146
<p>F THE EMISSION EQUATION.....</p> <p style="padding-left: 40px;">Doppler Effects and the Emission Equation Quantum Mechanics and the Emission Equation Connection Between the Emission Equation and the Refractive Index Surfaces</p>	150

	Page
G	REFRACTIVE INDEX DIAGRAMS 161
	Cold Plasma Real Refractive Index Surfaces
	Refractive Index Curves for Model H
	Refractive Index Surfaces for Model A
H	RELEVANT FORMULAS, DEFINITIONS, AND PHYSICAL CONSTANTS 192
	Physical Constants (MKS units, degrees Kelvin)
	Conversion Factors
	Plasma Parameters (MKS units and degrees Kelvin unless otherwise indicated)
	Formulas Involving Bessel Functions (Integer s)
	Formulas Involving the Plasma Dispersion Function $Z(\zeta)$
	Vector and Tensor Identities
	Formulas Involving the Dirac Delta Functions

SELECT LIST OF NOMENCLATURE
(See also table of constants in Appendix H)

Latin Symbol	Description	Page Intro.
<u>B</u>	Magnetic Induction	7
$\hat{e}_{+1}, \hat{e}_{-1}, \hat{e}_0$	Basis vectors in "polarized-wave" (P-W) space	111
<u>E</u>	Electric Field	7
f_s	Distribution Function	6
$g_{s\pm}, g_{s\pm 2}, g_{sx}$	Gyro elements	46
<u>J</u> ^(ex)	(External) current density	15
<u>k</u>	Wave propagation vector	15
<u>K</u>	Dielectric tensor	16
K_1, K_{-1}, K_0	Components of dielectric tensor for a cold plasma in P-W space	35
K_{-1}	Arithmetic mean of K_1 and K_{-1}	124
m_s	Particle mass	6

Latin Symbol	Description	Page Intro.
\underline{n}	Refractive index vector	20
N	Particle number density	7
P	Radiative power loss	61
\underline{P}	Pressure tensor	8
q_s	Plasma particle charge (positive or negative)	7
\underline{Q}	Heat flux tensor	8
T_s	Particle temperature	33
u_s	Thermal speed	33
\underline{V}	Velocity of radiating source	51
\underline{V}	Average velocity of plasma particle (usually written with a subscript s)	8
\underline{V}_g	Wave group velocity	130
X_s	Normalized plasma frequency squared	35

Latin Symbol	Description	Page Intro.
Y_s	Normalized gyro-frequency (positive or negative)	33
Z_s	Normalized collision frequency	44
Greek Symbol	Description	Page Intro.
α	Angle between phase and group velocities	130
α_s	Complex normalized plasma frequency	35
β_s	Complex normalized gyro frequency	33
$\underline{\beta}$	Normalized velocity of radiating source	51
γ	Relativistic mass correction factor	51
ϵ_s	Complex normalized thermal speed squared	34
ϑ	Angle between \underline{B}_0 and \underline{k} (or \underline{n})	130
ν_s	Effective collision frequency	12
$\underline{\underline{\mu}}_s$	Mobility tensor	15

Greek Symbol	Description	Page Intro.
ρ_s	Plasma particle mass density	11
ω	Angular wave frequency	15
ω_{bs}	Angular gyro-frequency (positive or negative)	18

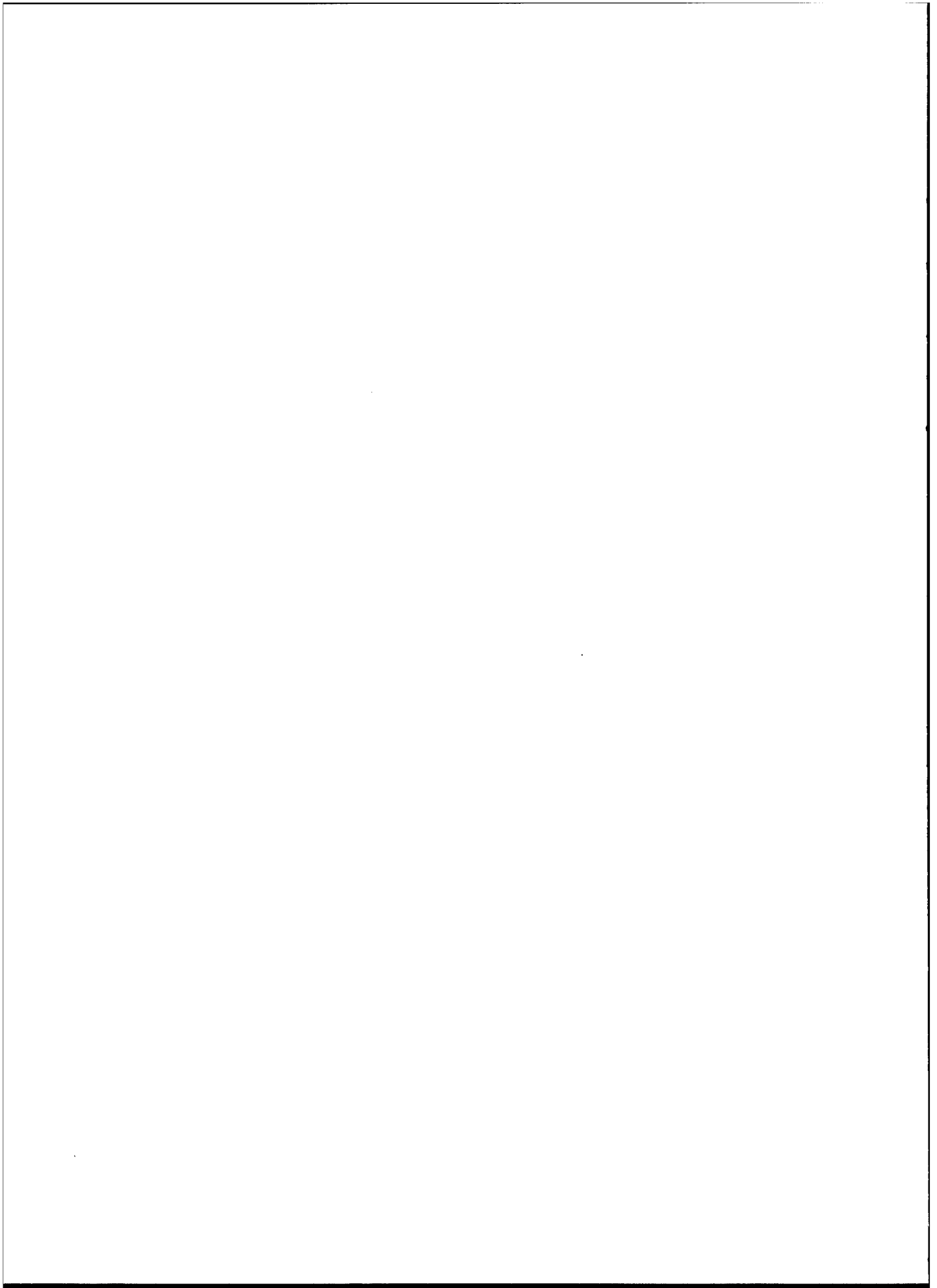
The form of the Fourier transform used in this thesis is

$$\underline{E}(\underline{r}, t) = (2\pi)^{-4} \int d^3k d\omega \underline{\mathcal{E}}(\underline{k}, \omega) e^{i\underline{k} \cdot \underline{r} - i\omega t}$$

with the inverse¹

$$\underline{\mathcal{E}}(\underline{k}, \omega) = \int d^3r dt \underline{E}(\underline{r}, t) e^{-i\underline{k} \cdot \underline{r} + i\omega t}.$$

¹ In this thesis, field quantities in (\underline{r}, t) space are shown as printed capital letters and their Fourier transforms by script capitals.



CHAPTER I

INTRODUCTION

In this thesis the term "plasma" is understood to mean a gas which is sufficiently ionized so that its dynamical behavior is dominated by electromagnetic effects. A "magnetoplasma" is a plasma with a magnetic field impressed upon it. The study of the plasma state of matter is a comparatively new branch of physics primarily because the natural occurrence of plasma on the earth's surface is nearly non-existent (except for transient plasmas caused by lightning). However, the sun and stars, interplanetary gases and the earth's upper atmosphere (ionosphere) are all examples of plasmas. In fact most of the universe is in the plasma state.

The advent of radio and in particular radio astronomy made possible the examination of these distant plasmas. In fact, it was in terms of the interaction between radio waves and the ionospheric plasma that the transmission of radio waves across the Atlantic was explained. More recently, the use of satellite and rocket-borne probes have made in-situ measurements possible in many of these plasmas, and for the first time many theoretical predictions about plasma behavior can be subjected to experimental verification. In addition to these naturally occurring plasmas, there are now many man made plasmas, such as those produced in gas discharge tubes and in high temperature plasma confinement devices for use in the study of thermonuclear power generation. Consequently, there is presently a great deal of interest in problems of radiation both in and through plasmas. This thesis investigates the radiation from sources which are moving in a warm magnetoplasma. In particular, we are interested in radiation from sources which are imbedded in the

Note: Manuscript submitted February 7, 1975.

ionospheric plasma surrounding the earth.

Charged Particle Radiation in Plasmas

The study of the radiation resulting from the uniform motion of a charged particle through a simple isotropic dielectric medium dates back to the experiments of Cerenkov during the period 1934-1938 and to the theoretical investigations of Frank and Tamm in 1937 [21]. Later, when radio astronomy was still in its infancy, it was suggested by Kiepenheuer that the non-thermal radio emissions from the sun might be due to radiation from beams of electrons moving through the plasma which forms the solar corona [36]. Also, the decametric noise bursts from Jupiter were interpreted in terms of radiation from suprathermic beams of charged particles streaming through plasmas [18]. Zheleznyakov [89] gives an extensive review of theory and experiment regarding radio emission from the sun and planets and states (p.569) that "... a noncoherent magneto-bremstrahlung¹ is most promising for interpreting the majority of the (solar) sporadic radio emission's components of the continuum type...". "Noise" observed by satellite-borne antennas in the magnetosphere has also been explained in terms of beam plasma interactions [34]. Most of the theories cited depend in great part on extending the original work of Frank and Tamm to include more complicated dielectric media such as anisotropic plasmas.

The energy loss from an electron moving with constant velocity parallel to the magnetic field lines of a magnetoplasma was first calculated by Kolomenskii [41] in 1956 using the Hamiltonian method. Cohen [12] included temperature effects but treated only isotropic plasmas. Tuan and Seshadri [81] gave some of the first numerical results for Cerenkov radiation in a cold anisotropic plasma and later

¹ Magneto-bremstrahlung is radiation caused by the accelerated motion of charged particles in a magnetic field. Magneto-bremstrahlung caused by relativistic electrons is usually called synchrotron radiation; the radiation of non-relativistic electrons in a magnetic field is sometimes called gyro-frequency radiation (since it occurs at the gyro-frequency and its lower harmonics) or cyclotron radiation.

Seshadri [65] also included temperature effects . Cerenkov radiation was studied via a kinetic approach by Kikuchi [38] . Sakurai and Ogawa [62] solved for the far fields of the spiraling charge in a cold magnetoplasma .

The present treatment differs from those given previously in the following ways:

- 1) The effects of collisions between plasma particles is retained in this thesis .
- 2) Effects of a non-isotropic kinetic pressure tensor are treated .
- 3) Coherent radiation from bunches of charged particles is examined .
- 4) The radiation from a charge spiraling in an anisotropic plasma is calculated including both electron and ion temperature effects .
- 5) A comparison is made of results using different plasma models .

Several different models of plasmas are used in addition to the popular cold plasma model . Model A is basically a quasi-cold plasma model with first order temperature corrections introduced via non-diagonal pressure tensors . This model can be derived from what is often referred to as the "full adiabatic theory" [4] . Model A, for certain frequencies where Landau damping is negligible gives results identical to those obtained using a kinetic theory analysis of the problem [6] . Model H is a warm plasma with temperature effects included via scalar pressures . This approach is essentially hydrodynamic in nature , and consequently does not include the effects of Landau damping . Also, we present some derivations based upon a kinetic theory approach, referred to as Model K . The various models are all identical in the limit of zero temperature and in this limit they reduce to the familiar "cold plasma" model .

Numerical results based on the use of these models are presented , and comparisons made with experimental data . In addition , some numerical results are given for coherent radiation from a group of charges

where the assumption is made that the charges radiate as a single macroscopic spheroid having a uniform charge density. MKSA units are used throughout the thesis with exceptions denoted explicitly.

The thesis concludes with an evaluation of the models used, their limitations and relative merits, and suggestions are made as to possible future theoretical refinements and applications of the theory. Several errors existing in the literature are also noted and discussed.

Antennas Radiating in the Ionosphere

Closely related to the free charge problem is that of an antenna radiating in the ionosphere. Like the problem of the free charge radiator, one is especially interested in the power fed into the surrounding plasma, the types of waves excited and the structure of the far zone radiation fields. However, when attempting to understand the operation of an ionospheric-embedded antenna there are several factors which serve to complicate the analysis. The following is a list of some of these factors.

1) A sheath will form about the antenna. The sheath exists due to the different mobilities of the negatively and positively charged constituent particles of the plasma [77,86], due to $\underline{v} \times \underline{B}$ induced potentials along the antenna as a consequence of its motion through the earth's magnetic field [57] and due to any potentials applied to the antenna terminals [54,59].

2) Since the plasma is not a perfect insulator, charges will flow between the antenna and plasma complicating the already difficult problem of determining the current distribution along the antenna [13].

3) As a result of finite temperatures of the ionospheric components acoustic type waves may also be excited and received by antennas [88].

4) At the low frequencies ions can react to the antenna excitations and their motion becomes important [9].

5) Collisions between plasma constituents causes damping of waves and makes the concept of radiation resistance ambiguous [23]. Collisions also enable coupling between different plasma modes and

losses must be introduced in cold-plasma calculations to prevent certain infinities [15].

6) Antenna motion causes Doppler shifts, in addition to spatial inhomogeneities such as wakes and shock fronts [35].

7) In the presence of the earth's magnetic field the kinetic pressure is more appropriately described by a tensor rather than by a simple scalar pressure [67].

8) Very modest potentials applied to the antenna terminals result in non-linear fields [49].

Presently, all treatments of the antenna problem have omitted some, and usually most, of these effects. Consequently, analyses tend to be too idealized to permit comparisons with experiment. In this thesis, we shall concentrate most of our efforts on the problems associated with items (3) - (7). Most of the other items are discussed in some detail in a paper by Baker, Weil, and Bearce [5].

CHAPTER II

GOVERNING EQUATIONS-HYDRODYNAMIC APPROACH

In this chapter we shall give the equations used to describe radiation in homogeneous plasmas via a hydrodynamic approach. The procedure will be to first calculate moments of the Boltzmann equation for each species of particle in the plasma; the electrically charged particles assumed moving under the influence of Lorentz forces. The simplest possible models are used for the collision terms appearing in the moments of Boltzmann equation in order to make the mathematics tractable and still retain some collision effects.

Using the Fourier-analyzed Maxwell curl equations and assuming the properties of the plasma can be described by a mobility or dielectric tensor, a "wave equation" is derived which gives the dependence of the electric field in the plasma on the "external" source currents generating this field. The resulting moment equations and the wave equation are then linearized and expressed in terms of "polarized wave" coordinates. These are the equations which form the basis for much of our work.

Moments of the Boltzmann Equation

The derivation presented here is very similar to that given by Delcroix [14], and Shkarofsky et.al. [69]. Our analysis begins with the Boltzmann equation, which we assume to adequately describe the motion of the plasma particles in phase space. For each species, s , of particles of mass m_s in the plasma there corresponds a distribution function, f_s , which in general will be a function of the position, \underline{r} , and velocity, \underline{w} , of each particle as well as time, t . If \underline{F}_s is the force acting on each particle, then the Boltzmann equation can be written

$$\partial f_s / \partial t + \underline{w} \cdot \nabla f_s + m_s^{-1} \underline{F}_s \cdot (\partial f_s / \partial \underline{w}) = (\delta f_s / \delta t)_{\text{int}}, \quad (2.1)$$

where the gradient in velocity space is defined by

$$\frac{\partial}{\partial \underline{w}} \equiv \hat{e}_{w_x} \frac{\partial}{\partial w_x} + \hat{e}_{w_y} \frac{\partial}{\partial w_y} + \hat{e}_{w_z} \frac{\partial}{\partial w_z} \quad (2.2)$$

and \hat{e}_{w_x} , \hat{e}_{w_y} and \hat{e}_{w_z} are unit vectors in velocity space. The interaction term, $(\delta f_s / \delta t)_{\text{int}}$, appearing in (2.1) represents changes in the

distribution function due to collisions between different species of particles as well as collisions between particles of the same species.

The force \underline{F}_s , under which the particles of charge q_s are accelerated, is the Lorentz force,

$$\underline{F}_s = q_s (\underline{E} + \underline{w} \times \underline{B}) \quad (2.3)$$

where \underline{E} and \underline{B} are the macroscopic electric and magnetic fields in the plasma. Since each species of particles obeys equations of the same form, we shall temporarily omit the subscript s to simplify the notation. Using the convention of summing over repeated latin subscripts on vector or tensor quantities (i.e. $\sum_j A_j B_j \equiv A_x B_x + A_y B_y + A_z B_z$), (2.1) is written

$$\partial f / \partial t + w_j \partial f / \partial x_j + m^{-1} F_j \partial f / \partial w_j = (\delta f / \delta t)_{\text{int}}. \quad (2.4)$$

Let $A(\underline{r}, \underline{w}, t)$ be a general function of position, velocity and time, and define the average, $\overline{A(\underline{r}, t)}$, by

$$\overline{A(\underline{r}, t)} \equiv N^{-1} \int A(\underline{r}, \underline{w}, t) f d^3 w, \quad (2.5)$$

where N is the number density

$$N = \int f d^3 w. \quad (2.6)$$

Here and elsewhere in this thesis, we use the convention that when the integration limits are not explicitly given, they are to be understood to span the whole space of the variable or variables involved. We also take the liberty of writing a single integral sign to represent a multiple integration whenever it is obvious from the form of the expression involved that a multiple integration is required.

We define the average velocity, \underline{V} , the kinetic pressure, \underline{P} , and the thermal energy flux tensor, \underline{Q} , as follows:

$$\underline{V} \equiv N^{-1} \int \underline{w} f d^3 w, \quad (2.7)$$

$$\underline{P} \equiv m \int (\underline{w} - \underline{V})(\underline{w} - \underline{V}) f d^3 w, \quad (2.8)$$

$$\underline{Q} \equiv m \int (\underline{w} - \underline{V})(\underline{w} - \underline{V})(\underline{w} - \underline{V}) f d^3 w. \quad (2.9)$$

Now to form moments of the Boltzmann equation, multiply (2.4) by A and integrate over all velocities. Consider the various terms separately.

$$\begin{aligned} \int A (\partial f / \partial t) d^3 w &= \frac{\partial}{\partial t} \int A f d^3 w - \int (\partial A / \partial t) f d^3 w \\ &= \partial (N \bar{A}) / \partial t - N \overline{(\partial A / \partial t)} \end{aligned} \quad (2.10)$$

$$\begin{aligned} \int A w_j (\partial f / \partial x_j) d^3 w &= \frac{\partial}{\partial x_j} \int A w_j f d^3 w - \int (\partial A / \partial x_j) w_j f d^3 w \\ &= \partial (N \bar{A} w_j) / \partial x_j - N \overline{(\partial A / \partial x_j) w_j} \end{aligned} \quad (2.11)$$

$$\begin{aligned} m^{-1} \int A F_j (\partial f / \partial w_j) d^3 w &= m^{-1} \int [A F_j (\partial f / \partial w_j) dw_j] dw_k dw_l, j \neq k \neq l \\ &= m^{-1} \int [A F_j f]_{-\infty}^{\infty} dw_k dw_l - \\ &\quad m^{-1} \int [\partial (A F_j) / \partial w_j] f d^3 w \\ &= - m^{-1} N \overline{\partial (A F_j) / \partial w_j} \end{aligned} \quad (2.12)$$

Note that in (2.12) we have set the term

$$A F_j f = 0 \text{ for } w_j = \pm \infty . \quad (2.13)$$

This ensures that the moments of f : N , \underline{V} , \underline{P} , ... remain finite and makes $\int [A F_j f]_{-\infty}^{\infty} dw_k dw_l = 0$. We may write the Lorentz force as

$$F_j = q (E_j + \epsilon_{jkl} w_k B_l) \quad (2.14)$$

with ϵ_{jkl} , the Levi-Civita symbol, defined by

$$\epsilon_{jkl} = \begin{cases} 1 & \text{if } jkl \text{ is an even permutation of } xyz \\ -1 & \text{if } jkl \text{ is an odd permutation of } xyz \\ 0 & \text{otherwise.} \end{cases} \quad (2.15)$$

We note that for the Lorentz force

$$\partial F_j / \partial w_j = 0 . \quad (2.16)$$

Therefore the right side of (2.12) simplifies to

$$- N m^{-1} \overline{(\partial A / \partial w_j)} F_j . \quad (2.17)$$

Finally, for the interaction term, we define the interaction operator Δ as

$$\Delta A \equiv N^{-1} \int A (\delta f / \delta t)_{\text{int}} d^3w . \quad (2.18)$$

Collecting the various terms obtained we arrive at the macroscopic equation

$$\begin{aligned} \partial (\overline{NA}) / \partial t - N \overline{\partial A / \partial t} + \partial (\overline{NA w_j}) / \partial x_j - N \overline{(\partial A / \partial x_j) w_j} \\ - N m^{-1} \overline{(\partial A / \partial w_j)} F_j = N \Delta A . \end{aligned} \quad (2.19)$$

In the following sections we shall obtain the first three moment equations by setting $A(\underline{r}, \underline{w}, t)$ equal to 1, $m \underline{w}$ and $m (\underline{w} - \underline{V})(\underline{w} - \underline{V})$, respectively.

Continuity Equation

Reintroducing the species subscript s , and putting $A_s = 1$ in (2.19), and inserting the averaged quantities N_s and \underline{V}_s , we obtain the continuity equation for particle number conservation.

$$\partial N_s / \partial t + \partial (N_s V_{sj}) / \partial x_j = N_s \Delta_s 1 = (\delta N_s / \delta t)_{int} \quad (2.20)$$

The source-term $(\delta N_s / \delta t)_{int}$ which appears in the continuity equation includes all short range interactions which change the number density. For the ionosphere, these interactions can be divided into two broad categories: those which result in production of ionization (ionization processes) and those which result in destruction of ionization (recombination processes). Production processes are solar photoionization and corpuscular ionization. The former is a result of particle-photon interactions, while the latter is a result of high energy particle-particle collisions. The primary recombination process responsible for the loss of ionization in the ionosphere is that of electron-ion recombination. Typical reaction times for these processes are given by Rishbeth and Garriott [61]. For studying radiation phenomena in the ionosphere, the source-terms appearing on the right side in (2.20) are small compared with the terms on the left since N_s is nearly constant over times of the order of a few typical radiation periods. Therefore we can neglect the term $(\delta N_s / \delta t)_{int}$ in (2.20) and obtain the familiar form of the continuity equation

$$\partial N_s / \partial t + \partial (N_s V_{sj}) / \partial x_j = 0. \quad (2.21)$$

Momentum Transport Equation

Setting $A_s = m_s \underline{w}$ in (2.19) gives

$$m_s \partial (N_s \underline{V}_s) / \partial t + m_s \partial (N_s \overline{w_j}) / \partial x_j - N_s \underline{F}_s = N_s m_s \Delta_s \underline{w}. \quad (2.22)$$

This is a vector equation which for the k^{th} component is written

$$m_s \partial (N_s V_{sk}) / \partial t + m_s \partial (N_s \overline{w_k w_j}) / \partial x_j - N_s \underline{F}_{sk} = N_s m_s \Delta_s w_k. \quad (2.23)$$

It is easy to show that

$$\overline{w_k w_j} = \overline{(w_k - V_{sk})(w_j - V_{sj})} + \overline{V_{sk} V_{sj}}. \quad (2.24)$$

Hence with the help of (2.24) and our definition of \underline{P} , and inserting the Lorentz force for \underline{F}_s , we can write (2.23) as

$$m_s \partial (N_s V_{sk}) / \partial t + \partial P_{skj} / \partial x_j + m_s \partial (N_s V_{sk} V_{sj}) / \partial x_j - N_s \alpha_s (E_k + \epsilon_{klm} V_{sl} B_m) = N_s m_s \Delta_s w_k. \quad (2.25)$$

If we make use of the continuity equation (2.21) this can be simplified to

$$\partial V_{sk} / \partial t + \rho_s^{-1} \partial P_{skj} / \partial x_j + V_{sj} \partial V_{sk} / \partial x_j - \alpha_s m_s^{-1} (E_k + \epsilon_{klm} V_{sl} B_m) = \Delta_s w_k \quad (2.26)$$

where we have introduced the mass density, ρ_s . To use this equation, an explicit and mathematically tractable form for the interaction operator $\Delta_s w_k$ must be found.

The most elementary technique which allows us to include some effects of collisions is the simple relaxation model, wherein the interaction term assumes the form

$$(\delta f / \delta t)_{\text{int}} = -\nu (f - f_o) \quad (2.27)$$

where f_0 is some equilibrium velocity distribution and ν^{-1} is the relaxation time for the distribution. This model is discussed at length by Tanenbaum [78]. Our primary objective in using this simple collision model is to ensure the proper selection of integration contours about certain singularities appearing in various integrands in this thesis, and not to obtain quantitative measures of the collision effects such as radiation absorption.

When the collision model (2.27) is used, we obtain for the interaction operator $\Delta_s \underline{w}$

$$\Delta_s \underline{w} = - N_s^{-1} \int \nu_s (\underline{w} f_s - \underline{w} f_{s0}) d^3w = - \nu_s (\underline{V}_s - \underline{V}_{s0}) \quad (2.28)$$

where \underline{V}_{s0} is some equilibrium average particle velocity. Thus our momentum transport equation becomes

$$\begin{aligned} \partial V_{sk} / \partial t + \rho_s^{-1} \partial P_{skj} / \partial x_j + V_{sj} \partial V_{sk} / \partial x_j - q_s m_s^{-1} (E_k + \epsilon_{klm} V_{sl} B_m) \\ = - \nu_s (V_{sk} - V_{sko}). \end{aligned} \quad (2.29)$$

Transport Equation for Kinetic Pressure

Replacing A_s by $m_s (\underline{w} - \underline{V}_s)(\underline{w} - \underline{V}_s)$ in (2.19), the result is a tensor equation. We look at the equation for the $(k,l)^{th}$ element of this tensor, considering each term of (2.19) in succession.

$$\partial (N \overline{A_{skl}}) / \partial t = \partial P_{skl} / \partial t \quad (2.30)$$

$$- N_s \overline{\partial A_{skl} / \partial t} = 0 \quad (2.31)$$

$$\begin{aligned} \partial (N_s \overline{A_{skl} w_j}) / \partial x_j = \partial Q_{sklj} / \partial x_j + (\partial V_{sj} / \partial x_j) P_{skl} \\ + V_{sj} \partial P_{skl} / \partial x_j \end{aligned} \quad (2.32)$$

$$\begin{aligned} - N_s \overline{(\partial A_{skl} / \partial x_j) w_j} = (\partial V_{sk} / \partial x_j) P_{slj} + \\ P_{skj} (\partial V_{sl} / \partial x_j) \end{aligned} \quad (2.33)$$

$$\begin{aligned}
-N_s m_s^{-1} \overline{(\partial A_{skl} / \partial w_j) F_{sj}} &= -q_s m_s^{-1} \epsilon_{kmn} P_{slm} B_n \\
&\quad - q_s m_s^{-1} \epsilon_{lmn} P_{skm} B_n \quad (2.34)
\end{aligned}$$

$$N_s \Delta_s A_{skl} = \rho_s \Delta_s (w_k - V_{sk})(w_l - V_{sl}) \quad (2.35)$$

Collecting these terms, we obtain the transport equation for kinetic pressure

$$\begin{aligned}
\partial P_{skl} / \partial t + \partial Q_{sklj} / \partial x_j + (\partial V_{sj} / \partial x_j) P_{skl} + V_{sj} \partial P_{skl} / \partial x_j + \\
(\partial V_{sk} / \partial x_j) P_{slj} + P_{skj} \partial V_{sl} / \partial x_j + \\
q_s m_s^{-1} (\epsilon_{knm} B_n P_{lm} + \epsilon_{lnm} B_n P_{km}) \\
= \rho_s \Delta_s (w_k - V_{sk})(w_l - V_{sl}). \quad (2.36)
\end{aligned}$$

As in the previous section, we again use the collision model (2.27) to obtain a tractable form for the interaction operator. This results in the relatively simple expression

$$\Delta_s m_s (\underline{w} - \underline{V}_s) (\underline{w} - \underline{V}_s) = -N_s^{-1} \nu_s (\underline{P}_s - \underline{P}_{s0}) \quad (2.37)$$

where \underline{P}_{s0} is some equilibrium kinetic pressure. In general, the equilibrium kinetic pressure \underline{P}_{s0} will be a scalar quantity as indicated for example in [66]. However, in the ionosphere, the temperatures corresponding to particle speeds parallel and perpendicular to the Earth's magnetic field are often unequal for times on the order of many cycles of the radiation. Hence, the unperturbed kinetic pressure in the ionospheric plasma is likely to be a tensor quantity corresponding to different pressures parallel and transverse to the Earth's magnetic field. Thus for our purposes we treat \underline{P}_{s0} appearing in (2.37) as the unperturbed kinetic pressure since, for the cases we wish to consider, the unperturbed pressure represents a quasi-equilibrium state. This

method of introducing losses into the kinetic pressure transport equation is used by Sharma [67].

In order to close the set of moment equations we shall use the adiabatic approximation $\nabla \cdot \underline{Q}_s = 0$ as used for example in [10,82]. Then (2.36) simplifies to

$$\begin{aligned} & \partial P_{skl} / \partial t + (\partial V_{sj} / \partial x_j) P_{skl} + V_{sj} \partial P_{skl} / \partial x_j + \\ & \quad (\partial V_{sk} / \partial x_j) P_{slj} + P_{skj} \partial V_{sl} / \partial x_j + \\ & \quad q_s m_s^{-1} (\epsilon_{knm} B_n P_{slm} + \epsilon_{lnm} B_n P_{skm}) \\ & = -\nu_s (P_{skl} - P_{sokl}) . \end{aligned} \quad (2.38)$$

An alternative procedure to closing the moment equations which does not require setting $\nabla \cdot \underline{Q}_s = 0$ is given by Oraevskii, et. al. [56].

"Wave Equation"

Before we can solve for the power fed into a plasma from a radiating source it is first necessary to determine the dependence of the electric field in the plasma upon the source current density $\underline{J}^{(ex)}$ which we often call the "external" current density. The purpose of this section is to derive this functional dependence. The relation between the electric field and the source current as derived here is often called the "wave equation", for it is simply a generalization of the free space wave equation to the case of complex dielectric media.

We begin the derivation by Fourier-analyzing the Maxwell curl equations (MKSA units). Assuming that all field quantities can be considered to be made up locally of a superposition of plane waves $\exp(i \underline{k} \cdot \underline{r} - i \omega t)$ with \underline{k} the wave propagation vector and ω the radian frequency, these equations can be written,

$$\underline{k} \times \underline{\mathcal{E}} = \omega \underline{\mathcal{B}} \quad (2.39)$$

and

$$i \mu_0^{-1} \underline{k} \times \underline{\mathcal{B}} = -i \epsilon_0 \omega \underline{\mathcal{E}} + \sum_s N_s q_s \underline{\mathcal{V}}_s + \underline{\mathcal{J}}^{(ex)}, \quad (2.40)$$

where the convention will be to use script capital letters for the Fourier transformed fields. $\underline{\mathcal{J}}^{(ex)}$ is the Fourier transform of an external current density which for our purposes will be taken as flowing independently of the plasma medium in which it is embedded, and $N_s q_s \underline{\mathcal{V}}_s$ is a Fourier transformed convection current in the plasma. μ_0 and ϵ_0 are the usual permeability and relative permittivity of free space. The summation is over all particle species in the plasma. If the plasma is described in terms of a mobility tensor $\underline{\mu}_s$ which relates $\underline{\mathcal{V}}_s$ to $\underline{\mathcal{E}}$ via

$$\underline{\mathcal{V}}_s = \underline{\mu}_s \cdot \underline{\mathcal{E}} \quad (2.41)$$

then (2.40) can be written as

$$i \mu_0^{-1} \underline{k} \times \underline{\beta} = -i \epsilon_0 \omega \underline{\mathcal{E}} + \sum_s N_s q_s \underline{\mu}_s \cdot \underline{\mathcal{E}} + \underline{j}^{(ex)}. \quad (2.42)$$

The relation between the "induced" current $\underline{j}_s^{(in)}$ and the electric field given by

$$\underline{j}_s^{(in)} \equiv N_s q_s \underline{\gamma}_s = \underline{\sigma}_s \cdot \underline{\mathcal{E}} \quad (2.43)$$

defines the often used conductivity tensor $\underline{\sigma}_s$ which is obviously related to the mobility tensor by

$$\underline{\sigma}_s = N_s q_s \underline{\mu}_s. \quad (2.44)$$

Defining the dielectric tensor \underline{K} by

$$\underline{K} = \underline{I} + i (\epsilon_0 \omega)^{-1} \sum_s N_s q_s \underline{\mu}_s = \underline{I} + i (\epsilon_0 \omega)^{-1} \sum_s \underline{\sigma}_s, \quad (2.45)$$

(2.42) becomes

$$i \mu_0^{-1} \underline{k} \times \underline{\beta} = -i \omega \epsilon_0 \underline{K} \cdot \underline{\mathcal{E}} + \underline{j}^{(ex)}. \quad (2.46)$$

Solving (2.39) for $\underline{\beta}$ and inserting the result into (2.46) gives the single equation for $\underline{\mathcal{E}}$, namely,

$$\underline{k} \times (\underline{k} \times \underline{\mathcal{E}}) + (\omega^2 / c^2) \underline{K} \cdot \underline{\mathcal{E}} = -i \omega \mu_0 \underline{j}^{(ex)}, \quad (2.47)$$

where c is the velocity of light in a vacuum. Using the vector identity

$$\underline{k} \times (\underline{k} \times \underline{\mathcal{E}}) = \underline{k} (\underline{k} \cdot \underline{\mathcal{E}}) - k^2 \underline{\mathcal{E}} \quad (2.48)$$

we can write the "wave equation" for $\underline{\mathcal{E}}$

$$-\underline{k} (\underline{k} \cdot \underline{\mathcal{E}}) + k^2 \underline{\mathcal{E}} - (\omega^2 / c^2) \underline{K} \cdot \underline{\mathcal{E}} = i \omega \mu_0 \underline{j}^{(ex)}. \quad (2.49)$$

At this point we have only a formal relationship between the electric field and the source or "external" current density, since we have not yet specified the components of the dielectric tensor $\underline{\underline{K}}$. What we are doing is putting all of the complexities of the plasma into this, as yet unspecified, tensor. Provided that the dielectric tensor components are independent of the electric field, the "wave equation" can be straight-forwardly inverted to yield an expression for the electric field. When the dielectric tensor depends upon the electric field, the radiation problem becomes an enormously complicated nonlinear problem. Such situations are not at all difficult to realize in practice. For example, an electric dipole will drive a plasma in which it is embedded in a nonlinear fashion when only a few volts, i.e. $\gtrsim 1$ volt, are placed across its terminals [49]. In this thesis, we shall restrict ourselves to linear plasma responses. Analyses of the nonlinear antenna-plasma problem are given by Baker, Weil, and Bearce [5] and Shkarofsky [68] which treat the problem of the input impedance of an antenna under large drive levels.

Linearization and Transformation

Till now, all the field quantities \underline{E} , \underline{B} , $\underline{\underline{P}}_s$, \underline{V}_s , etc. have referred to the total field. Now we wish to consider all field quantities as being composed of an unperturbed part indicated by a subscript, o, and a small perturbation caused by an external source which is written without the subscript o. We shall assume that the present field quantities can be replaced as follows:

$$\begin{aligned} \underline{E} &\rightarrow 0 + \underline{E} & , & & \underline{B} &\rightarrow \underline{B}_o + \underline{B} & , & & \underline{V}_s &\rightarrow 0 + \underline{V}_s & , \\ \underline{N}_s &\rightarrow \underline{N}_{so} + \underline{N}_s & , & & \underline{\rho}_s &\rightarrow \underline{\rho}_{so} + \underline{\rho}_s & , & & \underline{\underline{P}}_s &\rightarrow \underline{\underline{P}}_{so} + \underline{\underline{P}}_s & . \end{aligned} \quad (2.50)$$

The first term to the right of each arrow represents the unperturbed value of the respective field while the second represents only the perturbed field. Note that when no source is present, the plasma is assumed to be

at rest ($\underline{V}_{s0} = 0$) with no ambient electric field ($\underline{E}_0 = 0$) but permeated by a constant magnetic field ($\underline{B}_0 = B_0 \hat{e}_z$) directed along the positive z-axis. Retaining only terms to first order in the perturbation fields the moment equations become

$$\partial N_s / \partial t + N_{s0} \partial V_{sj} / \partial x_j = 0 \quad (2.51)$$

$$\begin{aligned} \partial V_{sk} / \partial t + \rho_{s0}^{-1} \partial P_{skj} / \partial x_j - q_s m_s^{-1} (E_k + \epsilon_{klm} V_{sl} B_{0m}) \\ = -\nu_s V_{sk} \end{aligned} \quad (2.52)$$

$$\begin{aligned} \partial P_{skl} / \partial t + (\partial V_{sj} / \partial x_j) P_{sokl} + (\partial V_{sk} / \partial x_j) P_{solj} + \\ P_{sokj} \partial V_{sl} / \partial x_j + q_s m_s^{-1} (\epsilon_{knm} B_{0n} P_{slm} + \epsilon_{lnm} B_{0n} P_{skm} + \\ \epsilon_{knm} B_{0n} P_{solm} + \epsilon_{lnm} B_{0n} P_{sokm}) = -\nu_s P_{skl} . \end{aligned} \quad (2.53)$$

This amounts to a linearization of the moment equations.

We shall perform a double transformation of the moment equations as follows: First, we shall Fourier-analyze them and second, we shall express the resultant equations in terms of Polarized-Wave (P-W) space. For a discussion of Polarized-Wave space see Appendix A. Field quantities which depend on the Fourier transform variables (\underline{k} , ω) will be designated by capital script letters as previously indicated.

The first two moment equations, (2.51) and (2.52), become

$$-\omega \eta_s + N_{s0} k - \gamma \nu_s \gamma = 0 \quad (2.54)$$

$$\begin{aligned} -i\omega \gamma_{s\sigma} + i\rho_{s0}^{-1} \varphi_{s\sigma} - \gamma k_\gamma - q_s m_s^{-1} \delta_\sigma + i\sigma \omega_{bs} \gamma_{s\sigma} \\ = -\nu_s \gamma_{s\sigma} . \end{aligned} \quad (2.55)$$

The radian gyrofrequency ω_{bs} appearing in (2.55) is defined as

$\omega_{bs} \equiv q_s B_0 / m_s$, and contains the sign of the charge.

As in the case of repeated latin subscripts, we use the summation convention of summing over repeated Greek subscripts on vector and tensor quantities. In this thesis, Greek summation indices take on the values +1, -1, 0. By way of illustration we write for vectors A and B

$$\underline{A} \cdot \underline{B} = \sum_{\nu} A_{-\nu} B_{\nu} \equiv A_{-\nu} B_{\nu} = A_{-1} B_1 + A_1 B_{-1} + A_0 B_0. \quad (2.56)$$

Greek indices can also appear as algebraic quantities. This feature considerably simplifies the form of many equations. For example,

$$\sum_{\nu} \nu A_{-\nu} B_{\nu} \equiv \nu A_{-\nu} B_{\nu} = A_{-1} B_1 - A_1 B_{-1}. \quad (2.57)$$

Note, however, that no summation is implied in the following examples containing vectors A and B and Bessel function J_{σ} :

$$\sigma A_{-\sigma} B_{\nu}, \quad J_{\sigma} B_{\sigma} \quad (2.58)$$

since σ does not appear as a repeated subscript on vector or tensor quantities.

In the transport equation for kinetic pressure (2.53), we first Fourier-analyze this equation and then eliminate $\underline{\beta}$ by using the Maxwell equation (2.39) and the identity (H.46). Then transforming to P-W space, realizing that in cartesian space $\underline{\varrho}_s$ is symmetric, we obtain

$$\begin{aligned} & \left(-i\omega + \nu_s + i\omega_{bs}(\sigma + \lambda) \right) \varrho_{s\sigma\lambda} = -i k_{-\gamma} \gamma_{s\gamma} P_{so\sigma\lambda} - i \gamma_{s\sigma} k_{-\gamma} P_{so\gamma\lambda} - \\ & i P_{so\sigma-\gamma} k_{\gamma} \gamma_{s\lambda} - q_s m_s^{-1} \omega^{-1} \left(\varrho_{\sigma-\gamma} k_{-\gamma} P_{so\gamma\lambda} - \right. \\ & \left. k_{\sigma} \varrho_{-\gamma} P_{so\gamma\lambda} + P_{so\sigma-\gamma} k_{\gamma} \varrho_{\lambda} - P_{so\sigma-\gamma} \varrho_{\gamma} k_{\lambda} \right). \quad (2.59) \end{aligned}$$

Linearizing the constitutive relation (2.43) we get

$$\underline{\varrho}_s^{(in)} = N_{so} q_s \underline{\gamma}_s = \underline{\sigma}_s \cdot \underline{\varrho}. \quad (2.60)$$

Hence, in the linear regime

$$\underline{\underline{\sigma}}_s = N_{s0} q_s \underline{\underline{\mu}}_s , \quad (2.61)$$

and from (2.45) the linearized dielectric, mobility and conductivity tensors are connected by

$$\underline{\underline{K}} = \underline{\underline{I}} + i (\epsilon_0 \omega)^{-1} \sum_s N_{s0} q_s \underline{\underline{\mu}}_s = \underline{\underline{I}} + i (\epsilon_0 \omega)^{-1} \sum_s \underline{\underline{\sigma}}_s . \quad (2.62)$$

The "wave equation" (2.49) looks formally the same after linearization. In terms of P-W space it becomes

$$(n^2 I_{\sigma-\gamma} - K_{\sigma-\gamma} - n_{\sigma} n_{-\gamma}) \underline{\underline{\mathcal{E}}}_{\gamma} = i (\omega \epsilon_0)^{-1} \underline{\underline{\mathcal{J}}}_{\sigma}^{(ex)} \quad (2.63)$$

which is written using the refractive index vector \underline{n} , defined by $\underline{n} = c \underline{k} / \omega$. The quantity $I_{\sigma-\gamma}$ is a component of the identity tensor in P-W space. $I_{\sigma-\gamma} = 1$ if the algebraic quantity $\sigma - \gamma = 0$ and $I_{\sigma-\gamma} = 0$ if $\sigma - \gamma \neq 0$.

If $\underline{\underline{\mathcal{J}}}_{\sigma}^{(ex)} = 0$, then the "wave equation" reduces to

$$(n^2 I_{\sigma-\gamma} - K_{\sigma-\gamma} - n_{\sigma} n_{-\gamma}) \underline{\underline{\mathcal{E}}}_{\gamma} = 0. \quad (2.64)$$

In order for there to exist non-trivial solutions to this equation, the determinant of the matrix multiplying $\underline{\underline{\mathcal{E}}}$ must vanish, that is,

$$\det (n^2 I_{\sigma-\gamma} - K_{\sigma-\gamma} - n_{\sigma} n_{-\gamma}) = 0. \quad (2.65)$$

This is referred to as the dispersion relation because it gives the functional dependence between frequency and wave propagation or refractive index vector.

The linearized and transformed equations given in this chapter are collectively referred to as the "governing equations" - hydrodynamic approach.

CHAPTER III

GOVERNING EQUATIONS-KINETIC APPROACH

In the previous chapter we obtained a set of equations used for studying plasma phenomena which are based on a hydrodynamic approach. In the hydrodynamic approach one does not work directly with the Boltzmann equation but rather with the moments of this equation. Hence, this approach can not describe those phenomena which depend on the explicit form of the distribution function rather than just on averages obtained with it. However, in this chapter we shall work directly with the linearized Boltzmann equation. We write down a formal solution of this equation and make the connection between the solution of the Boltzmann equation and the expression for the dielectric tensor which describes a warm magnetoplasma. Having obtained an expression for the plasma dielectric tensor, we can then combine this with the Maxwell equations, as done in the previous chapter, to get a set of equations governing radiation in homogeneous plasmas based upon a kinetic approach.

A great deal of the material which appears in this chapter is based on the numerous Russian investigations in this area; see for example the book by Klimontovich [39]. We also found the papers by Bernstein [7] and Kikuchi [38] to be extremely useful in this regard.

As in the previous chapter, our starting point is the Boltzmann equation which we write in the form

$$\partial f / \partial t + \underline{w} \cdot \nabla f + m^{-1} q (\underline{E} + \underline{w} \times \underline{B}) \cdot (\partial f / \partial \underline{w}) = (\partial f / \partial t)_{\text{int}} \quad (3.1)$$

where we use the same notation as in the previous chapter. An equation of the same form holds for each species of charged particles in the plasma.

Using the simple collision model (2.27) to approximate the interaction term and linearizing in a manner similar to that used in the previous chapter with $f \rightarrow f + f_0$, we get

$$(\partial f / \partial t) + \underline{w} \cdot \nabla f + m^{-1} q (\underline{w} \times \underline{B}_0) \cdot (\partial f / \partial \underline{w}) + \nu f = -m^{-1} q (\partial f_0 / \partial \underline{w}) \cdot (\underline{E} + \underline{w} \times \underline{B}). \quad (3.2)$$

Note that in Klimontovich's book that his eqn. (9.4) is missing the term $-m^{-1} q (\partial f_0 / \partial \underline{w}) \cdot \underline{w} \times \underline{B}$ which occurs in our corresponding eqn. (3.2). He claims that this term is identically zero if the distribution function f_0 is of the form $f_0(\underline{w}) = f_0(w_\perp^2, w_z^2)$. However, this condition alone is not sufficient to guarantee the vanishing of the additional term. To see this, consider the particular distribution function

$$f_0 = e^{-\alpha w_\perp^2 - \beta w_z^2}. \quad (3.3)$$

If $\alpha \neq \beta$, then $\partial f_0 / \partial \underline{w}$ is clearly not parallel to \underline{w} and therefore $(\partial f_0 / \partial \underline{w}) \cdot \underline{w} \times \underline{B}$ is not always zero. Hence this term must be retained if we are to allow for such ambient undisturbed distribution functions such as given by (3.3).

We find it convenient to express those terms which derive from the Lorentz force in terms of "polarized-wave" space. Thus we write

$$(\partial f / \partial t) + w_j (\partial f / \partial x_j) + i \omega_p \gamma w_\perp (\partial f / \partial \underline{w}) + \nu f = -m^{-1} q (\partial f_0 / \partial \underline{w}) \cdot [\underline{E}_\gamma + (\underline{w} \times \underline{B})_\gamma]. \quad (3.4)$$

From Appendix A we use the relation

$$\left(\frac{\partial}{\partial \underline{w}} \right)_\gamma \equiv \left(\gamma^2 2^{-\frac{1}{2}} \frac{\partial}{\partial w_\perp} + i \gamma 2^{-\frac{1}{2}} w_\perp^{-1} \frac{\partial}{\partial \phi} + (1 - \gamma^2) \frac{\partial}{\partial w_z} \right) e^{i \gamma \phi} \quad (3.5)$$

where the velocity is written in cylindrical (w_\perp, ϕ, w_z) coordinates, to obtain

$$\begin{aligned}
 (\partial f / \partial t) + w_{\perp} \cos \phi (\partial f / \partial x) + w_{\perp} \sin \phi (\partial f / \partial y) + w_z (\partial f / \partial z) \\
 - \omega_b (\partial f / \partial \phi) + \nu f = -m^{-1} q (\partial f / \partial \underline{w})_{\gamma} [E_{\gamma} + (\underline{w} \times \underline{B})_{\gamma}] . \quad (3.6)
 \end{aligned}$$

Consider solutions of the equations

$$\begin{aligned}
 dx/dt = w_{\perp} \cos \phi, \quad dy/dt = w_{\perp} \sin \phi, \quad dz/dt = w_z, \\
 dw_{\perp}/dt = 0, \quad d\phi/dt = -\omega_b, \quad dw_z/dt = 0, \quad (3.7)
 \end{aligned}$$

which are the characteristics[32] of the homogeneous linearized Boltzmann equation. The solutions of these characteristic equations connects the values of \underline{r} , \underline{w} at time t with the values of \underline{R} , \underline{W} at time t' . Here, \underline{r} , \underline{R} are position vectors with cartesian coordinates (x, y, z) and (X, Y, Z) respectively and \underline{w} , \underline{W} are velocity vectors with cartesian coordinates (w_x, w_y, w_z) and (W_x, W_y, W_z) respectively. Thus

$$\underline{R}(t', t, \underline{w}, \underline{r}) = \underline{R}(0, t-t', \underline{w}, \underline{r}) \quad \text{and} \quad \underline{W}(t', t, \underline{w}) = \underline{W}(0, t-t', \underline{w}). \quad (3.8)$$

The solutions of (3.7) are

$$\begin{aligned}
 x &= X + \omega_b^{-1} W_{\perp} \sin \Phi - \omega_b^{-1} W_{\perp} \sin [\Phi - \omega_b (t - t')] \\
 y &= Y - \omega_b^{-1} W_{\perp} \cos \Phi + \omega_b^{-1} W_{\perp} \cos [\Phi - \omega_b (t - t')] \\
 z &= Z + W_z (t - t') \\
 w_{\perp} &= W_{\perp} \\
 \phi &= \Phi - \omega_b (t - t') \\
 w_z &= W_z . \quad (3.9)
 \end{aligned}$$

The inverse relations are

$$\begin{aligned}
 X &= x - \omega_b^{-1} w_1 \sin [\phi - \omega_b (t' - t)] + \omega_b^{-1} w_1 \sin \phi \\
 Y &= y + \omega_b^{-1} w_1 \cos [\phi - \omega_b (t' - t)] - \omega_b^{-1} w_1 \cos \phi \\
 Z &= z + w_z (t' - t) \\
 W_1 &= w_1 \\
 \Phi &= \phi - \omega_b (t' - t) \\
 W_z &= w_z .
 \end{aligned} \tag{3.10}$$

Using the relations (3.10) we can now write the linearized Boltzmann equation in the form

$$\begin{aligned}
 f(\underline{r}, \underline{w}, t) &= e^{-\nu(t-t_0)} f(\underline{R}(0, t-t_0, \underline{w}, \underline{r}), W(0, t-t_0, w), t_0) \\
 &\quad - m^{-1} q \int_{t_0}^t e^{-\nu(t-t')} (\partial f_0 / \partial \underline{w})_{-\gamma, \underline{w} \rightarrow \underline{W}(0, t-t', \underline{w})} \{ E_\gamma(\underline{R}(0, t-t', \underline{w}, \underline{r}), t') \\
 &\quad + [\underline{W}(0, t-t', \underline{w}) \times \underline{B}(\underline{R}(0, t-t', \underline{w}, \underline{r}), t')]_\gamma \} dt'
 \end{aligned} \tag{3.11}$$

where we take $t > t_0$. To verify that (3.11) and (3.6) are equivalent, substitute this expression for $f(\underline{r}, \underline{w}, t)$ into (3.6) and differentiate directly using the formula

$$\frac{d}{da} \int_{\psi(a)}^{\varphi(a)} f(x, a) dx = f(\varphi(a), a) \frac{d\varphi(a)}{da} - f(\psi(a), a) \frac{d\psi(a)}{da} + \int_{\psi(a)}^{\varphi(a)} \frac{\partial}{\partial a} f(x, a) dx \tag{3.12}$$

for differentiating a definite integral with respect to a parameter. In this manner it can be readily shown that our expression for $f(\underline{r}, \underline{w}, t)$ does indeed satisfy the differential equation (3.6).

The first term on the right hand side of (3.11) is determined by the initial value of the function f , the collision frequency ν , and the time

lapse $t-t_0$. It is the solution of the homogeneous equation obtained from (3.6), while the second term is the solution of the non-homogeneous equation (3.6). If $t-t_0$ (t_0 is the initial point in time) is greater than the time required for the establishment of steady conditions, that is $t-t_0 \gg 1/\nu$, then we can make the initial point in time in (3.11) approach $-\infty$. This defines the connection between the distribution function and the electromagnetic field vectors \underline{E} and \underline{B} for a steady (stationary) process. Below we shall take $t_0 = -\infty$. In this case the first term on the right hand side of equation (3.11) goes to zero.

Using the distribution function one may obtain the current density \underline{J} for a given species via the usual relation

$$\underline{J} = q \int \underline{w} f d^3w. \quad (3.13)$$

Reintroducing the subscript s to distinguish various species of charged particles the total current density is written

$$\underline{J} = \sum_s \underline{J}_s. \quad (3.14)$$

Using (3.11), the induced currents $\underline{J}_s^{(in)}$, which are proportional to the electric and magnetic fields in the plasma, can be written

$$\begin{aligned} \underline{J}_s^{(in)} = -m_s^{-1} q_s^2 \int_{-\infty}^t dt' \int d^3w e^{-\nu_s(t-t')} \underline{w} \left(\frac{\partial f_{s0}}{\partial \underline{w}} \right)_{-\gamma, \underline{w} \rightarrow \underline{W}(0, t-t', \underline{w})} \\ \left\{ \underline{E}_\gamma(\underline{R}(0, t-t', \underline{w}, \underline{r}), t') + \left[\underline{W}(0, t-t', \underline{w}) \times \underline{B}_\gamma(\underline{R}(0, t-t', \underline{w}, \underline{r}), t') \right] \right\}. \end{aligned} \quad (3.15)$$

Applying the space Fourier transform to our expression for the induced currents $\underline{J}_s^{(in)}(\underline{r}, t)$ and expressing \underline{E} and \underline{B} in terms of their Fourier transforms in \underline{k} -space, we obtain

$$\begin{aligned}
\underline{\ell}_S(\underline{k}, t) &= -m_S^{-1} \alpha_S^2 \int d^3r \int_{-\infty}^t dt' \int d^3w \underline{w} \left(\partial f_{SO} / \partial \underline{w} \right)_{-\gamma, \underline{w} \rightarrow \underline{W}(0, t-t', \underline{w})} \\
&\quad (2\pi)^{-3} \int d^3k' e^{i\underline{k}' \cdot \underline{R}(0, t-t', \underline{w}, \underline{r}) - i\underline{k} \cdot \underline{r} - \nu_S(t-t')} \left\{ \mathcal{E}_\gamma(\underline{k}', t') \right. \\
&\quad \left. + \left[\underline{W}(0, t-t', \underline{w}) \times \underline{\mathcal{B}}(\underline{k}', t') \right]_\gamma \right\} . \quad (3.16)
\end{aligned}$$

Noting from (3.10) that

$$\underline{R}(0, t-t', \underline{w}, \underline{r}) = \underline{r} + \underline{R}(0, t-t', \underline{w}, 0), \quad (3.17)$$

changing the orders of integration, and performing the integrations over d^3r and d^3k' results in the following expression

$$\begin{aligned}
\underline{\ell}_S(\underline{k}, t) &= -m_S^{-1} \alpha_S^2 \int_{-\infty}^t dt' \int d^3w \underline{w} \left(\partial f_{SO} / \partial \underline{w} \right)_{-\gamma, \underline{w} \rightarrow \underline{W}(0, t-t', \underline{w})} \\
&\quad e^{i\underline{k} \cdot \underline{R}(0, t-t', \underline{w}, 0) - \nu_S(t-t')} \\
&\quad \left\{ \mathcal{E}_\gamma(\underline{k}, t') + \left[\underline{W}(0, t-t', \underline{w}) \times \underline{\mathcal{B}}(\underline{k}, t') \right]_\gamma \right\} . \quad (3.18)
\end{aligned}$$

Carrying out a Fourier transform of $\underline{\ell}_S(\underline{k}, t)$ with respect to time we obtain

$$\begin{aligned}
\underline{\ell}_S(\underline{k}, \omega) &= -m_S^{-1} \alpha_S^2 \int_{-\infty}^{\infty} dt e^{i\omega t} \int_{-\infty}^t dt' \int d^3w \underline{w} \left(\partial f_{SO} / \partial \underline{w} \right)_{-\gamma, \underline{w} \rightarrow \underline{W}(0, t-t', \underline{w})} \\
&\quad e^{i\underline{k} \cdot \underline{R}(0, t-t', \underline{w}, 0) - \nu_S(t-t')} \\
&\quad \left\{ \mathcal{E}_\gamma(\underline{k}, t') + \left[\underline{W}(0, t-t', \underline{w}) \times \underline{\mathcal{B}}(\underline{k}, t') \right]_\gamma \right\} . \quad (3.19)
\end{aligned}$$

We make the following change of variables:

$$\begin{aligned}\tau &= t - t' \\ \xi &= t',\end{aligned}\quad (3.20)$$

which enables us to put $\underline{g}_s(\underline{k}, \omega)$ into the form

$$\begin{aligned}\underline{g}_s(\underline{k}, \omega) &= -m_s^{-1} q_s^2 \int_0^\infty d\tau \int d^3 \underline{w} \underline{w} \left(\partial f_{s0} / \partial \underline{w} \right)_{-\underline{\gamma}, \underline{w} \rightarrow \underline{W}(0, \tau, \underline{w})} \\ &\quad e^{-\nu_s \tau + i\omega \tau + i\underline{k} \cdot \underline{R}(0, \tau, \underline{w}, 0)} \\ &\quad \left[\int_{-\infty}^\infty d\xi \left\{ \delta_\gamma(\underline{k}, \xi) + \left[\underline{W}(0, \tau, \underline{w}) \times \underline{\beta}(\underline{k}, \xi) \right]_\gamma \right\} e^{i\omega \xi} \right].\end{aligned}\quad (3.21)$$

Noting that

$$\int_{-\infty}^\infty d\xi \delta_\gamma(\underline{k}, \xi) e^{i\omega \xi} = \delta_\gamma(\underline{k}, \omega) \quad (3.22)$$

and similarly for $\underline{\beta}(\underline{k}, \xi)$ and replacing the dummy variable τ by t , we find that

$$\begin{aligned}\underline{g}_s(\underline{k}, \omega) &= -m_s^{-1} q_s^2 \int_0^\infty dt \int d^3 \underline{w} \underline{w} \left(\partial f_{s0} / \partial \underline{w} \right)_{-\underline{\gamma}, \underline{w} \rightarrow \underline{W}(0, t, \underline{w})} \\ &\quad e^{-\nu_s t + i\omega t + i\underline{k} \cdot \underline{R}(0, t, \underline{w}, 0)} \\ &\quad \left\{ \delta_\gamma(\underline{k}, \omega) + \left[\underline{W}(0, t, \underline{w}) \times \underline{\beta}(\underline{k}, \omega) \right]_\gamma \right\}.\end{aligned}\quad (3.23)$$

Eliminating $\underline{\beta}$ by using the transformed Maxwell equation (2.39) and factoring the quantity δ_γ we obtain

$$\begin{aligned}
\underline{\underline{g}}_S(\underline{k}, \omega) = & -m_S^{-1} q_S^2 \int_0^\infty dt \int d^3 \underline{w} \underline{w} \quad (\partial f_{SO} / \partial \underline{w})_{-\lambda, \underline{w} \rightarrow \underline{W}(0, t, \underline{w})} \\
& e^{-\nu_S t + i\omega t + i\underline{k} \cdot \underline{R}(0, t, \underline{w}, 0)} \left\{ I_{\lambda-\gamma} \left[1 - \omega^{-1} \underline{k} \cdot \underline{W}(0, t, \underline{w}) \right] \right. \\
& \left. + \omega^{-1} k_\lambda W_{-\gamma}(0, t, \underline{w}) \right\} \delta_\gamma
\end{aligned} \tag{3.24}$$

Comparing our definition of the conductivity tensor $\underline{\underline{\sigma}}_S$, given by (2.43), with (3.24) we find that

$$\begin{aligned}
\sigma_{S\mu-\gamma} = & -m_S^{-1} q_S^2 \int_0^\infty dt \int d^3 \underline{w} w_\mu \quad (\partial f_{SO}(\underline{w}) / \partial \underline{w})_{-\lambda, \underline{w} \rightarrow \underline{W}(0, t, \underline{w})} \\
& e^{-\nu_S t + i\omega t + i\underline{k} \cdot \underline{R}(0, t, \underline{w}, 0)} \left\{ I_{\lambda-\gamma} \left[1 - \omega^{-1} \underline{k} \cdot \underline{W}(0, t, \underline{w}) \right] \right. \\
& \left. + \omega^{-1} k_\lambda W_{-\gamma}(0, t, \underline{w}) \right\} .
\end{aligned} \tag{3.25}$$

Using the expression for \underline{R} given by (3.10) and expressing \underline{k} in cylindrical (k_\perp, ϕ, k_z) coordinates, we can write

$$\underline{k} \cdot \underline{R}(0, t, \underline{w}, 0) = k_\perp \omega_{BS}^{-1} w_\perp \left[\sin(\phi - \phi - \omega_{BS} t) - \sin(\phi - \phi) \right] - k_z w_z t. \tag{3.26}$$

Introducing the identity

$$e^{ik_\perp \omega_{BS}^{-1} w_\perp \sin(\phi - \phi - \omega_{BS} t)} = \sum_{p=-\infty}^{\infty} J_p(k_\perp \omega_{BS}^{-1} w_\perp) e^{ip(\phi - \phi) - ip\omega_{BS} t} \tag{3.27}$$

and using the equality

$$(\partial f_{SO}(\underline{w})/\partial \underline{w})_{-\lambda, \underline{w} \rightarrow \underline{W}(0, t, \underline{w})} = e^{-i\lambda \omega_{bS} t} (\partial f_{SO}(\underline{w})/\partial \underline{w})_{-\lambda} \quad (3.28)$$

which presupposes $f_{SO}(\underline{W}) = f_{SO}(\underline{w})$ which is true for distributions of the form $f_{SO}(w_{\perp}, w_z)$, we can now write the plasma conductivity as

$$\sigma_{s\mu-\gamma} = -m^{-1} q_s^2 \int_0^{\infty} dt \int d^3w w_{\mu} [A_{-\gamma} f_{SO}(\underline{w})] e^{-i\gamma \phi} \sum_{p=-\infty}^{\infty} J_p(\xi) e^{ip(\varphi-\phi) - i\xi \sin(\varphi-\phi) + [-\nu_s + i\omega - i(p+\gamma)\omega_{bS} - ik_z w_z]t} \quad (3.29)$$

where

$$\xi \equiv k_{\perp} \omega_{bS}^{-1} w_{\perp}, \quad (3.30)$$

and \underline{A} is the vector operator with components

$$A_{\pm 1} \equiv 2^{-\frac{1}{2}} \left[(1 - \omega^{-1} k_z w_z) \frac{\partial}{\partial w_{\perp}} + \omega^{-1} k_z w_{\perp} \frac{\partial}{\partial w_z} \right], \quad (3.31)$$

and

$$A_0 \equiv \omega^{-1} k_{\perp} \cos(\varphi - \phi - \omega_{bS} t) \left[w_z \frac{\partial}{\partial w_{\perp}} - w_{\perp} \frac{\partial}{\partial w_z} \right] + \frac{\partial}{\partial w_z}. \quad (3.32)$$

Performing the integration over t gives

$$\sigma_{s\mu-\gamma} = i m_s^{-1} q_s^2 k_z^{-1} \int d^3w w_{\mu} [C_{\gamma} f_{SO}(\underline{w})] e^{-i\gamma \phi} \sum_{p=-\infty}^{\infty} J_p(\xi) e^{ip(\varphi-\phi) - i\xi \sin(\varphi-\phi)} \quad (3.33)$$

where

$$C_{\pm 1} \equiv \left[w_z - (\omega + i\nu_s - (p \pm 1)\omega_{bS})/k_z \right]^{-1} A_{\pm 1} \quad (3.34)$$

and

$$\begin{aligned}
C_0 \equiv & \frac{1}{2} \omega^{-1} k_z \left\{ \left[w_z - (\omega + i\nu_s - (p+1)\omega_{bs})/k_z \right]^{-1} e^{i(\varphi-\phi)} \right. \\
& + \left. \left[w_z - (\omega + i\nu_s - (p-1)\omega_{bs})/k_z \right]^{-1} e^{-i(\varphi-\phi)} \right\} \left[w_z \frac{\partial}{\partial w_z} - w_z \frac{\partial}{\partial w_z} \right] \\
& + \left[w_z - (\omega + i\nu_s - p\omega_{bs})/k_z \right]^{-1} \frac{\partial}{\partial w_z} . \tag{3.35}
\end{aligned}$$

Since we have already assumed that f_{so} is independent of the azimuthal angle ϕ , the integration over ϕ can also be carried out at this time. Noting the equality

$$\int_0^{2\pi} e^{i(\ell\phi - \xi \sin\phi)} d\phi = 2\pi J_\ell(\xi) , \tag{3.36}$$

the result of this integration can be written

$$\begin{aligned}
\sigma_{s\mu-\gamma} = & i 2\pi m_s^{-1} \alpha_s^2 k_z^{-1} e^{i(\mu-\gamma)\varphi} \sum_{p=-\infty}^{\infty} \int_0^{\infty} dw_z \int_{-\infty}^{\infty} dw_z w_z S_\mu J_{p-\mu}(\xi) J_{p-\gamma}(\xi) \\
& \left\{ \frac{\mathcal{O}_{-\gamma} f_{so} - D_{-\gamma} [w_z (\partial f_{so}/\partial w_z) - w_z (\partial f_{so}/\partial w_z)]}{w_z - (\omega + i\nu_s - p\omega_{bs})/k_z} \right\} \tag{3.37}
\end{aligned}$$

where S_μ defined by

$$w_\mu = S_\mu e^{i\mu\phi} \tag{3.38}$$

is the ϕ independent part of w_μ . Thus

$$S_\mu = \mu^2 2^{-\frac{1}{2}} w_z + (1-\mu^2) w_z . \tag{3.39}$$

Similarly we have also used the vector operator \mathcal{O}_α where $\mathcal{O}_\alpha f_{so}$ is defined as the ϕ independent part of $(\partial f_{so}/\partial \underline{w})_\alpha$, assuming f_{so} is independent of ϕ , hence

$$\mathcal{O}_\lambda = \lambda^2 2^{-\frac{1}{2}} \frac{\partial}{\partial w_z} + (1-\lambda^2) \frac{\partial}{\partial w_z} . \tag{3.40}$$

Finally, we have introduced the vector \underline{D} , defined by

$$D_{\lambda} = -\lambda^2 2^{-\frac{1}{2}} \omega^{-1} k_z + (1 - \lambda^2) p Y_s w_{\perp}^{-1} . \quad (3.41)$$

Having obtained an expression for the conductivity of a plasma, we can then combine this information with the Maxwell equations, as done for example in the previous chapter. The result is a set of equations governing radiation in homogeneous plasmas based on a kinetic theory description of the plasma. We call these the "governing equations"-kinetic approach.

CHAPTER IV

DERIVATION OF DIELECTRIC TENSOR

The approach we have taken has been to restrict all of the medium complexities to the dielectric tensor. Hence, by modeling the plasma, we mean giving an explicit form to the dielectric tensor. This chapter is devoted to giving alternative expressions for the dielectric tensor based upon our different plasma models.

We are going to analyze three plasma models. The first model is based upon a hydrodynamic description of the plasma using scalar pressure theory. We call this Model H and refer to it as the Hydrodynamic Model. The second model is based upon a kinetic description of the plasma and is referred to as Model K or the Kinetic Model. The third model we shall use is derivable from both the hydrodynamic and kinetic approaches using suitable approximations but not limiting the pressure to be isotropic. It is sometimes referred to as the Full Adiabatic Model [10]; our Model A.

Model H

Model H assumes an isotropic pressure, that is,

$$\underline{\underline{P}}_s = P_s \begin{bmatrix} 1 & 0 & 0 \\ 0 & 1 & 0 \\ 0 & 0 & 1 \end{bmatrix}. \quad (4.1)$$

The scalar pressure P_s is assumed to obey the adiabatic equation of state

$$P_s N_s^{-\gamma'_s} = \text{constant} \quad (4.2)$$

where γ'_s is the specific heat. In the linear approximation

$$dP_s = (\gamma'_s P_{s0} / N_{s0}) dN_s \quad (4.3)$$

where the equation

$$P_{s0} = N_{s0} K T_s \quad (4.4)$$

relates the unperturbed pressure number density and temperature.

K is Boltzmann's constant. Rearranging terms

$$dP_s = \gamma'_s K T_s dN_s = m_s u_s^2 dN_s \quad (4.5)$$

where u_s is the "sound" speed defined by

$$u_s^2 = \gamma'_s K T_s / m_s . \quad (4.6)$$

The value of the specific heat γ'_s is a somewhat complicated function of wave frequency and particle collision frequency [17], and different values are obtained depending upon the assumptions which are made. However, the various assumptions do not seriously affect calculated results as long as one considers a linearized theory [58]. The actual numerical constant can be absorbed by using an appropriate sound velocity. In our numerical calculations we use $\gamma'_s = 3$.

As a result of these considerations, the linearized continuity equation can now be written as

$$N_{s0} m_s u_s^2 \nabla \cdot \underline{V}_s = - \partial P_s / \partial t. \quad (4.7)$$

Since we have assumed that the various plasma constituents obey adiabatic equations of state, it will not be necessary to use the pressure transport equation. The momentum conservation equation (2.55) with $\varphi_{s\lambda - \sigma} k_\sigma$ now replaced by $\varphi_s k_\lambda$ becomes

$$(-i\omega + \nu_s + i\lambda \omega_{bs}) \nu_{s\lambda} = q_s m_s^{-1} \mathcal{E}_\lambda - i\rho_{s0}^{-1} \varphi_s k_\lambda , \quad (4.8)$$

or, solving for $\nu_{s\lambda}$, and introducing the notation

$$\Gamma_s \equiv 1 + i\nu_s / \omega , Y_s \equiv \omega_{bs} / \omega , \beta_s = Y_s / \Gamma_s , \quad (4.9)$$

we have

$$\underline{v}_{s\lambda} = [m_s \Gamma_s \omega (1 - \lambda \beta_s)]^{-1} (i q_s \mathcal{E}_\lambda + \varphi_s k_\lambda / N_{so}) . \quad (4.10)$$

Note that \underline{v}_s , like ω_{bs} , contains the sign of the charge.

We can solve for φ_s in terms of \mathcal{E}_λ by forming the dot product $\underline{k} \cdot \underline{v}_s$ using (4.10) and substituting for $\underline{k} \cdot \underline{v}_s$ from the Fourier-analyzed continuity equation which we write as

$$\underline{k} \cdot \underline{v}_s = (\rho_{so} u_s^2)^{-1} \omega \varphi_s . \quad (4.11)$$

As a result of this procedure we obtain the relation

$$\varphi_s / N_{so} = (i q_s \epsilon_s c^2 / \omega^2 D_s) k_{-\gamma} (1 - \gamma \beta_s)^{-1} \mathcal{E}_\gamma \quad (4.12)$$

where the complex normalized thermal speed squared is given by

$$\epsilon_s \equiv u_s^2 / (c^2 \Gamma_s) , \quad (4.13)$$

and the complex "gyro-element" g_{sx} is defined by

$$g_{sx} \equiv (1 - \beta_s^2)^{-1} , \quad (4.14)$$

and

$$D_s = 1 - \epsilon_s (n_x^2 g_{sx} + n_z^2) . \quad (4.15)$$

Combining equations (4.10) and (4.12), we get

$$\underline{v}_{s\lambda} = i q_s [m_s \Gamma_s \omega (1 - \lambda \beta_s)]^{-1} (\mathcal{E}_\lambda + \epsilon_s (1 - \gamma \beta_s)^{-1} D_s^{-1} n_\lambda n_{-\gamma} \mathcal{E}_\gamma) . \quad (4.16)$$

Therefore the mobility tensor elements $\mu_{s\lambda-\gamma}$ are of the form

$$\mu_{s\lambda-\gamma} = i q_s [m_s \Gamma_s \omega (1 - \lambda \beta_s)]^{-1} [I_{\lambda-\gamma} + \epsilon_s n_\lambda n_{-\gamma} (1 - \gamma \beta_s)^{-1} / D_s] \quad (4.17)$$

Defining the magnetoionic variable

$$X_s \equiv N_{s0} \alpha_s^2 / \epsilon_0 m_s \omega^2 \quad (4.18)$$

and the complex magnetoionic variable

$$\alpha_s^2 = X_s / \Gamma_s, \quad (4.19)$$

the dielectric tensor elements obtained from (2.62) are given by

$$K_{\lambda-\gamma} = I_{\lambda-\gamma} - \sum_s \alpha_s^2 (1-\lambda\beta_s)^{-1} [I_{\lambda-\gamma} + \epsilon_s n_\lambda n_{-\gamma} (1-\gamma\beta_s)^{-1} / D_s]. \quad (4.20)$$

In a cold plasma (i.e. one in which $\epsilon_s = 0$), the dielectric tensor simplifies to

$$K_{\lambda-\gamma} = K_\lambda I_{\lambda-\gamma} \quad (4.21)$$

where

$$K_\lambda = 1 - \sum_s \alpha_s^2 (1-\lambda\beta_s)^{-1}, \quad (\lambda=1, -1, 0) \quad (4.22)$$

is a diagonal element of the cold plasma dielectric tensor. Since K_λ is neither a vector or tensor quantity, the summation convention does not apply to it. In terms of K_λ , we can write (4.20) as

$$K_{\lambda-\gamma} = K_\lambda I_{\lambda-\gamma} - \sum_s \epsilon_s \alpha_s^2 (1-\lambda\beta_s)^{-1} (1-\gamma\beta_s)^{-1} n_\lambda n_{-\gamma} / D_s. \quad (4.23)$$

Explicitly, for cylindrical (n_\perp, ϕ, n_z) coordinates

$$K_{1-1} = K_1 - \frac{1}{2} n_1^2 \sum_s \epsilon_s \alpha_s^2 (1 - \beta_s)^{-2} / D_s \quad (4.24)$$

$$K_{00} = K_0 - n_z^2 \sum_s \epsilon_s \alpha_s^2 / D_s \quad (4.25)$$

$$K_{11} = -\frac{1}{2} n_1^2 e^{i2\varphi} \sum_s \epsilon_s \alpha_s^2 (1 - \beta_s^2)^{-1} / D_s \quad (4.26)$$

$$K_{10} = -2^{-\frac{1}{2}} n_1 n_z e^{i\varphi} \sum_s \epsilon_s \alpha_s^2 (1 - \beta_s)^{-1} / D_s \quad (4.27)$$

$$K_{01} = -2^{-\frac{1}{2}} n_1 n_z e^{i\varphi} \sum_s \epsilon_s \alpha_s^2 (1 + \beta_s)^{-1} / D_s \quad (4.28)$$

The remaining components of the dielectric tensor can easily be obtained from these if we note from the general form of $K_{\lambda-\gamma}$ that

$$K_{-\lambda\gamma}(\underline{n}, \omega) = K_{\lambda-\gamma}^*(\underline{n}, -\omega). \quad (4.29)$$

Model K

In Chapter III we derived an expression (3.37) for the plasma conductivity tensor using kinetic theory. If we now assume that f_{s0} can be described by the two-temperature Maxwellian distribution

$$f_{s0} = N_{s0} (2\pi)^{-3/2} u_{s\perp}^{-2} u_{s\parallel}^{-1} e^{-w_{\perp}^2/2u_{s\perp}^2 - w_z^2/2u_{s\parallel}^2} \quad (4.30)$$

with transverse and longitudinal thermal speeds defined by

$$u_{s\perp}^2 = KT_{s\perp}/m_s, \quad u_{s\parallel} = KT_{s\parallel}/m_s, \quad (4.31)$$

respectively, and insert this for f_{s0} into the conductivity equation (3.37), we obtain

$$\sigma_{s\mu-\gamma} = -i(2\pi)^{-2} \epsilon_0 \omega_{ps}^2 k_z^{-1} u_{s\perp}^{-2} u_{s\parallel}^{-1} e^{i(\mu-\gamma)\phi} \sum_{p=-\infty}^{\infty} \int_0^{\infty} dw_{\perp} \int_{-\infty}^{\infty} dw_z w_{\perp} S_{\mu} J_{p-\mu} J_{p-\gamma} e^{-w_{\perp}^2/2u_{s\perp}^2 - w_z^2/2u_{s\parallel}^2} \left\{ \frac{S_{-\gamma} u_{s-\gamma}^{-2} - D_{-\gamma} w_{\perp} w_z (u_{s\parallel}^{-2} - u_{s\perp}^{-2})}{w_z - (\omega + i\nu_{s-\mu} - p\omega_{bs})/k_z} \right\} \quad (4.32)$$

where $u_{s\gamma}$ (not a vector quantity) is defined by

$$u_{s\pm 1} \equiv u_{s\perp}, \quad u_{s0} \equiv u_{s\parallel}. \quad (4.33)$$

We can reduce the number of tensor elements which we have to calculate if we note the following symmetry property obtained from (4.32).

$$\sigma_{s\mu-\gamma}(\underline{n}, \omega) = \sigma_{s-\mu\gamma}^*(\underline{n}, -\omega) \quad (4.34)$$

The dielectric tensor, which is related to the conductivity by

$$\underline{\underline{K}} = \underline{\underline{I}} + i(\epsilon_0 \omega)^{-1} \sum_s \underline{\underline{\sigma}}_s, \quad (4.35)$$

also obeys the symmetry relation

$$K_{\mu-\gamma}(\underline{n}, \omega) = K_{-\mu\gamma}^*(\underline{n}, -\omega) . \quad (4.36)$$

Hence, we proceed to calculate only K_{1-1} , K_{00} , K_{11} , K_{10} , and K_{01} ; the symmetry property makes it a trivial exercise to obtain the other elements of the dielectric tensor from these.

In (4.32), the integrals over w_z can be expressed in terms of the "plasma dispersion function" $Z(\zeta)$ (see Appendix D), and the integrations over w_{\perp} are all related to Weber's second exponential integral [85] and are found in our Appendix D. Carrying out these integrations results in the following expressions for the dielectric tensor elements

$$K_{1-1} = 1 + \sum_s X_s 2^{-\frac{1}{2}} n_z^{-1} d_{s\parallel}^{-\frac{1}{2}} e^{-\mu_s} \sum_{p=-\infty}^{\infty} \left[Z(\zeta_p) + 2^{-\frac{1}{2}} n_z d_{s\parallel}^{\frac{1}{2}} (1-d_{s\perp}/d_{s\parallel}) Z'(\zeta_p) \right] \\ \left[-p I_p(\mu_s) + (1+p-\mu_s) I'_p(\mu_s) + \mu_s I''_p(\mu_s) \right] \quad (4.37)$$

$$K_{00} = 1 - \sum_s X_s 2^{-\frac{1}{2}} n_z^{-1} d_{s\parallel}^{-\frac{1}{2}} e^{-\mu_s} \sum_{p=-\infty}^{\infty} \zeta_p Z'(\zeta_p) \left[1-p Y_s(1-d_{s\parallel}/d_{s\perp}) \right] I_p(\mu_s) \quad (4.38)$$

$$K_{11} = e^{i2\varphi} \sum_s X_s 2^{-\frac{1}{2}} n_z^{-1} d_{s\parallel}^{-\frac{1}{2}} \mu_s e^{-\mu_s} \sum_{p=-\infty}^{\infty} \left[Z(\zeta_p) + 2^{-\frac{1}{2}} n_z d_{s\parallel}^{\frac{1}{2}} (1-d_{s\parallel}/d_{s\perp}) Z'(\zeta_p) \right] \left(I'_p(\mu_s) - I_p(\mu_s) \right) \quad (4.39)$$

$$K_{10} = -e^{i\varphi} \sum_s X_s Y_s 2^{-3/2} n_z^{-1} n_z^{-1} d_{s\parallel}^{-1} e^{-\mu_s} \sum_{p=-\infty}^{\infty} \left[1-p Y_s(1-d_{s\parallel}/d_{s\perp}) \right] \\ Z'(\zeta_p) \left[(p-\mu_s) I_p(\mu_s) + \mu_s I'_p(\mu_s) \right] \quad (4.40)$$

$$K_{01} = -e^{i\varphi} \sum_s X_s Y_s 2^{-3/2} n_z^{-1} n_z^{-1} d_{s\perp}^{-1} e^{-\mu_s} \sum_{p=-\infty}^{\infty} \left[Z'(\zeta_p) - 2^{-\frac{1}{2}} n_z d_{s\parallel}^{\frac{1}{2}} (1-d_{s\perp}/d_{s\parallel}) \zeta_p Z'(\zeta_p) \right] \left[(p+\mu_s) I_p(\mu_s) - \mu_s I'_p(\mu_s) \right] . \quad (4.41)$$

The argument ζ_p of the "plasma dispersion function" is given by

$$\zeta_p = (\omega + i\nu_s - p\omega_{bs}) / 2^{\frac{1}{2}} k_z u_{s\parallel} = (1 + i\nu_s/\omega - pY_s) / 2^{\frac{1}{2}} d_{s\parallel}^{\frac{1}{2}} n_z \quad (4.42)$$

and the argument μ_s of the modified Bessel function I_p is given by

$$\mu_s = k_{\perp}^2 u_{s\perp}^2 / \omega_{bs}^2 = n_{\perp}^2 d_{s\perp} / Y_s^2, \quad (4.43)$$

where $d_{s\parallel}$ and $d_{s\perp}$ are the normalized thermal speeds defined by

$$d_{s\parallel} = u_{s\parallel}^2 / c^2, \quad d_{s\perp} = u_{s\perp}^2 / c^2. \quad (4.44)$$

We also use the convention that

$$\frac{dZ(\zeta_p)}{d\zeta_p} \equiv Z'(\zeta_p) \quad (4.45)$$

with similar relations for $I'(\mu_s)$ and $I''(\mu_s)$.

Equations (4.37) - (4.41) are the dielectric tensor elements for our kinetic model which we call Model K.

Model A

The dielectric tensor for the Full Adiabatic Model¹ (Model A) is obtained from approximate solutions to the "governing equations" which were derived in the first few chapters. We find it illuminating to derive this model from both the moment equations and the Boltzmann equation, since such a procedure points out some of the similarities of the two approaches.

Derivation of Model A From Moment Equations

Our starting point is the "governing equations" found in Chapter II. We assume that the ambient plasma kinetic pressure is of the non-shear type. This enables us to write the ambient pressure tensor as a diagonal tensor. Allowing for differences between the pressure, $P_{S\parallel}$, along the magnetic field of our magnetoplasma and the pressures, $P_{S\perp}$, transverse to this field, we thus write

$$\underline{P}_{S0} = \begin{bmatrix} P_{S\perp} & 0 & 0 \\ 0 & P_{S\perp} & 0 \\ 0 & 0 & P_{S\parallel} \end{bmatrix} = \begin{bmatrix} P_{S\parallel} & 0 & 0 \\ 0 & P_{S\parallel} & 0 \\ 0 & 0 & P_{S\parallel} \end{bmatrix} + \begin{bmatrix} P_{S\perp} - P_{S\parallel} & 0 & 0 \\ 0 & P_{S\perp} - P_{S\parallel} & 0 \\ 0 & 0 & 0 \end{bmatrix}. \quad (4.46)$$

This expression for \underline{P}_{S0} has the same form both in the Cartesian and P-W spaces. Evidently we can write

$$P_{S0\alpha\lambda} = P_{S\parallel} I_{\alpha\lambda} + P_{S\Delta} \alpha^2 I_{\alpha\lambda} \quad (4.47)$$

where

$$P_{S\Delta} = P_{S\perp} - P_{S\parallel}. \quad (4.48)$$

Inserting this into equation (2.59), we have

¹ The model is full adiabatic because an adiabatic gas law is applied to all components of the pressure tensor rather than to a scalar pressure only.

$$\begin{aligned}
\varphi_{s\sigma\lambda} = & [-i\omega + \nu_s + i\omega_{bs}(\sigma + \lambda)]^{-1} \{ -iP_{s\parallel} I_{\sigma\lambda} k_{-\gamma} \gamma_{s\gamma} - \\
& iP_{s\Delta} \sigma^2 I_{\sigma\lambda} k_{-\gamma} \gamma_{s\gamma} - iP_{s\parallel} \gamma_{s\sigma} k_{-\gamma} - iP_{s\Delta} \gamma_{s\sigma} \gamma^2 k_{-\gamma} I_{\gamma\lambda} - \\
& iP_{s\parallel} k_{\sigma} \gamma_{s\lambda} - iP_{s\Delta} \sigma^2 k_{\sigma} \gamma_{s\lambda} - \\
& \omega^{-1} q_s m_s^{-1} [P_{s\Delta} \delta_{\sigma}^2 k_{-\lambda} - P_{s\Delta} k_{\sigma} \lambda^2 \delta_{\sigma} + P_{s\Delta} \sigma^2 k_{\sigma} \delta_{\sigma} - P_{s\Delta} \sigma^2 \delta_{\sigma} k_{\lambda}] \} \quad (4.49)
\end{aligned}$$

From (2.55) we obtain the desired form of the momentum transport equation.

$$(-i\omega + \nu_s + i\sigma\omega_{bs}) \gamma_{s\sigma} = q_s m_s^{-1} \delta_{\sigma} - \rho_{s0}^{-1} \varphi_{s\sigma-\lambda} k_{\lambda} \quad (4.50)$$

Inserting for $\varphi_{s\lambda-\gamma}$ using (4.49) gives

$$\begin{aligned}
(-i\omega + \nu_s + i\sigma\omega_{bs}) \gamma_{s\sigma} = & q_s m_s^{-1} \delta_{\sigma} - \rho_{s0}^{-1} \left\{ iP_{s\parallel} \left[\frac{k_{\sigma} k_{-\gamma}}{\omega + i\nu_s} + \right. \right. \\
& \left. \frac{k_{-\lambda} K_{\lambda} I_{\sigma-\gamma}}{\omega + i\nu_s - \omega_{bs}(\sigma - \lambda)} + \frac{k_{\sigma} k_{-\gamma}}{\omega + i\nu_s - \omega_{bs}(\sigma + \gamma)} \right] \gamma_{s\gamma} + iP_{s\Delta} \left[\frac{\sigma^2 k_{\sigma} k_{-\gamma}}{\omega + i\nu_s} + \right. \\
& \left. \frac{\lambda^2 k_{-\lambda} k_{\sigma} I_{\sigma-\gamma}}{\omega + i\nu_s - \omega_{bs}(\sigma - \lambda)} + \frac{\sigma^2 k_{\sigma} k_{-\gamma}}{\omega + i\nu_s - \omega_{bs}(\sigma + \gamma)} \right] \gamma_{s\gamma} + q_s (m_s \omega)^{-1} P_{s\Delta} \\
& \left. \left[\frac{(\gamma^2 - \sigma^2) k_{\sigma} k_{-\gamma}}{\omega + i\nu_s - \omega_{bs}(\sigma + \gamma)} + \frac{(\sigma^2 - \lambda^2) k_{-\lambda} k_{\sigma} I_{\sigma-\gamma}}{\omega + i\nu_s - \omega_{bs}(\sigma - \lambda)} \right] \delta_{\gamma} \right\}. \quad (4.51)
\end{aligned}$$

Defining

$$u_{s\parallel, \Delta, \perp}^2 \equiv \rho_{s0}^{-1} P_{s\parallel, \Delta, \perp} = K m_s^{-1} T_{s\parallel, \Delta, \perp} \quad (4.52)$$

and putting equation (4.51) into a form suitable for matrix inversion we obtain

$$\begin{aligned}
& \left\{ (-i\omega + \nu_s + i\sigma\omega_{bs}) I_{\sigma-\gamma} + iu_{s\parallel}^2 \left[\frac{k_{\sigma-\gamma} k_{\sigma-\gamma}}{\omega + i\nu_s} + \frac{k_{-\lambda} k_{\lambda} I_{\sigma-\gamma}}{\omega + i\nu_s - \omega_{bs}(\sigma-\lambda)} \right] + \right. \\
& \left. \frac{k_{\sigma-\gamma} k_{\sigma-\gamma}}{\omega + i\nu_s - \omega_{bs}(\sigma+\gamma)} \right] + iu_{s\Delta}^2 \left[\frac{\sigma^2 k_{\sigma-\gamma} k_{\sigma-\gamma}}{\omega + i\nu_s} + \frac{\lambda^2 k_{-\lambda} k_{\lambda} I_{\sigma-\gamma}}{\omega + i\nu_s - \omega_{bs}(\sigma-\lambda)} \right] + \\
& \left. \frac{\sigma^2 k_{\sigma-\gamma} k_{\sigma-\gamma}}{\omega + i\nu_s - \omega_{bs}(\sigma+\gamma)} \right\} \gamma_{s\gamma} = q_s m_s^{-1} \left\{ I_{\sigma-\gamma} + \frac{u_{s\Delta}^2}{\omega} \times \right. \\
& \left. \left[\frac{(\gamma^2 - \sigma^2) k_{\sigma-\gamma} k_{\sigma-\gamma}}{\omega + i\nu_s - \omega_{bs}(\sigma+\gamma)} + \frac{(\sigma^2 - \lambda^2) k_{-\lambda} k_{\lambda} I_{\sigma-\gamma}}{\omega + i\nu_s - \omega_{bs}(\sigma-\lambda)} \right] \right\} \delta_{\gamma}. \quad (4.53)
\end{aligned}$$

The accurate inversion of this equation is a very tedious process. Buneman [10] has pointed out that we may affect a first-order (i.e. linear in temperature) inversion of this equation if, for those terms on the left which contain components of the wave propagation vector \underline{k} , we substitute the expression for $\gamma_{s\gamma}$ obtained using the cold plasma approximation. The range of validity of this first-order inversion will be examined further when we re-derive Model A using kinetic theory in the next section. To perform this first-order inversion, in those terms which contain \underline{k} we use

$$(\gamma_{s\gamma})_{\text{cold}} = (-i\omega + \nu_s + i\gamma\omega_{bs})^{-1} q_s m_s^{-1} \delta_{\gamma} \quad (4.54)$$

which we get from (4.8) neglecting the pressure term. As a result we can solve for $\gamma_{s\sigma}$.

$$\begin{aligned}
\gamma_{s\sigma} = & q_s m_s^{-1} (-i\omega + \nu_s + i\sigma\omega_{bs})^{-1} \left\{ I_{\sigma-\gamma} + \frac{u_{s\Delta}^2}{\omega} \left[\frac{(\gamma^2 - \sigma^2) k_{\sigma} k_{-\gamma}}{\omega + i\nu_s - \omega_{bs}(\sigma + \gamma)} + \right. \right. \\
& \left. \left. \frac{(\sigma^2 - \lambda^2) k_{-\lambda} k_{\lambda} I_{\sigma-\gamma}}{\omega + i\nu_s - \omega_{bs}(\sigma - \lambda)} \right] - \frac{u_{s\parallel}^2 i}{-i\omega + \nu_s + i\gamma\omega_{bs}} \left[\frac{k_{\sigma} k_{-\gamma}}{\omega + i\nu_s} + \right. \right. \\
& \left. \left. \frac{k_{-\lambda} k_{\lambda} I_{\sigma-\gamma}}{\omega + i\nu_s - \omega_{bs}(\sigma - \lambda)} + \frac{k_{\sigma} k_{-\gamma}}{\omega + i\nu_s - \omega_{bs}(\sigma + \gamma)} \right] - \frac{u_{s\Delta}^2 i}{-i\omega + \nu_s + i\gamma\omega_{bs}} \right. \\
& \left. \left. \left[\frac{\sigma^2 k_{\sigma} k_{-\gamma}}{\omega + i\nu_s} + \frac{\lambda^2 k_{-\lambda} k_{\lambda} I_{\sigma-\gamma}}{\omega + i\nu_s - \omega_{bs}(\sigma - \lambda)} + \frac{\sigma^2 k_{\sigma} k_{-\gamma}}{\omega + i\nu_s - \omega_{bs}(\sigma + \gamma)} \right] \right\} \mathcal{E}_{\gamma}. \quad (4.55)
\end{aligned}$$

From (2.41) it follows that the mobility tensor is identifiable with the matrix multiplying \mathcal{E} in (4.55). Therefore from (4.55) and (2.62) we can write

$$\begin{aligned}
K_{\sigma-\gamma} = & I_{\sigma-\gamma} - \sum_s X_s (1 + iZ_s - \sigma Y_s)^{-1} \left\{ I_{\sigma-\gamma} + d_{s\Delta} \left[\frac{(\gamma^2 - \sigma^2) n_{\sigma} n_{-\gamma}}{1 + iZ_s - (\sigma + \gamma) Y_s} + \right. \right. \\
& \left. \left. \frac{(\sigma^2 - \lambda^2) n_{-\lambda} n_{\lambda} I_{\sigma-\gamma}}{1 + iZ_s - (\sigma - \lambda) Y_s} \right] + \frac{d_{s\parallel}}{1 + iZ_s - \gamma Y_s} \left[\frac{n_{\sigma} n_{-\gamma}}{1 + iZ_s} + \right. \right. \\
& \left. \left. \frac{n_{-\lambda} n_{\lambda} I_{\sigma-\gamma}}{1 + iZ_s - (\sigma - \lambda) Y_s} + \frac{n_{\sigma} n_{-\gamma}}{1 + iZ_s - (\sigma + \gamma) Y_s} \right] + \frac{d_{s\Delta}}{1 + iZ_s - \gamma Y_s} \right. \\
& \left. \left. \left[\frac{\sigma^2 n_{\sigma} n_{-\gamma}}{1 + iZ_s} + \frac{\lambda^2 n_{-\lambda} n_{\lambda} I_{\sigma-\gamma}}{1 + iZ_s - (\sigma - \lambda) Y_s} + \frac{\sigma^2 n_{\sigma} n_{-\gamma}}{1 + iZ_s - (\sigma + \gamma) Y_s} \right] \right\}. \quad (4.56)
\end{aligned}$$

In writing (4.56) we have introduced the following new quantities:

$$Z_s \equiv v_s / \omega ,$$

$$d_{s\parallel, s\Delta, s\perp} \equiv u_{s\parallel, s\Delta, s\perp}^2 / c^2 . \quad (4.57)$$

In cylindrical (n_\perp, ϕ, n_z) coordinates

$$n_\pm = 2^{-\frac{1}{2}} n_\perp e^{\pm i\phi} , \quad n_0 = n_z . \quad (4.58)$$

Hence, writing the components of the dielectric tensor in cylindrical coordinates we get

$$K_{1-1} = 1 - \sum_s X_s (1 + iZ_s - Y_s)^{-1} \left\{ 1 + d_{s\parallel} (1 + iZ_s - Y_s)^{-1} \right.$$

$$\left. \left[n_\perp^2 \left((1 + iZ_s)^{-1} + (1 + iZ_s - 2Y_s)^{-1} \right) + n_z^2 (1 + iZ_s - Y_s)^{-1} \right] \right.$$

$$+ d_{s\Delta} n_\perp^2 (1 + iZ_s - Y_s)^{-1} \left[(1 + iZ_s)^{-1} + (1 + iZ_s - 2Y_s)^{-1} \right]$$

$$\left. + d_{s\Delta} n_z^2 (1 + iZ_s - Y_s)^{-1} \right\} . \quad (4.59)$$

Defining

$$\Gamma_s = 1 + iZ_s$$

$$\alpha_s^2 = X_s / \Gamma_s , \quad \beta_s = Y_s / \Gamma_s$$

$$\epsilon_{s\parallel, s\Delta, s\perp} = d_{s\parallel, s\Delta, s\perp} / \Gamma_s , \quad (4.60)$$

the expression for K_{1-1} simplifies to

$$\begin{aligned}
K_{1-1} = & 1 - \sum_S \alpha_S^2 (1-\beta_S)^{-1} \left\{ 1 + \epsilon_{S\parallel} n_{\perp}^2 \left[\Gamma_S (1-\beta_S) \right]^{-1} \left[1 + (1-2\beta_S)^{-1} \right] \right. \\
& + \epsilon_{S\parallel} n_z^2 \left[\Gamma_S (1-\beta_S)(1-\beta_S) \right]^{-1} + \epsilon_{S\Delta} n_{\perp}^2 \left[\Gamma_S (1-\beta_S) \right]^{-1} \\
& \left. \left[1 + (1-2\beta_S)^{-1} \right] + \epsilon_{S\Delta} n_z^2 (1-\beta_S)^{-1} \right\} . \quad (4.61)
\end{aligned}$$

Also, we have from (4.56)

$$\begin{aligned}
K_{00} = & 1 - \sum_S \alpha_S^2 \left\{ 1 + (\epsilon_{S\parallel} / \Gamma_S) n_{\perp}^2 (1-\beta_S)^{-1} + (\epsilon_{S\parallel} / \Gamma_S) 3 n_z^2 - \right. \\
& \left. \left[\epsilon_{S\Delta} - (\epsilon_{S\Delta} / \Gamma_S) \right] n_{\perp}^2 (1-\beta_S)^{-1} \right\} \quad (4.62)
\end{aligned}$$

$$K_{11} = - \sum_S \alpha_S^2 (1-\beta_S)^{-1} (\epsilon_{S\parallel} + \epsilon_{S\Delta}) n_{\perp}^2 e^{i2\phi} / \Gamma_S \quad (4.63)$$

$$\begin{aligned}
K_{10} = & -2^{\frac{1}{2}} n_{\perp} n_z e^{i\phi} \sum_S \alpha_S^2 (1-\beta_S)^{-1} \left\{ (\epsilon_{S\parallel} + \epsilon_{S\Delta}) \left[1 + (1-\beta_S)^{-1} \right] / \Gamma_S - \right. \\
& \left. \epsilon_{S\Delta} (1-\beta_S)^{-1} \right\} \quad (4.64)
\end{aligned}$$

$$\begin{aligned}
K_{01} = & -2^{-\frac{1}{2}} n_{\perp} n_z e^{-i\phi} \sum_S \alpha_S^2 \left\{ (\epsilon_{S\parallel} / \Gamma_S) (1-\beta_S)^{-1} \left[1 + (1-\beta_S)^{-1} \right] + \right. \\
& \left. \epsilon_{S\Delta} (1-\beta_S)^{-1} \right\} \quad (4.65)
\end{aligned}$$

Noting from (4.56) that

$$K_{-\lambda\gamma}(\underline{n}, \omega) = K_{\lambda-\gamma}^*(\underline{n}, -\omega) \quad (4.66)$$

it is easy to obtain the four remaining components of the dielectric tensor.

Defining the "gyro-elements"

$$\begin{aligned} g_{s\pm} &\equiv (1 \pm \beta_s)^{-1} \\ g_{s\pm 2} &\equiv (1 \pm 2\beta_s)^{-1} \\ g_{sx} &\equiv (1 - \beta_s^2)^{-1} \end{aligned} \quad (4.67)$$

and writing the components of the dielectric tensor in cylindrical (n_\perp, φ, n_z) coordinates we finally obtain

$$\begin{aligned} K_{1-1} = & -n_\perp^2 \sum_s \alpha_s^2 g_{s-}^2 \left\{ \epsilon_{s\perp} (1 + g_{s-2}) / \Gamma_s \right\} + \left\{ 1 - \sum_s \alpha_s^2 g_{s-} \right. \\ & \left. \left[1 + n_z^2 (\epsilon_{s\Delta} g_{s-} + \epsilon_{s\parallel} g_{s-} g_{s-} / \Gamma_s) \right] \right\} \end{aligned} \quad (4.68)$$

$$\begin{aligned} K_{-11} = & -n_\perp^2 \sum_s \alpha_s^2 g_{s+}^2 \left\{ \epsilon_{s\perp} (1 + g_{s+2}) / \Gamma_s \right\} + \left\{ 1 - \sum_s \alpha_s^2 g_{s+} \right. \\ & \left. \left[1 + n_z^2 (\epsilon_{s\Delta} g_{s+} + \epsilon_{s\parallel} g_{s+} g_{s+} / \Gamma_s) \right] \right\} \end{aligned} \quad (4.69)$$

$$K_{11} = -n_\perp^2 e^{i2\varphi} \sum_s \frac{\epsilon_{s\perp}}{\Gamma_s} \alpha_s^2 g_{sx} \quad (4.70)$$

$$K_{-1-1} = -n_\perp^2 e^{-i2\varphi} \sum_s \frac{\epsilon_{s\perp}}{\Gamma_s} \alpha_s^2 g_{sx} \quad (4.71)$$

$$K_{10} = n_\perp n_z 2^{-\frac{1}{2}} e^{i\varphi} \sum_s \alpha_s^2 g_{s-} \left[\epsilon_{s\Delta} g_{s-} - \frac{\epsilon_{s\perp}}{\Gamma_s} (1 + g_{s-}) \right] \quad (4.72)$$

$$K_{-10} = n_{\perp} n_z 2^{-\frac{1}{2}} e^{-i\varphi} \sum_s \alpha_s^2 g_{s+} \left[\epsilon_{s\Delta} g_{s+} - \frac{\epsilon_{s\perp}}{\Gamma_s} (1 + g_{s+}) \right] \quad (4.73)$$

$$K_{0-1} = -n_{\perp} n_z 2^{-\frac{1}{2}} e^{-i\varphi} \sum_s \alpha_s^2 \left[\epsilon_{s\Delta} g_{s-} + \frac{\epsilon_{s\parallel}}{\Gamma_s} g_{s-} (1 + g_{s-}) \right] \quad (4.74)$$

$$K_{01} = -n_{\perp} n_z 2^{-\frac{1}{2}} e^{i\varphi} \sum_s \alpha_s^2 \left[\epsilon_{s\Delta} g_{s+} + \frac{\epsilon_{s\parallel}}{\Gamma_s} g_{s+} (1 + g_{s+}) \right] \quad (4.75)$$

$$K_{00} = n_{\perp}^2 \sum_s \alpha_s^2 \left\{ \epsilon_{s\Delta} g_{sx} - \frac{\epsilon_{s\perp}}{\Gamma_s} g_{sx} \right\} + \left\{ 1 - \sum_s \alpha_s^2 \left[1 + 3 n_z^2 \frac{\epsilon_{s\parallel}}{\Gamma_s} \right] \right\} \quad (4.76)$$

These are the components of the dielectric tensor for Model A as obtained from hydrodynamic theory.

In the limit where collisions are neglected, that is $\nu_s = 0$, these components simplify to

$$K_{1-1} = 1 - \sum_s X_s g_{s-} \left\{ 1 + d_{s\parallel} n_z^2 g_{s-} (g_{s-} - 1) + d_{s\perp} \left[n_z^2 g_{s-} + 2 n_{\perp}^2 g_{s-2} \right] \right\} \quad (4.77)$$

$$K_{00} = 1 - \sum_s X_s \left\{ 1 + d_{s\parallel} \left[3 n_z^2 + n_{\perp}^2 g_{sx} \right] \right\} \quad (4.78)$$

$$K_{11} = -n_{\perp}^2 e^{i2\varphi} \sum_s X_s d_{s\perp} g_{sx} \quad (4.79)$$

$$K_{10} = -2^{-1/2} n_{\perp} n_z e^{i\varphi} \sum_s X_s g_{s-} \left\{ d_{s\perp} + d_{s\parallel} g_{s-} \right\} \quad (4.80)$$

$$K_{01} = -2^{-1/2} n_{\perp} n_z e^{i\varphi} \sum_s X_s g_{s+} \left\{ d_{s\perp} + d_{s\parallel} g_{s+} \right\} \quad (4.81)$$

where Y_s replaces β_s in the "gyro-elements". The other components can be obtained from these using the symmetry relation

$$K_{-\lambda\gamma}(\underline{n}, \omega) = K_{\lambda-\gamma}^*(\underline{n}, -\omega).$$

Often it is of convenience to have the dielectric tensor components expressed in spherical (n, ϑ, φ) coordinates. We write the components in the form

$$K_{\lambda-\gamma} = K_{\lambda} I_{\lambda-\gamma} + n^2 K'_{\lambda-\gamma} \quad (4.82)$$

where K_{λ} is the cold plasma component of the dielectric tensor defined by (4.22) and $K'_{\lambda-\gamma}$ contains the temperature dependent terms. The temperature dependent terms are easily obtained via equations (4.68) - (4.76). They are

$$K'_{1-1} = -\sin^2 \vartheta \sum_S \alpha_S^2 g_{S-}^2 [\epsilon_{S\perp} (1+g_{S-}) / \Gamma_S] - \cos^2 \vartheta \sum_S \alpha_S^2 g_{S-} (\epsilon_{S\Delta} g_{S-} + \epsilon_{S\parallel} g_{S-} g_{S-} / \Gamma_S) \quad (4.83)$$

$$K'_{00} = \sin^2 \vartheta \sum_S \alpha_S^2 (\epsilon_{S\Delta} g_{S\Delta} - \epsilon_{S\perp} g_{S\Delta} / \Gamma_S) - \cos^2 \vartheta \sum_S \alpha_S^2 3 \epsilon_{S\parallel} / \Gamma_S \quad (4.84)$$

$$K'_{11} = -\sin^2 \vartheta e^{i2\varphi} \sum_S \epsilon_{S\perp} \alpha_S^2 g_{S\Delta} / \Gamma_S \quad (4.85)$$

$$K'_{10} = 2^{-\frac{1}{2}} \sin \vartheta \cos \vartheta e^{i\varphi} \sum_S \alpha_S^2 g_{S-} [\epsilon_{S\Delta} g_{S-} - \epsilon_{S\perp} (1+g_{S-}) / \Gamma_S] \quad (4.86)$$

$$K'_{01} = -2^{-\frac{1}{2}} \sin \vartheta \cos \vartheta e^{i\varphi} \sum_S \alpha_S^2 [\epsilon_{S\Delta} g_{S+} + \epsilon_{S\parallel} g_{S+} (1+g_{S+}) / \Gamma_S] \quad (4.87)$$

The remaining components of the dielectric tensor are easily obtained from these with the aid of the usual symmetry relations.

For the case when collisions are neglected, our expression for \underline{K} is consistent with the susceptibility matrix derived by Johnston [33].

Derivation of Model A From Kinetic Theory

The starting point for the derivation of the dielectric tensor for Model A from kinetic theory are the basic equations (4.37) through (4.41) which were obtained for the kinetic model (Model K). The basic equations are rewritten, using the approximations

$$|\zeta_p| \gg 1, \mu_s \ll 1. \quad (4.88)$$

That is, $Z(\zeta_p)$ and $Z'(\zeta_p)$ are replaced by their asymptotic expansions and $I_p(\mu)$, $I_p'(\mu)$, $I_p''(\mu)$, $e^{-\mu}$ are replaced by their small argument expansions. The various expansions can be found in Appendix H.

Recall that if collisions are neglected

$$\zeta_p = (\omega - p \omega_{bs}) / 2^{\frac{1}{2}} k_z u_{s\perp} = (1 - p Y_s) / 2^{\frac{1}{2}} n_z d_{s\parallel}^{\frac{1}{2}}, \quad (4.89)$$

while μ_s remains unchanged. Thus $|\zeta_p| \gg 1$ means, physically, that the frequency is not too close to the p th harmonic of the gyro-frequency. From our definitions of $u_{s\perp}^2$ and $u_{s\parallel}^2$ given by (4.31), we see that these quantities are proportional to the temperature. Then the basic equations are written in terms of these expansions and only quantities which are first order in the normalized thermal speeds $d_{s\perp}$ and $d_{s\parallel}$ are retained (sometimes simply referred to as first order in temperature). The results which are obtained are identical to those derived using a macroscopic approach with suitable approximations (equations (4.77) through (4.81)). As a result of retaining only those quantities which are first order in temperature, only the terms in the infinite series, $\sum_{p=-\infty}^{\infty}$, with $|p| \leq 2$ contribute to the final expression. From this manner of deriving Model A, it follows that Model A is a limiting case of Model K.

Unlike the derivation of Model A from the moment equations given in the preceding section, here the range of validity of Model A is given explicitly by the conditions (4.88). These conditions specify the regimes where Landau and cyclotron damping are negligible [37].

CHAPTER V

RADIATIVE POWER LOSS

Free electric charges, both ions and electrons, which are moving at suprathermic speeds through homogeneous magnetoplasmas lose some of their kinetic energy due to the fact that they radiate. When the plasma is very tenuous so that collision effects can be neglected, this becomes the dominant source of energy loss. In this thesis we consider radiation from both single point charges and also from macroscopic distributions of charges. In the latter case we choose a distribution of charges which is intended to simulate a bunching of suprathermic charged particles which may then radiate coherently.

We shall also consider radiation from satellite-borne antennas. Satellite-borne transmitting antennas in the ionosphere have radiation characteristics which are often very different from their free-space characteristics, especially when they are being driven at frequencies comparable to the natural frequencies of the ionospheric magnetoplasma.

In order to compute the radiated power from either a free charge or an antenna, our approach is to compute the quantity $\int \underline{J}^{(ex)} \cdot \underline{E} d^3r$ over the volume of the source. The problem is simplified if we first Fourier transform the external current densities, $\underline{J}^{(ex)}$, and the macroscopic electric field \underline{E} in the plasma. This approach has been successfully applied to radiation problems using cold plasma models [40], [50]. We will use this same method for warm plasmas. Therefore, in this chapter we shall first compute the Fourier transform, $\underline{J}^{(ex)}$, for various radiating sources. Having obtained the Fourier transformed $\underline{J}^{(ex)}$ and using the formal expression for the Fourier transformed electric field \underline{E} obtained in Appendix C, we then write down the formulas for the power

radiated by each of these sources. The chapter concludes with a discussion of reversible and irreversible power.

Source Currents and Their Fourier Transforms

Current Density for a Spiraling Point Charge

The current density, $\underline{J}^{(pt)}$, for a point charge of rest mass M and charge Q (positive or negative) spiraling with velocity \underline{V} about the z -axis, which we take as being oriented parallel to the external magnetic induction \underline{B}_0 , is given by

$$\underline{J}^{(pt)}(\underline{r}, t) = Q \underline{V}(t) \delta(\underline{r} - \underline{r}(t)) \quad (5.1)$$

where the position vector is given by

$$\underline{r}(t) = \hat{e}_x a \gamma \cos(\Omega t / \gamma) - \hat{e}_y a \gamma \sin(\Omega t / \gamma) + \hat{e}_z V_z t \quad (5.2)$$

and the velocity is

$$\underline{V}(t) = -\hat{e}_x V_\perp \operatorname{sgn} \Omega \sin(\Omega t / \gamma) - \hat{e}_y V_\perp \operatorname{sgn} \Omega \cos(\Omega t / \gamma) + \hat{e}_z V_z. \quad (5.3)$$

Ω is the signed gyro-frequency of the spiraling point charge $\Omega = Q B_0 / M$ (negative for electrons and positive for positively charged ions). The non-relativistic gyro-radius $a = V_\perp / |\Omega|$ and γ is the relativistic mass correction factor given by $\gamma = (1 - \beta_\perp^2 - \beta_z^2)^{-\frac{1}{2}}$ where $\beta_\perp = V_\perp / c$ and $\beta_z = V_z / c$. The function $\operatorname{sgn} \Omega$ is defined to be +1 when Ω is positive and -1 when Ω is negative.

In terms of P-W space, these equations can be written

$$\underline{r}(t) = \hat{e}_{+1} 2^{-\frac{1}{2}} a \gamma e^{-i \Omega t / \gamma} + \hat{e}_{-1} 2^{-\frac{1}{2}} a \gamma e^{i \Omega t / \gamma} + \hat{e}_0 V_z t \quad (5.4)$$

$$\underline{V}(t) = -\hat{e}_{+1} i 2^{-\frac{1}{2}} V_\perp \operatorname{sgn} \Omega e^{-i \Omega t / \gamma} + \hat{e}_{-1} i 2^{-\frac{1}{2}} V_\perp \operatorname{sgn} \Omega e^{i \Omega t / \gamma} + \hat{e}_0 V_z. \quad (5.5)$$

More concisely, we can write

$$V_{\nu}(t) = e^{-i\nu\pi/2} 2^{-\frac{1}{2}} \mathcal{J}_{\nu} e^{-i\nu\Omega t/\gamma} \quad (5.6)$$

where the vector component \mathcal{J}_{ν} is defined by

$$\mathcal{J}_{\nu} = \nu^2 V_{\perp} \operatorname{sgn} \Omega + (1-\nu^2) 2^{\frac{1}{2}} V_z. \quad (5.7)$$

These equations are used to compute the Fourier transform $\underline{g}^{(pt)}$. The integration over space is trivial because of the delta function appearing in (5.1). The result of the space integration is

$$\underline{g}_{\nu}^{(pt)}(\underline{k}, \omega) = Q \int V_{\nu}(t) e^{-i\underline{k} \cdot \underline{r}(t) + i\omega t} dt. \quad (5.8)$$

Referring to Appendix A, we can write $\underline{k} \cdot \underline{r}(t) = k_{\perp} r_{\nu}(t)$. Noting that in terms of cylindrical $(k_{\perp}, \varphi, k_z)$ coordinates

$$k_{\pm 1} = 2^{-\frac{1}{2}} k_{\perp} e^{\pm i\varphi}, \quad (5.9)$$

equation (5.8) can be written using (5.9)

$$\underline{g}_{\nu}^{(pt)}(\underline{k}, \omega) = Q \int dt V_{\nu}(t) e^{-ik_{\perp} a \gamma \cos(\Omega t/\gamma + \varphi)} e^{-i(k_z V_z - \omega)t}. \quad (5.10)$$

Using the property of Bessel functions that

$$e^{-ik_{\perp} a \gamma \cos(\Omega t/\gamma + \varphi)} = \sum_{p=-\infty}^{\infty} J_p(k_{\perp} a \gamma) e^{-ip(\pi/2 + \Omega t/\gamma + \varphi)} \quad (5.11)$$

(5.10) can also be written

$$\underline{g}_{\nu}^{(pt)}(\underline{k}, \omega) = Q \sum_{p=-\infty}^{\infty} J_p(k_{\perp} a \gamma) e^{-ip(\varphi + \pi/2)} \int dt V_{\nu}(t) e^{i(\omega - k_z V_z - p\Omega/\gamma)t}. \quad (5.12)$$

Inserting for $V_{\nu}(t)$ and integrating we get

$$\begin{aligned}
 \mathcal{J}_{\nu}^{(pt)}(\underline{k}, \omega) &= 2^{\frac{1}{2}} \pi Q \mathcal{J}_{\nu} e^{-i\nu\pi/2} \sum_{p=-\infty}^{\infty} J_p(k_{\perp} a \gamma) \\
 & e^{-ip(\varphi + \pi/2)} \delta(\omega - k_z V_z - (p + \nu) \Omega / \gamma) \quad . \quad (5.13)
 \end{aligned}$$

In terms of the refractive index, \underline{n} , this becomes

$$\begin{aligned}
 \mathcal{J}_{\nu}^{(pt)}(\underline{n}, \omega) &= 2^{\frac{1}{2}} \pi Q \mathcal{J}_{\nu} e^{-i\nu\pi/2} \sum_{p=-\infty}^{\infty} J_p(u) \\
 & e^{-ip(\varphi + \pi/2)} \delta(\omega - n_z \omega \beta_z - (p + \nu) \Omega / \gamma) \quad (5.14)
 \end{aligned}$$

where

$$u = k_{\perp} a \gamma = n_{\perp} a \gamma \omega / c. \quad (5.15)$$

Cerenkov radiation corresponds to $V_{\perp} = a = 0$, which means only the fundamental ($p = 0$) will be non-zero.

Current Density for an Extended Charge

In order to gain insight into the problem of coherent radiation from a bunch of charges, we shall also consider the problem of Cerenkov radiation from a uniformly charged ellipsoid (el) of revolution of mass M' whose center of mass, located at $x = 0, y = 0, z = z_0$, is moving parallel to \underline{B}_0 with a velocity $V_z \hat{e}_z$ as depicted in Figure 1. The ellipsoid is assumed at rest with respect to its center of mass.

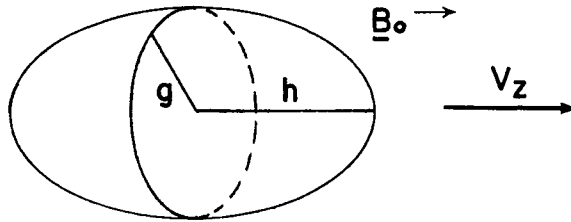


Fig. 1 . Sketch of geometry of charged ellipsoid. The ellipsoid is fixed relative to its center of mass

The axes of the ellipsoid are of lengths g and h as shown so that the volume of the ellipsoid is given by $\tau = (4/3) \pi g^2 h$. If Q' is the total charge contained within the ellipsoid, then the current density for such a source is given by

$$\underline{J}^{(el)}(\underline{r}, t) = \begin{cases} (Q'/\tau)\underline{V}(t) & , \text{inside ellipsoid} \\ 0 & , \text{outside ellipsoid.} \end{cases} \quad (5.16)$$

If $Q'/M' = Q/M$, which is the case we wish to study, then our previous formulas for the position and velocity of a point charge apply here to the center of mass of the ellipsoid.

The Fourier transform of $\underline{J}^{(el)}$ is given by

$$\underline{J}^{(el)}(\underline{k}, \omega) = (Q'/\tau) \int_{-\infty}^{\infty} dt \underline{V}(t) \int_{\text{vol. of el.}} d^3r e^{-i\underline{k} \cdot \underline{r} + i\omega t}. \quad (5.17)$$

In order to perform the last integration we need the equation for the surface of the ellipsoid as it moves. This is given by

$$(x^2 + y^2)/g^2 + (z - z_0)^2/h^2 = 1 \quad (5.18)$$

where $z_0 = V_z t$.

Making the change of variables

$$\eta = z - z_0, \quad (5.19)$$

the Fourier transform of $\underline{J}^{(el)}$ becomes

$$\underline{J}^{(el)}(\underline{k}, \omega) = (Q'/\tau) \int_{-\infty}^{\infty} dt \underline{V}(t) e^{-i(k_z V_z - \omega) t} \int_{\text{vol. of el.}} dx dy d\eta e^{-ik_x x - ik_y y - ik_z \eta} \quad (5.20)$$

which is nearly identical to what we had for a non-spiraling point charge with the exception of the integration over the ellipsoid volume. In fact,

it will be convenient to write

$$\underline{g}^{(el)} = D(g, h) \underline{g}^{(pt)} \quad (5.21)$$

where, in \underline{k} -space,

$$D(g, h) = \left(\frac{Q'}{Q} \right) \tau^{-1} \int_{\text{vol. of el.}} dx dy d\eta e^{-ik_x x - ik_y y - ik_z \eta}. \quad (5.22)$$

Switching to cylindrical coordinates via the transformations

$$\begin{aligned} k_x &= k_{\perp} \cos \varphi, & k_y &= k_{\perp} \sin \varphi, & k_z &= k_z \\ x &= \rho \cos \Phi, & y &= \rho \sin \Phi, & \eta &= \eta \end{aligned} \quad (5.23)$$

and making use of the identity

$$\cos(A - B) = \cos A \cos B + \sin A \sin B \quad (5.24)$$

our expression for $D(g, h)$, which we will call the "form factor", becomes

$$\begin{aligned} D(g, h) &= Q'(Q\tau)^{-1} \int_0^g \rho d\rho \int_0^{2\pi} d\Phi \int_{-\sqrt{f(\rho)}}^{+\sqrt{f(\rho)}} d\eta \\ &e^{-ik_{\perp} \rho \cos(\varphi - \Phi) - ik_z \eta} \end{aligned} \quad (5.25)$$

where, on the surface of the ellipsoid,

$$\eta = \pm h \sqrt{1 - \rho^2/g^2} = \pm \sqrt{f(\rho)}. \quad (5.26)$$

The integration over η is straight-forward, while the integration over Φ is given by

$$\int_0^{2\pi} e^{-ik_{\perp} \rho \cos(\varphi - \Phi)} d\Phi = 2\pi J_0(k_{\perp} \rho). \quad (5.27)$$

Hence, the "form factor" becomes

$$D(g, h) = 4\pi Q' (Q \tau k_z)^{-1} \int_0^g d\rho \rho J_0(k_\perp \rho) \sin(hk_z \sqrt{1 - \rho^2/g^2}). \quad (5.28)$$

From [26, p.761] we find that this integral is evaluated. Hence we can write

$$D(g, h) = 3 (Q'/Q) (\pi/2)^{\frac{1}{2}} \chi^{-3/2} J_{3/2}(\chi) \quad (5.29)$$

where

$$\chi \equiv (k_\perp^2 g^2 + k_z^2 h^2)^{\frac{1}{2}} = (\omega/c) (n_\perp^2 g^2 + n_z^2 h^2)^{\frac{1}{2}}. \quad (5.30)$$

Note that in the limit $g \rightarrow 0, h \rightarrow 0$

$$J_{3/2} \approx (2/\pi)^{\frac{1}{2}} \chi^{3/2} / 3 \quad (5.31)$$

so that for a point source with $Q' = Q$, the form factor $D(g, h) \rightarrow 1$.

Current Density for an Electric Dipole Antenna

For the calculation of many physical quantities, like the fields at great distances or the real power radiated, many current configurations $\underline{J}(\underline{r}, t)$, which are concentrated in an electrically small region, can be considered equivalent to an elementary dipole (see e.g. [76]). Therefore we shall examine the radiation from an oscillating point dipole whose dipole moment \underline{P} is specified

$$\underline{P} = \underline{p} \cos \omega_0 t \delta(\underline{r}) \quad (5.32)$$

where ω_0 is the angular operating frequency of the antenna and \underline{p} is the static dipole moment. The equivalent static dipole moment is given by

$$\underline{p} = \int \underline{r}' \rho(\underline{r}', t') d^3r', \quad (5.33)$$

where t' assumes the value which maximizes the integral. We can also think of \underline{p} as being equivalent to two point charges $+Q$ and $-Q$ separated

by a distance d , such that

$$\underline{p} = Q \underline{d} \quad (5.34)$$

where the vector \underline{d} extends from the negative to the positive charge. Assuming that the charge density varies in time like \underline{p} , we can also write

$$\rho = -Q \left[\delta \left(\underline{r} + \frac{1}{2} \underline{d} \right) - \delta \left(\underline{r} - \frac{1}{2} \underline{d} \right) \right] \cos \omega_0 t. \quad (5.35)$$

The current density associated with this oscillating dipole is given by

$$\underline{J} = \partial \underline{p} / \partial t = -\omega_0 \underline{p} \sin \omega_0 t \delta(\underline{r}). \quad (5.36)$$

Allowing our dipole antenna to move with the non-relativistic velocity \underline{V} with respect to the undisturbed plasma, the current density then becomes

$$\underline{J}(\underline{r}, t) = -\omega_0 \underline{p} \sin \omega_0 t \delta(\underline{r} - \underline{V}t) - Q \underline{V} \cos \omega_0 t \left[\delta \left(\underline{r} + \frac{1}{2} \underline{d} - \underline{V}t \right) - \delta \left(\underline{r} - \frac{1}{2} \underline{d} - \underline{V}t \right) \right]. \quad (5.37)$$

Treating the case of a dipole oriented parallel with \underline{B}_0 and moving along \underline{B}_0 (i.e. letting $\underline{p} = p_z \hat{e}_z$, $\underline{d} = d_z \hat{e}_z$, and $\underline{V} = V_z \hat{e}_z$), the current density is written

$$J_x(\underline{r}, t) = J_y(\underline{r}, t) = 0 \quad (5.38)$$

$$J_z(\underline{r}, t) = -\omega_0 p_z \sin \omega_0 t \delta(\underline{r} - V_z t \hat{e}_z) - Q V_z \cos \omega_0 t \left[\delta \left(\underline{r} + \frac{1}{2} d_z \hat{e}_z - V_z t \hat{e}_z \right) - \delta \left(\underline{r} - \frac{1}{2} d_z \hat{e}_z - V_z t \hat{e}_z \right) \right]. \quad (5.39)$$

Applying the Fourier transform to the ν^{th} component (P-W space) of the current density and performing the space integrations with the aid of the delta functions, we obtain

$$J_1(\underline{k}, \omega) = J_{-1}(\underline{k}, \omega) = 0 \quad (5.40)$$

$$J_0(\underline{k}, \omega) = -\omega_0 p_z \int \sin \omega_0 t e^{-ik_z V_z t + i\omega t} dt - \\ V_z Q 2i \sin(k_z \frac{1}{2} d_z) \int \cos \omega_0 t e^{-ik_z V_z t + i\omega t} dt. \quad (5.41)$$

Since we are assuming our dipole is very small, we take $|\frac{1}{2} k_z d_z| \ll 1$. Therefore, $2Q \sin(\frac{1}{2} k_z d_z)$ can be replaced by $k_z p_z$. Thus we can then write

$$J_0(\underline{k}, \omega) = -\omega_0 p_z \int \sin \omega_0 t e^{i(\omega - k_z V_z) t} dt - \\ V_z i k_z p_z \int \cos \omega_0 t e^{i(\omega - k_z V_z) t} dt. \quad (5.42)$$

The first term represents a current density which will excite radiation due the oscillating dipole moment, while the current density represented by the second term will excite Cerenkov radiation. In most cases, the second term is negligible, however, at very low frequencies and small wavelengths ω_0 can become comparable to $V_z k_z$ and in that case the Cerenkov contribution to the radiation becomes important. Thus the Cerenkov term will manifest itself first in its effects on thermal mode excitation, since these modes have the shortest wavelengths.

The remaining integrals over time can be expressed in terms of delta functions, so that we finally obtain

$$J_0(\underline{k}, \omega) = i\pi \omega_0 p_z [\delta(\omega + \omega_0 - k_z V_z) - \delta(\omega - \omega_0 - k_z V_z)] - \\ i\pi k_z p_z V_z [\delta(\omega + \omega_0 - k_z V_z) + \delta(\omega - \omega_0 - k_z V_z)] \quad (5.43)$$

or, in terms of the refractive index and the normalized velocity $\underline{\beta} = \underline{V}/c$,

$$\begin{aligned}
g_0(\underline{n}, \omega) &= i\pi(\omega_0 p_z - n_z p_z \omega \beta_z) \delta(\omega + \omega_0 - n_z \beta_z \omega) \\
&\quad - i\pi(\omega_0 p_z + n_z p_z \omega \beta_z) \delta(\omega - \omega_0 - n_z \beta_z \omega). \quad (5.44)
\end{aligned}$$

Current Density for a Loop Antenna

The current density for a stationary filamentary loop antenna of radius r_0 , oriented with its symmetry axis parallel to the magnetic field \underline{B}_0 can be written in cylindrical (ρ, ϕ, z) coordinates as

$$\underline{J}(\underline{r}, t) = I_0 r_0 \frac{\delta(\rho - r_0)}{\rho} \delta(z) \cos \omega_0 t \hat{e}_\phi \quad (5.45)$$

where ω_0 is the radian operating frequency and I_0 is the maximum current in the loop. When the antenna has a translational velocity $\underline{V} = V_z \hat{e}_z$, the current density becomes

$$\underline{J}(\underline{r}, t) = I_0 r_0 \frac{\delta(\rho - r_0)}{\rho} \delta(z - V_z t) \cos \omega_0 t \hat{e}_\phi. \quad (5.46)$$

The unit vector \hat{e}_ϕ is related to the Cartesian unit vectors via

$$\hat{e}_\phi = -\sin \phi \hat{e}_x + \cos \phi \hat{e}_y. \quad (5.47)$$

Expressing \hat{e}_x and \hat{e}_y in terms of the basis vectors for P-W space, we get

$$\hat{e}_\phi = \frac{i}{\sqrt{2}} [e^{i\phi} \hat{e}_1 - e^{-i\phi} \hat{e}_{-1}]. \quad (5.48)$$

Therefore in P-W space we have for our loop

$$\underline{J}_\nu(\underline{r}, t) = \frac{\nu i}{\sqrt{2}} e^{i\nu\phi} I_0 r_0 \frac{\delta(\rho - r_0)}{\rho} \delta(z - V_z t) \cos \omega_0 t. \quad (5.49)$$

The Fourier transform is given by

$$g_{\nu}(\underline{k}, \omega) = \int \rho d\rho d\phi dz dt J_{\nu}(\underline{r}, t) e^{-i(k_x \rho \cos \phi + k_y \rho \sin \phi + k_z z - \omega t)}. \quad (5.50)$$

Inserting for J_{ν} and performing the ρ and z integrations leaves

$$g_{\nu}(\underline{k}, \omega) = I_0 r_0 \nu i 2^{-\frac{1}{2}} \int d\phi dt \cos \omega_0 t e^{-i(k_x r_0 \cos \phi + k_y r_0 \sin \phi - \nu \phi) - i(k_z V_z - \omega) t}. \quad (5.51)$$

Expressing \underline{k} in cylindrical (k_{\perp}, ϕ, k_z) coordinates, we can write

$$e^{-i(k_x r_0 \cos \phi + k_y r_0 \sin \phi)} = e^{-ik_{\perp} r_0 \cos(\phi - \phi)}. \quad (5.52)$$

Using the identity

$$e^{-ik_{\perp} r_0 \cos(\phi - \phi)} = \sum_{p=-\infty}^{\infty} J_p(k_{\perp} r_0) e^{-ip(\phi - \phi + \pi/2)} \quad (5.53)$$

the integration over ϕ is easily performed yielding,

$$g_{\nu}(\underline{k}, \omega) = I_0 r_0 \nu i 2^{\frac{1}{2}} \pi J_{-\nu}(k_{\perp} r_0) e^{i\nu(\phi + \pi/2)} \int dt \cos \omega_0 t e^{-i(k_z V_z - \omega) t}. \quad (5.54)$$

The remaining integral over time can be expressed in terms of delta functions

$$g_{\nu}(\underline{k}, \omega) = I_0 r_0 \nu i 2^{\frac{1}{2}} \pi^2 J_{-\nu}(k_{\perp} r_0) e^{i\nu(\phi + \pi/2)} [\delta(\omega + \omega_0 - k_z V_z) + \delta(\omega - \omega_0 - k_z V_z)]. \quad (5.55)$$

In terms of the refractive index, this is

$$f_{\nu}(\underline{n}, \omega) = I_0 r_0 \nu i 2^{\frac{1}{2}} \pi^2 J_{-\nu}(u) e^{i\nu(\omega + \pi/2)} [\delta(\omega + \omega_0 - n_z \omega \beta_z) + \delta(\omega - \omega_0 - n_z \omega \beta_z)], \quad (5.56)$$

where the argument of the Bessel function is

$$u = n_{\perp} \omega r_0 / c, \quad (5.57)$$

and $\beta_z = V_z / c$ is the normalized velocity.

Power Loss Formulas

This section contains the formulas for the power radiated by the various current sources treated in the previous section. The formulas are derived in such a manner as to be independent of the particular model (A or H) chosen for the plasma. For each source considered the power loss is written in terms of a single integral which can be readily evaluated numerically.

Power Radiated by Point Charge

The rate at which energy is radiated from a current source $\underline{J}^{(ex)}(\underline{r}, t)$ is expressible as

$$P = - \int \underline{J}^{(ex)}(\underline{r}, t) \cdot \underline{E}(\underline{r}, t) d^3r. \quad (5.58)$$

The superscript (ex) indicates that this current is external to the plasma in the sense that it is not used to compute the medium constitutive relations. In terms of polarized-wave space the radiative power loss becomes

$$P = - \int J_{-\nu}^{(ex)}(\underline{r}, t) E_{\nu}(\underline{r}, t) d^3r. \quad (5.59)$$

Representing $J_{-\nu}^{(ex)}$ and E_{ν} by their Fourier transforms, we obtain

$$P = - (2\pi)^{-8} \int d^3r d^3k d\omega d^3k' d\omega' \mathcal{J}_{-\nu}^{(ex)}(\underline{k}', \omega') \mathcal{E}_{\nu}(\underline{k}, \omega) e^{i(\underline{k}' + \underline{k}) \cdot \underline{r} - i(\omega' + \omega)t} \quad (5.60)$$

In terms of the refractive index, this is

$$P = - (2\pi)^{-8} c^{-6} \int d^3r d^3n d\omega d^3n' d\omega' |\omega^3| |\omega'^3| \mathcal{J}_{-\nu}^{(ex)}(\underline{n}', \omega') \mathcal{E}_{\nu}(\underline{n}, \omega) e^{i(\underline{n}' \omega'/c + \underline{n} \omega/c) \cdot \underline{r} - i(\omega' + \omega)t} \quad (5.61)$$

Changing orders of integration and integrating over \underline{r} , we get the factor

$$(2\pi)^3 \delta(\underline{n}' \omega'/c + \underline{n} \omega/c) = (2\pi c)^3 |\omega'|^{-3} \delta(\underline{n}' + \underline{n} \omega/\omega') \quad (5.62)$$

which enables us to integrate over \underline{n}' getting

$$P = - (2\pi)^{-5} c^{-3} \int d^3n d\omega d\omega' |\omega^3| \mathcal{J}_{-\nu}^{(ex)}(-\underline{n} \omega/\omega', \omega') \mathcal{E}_{\nu}(\underline{n}, \omega) e^{-i(\omega' + \omega)t} \quad (5.63)$$

Inserting for \mathcal{E}_{ν} using (C.5) and substituting for $\mathcal{J}_{-\nu}^{(ex)}$ our expression (5.14) derived for a spiraling point charge, the power loss becomes

$$P = -i Q^2 (16 \pi^3 \epsilon_0 c^3)^{-1} \int d^3n d\omega d\omega' \omega^2 \operatorname{sgn} \omega \sum_{p, p' = -\infty}^{\infty} \mathcal{J}_{-\nu}^p \mathcal{J}_{-\nu}^{p'} e^{i(\nu - \sigma + p - p')\pi/2} e^{-i(\omega' + \omega)t} e^{-i(p' + p - \nu + \sigma)\varphi} \lambda_{\nu - \sigma} J_p J_{p'} \Lambda^{-1} \delta(\omega' + n_z \omega \beta_z - (p - \nu)\Omega/\gamma) \delta(\omega - n_z \omega \beta_z - (p' + \sigma)\Omega/\gamma) \quad (5.64)$$

The argument of the Bessel functions is $u = n_{\perp} a \gamma \omega/c$. Expressing d^3n as $n_{\perp} dn_{\perp} d\varphi dn_z$, the integration over φ gives a factor (2π) when $p' = -(p - \nu + \sigma)$ and zero otherwise. Hence,

$$\begin{aligned}
P = & -i Q^2 (8\pi^2 \epsilon_0 c^3)^{-1} \int n_{\perp} dn_{\perp} dn_z d\omega d\omega' \omega^2 \operatorname{sgn} \omega \sum_{p=-\infty}^{\infty} e^{i(\nu-\sigma)\pi} \\
& \int_{-\nu}^{\nu} \int_{\sigma}^{\sigma} e^{-i(\omega'+\omega)t} \lambda_{\nu-\sigma} \Lambda^{-1} J_p J_{p-\nu+\sigma} \delta(\omega'+n_z \omega \beta_z - (p-\nu)\Omega/\gamma) \\
& \delta(\omega - n_z \omega \beta_z + (p-\nu)\Omega/\gamma). \quad (5.65)
\end{aligned}$$

Integrating over ω' reduces our expression for the power loss to

$$\begin{aligned}
P = & -i Q^2 (8\pi^2 \epsilon_0 c^3)^{-1} \int n_{\perp} dn_{\perp} dn_z d\omega \omega^2 \operatorname{sgn} \omega \sum_{p=-\infty}^{\infty} \int_{-\nu}^{\nu} \int_{\sigma}^{\sigma} e^{i(\nu-\sigma)\pi} \\
& \Lambda^{-1} \lambda_{\nu-\sigma} J_p J_{p-\nu+\sigma} \delta(\omega - n_z \omega \beta_z + (p-\nu)\Omega/\gamma) \\
& e^{-i[\omega - n_z \omega \beta_z + (p-\nu)\Omega/\gamma]t}. \quad (5.66)
\end{aligned}$$

Writing

$$P = \int_{-\infty}^0 \mathcal{J} d\omega + \int_0^{\infty} \mathcal{J} d\omega, \quad (5.67)$$

assuming that $\lambda_{\nu-\sigma}(\underline{n}, \omega) = \lambda_{-\nu\sigma}^*(\underline{n}, -\omega)$, and making the following changes of variables $\omega \rightarrow -\omega$, $\nu \rightarrow -\nu$, $\sigma \rightarrow -\sigma$, $p \rightarrow -p$ in the integration over negative frequencies, we find that

$$P = \int_0^{\infty} \mathcal{J}^* d\omega + \int_0^{\infty} \mathcal{J} d\omega = 2 \operatorname{Re} \int_0^{\infty} \mathcal{J} d\omega. \quad (5.68)$$

Thus

$$\begin{aligned}
P = & -\operatorname{Re} i Q^2 (4\pi^2 \epsilon_0 c^3)^{-1} \int_0^{\infty} d\omega \int n_{\perp} dn_{\perp} dn_z \omega^2 \\
& \sum_{p=-\infty}^{\infty} \int_{-\nu}^{\nu} \int_{\sigma}^{\sigma} \Lambda^{-1} \lambda_{\nu-\sigma} J_p J_{p-\nu+\sigma} e^{i(\nu-\sigma)\pi} \\
& \delta(\omega - n_z \omega \beta_z + (p-\nu)\Omega/\gamma) e^{-i[\omega - n_z \omega \beta_z + (p-\nu)\Omega/\gamma]t}. \quad (5.69)
\end{aligned}$$

Replacing p by $p + \nu$, we get

$$P = -\operatorname{Re} i Q^2 (4\pi^2 \epsilon_0 c^3)^{-1} \int_0^\infty d\omega \int n_\perp dn_\perp dn_z \omega^2 \sum_{p=-\infty}^\infty \omega_{-\nu} \omega_\sigma \lambda_{\nu-\sigma} \Lambda^{-1} J_{p+\nu} J_{p+\sigma} e^{i(\nu-\sigma)\pi} \delta(\omega - n_z \omega \beta_z + p\Omega/\gamma) e^{-i(\omega - n_z \omega \beta_z + p\Omega/\gamma)t}. \quad (5.70)$$

If $\beta_z \neq 0$,

$$\delta(\omega - n_z \omega \beta_z + p\Omega/\gamma) = |\omega|^{-1} |\beta_z|^{-1} \delta(n_z - \beta_z^{-1}(1+pY/\gamma)) \quad (5.71)$$

which allows us to integrate over n_z . Thus for $\beta_z \neq 0$,

$$P = -\operatorname{Re} i Q^2 (4\pi^2 \epsilon_0 |V_z| c^2)^{-1} \int_0^\infty d\omega \int_0^\infty n_\perp dn_\perp \omega \sum_{p=-\infty}^\infty \omega_{-\nu} \omega_\sigma \lambda_{\nu-\sigma} \Lambda^{-1} J_{p+\nu} J_{p+\sigma} e^{i(\nu-\sigma)\pi} \Big|_{n_z = \beta_z^{-1}(1+pY/\gamma)} \quad (5.72)$$

where

$$n_z = \beta_z^{-1} (1 + p Y/\gamma) \quad (5.73)$$

is the so-called emission equation for a spiraling charge. Here

$$Y \equiv \Omega / \omega. \quad (5.74)$$

The only plane waves which can exist in the plasma are those whose refractive indexes satisfy the dispersion equation $\Lambda = 0$. Knowing the roots of the dispersion equation, which we assume can be written as a polynomial in the variable n_\perp^2 , the fundamental theorem of algebra allows us to write

$$\Lambda = C(\omega) \prod_m (n_\perp^2 - n_{\perp m}^2) \quad (5.75)$$

where n_{1m}^2 represents the m^{th} root of the dispersion equation. Hence we write the power loss as:

$$P = -\text{Re} i Q^2 (4\pi^2 \epsilon_0 |V_z|^2 c^2)^{-1} \int_0^\infty d\omega \int_0^\infty dn_\perp n_\perp \omega \sum_{p=-\infty}^\infty e^{i(\nu-\sigma)\pi} \lambda_{\nu-\sigma} \left[C(\omega) \prod_m (n_{1m}^2 - n_\perp^2) \right]^{-1} J_{p+\nu} J_{p+\sigma} \Big|_{n_z = \beta_z^{-1}(1+pY/\gamma)} \quad (5.76)$$

Write the power loss as

$$P = -\text{Re} i Q^2 (4\pi^2 \epsilon_0 |V_z|^2 c^2)^{-1} \int_0^\infty d\omega \frac{\omega}{C(\omega)} \sum_{p=-\infty}^\infty \lambda_{\nu-\sigma} e^{i(\nu-\sigma)\pi} \int_0^\infty \frac{\lambda_{\nu-\sigma} J_{p+\nu} J_{p+\sigma}}{\prod_m (n_{1m}^2 - n_\perp^2)} n_\perp dn_\perp \Big|_{n_z = \beta_z^{-1}(1+pY/\gamma)} \quad (5.77)$$

From Appendix C we note that the terms of the adjoint matrix have the form $n_\perp^{\nu-\sigma+2k}$ where $k = 0, 1, 2, \dots$. Referring to Appendix D where we have evaluated the integral

$$\int_0^\infty \frac{x^{\rho+1} J_{p+\nu}(ax) J_{p+\sigma}(ax)}{\prod_m (x^2 - z_m^2)} dx \quad (5.78)$$

and setting $\rho = \nu - \sigma + 2k$, $x = n_\perp$, etc. we find that the power loss can be expressed as

$$P = \text{Re} Q^2 (8\pi \epsilon_0 |V_z|^2 c^2)^{-1} \int_0^\infty d\omega \sum_j \frac{\omega}{C(\omega)} \sum_{p=-\infty}^\infty \lambda_{\nu-\sigma} e^{i(\nu-\sigma)\pi} \lambda_{\nu-\sigma} J_{p+\nu} \prod_{m \neq j} (n_{1j}^2 - n_{1m}^2)^{-1} \begin{cases} H_{p+\sigma}^{(1)} & , \text{Im } n_{1j} > 0 \\ (-1) H_{p+\sigma}^{(2)} & , \text{Im } n_{1j} < 0 \end{cases} \Big|_{n_z = \beta_z^{-1}(1+pY/\gamma)} \quad (5.79)$$

See the paragraph following eqn. (5.81) for a discussion of the expression for P corresponding to (5.79) when $\text{Im } n_{1j} = 0$.

The Hankel functions have the same argument as the ordinary Bessel function, namely $u = n_{\perp} a \gamma \omega / c$.

The subscripts j and m range from 1 up to the number of wave modes which can exist in the plasma at any given frequency. For a cold plasma there exists two modes, for a plasma with only warm electrons there exists three modes, and for a two component plasma with both ions and electrons warm there may exist up to four wave modes. When we do not allow for losses in the plasma, the imaginary part of $n_{\perp j}$ is either zero or else the roots occur in conjugate pairs. Suppose the roots $n_{\perp 1}$ and $n_{\perp 2}$ are conjugates and let \mathcal{J} be defined by

$$P = \text{Re} \int_0^{\infty} \sum_{j=1}^n \mathcal{J}_j d\omega. \quad (5.80)$$

Comparing (5.79) and (5.80) and assuming $n_{\perp 1} = n_{\perp 2}^*$ we can write

$$P = \text{Re} \int_0^{\infty} \left[\mathcal{J}_1 - \mathcal{J}_1^* + \sum_{j=3}^n \mathcal{J}_j \right] d\omega = \text{Re} \int_0^{\infty} \sum_{j=3}^n \mathcal{J}_j d\omega. \quad (5.81)$$

Hence, complex conjugate roots contribute no net radiation losses.

The case when $\text{Im} n_{\perp j} = 0$ is more difficult because the integrand of (5.77) has a singular point on the axis of integration. Several methods are available for determining how to deform the contour of integration so as to avoid this singularity. Perhaps the most direct method is to allow for small collision losses in the plasma in order to determine how the poles $n_{\perp j}$ move off the real axis. This then indicates how the contour of integration should be deformed. Once the proper integration path is determined, we can return to the limit of a lossless plasma [24]. Another method is to represent the electric field excited by the source as a superposition of plane waves and require that each constituent plane wave carry energy away from the source [20]. Still another method is to invoke causality which requires that the source current must precede the excited field [79]. These are all examples

of what is usually called the "radiation condition" and they all give equivalent results. The "radiation condition" must be invoked in order to determine which solution (equations (5.79)) is physically correct.

Electric fields which obey the "radiation condition" are often referred to as "retarded" or "outgoing" fields and denoted by $\underline{E}_{\text{ret}}$ or $\underline{E}_{\text{out}}$. Fields which do not obey the "radiation condition" are referred to as "advanced" or "incoming" fields and are denoted by $\underline{E}_{\text{adv}}$ or $\underline{E}_{\text{in}}$. Note that in (5.79) one equation represents a power loss due to the work done by "retarded" or "outgoing" electric fields while the other equation refers to the work done by the "advanced" or "incoming" electric fields. In the section on reversible and irreversible power which appears in this chapter, we discuss the computation of power loss using "incoming" and "outgoing" electric fields.

Power Radiated by Extended Charge Source

For the extended charge source discussed in the first part of this chapter and for a collisionless plasma, the power loss formula is given by the $p = 0$ term of equation (5.79) with the quantity $D^2(g, h)$ (see equation 5.29) multiplying the integrand.

Power Radiated by Electric Dipole Antenna

The physical quantity we wish to compute is the time average (over a period $2\pi/\omega_0$) of the power lost through radiation, \bar{P} . This is given by

$$\bar{P} = - (\omega_0/2\pi) \int_0^{2\pi/\omega_0} \int \underline{J}(\underline{r}, t) \cdot \underline{E}(\underline{r}, t) d^3r dt. \quad (5.82)$$

Expressing the dot product in terms of P-W space, applying the Fourier transform to \underline{J} and \underline{E} , writing the result in terms of the refractive index, and integrating over \underline{r} and \underline{n}' as done for the case of a spiraling charge, we obtain

$$\bar{P} = - (2\pi)^{-6} c^{-3} \omega_0 \int_0^{2\pi/\omega_0} dt \int n_{\perp} dn_{\perp} dn_z d\varphi d\omega d\omega' |\omega^3| \mathcal{E}_{-\nu}(-\underline{n} \omega/\omega', \omega') \mathcal{E}_{\nu}(\underline{n}, \omega) e^{-i(\omega' + \omega)t}. \quad (5.83)$$

Considering the case of an elementary electric dipole antenna oriented parallel with \underline{B}_0 and moving along the direction of the magnetic field of an anisotropic plasma, we substitute expression (5.44) for the current density into (5.83) and replace \mathcal{E}_{ν} in (5.83) by (C.5) to obtain

$$\begin{aligned} \bar{P} = & i(64 \pi^4 c^3 \epsilon_0)^{-1} \omega_0 \int_0^{2\pi/\omega_0} dt \int d^3n d\omega d\omega' |\omega^3| \\ & [(\omega_0 p_z + n_z p_z \omega \beta_z) \delta(\omega' + \omega_0 + n_z \beta_z \omega) \\ & - (\omega_0 p_z - n_z p_z \omega \beta_z) \delta(\omega' - \omega_0 + n_z \beta_z \omega)] \\ & e^{-i(\omega' + \omega)t} \omega^{-1} \Lambda^{-1} \lambda_{\infty} [(\omega_0 p_z - n_z p_z \omega \beta_z) \delta(\omega + \omega_0 - n_z \beta_z \omega) \\ & - (\omega_0 p_z + n_z p_z \omega \beta_z) \delta(\omega - \omega_0 - n_z \beta_z \omega)] . \end{aligned} \quad (5.84)$$

Integrating with respect to ω and ω' using the delta functions and performing the time averaging results in the expression

$$\bar{P} = - \{ i (32 \pi^3 c^3 \epsilon_0)^{-1} \int d^3n \omega^2 \operatorname{sgn} \omega \omega_0^2 p_z^2 |1 - n_z \beta_z|^{-3}$$

$$\Lambda^{-1} \lambda_{00} \} \Big|_{\omega = \omega_0 / (1 - n_z \beta_z)} - \{ " \} \Big|_{\omega = -\omega_0 / (1 - n_z \beta_z)}. \quad (5.85)$$

Expressing the index of refraction in terms of cylindrical (n_\perp, φ, n_z) coordinates, the integration over φ yields an additional factor 2π . The symmetry properties of the integrand allow us to write the result as

$$\bar{P} = - \operatorname{Re} i (8 \pi^2 c^3 \epsilon_0)^{-1} \int n_\perp dn_\perp dn_z \omega^2 \omega_0^2 p_z^2 \lambda_{00}$$

$$(1 - n_z \beta_z)^{-3} \Lambda^{-1} \Big|_{\omega = \omega_0 / (1 - n_z \beta_z)}. \quad (5.86)$$

Writing the determinant Λ as

$$\Lambda = C(\omega) \prod_m^n (n_\perp^2 - n_{\perp m}^2), \quad (5.87)$$

we see that the integral is closely related to (D.1) when the plasma is collisionless. To see this set $s = t = 0$ in (D.1) and then take $\lim_{a \rightarrow 0} \operatorname{Re} i \times$ (D.1). Evaluating the integral over n_\perp in this manner we obtain the following result for a collisionless plasma

$$\bar{P} = \pm \sum_j (16 \pi c^3 \epsilon_0)^{-1} \int dn_z \omega^2 p_z^2 \omega_0^2 \lambda_{00} (1 - n_z \beta_z)^{-3}$$

$$\left[C(\omega) \prod_{m \neq j}^n (n_{\perp j}^2 - n_{\perp m}^2) \right]^{-1} \Big|_{\omega = \omega_0 / (1 - n_z \beta_z)} \quad (5.88)$$

The sums and products range over the various propagating modes which can exist in the plasma. The sign of (5.88) is chosen so as to satisfy the radiation condition. The remaining integration can easily be performed numerically to yield the total radiated power from this antenna.

Note that when $n_z = 1/\beta_z$, the integrand has a singularity. This singularity can be removed by allowing for a dipole of finite size. These findings are in agreement with those given by McKenzie [53] for the case of a cold uniaxial plasma.

Power Radiated by Loop Antenna

The time averaged power loss \bar{P} can be expressed as

$$\bar{P} = - \lim_{T \rightarrow \infty} \frac{1}{T} \int_{-\frac{1}{2}T}^{\frac{1}{2}T} dt \int d^3r \underline{J}(\underline{r}, t) \cdot \underline{E}(\underline{r}, t) . \quad (5.89)$$

Following our usual procedures, we write this as

$$\bar{P} = - \lim_{T \rightarrow \infty} \frac{1}{T} \int_{-\frac{1}{2}T}^{\frac{1}{2}T} dt \int (2\pi)^{-5} c^{-3} d^3n d\omega d\omega' |\omega|^3 \mathcal{J}_{-\nu}(-\underline{n} \omega/\omega', \omega') \mathcal{E}_{\nu}(\underline{n}, \omega) e^{-i(\omega' + \omega)t} . \quad (5.90)$$

Treating the case of a filamentary loop antenna oriented with its symmetry axis parallel to the magnetic field \underline{B}_0 and moving with a velocity $\underline{V} = V_z \hat{e}_z$, we substitute for $\mathcal{J}_{-\nu}$ from (5.56) and insert for \mathcal{E}_{ν} from (C.5). The result is

$$\begin{aligned} \bar{P} = & - \lim_{T \rightarrow \infty} \frac{I_0^2 r_0^2 i}{16 \pi c^3 \epsilon_0} \frac{1}{T} \int_{-\frac{1}{2}T}^{\frac{1}{2}T} dt \int d^3n d\omega d\omega' \\ & \omega^2 \operatorname{sgn} \omega \nu J_{\nu} \lambda_{\nu-\sigma} \sigma J_{-\sigma} \Lambda^{-1} e^{i(\nu+\sigma)\pi/2} e^{-i(\omega' + \omega)t} \\ & \left\{ \delta(\omega' + \omega_0 + n_z \omega \beta_z) \delta(\omega + \omega_0 - n_z \omega \beta_z) + \right. \\ & \delta(\omega' + \omega_0 + n_z \omega \beta_z) \delta(\omega - \omega_0 - n_z \omega \beta_z) + \\ & \delta(\omega' - \omega_0 + n_z \omega \beta_z) \delta(\omega + \omega_0 - n_z \omega \beta_z) + \\ & \left. \delta(\omega' - \omega_0 + n_z \omega \beta_z) \delta(\omega - \omega_0 - n_z \omega \beta_z) \right\} . \quad (5.91) \end{aligned}$$

Performing the time and radian frequency integrations and taking the limit, we obtain

$$\begin{aligned} \bar{P} = - \left\{ \frac{I_0^2 r_0^2 i}{16 \pi c^3 \epsilon_0} \int d^3 n \left| 1 - n_z \beta_z \right|^{-1} \omega^2 \operatorname{sgn} \omega \nu J_\nu \lambda_{\nu-\sigma} \sigma J_{-\sigma} \Lambda^{-1} \right. \\ \left. e^{i(\nu+\sigma)\pi/2} \right\}_{\omega = \omega_0 (1 - n_z \beta_z)^{-1}} \\ \left\{ \text{"} \right\}_{\omega = -\omega_0 (1 - n_z \beta_z)^{-1}} \quad (5.92) \end{aligned}$$

Assuming the usual symmetry property, $K_{\nu-\sigma}(\underline{n}, \omega) = K_{-\nu\sigma}^*(\underline{n}, -\omega)$ for the components of the dielectric tensor, the power loss can be written

$$\begin{aligned} \bar{P} = - \operatorname{Re} \frac{I_0^2 r_0^2 i}{8 \pi c^3 \epsilon_0} \int n_\perp dn_\perp dn_z d\varphi (1 - n_z \beta_z)^{-1} \\ \omega^2 \nu J_\nu \lambda_{\nu-\sigma} \sigma J_{-\sigma} \Lambda^{-1} e^{i(\nu+\sigma)\pi/2} \Big|_{\omega = \omega_0 / (1 - n_z \beta_z)} \quad (5.93) \end{aligned}$$

Writing out the summations and performing the trivial integration over φ , it is easily verified that

$$\begin{aligned} \bar{P} = - \operatorname{Re} \frac{I_0^2 r_0^2 i}{2 c^3 \epsilon_0} \int n_\perp dn_\perp dn_z \omega^2 \Lambda^{-1} \\ I_1^2 \lambda_{YY} (1 - n_z \beta_z)^{-1} \Big|_{\omega = \omega_0 / (1 - n_z \beta_z)} \quad (5.94) \end{aligned}$$

Since the integral over n_\perp is of the form assumed in (D.1), this integral can be evaluated. The expression for the time averaged power loss then becomes

$$\bar{P} = \sum_{j=1}^n \frac{r_0^2 r_0^2 \pi}{4 c^3 \epsilon_0} R_e \int dn_z \omega^2 J_1(u_j) \lambda_{YY} [C(\omega) \prod_{m \neq j}^n (n_{\perp j}^2 - n_{\perp m}^2)]^{-1}$$

$$(1 - n_z \beta_z)^{-1} \begin{cases} H_1^{(1)}(u_j) & , \text{Im } n_{\perp j} > 0 \\ -H_1^{(2)}(u_j) & , \text{Im } n_{\perp j} < 0 \end{cases} \Bigg|_{\omega = \omega_0 / (1 - n_z \beta_z)} \quad (5.95)$$

The argument of the Bessel functions is

$$u_j = n_{\perp j} \omega r_0 / c. \quad (5.96)$$

The sum over j is a sum over the various propagating modes which can exist in the plasma.

When $\text{Im } n_{\perp j} = 0$, the appropriate expression for \bar{P} is the solution given in (5.95) which satisfies the radiation condition.

Reversible and Irreversible Power

Previously, we wrote the expression for the power radiated from a point charge source $\underline{J}^{(ex)}$ as

$$P = - \int \underline{J}^{(ex)} \cdot \underline{E} \, d^3r \quad (5.97)$$

and we required that \underline{E} obey the "radiation condition". Thus, we actually use

$$P = - \int \underline{J}^{(ex)} \cdot \underline{E}_{out} \, d^3r. \quad (5.98)$$

For a point charge spiraling in a vacuum, a different formula is customarily used, namely [64],

$$P = -\frac{1}{2} \int \underline{J}^{(ex)} \cdot (\underline{E}_{out} - \underline{E}_{in}) \, d^3r. \quad (5.99)$$

In this section we intend to show that both formulas (5.98) and (5.99) yield identical results for a lossless plasma.

Having already evaluated (5.97), the proof that (5.98) and (5.99) are equivalent for a charge spiraling in a lossless plasma is rather simple. From (5.79) we find that the two expressions $\int \underline{J}^{(ex)} \cdot \underline{E}_{out} \, d^3r$ and $\int \underline{J}^{(ex)} \cdot \underline{E}_{in} \, d^3r$ are given by

$$\pm Q^2 (8 \pi \epsilon_0 |V_z| c^2)^{-1} \int_0^\infty d\omega \frac{\omega}{C(\omega)} \sum_j \sum_{p=-\infty}^\infty \rho_{-p}^j \rho_p^j \sigma e^{i(\nu-\sigma)\pi} \lambda_{\nu-\sigma} J_{P+\nu} J_{P+\sigma} \prod_{m \neq j} (n_{\perp j}^2 - n_{\perp m}^2)^{-1} \quad (5.100)$$

where one solution corresponds to using \underline{E}_{out} and the other corresponds to using \underline{E}_{in} . Since the two solutions are negatives of each other it follows that (5.99) is equivalent to (5.98).

We should note that this question of what is the proper expression to use for calculating radiation losses in a magnetoplasma is not new. Several years ago Lee and Papas [46] suggested that the so-called "infinity catastrophe" which predicted infinite power radiating from a point dipole located in a cold magnetoplasma [15,73,87] was due to using only outgoing waves as in (5.98) instead of using the "correct" combination of waves as in (5.99) when computing radiation losses. The question was vigorously argued in a series of articles which appeared shortly thereafter [44,45,72,83]. More recently, the issue was re-settled by Snyder and Weitzner [71] who showed that the assertion made by Lee and Papas was false, and that as far as real radiated power from a Hertz dipole is concerned, both formulations give the same results. Hence, our similar findings for a spiraling charge source are not completely unexpected. Thus it follows that for both antennas and free charge sources, either formula (5.98) or (5.99) may be used for computing the radiation loss.

CHAPTER VI

NUMERICAL RESULTS

In this chapter we present some numerical results for free charge sources obtained by using the plasma Models H and A described in this thesis.

Results Using Model H

The background plasma chosen for this model is composed of thermal electrons and protons with an isotropic temperature of 2000°K . As pointed out in the discussion following equation (4.6), the value of the specific heat γ'_s is somewhat arbitrary. Our results might also be thought of as representing a 6000° plasma with $\gamma'_s = 1$. All our calculations are for the "operating line" $R^2 \equiv (f_{be}^2/f_{pe}^2) = 0.4$ as shown in Fig. 2.

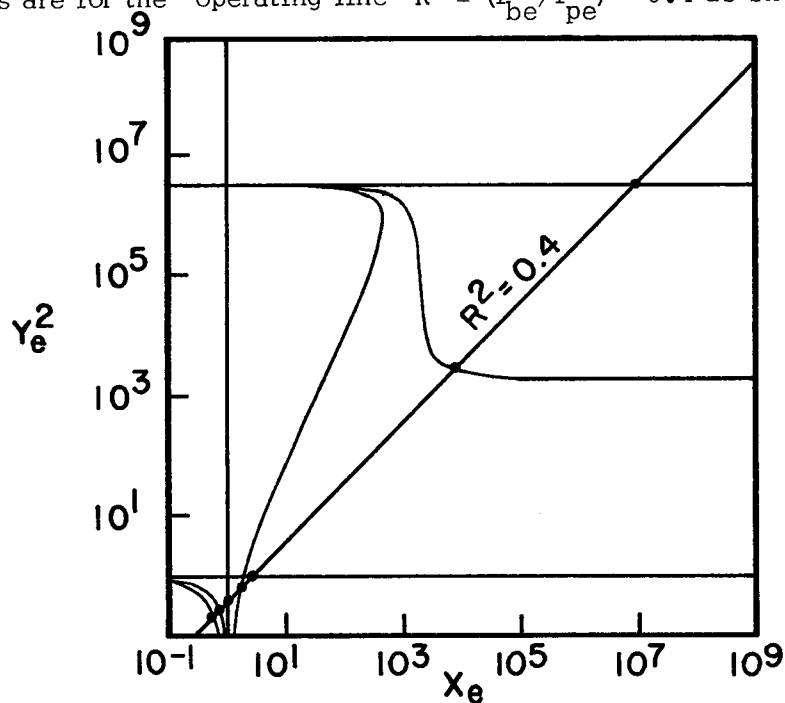


Fig. 2. Sketch of the "operating line" $R^2 = 0.4$ superimposed on the CMA diagram

The "operating line" intersects the principal cutoff and resonance lines at the points shown on the CMA diagram of Figure 2. The corresponding values of X_e at these intersection points are given in Table 1.

TABLE 1
VALUES OF X_e CORRESPONDING TO PRINCIPAL RESONANCES
AND CUTOFFS FOR THE OPERATING LINE $R^2 = 0.4$

X_e	Name of Cutoff or Resonance	Log X_e
.537	Electron cyclotron cutoff	-0.27
.714	Upper hybrid resonance	-0.15
1.00	Plasma cutoff	0.00
1.86	Ion cyclotron cutoff	0.27
2.50	Electron gyro-resonance	0.40
6.43×10^3	Lower hybrid resonance	3.81
8.43×10^6	Ion-gyro resonance	6.93

Figure 3 gives the power spectral density for a non-spiraling electron. For the non-spiraling electron, the total power spectral density consists only of the Cerenkov term $p = 0$. As expected from cold plasma results [52], [80], there are peaks in the power spectrum at the upper and lower hybrid resonances. The cold plasma results yield infinities in the calculated power spectrum at these resonances. Most noticeable when thermal effects are included are the additional modes which appear. These are mode 4, and an extension of mode 3 to frequencies above the UHR. The numbering scheme used here is of no particular physical significance, but rather for convenience in discussing the results. Note that a considerable proportion of the total power is in the form of radiation in the thermal mode at frequencies just above the UHR. This thermal mode has its origin in electron temperature effects whereas mode 4 here has its origin in the ion temperature.

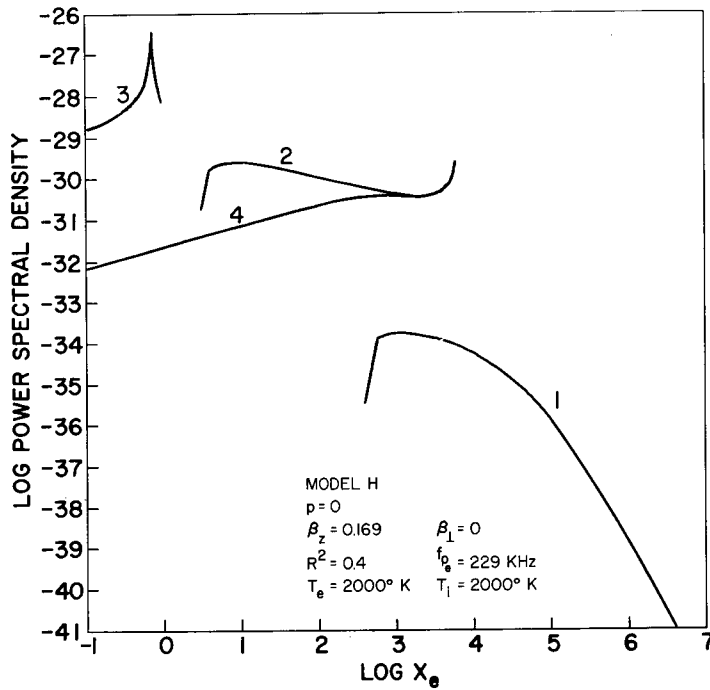


Fig. 3 . Power spectral density for a non-spiraling electron

Figure 4 shows the effects caused by the spiraling motion of the source charge. Two very pronounced effects are immediately noticed: first, the power spectrum exhibits an oscillatory pattern and secondly, the spectral power density in the thermal modes is greatly reduced from the non-spiraling case shown in the previous figure. The oscillatory pattern is due to interference between waves excited at different points on the orbit of the spiraling charge, and the overall decrease in the spectral power density amplitude for modes 3 and 4 is due to the apparent charge smearing effect the rotational motion gives. This apparent smearing effect is very similar to that obtained by considering finite vs. infinitesimal electric dipole antennas [73], and most affects those waves which have small wavelengths in the radial direction. Note that the upper envelopes on the oscillatory patterns somewhat resemble the shapes of the corresponding curves for the non-spiraling charge. We should point out that in certain frequency regimes relatively few points

have been plotted which accounts for the rather jagged envelopes in the oscillatory patterns for X_e less than 0.5 or greater than 2.5. In particular, the behavior of mode 2 near the LHR ($X_e \approx 6 \times 10^3$) is not adequately shown in these figures due to the fact that the plasma index of refraction is rapidly changing with frequency near the LHR.

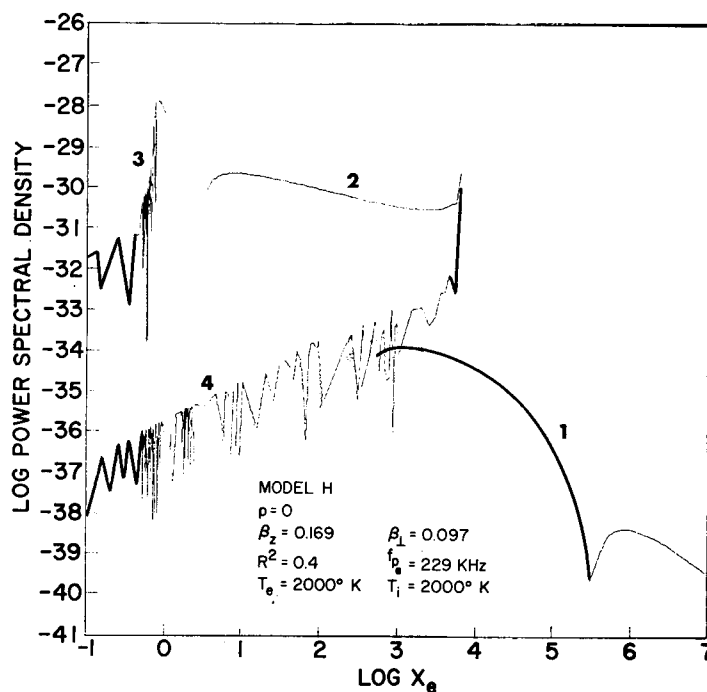


Fig. 4 . The contribution to the total power spectral density due to Cerenkov radiation from a spiraling charge

Figure 5 shows the contribution to the spectral power density due to normal Doppler emission at the harmonic $p = -1$. Note that in the regime between the electron gyro-frequency and the LHR mode 2 shows a lower radiation loss as compared with the Cerenkov contribution $p = 0$. This is consistent with cold plasma calculations at these frequencies which show that the Cerenkov term is the dominant one [48]. Also note that for frequencies below the LHR two new modes appear. These modes, which are due to thermal effects, show a relatively low power density. Figure 6 shows very similar results for anomalous Doppler emission at $p = 1$.

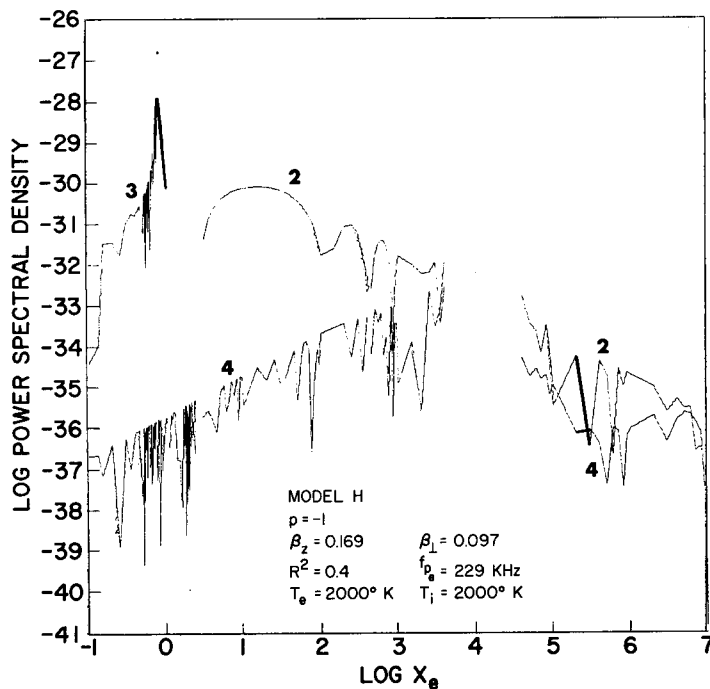


Fig. 5 . Contribution to the total power spectral density for a spiraling electron due to normal Doppler emission at the harmonic $p = -1$

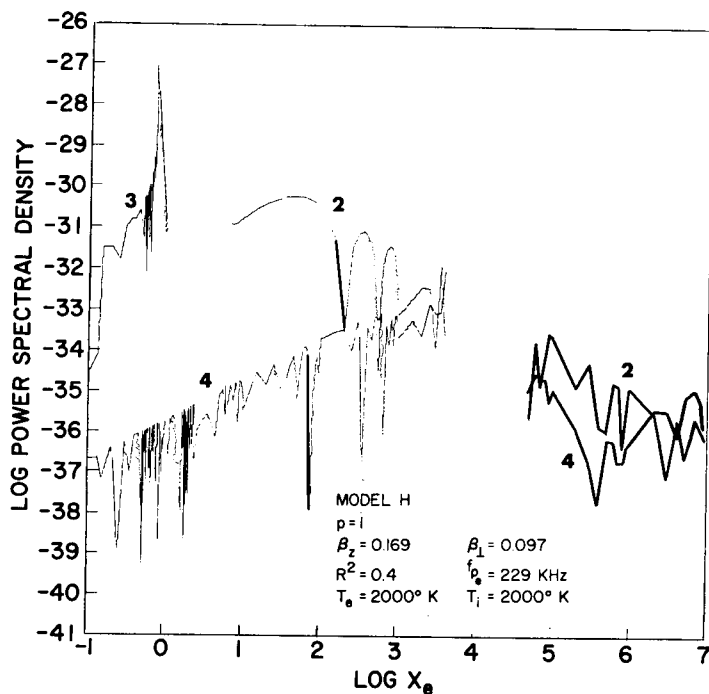


Fig. 6 . Contribution to the total power spectral density for a spiraling electron due to anomalous Doppler emission at the harmonic $p = 1$

The directions of the phase velocities for the excited waves corresponding to the power spectra shown in the previous figures are shown in the next figures. The curves are obtained by first solving the emission equation for n_z and then using this value for n_z in the dispersion equation to find n_{\perp} . The phase velocity direction is then given by $\vartheta = \tan^{-1}(n_{\perp}/n_z)$. The phase velocity direction, ϑ , is independent of the radial velocity V_{\perp} of the spiraling charge, since the emission equation does not depend on V_{\perp} . For Cerenkov radiation, Figure 7, the wave phase velocity component along the magnetic field is in the same direction as the particle velocity V_z . Such is not always the case for magneto-bremmstrahlung, as noted, for example, by comparing Figures 8 and 9.

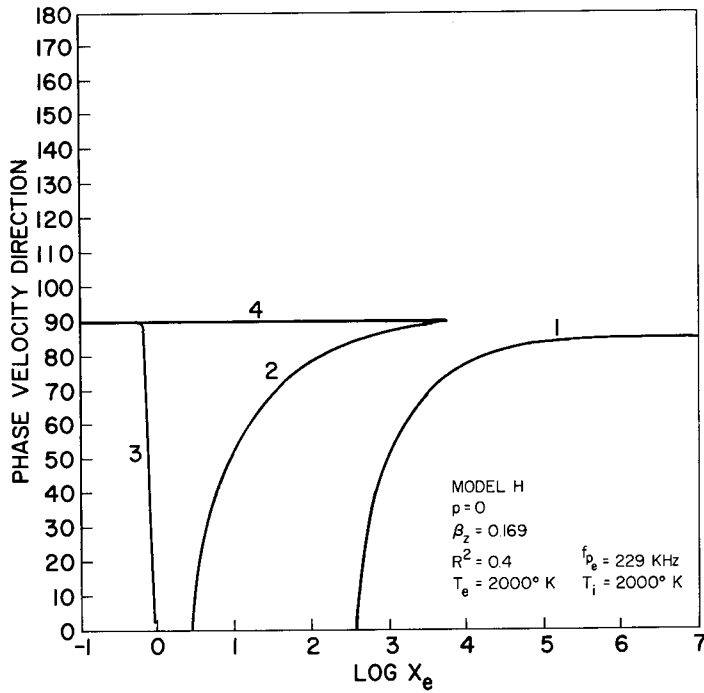


Fig. 7 . Phase velocity directions of the various waves excited by Cerenkov radiation

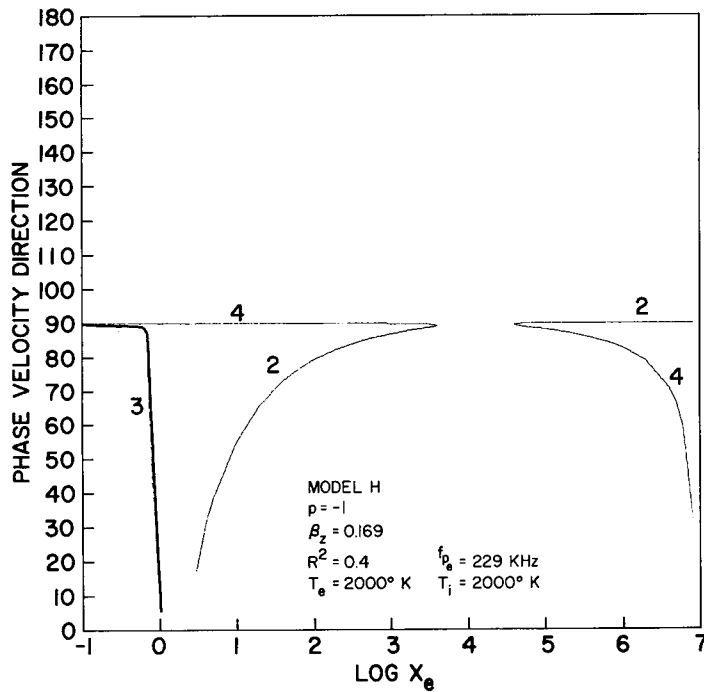


Fig. 8 . Phase velocity directions of the various waves excited by normal Doppler emission at the harmonic $p = -1$

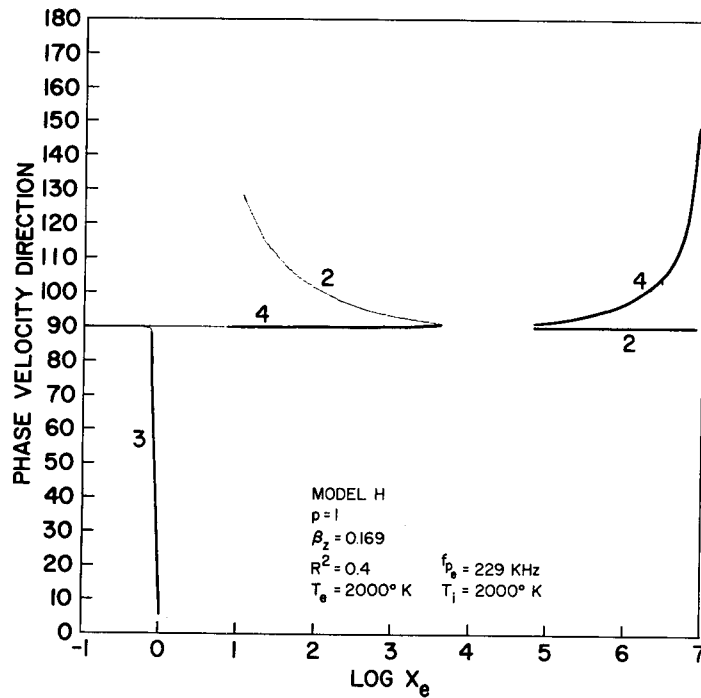


Fig. 9 . Phase velocity directions of the various waves excited by anomalous Doppler emission at the harmonic $p = 1$

When discussing the propagation of radiation in an slowly varying inhomogeneous magnetoplasma it is important to know in what direction the waves which are excited propagate. Herein lies the usefulness of these plots. However, in addition to specifying the directions in which the excited waves propagate, we must also determine the direction of energy propagation in order to trace the path of the radiation. Generally the wave phase velocity direction and the group velocity or Poynting vector are not colinear in a magnetoplasma. In Appendix B we gave the method for finding the direction of energy flow. Applying this method we obtain Figures 10 through 12 which show the direction of energy flow for the various modes at the various frequencies corresponding to the parameters used previously. The angle θ^0 represents energy propagation parallel to the magnetic field. The negative sign before an angle indicates that the radial component of the group velocity ($V_{g,r}$) is antiparallel to the radial component of the associated phase velocity. Note that the

direction of energy flow is strongly affected by the frequency of the emitted radiation. Note also that for the low frequencies mode 2 exhibits a strong guiding effect which tends to keep the energy propagating along the magnetic field. This is the familiar Whistler mode of propagation [30].

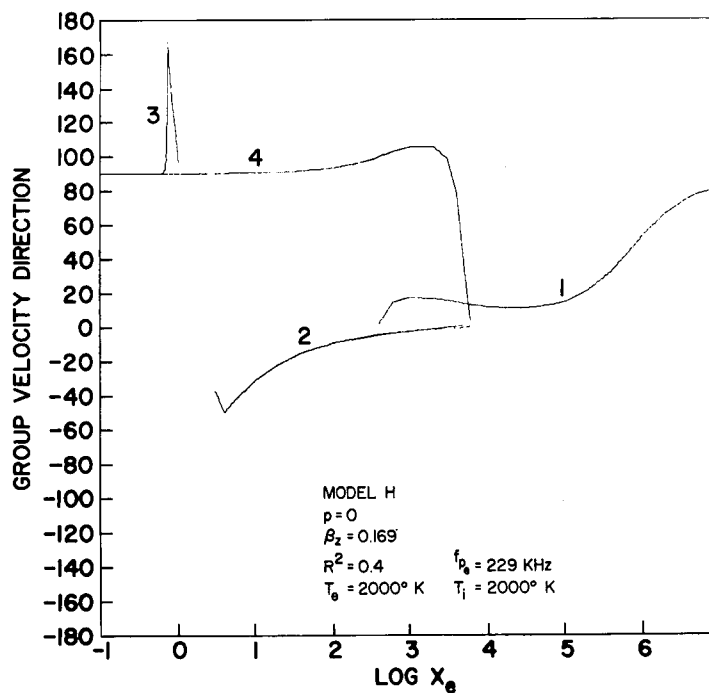


Fig. 10 . The direction of energy propagation associated with the various waves excited by Cerenkov radiation. Negative angles indicate oppositely directed radial components of the phase and group velocity vectors

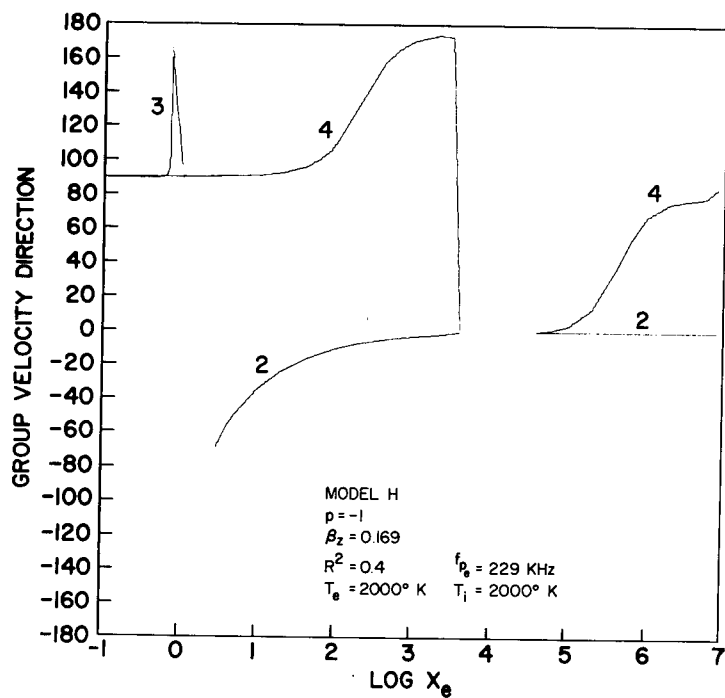


Fig. 11 . The direction of energy propagation associated with the various waves excited by normal Doppler emission at the harmonic $p = -1$. Negative angles indicate oppositely directed radial components of the phase and group velocity vectors

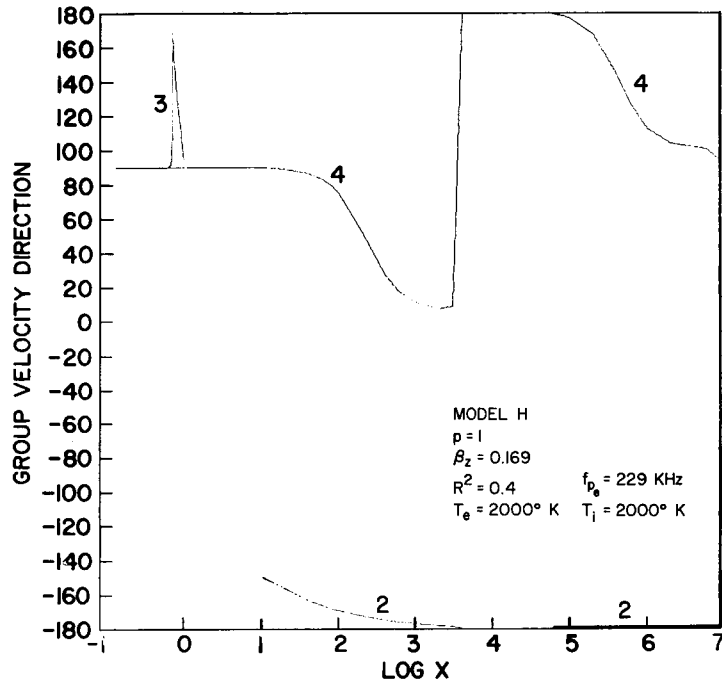


Fig. 12 . The direction of energy propagation associated with the various waves excited by anomalous Doppler emission at the harmonic $p = 1$. Negative angles indicate oppositely directed radial components of the phase and group velocity vectors

The power spectra which we have shown thus far have been for a single electron. We consider now what happens when we have a bunch of electrons moving together. Many of the resulting phenomena can be understood by analyzing the simple case of particles moving parallel to the magnetic field and bunched in the form of a sphere of uniform charge density N_b and radius g . The mathematical result of this bunching is that our expression for the spectral power density (the integrand of equation (5.79) with $p = 0$) has now to be multiplied by the form factor $D(g)$ squared, where from (5.29), we have for $g = h$ that

$$D(g) = N_b (2\pi g/k)^{3/2} J_{3/2}(gk). \quad (6.1)$$

The propagation vector k equals $2\pi/\lambda$ where λ is the wavelength in the medium. Thus if there is only a small fraction of a wavelength in the dimension $2\pi g$, then $kg \ll 1$ and the Bessel function can be replaced by its small argument approximation. In this case

$$D^2 = [N_b (4\pi g^3/3)]^2 \quad (6.2)$$

$$= [\text{total number particles in bunch}]^2, \quad kg \ll 1,$$

which we quite expect. On the other hand if there are many wavelengths in a dimension $2\pi g$, then $kg \gg 1$. Since $J_{3/2}$ is a rapidly oscillating function for large arguments consider only the envelope of maximas, D_{env}^2 . If we do this using the asymptotic form for $J_{3/2}$, we get

$$\begin{aligned} D_{\text{env}}^2 &= [N_b (4\pi g^3/3)]^2 / (k^2 g^2/3)^2 \\ &= [\text{total number particles in bunch}]^2 / (k^2 g^2/3)^2, \quad kg \gg 1. \end{aligned} \quad (6.3)$$

Now if the particles in the bunch were radiating incoherently, then the spectral power density would be increased by a factor equal to the total number of radiating particles, in our case, $N_b (4\pi g^3/3)$. Therefore, if for some wave $(k^2 g^2/3)^2 > N_b (4\pi g^3/3) = \text{number of radiating particles}$, then the power radiated into that mode is less than it would be if the charges were not bunched but rather were radiating incoherently.

Figure 13 illustrates these conclusions. The curves marked a are for a single electron while those marked b and c are for spherical charge bunches of radii 10 cm and 1 meter respectively having a uniform charge density of 10^5 particles per cubic meter. Note that for most frequencies and modes the greater the number of radiating charges, the greater is the radiation loss. However, at the very high frequencies ($X_e \approx 0.1$), and for the modes having spectral power densities $\approx 10^{-32}$, we see that bunching sometimes causes less energy to be radiated than for a single charge. These are the thermal modes having very short wavelengths. The point to be made here is that there is a limit to the size of our

bunch, beyond which the charges radiate even less at a given frequency and into a given mode than they would if they radiated incoherently. In a magnetoplasma this critical size is a function of the shape of the bunch as well as of the magnitude and direction of the wave propagation vector \underline{k} .

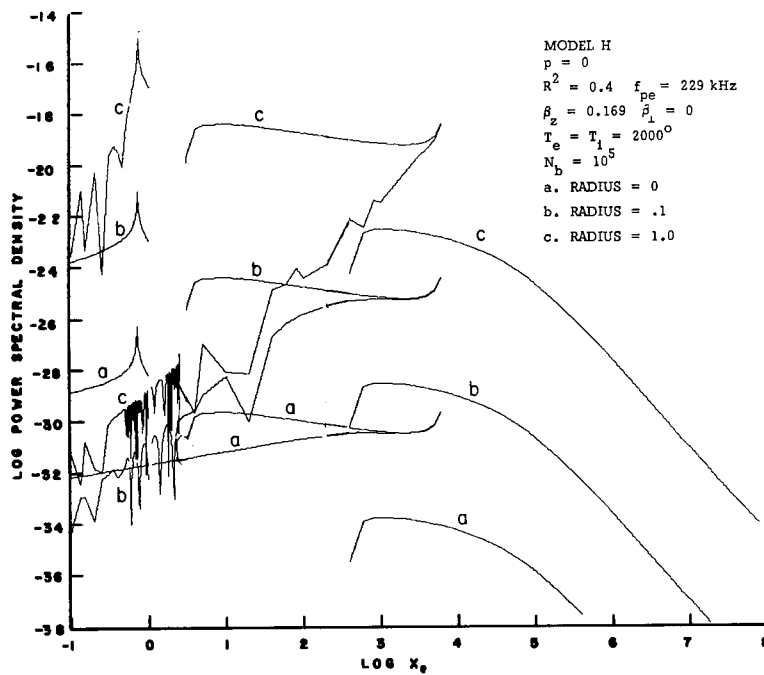


Fig. 13. Comparison of the power spectral densities for a) a point charge source, b) a spherical source of radius 10 cm and uniform density N_b , and c) a spherical source of radius 1 m and with a uniform number density N_b

Results Using Model A

From our derivation of the dielectric tensor elements for Model A using the kinetic theory approach, we find that this model is valid provided that the following inequalities are satisfied,

$$|\zeta_p| \gg 1 \quad \text{and} \quad \mu_s \ll 1, \quad (6.4)$$

where for a collisionless plasma

$$\zeta_p = (1 - p Y_s) / n_z (2 d_{s\parallel})^{\frac{1}{2}} \quad (6.5)$$

and

$$\mu_s = n_{\perp}^2 d_{s\perp} / Y_s^2. \quad (6.6)$$

We shall only show numerical results for the Cerenkov radiation from a particle. We shall also restrict ourselves to the high frequency end of the power spectrum where ion motion can be neglected. Therefore, the emission equation we use is given simply as

$$n_z = \beta_z^{-1}. \quad (6.7)$$

In our computations the Model A is assumed to be valid for

$$|\zeta_p| \geq 2 \quad \text{and} \quad \mu_e \leq 0.5. \quad (6.8)$$

Using the emission equation, this requires that

$$|1 - p Y_e| \geq 2^{3/2} \beta_z^{-1} (d_{e\parallel})^{\frac{1}{2}}. \quad (6.9)$$

For an unperturbed temperature $T_{e\parallel} = T_{e\perp} = 6000^\circ$ hence isotropic unperturbed pressure to compare with the Model H results, and a particle speed $\beta_z = 0.169$, we have that

$$|1 - p Y_e| \gtrsim 1.7 \times 10^{-2} \quad (6.10)$$

and, from $\mu_e \leq 0.5$, we also have that

$$n_{\perp}^2 \lesssim 5 \times 10^5 Y_e^2. \quad (6.11)$$

In terms of our abscissa variable X_e , these inequalities become

$$|1 + 0.63 p X_e^{\frac{1}{2}}| \geq 1.7 \times 10^{-2} \quad (6.12)$$

and

$$n_1^2 \leq 2 \times 10^5 X_e \quad (6.13)$$

for the operating line $R^2 = 0.4$. Thus $|\zeta_p| \geq 2$ for all values of X_e except for values which lie very near to the harmonics of the electron gyro-frequency, that is, $X_e = 2.50, .625, .277, .156, .100$, etc.

The power spectral density for a non-spiraling electron as calculated from this model is shown in Figure 14. The dashed portions of the curves indicate where the adiabatic model fails, that is, at least one of our inequalities was not met in those regimes. The most noteworthy result is that there are two modes excited in the regime between the UHR and the electron plasma frequency having nearly the same power spectrum. In fact, on the scale of our graph it is difficult to distinguish the two curves. However, their existence is readily apparent in the plots of phase and group velocity directions. When we compare Figure 14 with Figure 3 for the hydrodynamic model, we see that only one such high energy mode was predicted by Model H. (Note: 1) the various mode numbers used in the two models bear no relation to each other and 2) mode 4 of Model H is due to second order temperature effects, while Model A retains only first order temperature effects. Thus we do not expect any mode corresponding to number 4 of Model H for the Model A). Also note from Figure 14 that there exists a frequency band between $X_e \approx .62$ and $X_e \approx .72$ where no radiation occurs as predicted by Kikuchi [38]. This is in contrast to the continuous spectrum shown in Figure 3 for Model H. Also different in the two models is the appearance of a radiated wave in the regime below the electron plasma frequency and above the electron gyro-frequency for Model A.

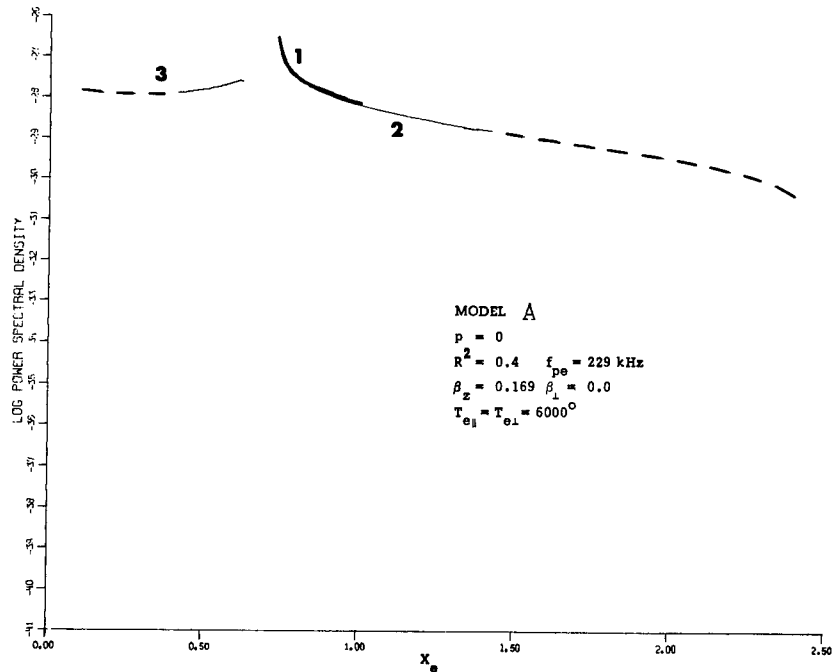


Fig.14 . Power spectral density at high frequencies for Cerenkov radiation from a non-spiraling electron obtained using Model A. Dashed lines indicate regions where model is not valid

Figure 15 shows the power spectrum for a spiraling charge. As with Model H we see the effects of wave interference manifested in the oscillations of the power spectrum. Similar differences to those noted previously for the non-spiraling electron are found on comparing Figure 15 with the corresponding Figure 4 obtained with Model H. As also noted for Model H, the rather jagged upper envelopes on the curves is due to the rather limited number of abscissa points plotted.

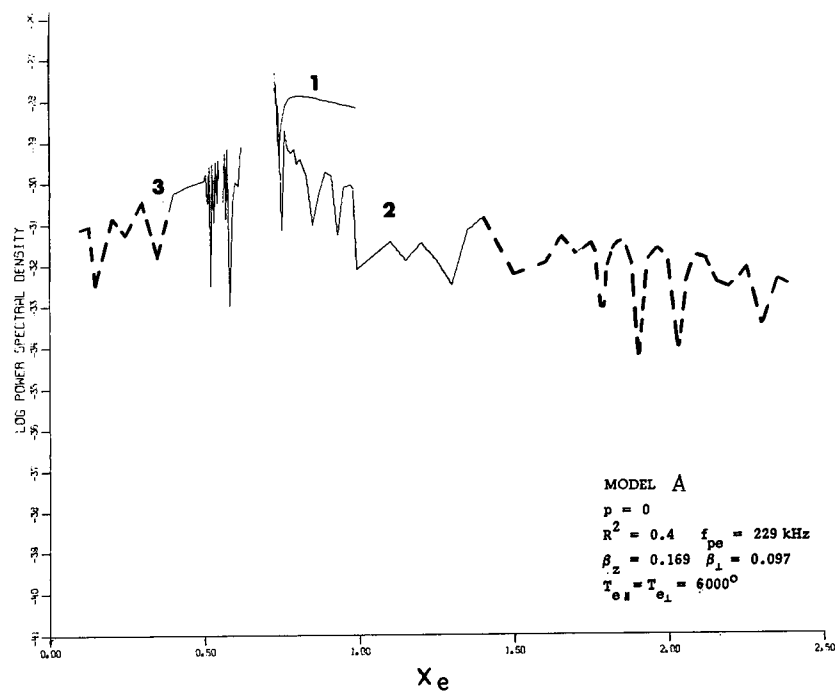


Fig. 15 . Power spectral density at high frequencies for Cerenkov radiation from a spiraling electron obtained using Model A. Dashed lines indicate regions where model is not valid

Figure 16 gives the spectrum of phase velocity directions excited by the Cerenkov emissions. This spectrum is quite different than the one obtained for Model H (see Figure 7). This is expected because of the additional high energy mode and the emission gap at $.62 < X_e < .72$ which we find in Model A.

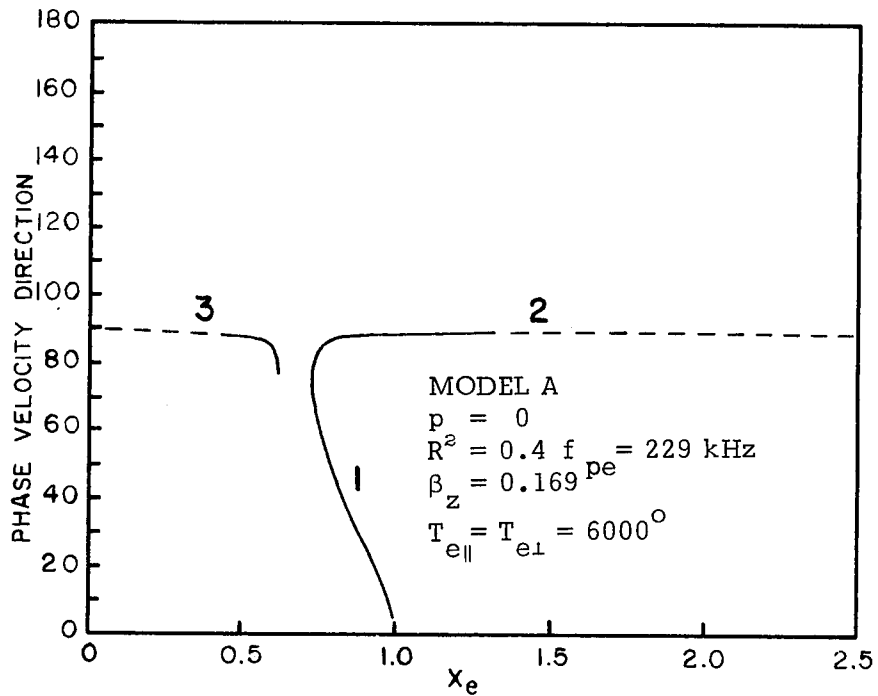


Fig. 16. High frequency spectrum of phase velocity directions excited by Cerenkov emissions obtained using Model A. Dashed lines indicate regions where model is not valid

Figure 17 shows that the new mode 2 propagates with a group velocity which has a radial component antiparallel to the radial component of the associated phase velocity vector. This is indicated by the negative angles in Figure 17.

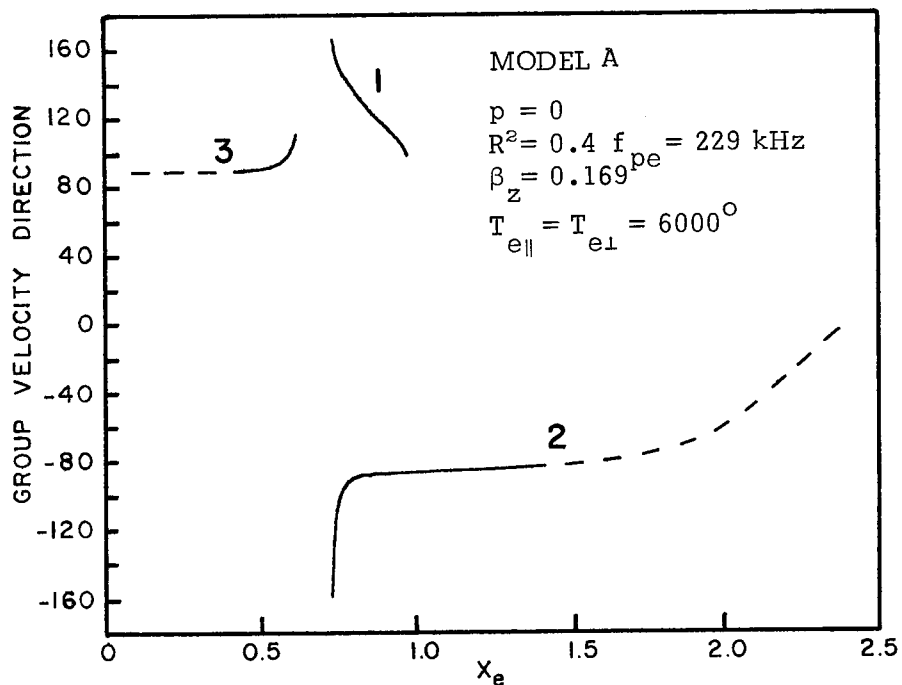


Fig. 17. High frequency spectrum of group velocity directions excited by Cerenkov emissions obtained using Model A. Dashed lines indicate regions where model is not valid

CHAPTER VII

POTENTIAL APPLICATIONS OF THEORY

In the previous chapters we developed a theory for computing the radiation losses from free electric charges and antennas moving through a warm magnetoplasma. Here we discuss some areas where this theory is applicable. We first discuss its possible application to explain noise generation in the ionosphere, and secondly we discuss its potential application to the problem of radiation from satellite-borne antennas in the ionosphere.

Noise Generation in the Ionosphere

The main contribution to the natural atmospheric noise observed at low frequencies using ground-based receivers is caused by lightning. When a lightning flash occurs, the electromagnetic noise which it generates can propagate to a distant receiver by different paths. Figure 18 depicts the "direct" path from the lightning flash, L, to the receiver, R, and Figure 19 shows the so-called Whistler path in which the

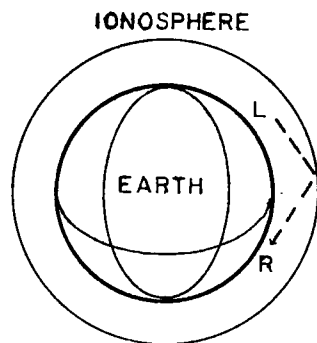


Fig. 18 . "Direct" path from L to R

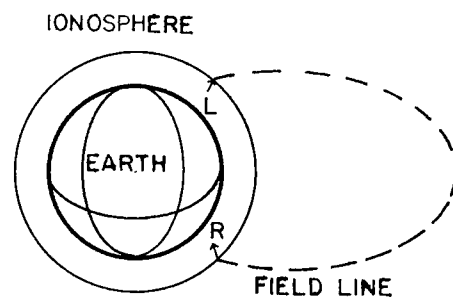


Fig. 19 . Whistler path from L to R

noise from L penetrates the ionosphere near the source and then travels along the Earth's magnetic field to a receiver located near the opposite end of the same field line. Along that portion of the Whistler path which is in the ionosphere, the higher frequency components of the noise travel faster than the lower frequency components. If a high gain audio amplifier is connected to the receiving antenna R, a descending tone can be heard--hence the name Whistler. While studying Whistlers, investigators noted that there also existed a continuous component of atmospheric noise at frequencies below 10 MHz that appeared to be of cosmic origin [60]. Ellis [19] discussed the possibility that the portion of this noise at frequencies of hundreds of kilohertz was due to Cerenkov radio emission by auroral particles approaching the Earth. He concluded that the flux density of this radiation might be as high as $10^{-21} \text{ Wm}^{-2} \text{ Hz}^{-1}$. Such power flux densities are well above the minimum observable. Subsequent analysis of natural atmospheric noise showed that much of the discrete VLF (30 kHz to ≈ 3 kHz) noise observed also had its origins in the exosphere rather than in lightning bursts [25]. However, comparisons between theory and observations were largely speculative at that time since no direct measurements of suspected source currents in the exosphere were available.

Experiments performed aboard the Earth orbiting Injun 3 satellite indicate that VLF hiss emissions are often correlated with precipitated high energy electrons [28]. In one of the cases cited in [28] (March 3 event), the energy balance is as follows: VLF energy flux less than 10 kHz = $8.0 \times 10^{-7} \text{ erg cm}^{-2} \text{ sec}^{-1}$, electron energy flux equals $10 \text{ ergs cm}^{-2} \text{ sec}^{-1}$. In addition, observations seem to indicate that VLF hiss is generated near the high-latitude (or large L^1) boundary termination of particle trapping by the Earth's magnetic field.

¹ If the Earth's magnetic field is approximated by a dipole field, the L value is equal to the distance from the center of the Earth measured in Earth radii, at which a particular magnetic field line crosses the magnetic equator. Further discussion of this quantity can be found in McIlwain [51].

Liemohn [47] applied the results of the theory of Cerenkov and cyclotron radiation in a dispersive medium to the interpretations of the very-low-frequency (VLF) and low-frequency (LF) emissions from the magnetosphere (3 to 300 kHz) using the following assumptions:

- 1) The source of the noise was postulated to be suprathermic electrons streaming through the ambient plasma and radiating incoherently.
- 2) The energy radiated by each electron into the Whistler mode is assumed to propagate along the Earth's magnetic field lines.
- 3) The Earth's magnetic field is approximated by a dipole field.
- 4) The total spectral power density observed near the base of the ionosphere is taken as

$$P(f) \cdot N_Q \cdot V_B$$

where $P(f)$ is the average power loss per electron at the frequency f as calculated using cold plasma theory, N_Q is the number density of suprathermic electrons and V_B is the volume of the flux tube containing the source electrons. Liemohn took $P(f) \sim 10^{-30} \text{ WHz}^{-1}$, $N_Q \sim 0.1 \text{ electrons/cm}^3$ and $V_B \sim 10^{10} \text{ cm}^3$ (corresponding to $L = 3$). With these rough approximations, the incoherent radiation flux at the base of the flux tube (calculated to be $\sim 10^{-21} \text{ W/cm}^2 \text{ Hz}$) was found to be several orders of magnitude below the observed power level (taken as $10^{-14} \text{ W/cm}^2 \text{ Hz}$).

Several years later, Jorgensen [34] performed very similar calculations. The reason for doing the recalculation was based on the following three reasons:

- 1) The observed power with which the calculated power was compared was claimed to be $10^{-10} \text{ Wm}^{-2} \text{ Hz}^{-1}$, whereas preliminary results obtained by the VLF experiment in the OGO 2 satellite, which are reported in [34], indicate a maximum spectral density of about $10^{-12} \text{ Wm}^{-2} \text{ Hz}^{-1}$.

2) Although the noise was observed at latitudes where the magnetic shell parameter L is about 7 and higher [28], the tube of lines of force, the volume of which was used in the total power calculation, was located by Liemohn at $L = 3$, and so the volume used was much too small.

3) The density of the energetic particles was taken to be 0.1 cm^{-3} , but densities of electrons with energies between 1 and 10 keV observed in the auroral zone have been found to be almost 2 orders of magnitude higher.

In view of the factors discussed above, the models used in earlier works considering Cerenkov radiation as a mechanism for VLF and LF emissions probably were unrealistic, and so the new attempt was considered worthwhile. In summary, Jorgensen points out that typical noise spectra in the VLF and LF ranges observed from the ground (Byrd Station) and in space (OGO 2) exhibit similar characteristics with a peak spectral density near 10 kHz. Maximum spectral densities observed on the ground and in space are about 10^{-14} and $10^{-12} \text{ Wm}^{-2} \text{ Hz}^{-1}$, respectively, but usually the peak spectral densities observed are one or two orders of magnitude lower.

Jorgensen does not consider the difference of about 2 orders of magnitude between the maximum observed spectral density ($10^{-12} \text{ Wm}^{-2} \text{ Hz}^{-1}$) and the maximum calculated spectral density ($10^{-14} \text{ Wm}^{-2} \text{ Hz}^{-1}$) as a serious problem because the calculated noise spectrum is based only on radiation from energies above 1 keV. The contribution to the radiation from electrons with energies below 1 keV were not included in his calculations because at the time Jorgensen's calculations were performed, knowledge of auroral electrons with energies below 1 keV was poor. Jorgensen concludes that the emission known as auroral hiss and polar lower hybrid resonance noise may be generated by an incoherent Cerenkov process in contrast to the earlier work by Liemohn [47] and others.

Lim and Laaspere [48] extended the theoretical computations of Cerenkov noise emission to include the low energy particles neglected by Jorgensen. In addition to including the very soft electrons in their calculations, they also made their calculations for a magnetic latitude of 78° as opposed to the 70° latitude used by Jorgensen. While Jorgensen's value is appropriate for auroral hiss observed near midnight, they point out that satellite results have shown that these emissions are most intense at about noon magnetic local time¹ in the region of the day-time "polar cusp" at about 78° invariant latitude².

In the course of their study, they became aware of a weakness in the cold plasma theories which is generally called the "infinity catastrophe", and is caused by the fact that as the electron energy E decreases, the intensity of Cerenkov radiation from it increases as $E^{-\frac{1}{2}}$. They note that the $E^{-\frac{1}{2}}$ dependence of the radiated power cannot continue without limit as E decreases, since net radiation from an electron should certainly cease as the electron's energy becomes comparable to the thermal energy of the background electrons.

There is experimental evidence that similar phenomena occur at frequencies just below the upper hybrid resonance frequency, around a few megahertz [27], [29]. In this regime of the CMA diagram, the cold plasma refractive index surfaces are unbounded in certain resonance directions resulting in infinities in computed power spectra similar to the previously discussed case of the lower frequencies.

The source of the "infinity catastrophe" lies in the shape of the cold plasma refractive index surfaces in regimes of the CMA diagram where resonance cones exist (see e.g. Figures 30 and 32). Note that in the resonance regimes there is no lower limit on the electron parallel velocity which satisfied the Cerenkov radiation condition $V_z = c/n_z$:

¹ Magnetic Local Time (MLT) is defined as the local time at the intersection with the magnetic equator of the field line passing through the satellite.

² The invariant latitude of a satellite is the magnetic latitude at which the magnetic field line passing through the satellite intersects the Earth's surface.

no matter how small V_z is, one can always find a real n_{\perp} such that the emission equation is satisfied. As $V_z \rightarrow 0$, $n \rightarrow \infty$ in these regimes. We shall examine this problem in the light of the theory developed in this thesis.

We can classify the methods for eliminating the "infinity catastrophe" into two categories. In the first category are those methods which seek to prevent $n \rightarrow \infty$ by making the mathematical model of the plasma more realistic. These methods likely include the allowance for collision and/or thermal effects in the description of the plasma. The second category contains those methods which allow $n \rightarrow \infty$ but limit the amount of power which can radiate into directions where n is very large. This is the technique most often employed. Generally, in this approach one simply neglects the radiation into directions where n is greater than some cutoff value. Another possibility, using this kind of approach, is to allow for sources of finite size. When the sources can be modeled in this way, the "infinity catastrophe" is eliminated in a more consistent and realistic manner than is possible by simply imposing a cutoff on n .

Consider these methods in more detail. First consider the case when thermal effects are included in the description of the plasma as in our Models A and H but collision effects are neglected. The refractive index for such cases is not always finite. That this is so, can be seen by examining the refractive index surfaces for Models A and H as given in Appendix G. For example, when $X_e = .8$ Model A has resonance cones ($n \rightarrow \infty$) as shown in Figure 52. Note, however, that at the same value of X_e , Model H has bounded refractive surfaces. The surfaces for Model H are not bounded for all values of X_e , however, as seen for example in Figure 42. Therefore when collisions are neglected, the inclusion of plasma thermal effects in the manner of Models A or H will not lead to the elimination of the "infinity catastrophe" for a point charge source.

When collision effects are introduced into Models A and H, the refractive index is likely to remain finite everywhere as it does for the case of a cold plasma with collisions [15]. However, in the magneto-

spheric plasma surrounding the Earth, collision frequencies are often very low. The introduction of such small collision losses into Models A and H may still lead to unrealistically high values of the refractive index. In these cases one should use improved models for the plasma, such as our Model K, or else allow for sources of sufficient size such that the power which is radiated in the form of waves corresponding to very large refractive indexes is negligible.

For example, consider radiation from an extended charge source. In Chapter V we give the power radiated by a uniformly charged ellipsoid of revolution which is moving along the magnetic field of an anisotropic plasma. Such a source might approximate a collection of point charges in a beam which have been bunched by plasma waves.

For very large refractive indexes, the Fourier transformed current density for this source behaves like $1/n_z^2$ or like V_z^2 if one uses the Cerenkov condition $n_z = c/V_z$. Since the power radiated goes like the square of the current density, we find that for an extended source the power decreases like V_z^3 instead of increasing like $1/V_z$ which is the case for a point charge. Hence, such an extended source has a finite power spectral density irrespective of any infinities which exist in the refractive index.

While studying the problem of radiation from spiraling charges we noted that Model A predicted that a relatively large portion of energy could be radiated into the thermal mode at frequencies near the upper hybrid resonance. Since there appears to be an enhanced band of noise in the ionosphere at these frequencies, it would appear from our numerical results using Model A that part of this noise (sometimes referred to as "region 3 noise" [42]) may have its source in Cerenkov and cyclotron radiation from suprathermic electrons radiating into electroacoustic (thermal) modes.

To check such a hypothesis would require that the source of the "noise" be located and described. When studying VLF hiss, most investigators assume that the source electrons are located approximately on the same field line as the receiver, since VLF Whistler mode radiation often propagates nearly along the magnetic field lines. At frequencies near the UHR, the calculation of the trajectory of radiation propagation is quite complicated, especially if thermal effects are taken into account [4] (which could be important). Because of the difficulties involved in tracing a ray backwards from the receiver to the source electrons at these UHR frequencies, our knowledge of the location of the source of this noise is very poor. Thus an adequate check of the results predicted by Model A regarding region 3 noise must await the development of a theory for locating where the sources are; a search of experimental data concerning the description of the sources is then in order. Once the sources are described the theory given here may be applied.

The radiation from free charges also has potential as an element of a communications system (so-called free-charge antennas). The feasibility of using free-charge-radiators in a controlled manner has recently been examined using cold plasma theory [16]. The warm plasma theory developed in this thesis can be applied to this problem.

Antennas in the Ionosphere

The theory given in this thesis can likewise be applied to communication systems which involve a source antenna in the plasma. In particular, our treatment of this problem differs from most previous studies [53], [70] in that we have treated antenna motion and plasma thermal effects simultaneously.

The study of the radiation losses from a transmitting antenna are important for an understanding of antenna efficiency. Thermal mode excitation could be a major limitation to the maximum realizable efficiency of an antenna in the ionosphere. Using the formulas developed in this thesis, loop and dipole antennas can be compared with one another with regard to their susceptibility for exciting thermal modes.

Although we have derived expressions for the total power radiated by various antennas, it is sometimes more useful to obtain radiation patterns for these antennas. If the antenna is located high up in the ionosphere so that the energy propagation can be described by "ray theory", then it is often most convenient to obtain these radiation patterns in terms of wave normal space (\underline{k} -space). Only slight modification of several formulas given in this thesis are necessary to obtain expressions for \underline{k} -space radiation patterns for the loop and dipole antennas.

In our expressions (5.95) and (5.88) for the power radiated by moving loop and electric dipole antennas, we note from the emission equation that a band of frequencies are emitted. The width of this band depends on the magnitude of n_z . Those modes which have n_z very large, such as the thermal modes, will show large frequency spreading. The formulas given in this thesis allow for the systematic study of the complex phenomenon of Doppler shifted radiation from sources moving in warm anisotropic plasmas.

CHAPTER VIII

CONCLUSIONS

Before presenting our conclusions we first review both the motivation behind this study, and its objectives. The motives for this study are found in both experimental observations and in paradoxical theoretical predictions. The experimental observations we refer to are the discovery of rather intense radio noise¹ in the ionosphere at frequencies below the upper hybrid resonance frequency and above the electron plasma frequency [84, 31, 27, 1]. This noise has been correlated with fluxes of supra-thermic electrons also observed in the vicinity of the intense radio noise [42]. It was suggested that these energetic electrons may be the source of this radio noise via the Cerenkov and cyclotron radiation which they emit. However, theoretical estimates of the amount of Cerenkov and cyclotron radiation emitted by an electron in this frequency band, based upon cold plasma theory, lead to the paradoxical result that the energy radiated becomes infinite as the particle speed approaches zero ("infinity-catastrophe") [63], [48]. The original objectives of this study were: 1) to modify the cold plasma theory so as to eliminate the "infinity catastrophe" and, 2) to apply the improved theory to test the hypothesis that the observed "region 3" radio noise is due to Cerenkov and cyclotron radiation.

In order to eliminate infinities in computed power spectra, it was decided to discard the cold plasma model in favor of a more realistic plasma model which would allow for thermal effects. In addition, the new model was to include collision effects. As a further means of

¹ This is sometimes referred to as "region 3 noise" because it relates to region 3 of the CMA diagram.

eliminating power infinities and at the same time treat the case of coherent radiation from charge bunches, it was decided that the problem of Cerenkov radiation from an extended source would also be investigated. Since there are several ways in which plasma thermal effects can be modeled, an additional objective developed; to compare Cerenkov and cyclotron radiation spectra as computed using the various models.

Due to the unforeseen complexity and magnitude of the work required to modify cold plasma theory as indicated in objective 1), very little effort was given to applications of our theory as related to the previously stated objective 2). However, we believe that the theory of Cerenkov radiation and magneto-bremstrahlung developed in this thesis is the best theory currently available for analyzing "region 3 noise" in terms of these processes.

Modifications of cold plasma theory to allow for finite plasma temperatures are generally made using either hydrodynamic or kinetic theory. The hydrodynamic theory is based upon equations derived by taking successive velocity moments of the Boltzmann equation. In order to close the set of moment equations the assumption of negligible heat flow is made (adiabatic approximation). The kinetic theory is based upon computation with the Boltzmann equation directly instead of working with its moments. As is usually the case for both the hydrodynamic and kinetic theories, the governing equations were linearized in this thesis.

We found that by transforming the governing equations to Polarized-Wave space and working in this space, we were often able to express rather complicated results very concisely.

The conductivity tensor and the closely related dielectric tensor are of the utmost importance in our theory, since they determine how the plasma is modeled. Consequently, we have given very detailed derivations of the dielectric tensor for the various models, and we have indicated where errors exist in previous published derivations. Note that

although the dielectric tensor for Model A is derivable using either a macroscopic or kinetic theory, the latter theory also gives the regions of validity of this model very straightforwardly.

The tractability of analytic solutions to many problems involving radiation in plasmas, depends largely upon the complexity of the dielectric tensor. Note in particular, that the dielectric tensor for our Models A and H allow us to perform the integrations required to obtain the power spectral density from a radiating charge without resorting to difficult integrations involving branch points and branch cuts. Such is generally not the case when working with the full kinetic expression for the dielectric tensor. However, we wish to point out a potentially promising extension of our results which might allow for some of the features of the kinetic theory such as Landau and cyclotron damping.

Kikuchi [37] in a very interesting paper gives various explicit formulas for the dielectric tensor which include the effects of Landau and cyclotron damping. These formulas are obtained starting with the dielectric tensor of kinetic theory. Kikuchi then takes various expansions of the transcendental functions appearing in this tensor. Substituting for these functions the proper expansions, and neglecting high order temperature effects, he is able to obtain fairly tractable formulas for the dielectric tensor. It appears possible that using Kikuchi's formulas, the power spectral density of radiation from a charge spiraling in a homogeneous magnetoplasma can be obtained analytically in a relatively straightforward manner. This would include the phenomena of Landau and cyclotron damping, which we have not been able to treat in this thesis.

In the opposite case, where thermal effects are completely negligible (cold plasma theory), we have shown that our simplified formula for the power spectral density for a spiraling point charge is identical to that obtained by Trulsen and Fejer (TF) [80] using a different approach. Since (TF) and Liemohn [47] are in disagreement as to this formula, our results support the conclusion that the formula of TF is correct and that of Liemohn is incorrect.

By including finite size charge sources we have been able to eliminate the "infinity catastrophe" independent of whether a cold or warm plasma model is assumed.

In addition to Cerenkov and cyclotron radiation via the cold plasma modes, our numerical results clearly show that there are also emissions into the new thermal modes described by warm plasma theory. It is also obvious from our results that the radiating bands for the cold plasma modes and the thermal modes are not identical. Indeed, there are even differences in the radiation bands for the thermal modes depending on the particular warm plasma model used (i.e. Model A or H).

Most cases which we have studied predict significantly greater radiation losses into the cold plasma vs. the warm plasma modes. A noteworthy exception occurs in "region 3" of the CMA diagram when Model A is used. Recall that this is the regime where excessive radio noise was observed in the ionosphere. In this regime radiation losses into the thermal modes may be a very significant part of the total energy radiated. Because the cold and warm plasma modes have very different propagation characteristics in this regime, the thermal mode contribution to "region 3 noise" observed by a receiver in the ionosphere and the corresponding contribution to this noise due to the cold plasma modes will likely have different source locations. Hence, thermal effects may be very important in understanding the mechanism of "region 3 noise".

During our study of Cerenkov and cyclotron radiation we did not find any significant changes in computed power spectral densities for spiraling charges when we replaced the scalar pressure with an anisotropic pressure in Model A. The anisotropic pressure model, however, was not extensively tested so that no general conclusions were obtained.

With regard to the "infinity catastrophe" we wish to point out that in both Models A and H there exist certain modes having resonance directions such that the refractive index $n \rightarrow \infty$ in these directions. We find that the cold plasma index infinities at the LHR and UHR are elimin-

ated by allowing for plasma thermal effects; however, the thermal modes themselves have resonance cones which may lead to an "infinity catastrophe".

Refractive index plots for Model A seem to indicate that this model is strictly valid only in the vicinity of the upper and lower hybrid resonances. Away from these frequencies the refractive index is so large that the basic approximations used to derive the model are no longer valid.

We find that the results of computations based on Models A and H can often differ drastically from one another. In particular, large differences were noted at frequencies near the upper hybrid resonance.

The method of analyzing radiation from spiraling charges was found to be easily adapted to the study of radiation from moving antennas. However, in the expression for the power radiated by a moving point dipole antenna a singularity was noted for those cases where $n_z = 1/\beta_z$.

It was noted that by a slight alteration of our derivation of the power loss formulas radiation patterns in wave normal space could be obtained. These are particularly useful as inputs to ray tracing theories.

The Doppler spread of frequencies caused by antenna motion can be analyzed straightforwardly using the formulas given in the thesis.

APPENDIX A

POLARIZED-WAVE (P-W) SPACE

In solving problems involving anisotropic plasma media, it is often the case that the equations which must be manipulated are greatly simplified when expressed in terms of "polarized-wave" space. This appendix is devoted to a discussion of "polarized-wave" space insofar as is required for understanding its use in this thesis.

The underlying reason that the equations simplify when written in P-W space is that the curl operator ($\hat{e}_z \times$) which appears so often in problems involving anisotropic plasmas becomes a diagonal tensor in P-W space as shown in the next section. The transformations relating quantities in Cartesian space to corresponding quantities in "polarized-wave" space are given in this appendix along with the explanation of why it is referred to as "polarized-wave" space.

Diagonalizing the Matrix for ($\hat{e}_z \times$)

Consider the vector product $\hat{e}_z \times \underline{e}$. This product may be written

$$\hat{e}_z \times \underline{e} = \begin{bmatrix} 0 & -1 & 0 \\ 1 & 0 & 0 \\ 0 & 0 & 0 \end{bmatrix} \begin{bmatrix} e_x \\ e_y \\ e_z \end{bmatrix}. \quad (\text{A.1})$$

We seek eigenvectors and eigenvalues (λ) such that

$$\begin{bmatrix} 0 & -1 & 0 \\ 1 & 0 & 0 \\ 0 & 0 & 0 \end{bmatrix} \begin{bmatrix} e_x \\ e_y \\ e_z \end{bmatrix} = \lambda \begin{bmatrix} e_x \\ e_y \\ e_z \end{bmatrix}. \quad (\text{A.2})$$

This system of equations has a non-trivial solution only if

$$\lambda (\lambda^2 + 1) = 0 . \quad (A.3)$$

Thus there are three possible eigenvalues, namely, $\lambda = +i, -i, \text{ or } 0$.

The corresponding eigenvectors $\underline{e}_{+1}, \underline{e}_{-1}, \underline{e}_0$ have directions specified by

$$\begin{aligned} \underline{e}_{+1} &\propto (\hat{e}_x - i \hat{e}_y) \\ \underline{e}_{-1} &\propto (\hat{e}_x + i \hat{e}_y) \\ \underline{e}_0 &\propto \hat{e}_z \end{aligned} \quad (A.4)$$

where we shall fix the proportionality constants by requiring these vectors to be of unit norm.

If \underline{e} is a complex vector

$$\underline{e} = \underline{e}' + i \underline{e}'' \quad (A.5)$$

with \underline{e}' and \underline{e}'' real, then we define the norm of \underline{e} , $\|\underline{e}\|$, as

$$\|\underline{e}\| \equiv + (\underline{e}^* \cdot \underline{e})^{\frac{1}{2}} = + (e'^2 + e''^2)^{\frac{1}{2}} , \quad (A.6)$$

which is a positive real number. The length of \underline{e} , $|\underline{e}|$, is defined as

$$|\underline{e}| \equiv \pm (\underline{e}^2)^{\frac{1}{2}} = \pm (\underline{e} \cdot \underline{e})^{\frac{1}{2}} = \pm (e'^2 - e''^2 + i 2\underline{e}' \cdot \underline{e}'')^{\frac{1}{2}} \quad (A.7)$$

which is a complex number, sign undetermined.

The eigenvectors of unit norm, $\hat{e}_{+1}, \hat{e}_{-1}, \hat{e}_0$, have cartesian components

$$\begin{aligned} \hat{e}_{+1} &= 2^{-\frac{1}{2}} (\hat{e}_x - i \hat{e}_y) \\ \hat{e}_{-1} &= 2^{-\frac{1}{2}} (\hat{e}_x + i \hat{e}_y) \\ \hat{e}_0 &= \hat{e}_z . \end{aligned} \quad (A.8)$$

They are linearly independent and can therefore serve as a set of basis vectors. In terms of this set of basis vectors, the cartesian unit vectors are given by

$$\begin{aligned}\hat{e}_x &= 2^{-\frac{1}{2}} (\hat{e}_{+1} + \hat{e}_{-1}) \\ \hat{e}_y &= i 2^{-\frac{1}{2}} (\hat{e}_{+1} - \hat{e}_{-1}) \\ \hat{e}_z &= \hat{e}_0.\end{aligned}\quad (\text{A.9})$$

Transformations Between Cartesian and "Polarized-Wave" Spaces

A vector, \underline{E} , will have components

$$\begin{aligned}\underline{E} &= E_1 \hat{e}_{+1} + E_{-1} \hat{e}_{-1} + E_0 \hat{e}_0 \\ &= E_x \hat{e}_x + E_y \hat{e}_y + E_z \hat{e}_z \\ &= 2^{-\frac{1}{2}} (E_x + i E_y) \hat{e}_{+1} + 2^{-\frac{1}{2}} (E_x - i E_y) \hat{e}_{-1} + E_z \hat{e}_0\end{aligned}\quad (\text{A.10})$$

which leads to the vector transformation matrix, \underline{T} .

$$\begin{bmatrix} E_1 \\ E_{-1} \\ E_0 \end{bmatrix} = 2^{-\frac{1}{2}} \begin{bmatrix} 1 & i & 0 \\ 1 & -i & 0 \\ 0 & 0 & 2^{\frac{1}{2}} \end{bmatrix} \begin{bmatrix} E_x \\ E_y \\ E_z \end{bmatrix} = \underline{T} \cdot \begin{bmatrix} E_x \\ E_y \\ E_z \end{bmatrix}\quad (\text{A.11})$$

\underline{T}^{-1} is given by

$$\begin{bmatrix} E_x \\ E_y \\ E_z \end{bmatrix} = 2^{\frac{1}{2}} \begin{bmatrix} 1 & 1 & 0 \\ -i & i & 0 \\ 0 & 0 & 2^{\frac{1}{2}} \end{bmatrix} \begin{bmatrix} E_1 \\ E_{-1} \\ E_0 \end{bmatrix} = \underline{T}^{-1} \cdot \begin{bmatrix} E_1 \\ E_{-1} \\ E_0 \end{bmatrix}\quad (\text{A.12})$$

Suppose $\underline{E}(\underline{r}, t) = \underline{\mathcal{E}}(\underline{k}, \omega) e^{ikz - i\omega t}$ represents the electric field associated with a plane wave of real amplitude $\underline{\mathcal{E}}$ propagating along the z-axis. From our transformation matrix

$$\delta_1 = 2^{-\frac{1}{2}} (\delta_x + i \delta_y), \quad \delta_{-1} = 2^{-\frac{1}{2}} (\delta_x - i \delta_y), \quad \delta_0 = \delta_z. \quad (\text{A.13})$$

Therefore, $\delta_1 \neq 0, \delta_{-1} = \delta_0 = 0$ refers to a left circularly polarized (LCP) transverse electromagnetic (TEM) wave. Similarly, $\delta_1 \neq 0, \delta_1 = \delta_0 = 0$ and $\delta_z \neq 0, \delta_1 = \delta_{-1} = 0$ refer to waves which are right circularly polarized (RCP) TEM and longitudinally polarized respectively. By definition, the electric field of a RCP wave rotates in a clockwise manner when viewed looking in the direction of the magnetic field, conversely the LCP wave rotates counterclockwise. For this reason the coordinate system having $(\hat{e}_{+1}, \hat{e}_{-1}, \hat{e}_0)$ as basis vectors is sometimes referred to as the "polarized-wave" (P-W) coordinate system.

If $\underline{\underline{C}}$ is a tensor in Cartesian space and $\underline{\underline{K}}$ is its transform in P-W space, then

$$\underline{\underline{K}} = \underline{\underline{T}} \underline{\underline{C}} \underline{\underline{T}}^{-1} \quad \text{and} \quad \underline{\underline{C}} = \underline{\underline{T}}^{-1} \underline{\underline{K}} \underline{\underline{T}}. \quad (\text{A.14})$$

Tensors written in P-W space are arranged as follows. Rows are labeled in the same manner as column vectors. Hence the top row is the +1 row, the middle row is the -1 row and the last row is the 0 row. Columns are labeled in such a manner that the product of a tensor $\underline{\underline{K}}$ and a column vector $\underline{\underline{E}}$ obeys the relation

$$\underline{\underline{K}} \cdot \underline{\underline{E}} = K_{\mu - \nu} E_{\nu}. \quad (\text{A.15})$$

According to this scheme the columns are ordered -1, +1, 0 when read from left to right.

If

$$\underline{\underline{K}} = \begin{bmatrix} K_{1-1} & K_{11} & K_{10} \\ K_{-1-1} & K_{-11} & K_{-10} \\ K_{0-1} & K_{01} & K_{00} \end{bmatrix} \quad \text{and} \quad \underline{\underline{C}} = \begin{bmatrix} C_{xx} & C_{xy} & C_{xz} \\ C_{yx} & C_{yy} & C_{yz} \\ C_{zx} & C_{zy} & C_{zz} \end{bmatrix} \quad (\text{A.16})$$

then the components of $\underline{\underline{K}}$ and $\underline{\underline{C}}$ are related as follows:

$$\begin{aligned} K_{1-1} &= 2^{-1} (C_{xx} + C_{yy}) + i 2^{-1} (C_{yx} - C_{xy}) \\ K_{11} &= 2^{-1} (C_{xx} - C_{yy}) + i 2^{-1} (C_{yx} + C_{xy}) \\ K_{-1-1} &= 2^{-1} (C_{xx} - C_{yy}) - i 2^{-1} (C_{yx} + C_{xy}) \\ K_{-11} &= 2^{-1} (C_{xx} + C_{yy}) - i 2^{-1} (C_{yx} - C_{xy}) \\ K_{10} &= 2^{-\frac{1}{2}} (C_{xz} + i C_{yz}) \\ K_{-10} &= 2^{-\frac{1}{2}} (C_{xz} - i C_{yz}) \\ K_{0-1} &= 2^{-\frac{1}{2}} (C_{zx} - i C_{zy}) \\ K_{01} &= 2^{-\frac{1}{2}} (C_{zx} + i C_{zy}) \\ K_{00} &= C_{zz} \end{aligned} \quad (\text{A.17})$$

or inversely,

$$\begin{aligned} C_{xx} &= 2^{-1} (K_{1-1} + K_{11} + K_{-1-1} + K_{-11}) \\ C_{yy} &= 2^{-1} (K_{1-1} - K_{11} - K_{-1-1} + K_{-11}) \\ C_{zz} &= K_{00} \\ C_{xy} &= i 2^{-1} (K_{1-1} - K_{11} + K_{-1-1} - K_{-11}) \\ C_{yx} &= -i 2^{-1} (K_{1-1} + K_{11} - K_{-1-1} - K_{-11}) \\ C_{xz} &= 2^{-\frac{1}{2}} (K_{10} + K_{-10}) \\ C_{zx} &= 2^{-\frac{1}{2}} (K_{0-1} + K_{01}) \\ C_{yz} &= i 2^{-\frac{1}{2}} (-K_{10} + K_{-10}) \\ C_{zy} &= i 2^{-\frac{1}{2}} (K_{0-1} - K_{01}) \end{aligned} \quad (\text{A.18})$$

Note from the previous relations that $\underline{\underline{C}}^T$ corresponds to $\underline{\underline{R}}^T$ where the transpose of $\underline{\underline{R}}$ is defined by

$$(\underline{\underline{R}}_{\mu\nu})^T = \underline{\underline{R}}_{\nu\mu} \quad (\text{A.19})$$

or more explicitly,

$$\underline{\underline{C}}^T = \begin{bmatrix} C_{xx} & C_{yx} & C_{zx} \\ C_{xy} & C_{yy} & C_{zy} \\ C_{xz} & C_{yz} & C_{zz} \end{bmatrix} \quad \underline{\underline{R}}^T = \begin{bmatrix} R_{-11} & R_{11} & R_{01} \\ R_{-1-1} & R_{1-1} & R_{0-1} \\ R_{-10} & R_{10} & R_{00} \end{bmatrix} \cdot \quad (\text{A.20})$$

With this definition of the transpose, $\underline{\underline{R}}^T$ is not equivalent to the matrix $\underline{\underline{R}}$ with rows and columns interchanged.

Sometimes a vector \underline{k} is most conveniently expressed in either cylindrical (k_{\perp} , k_z , φ) or spherical (k , ϑ , φ) coordinates, hence we also use the transform from Cartesian to P-W space to write

$$\begin{aligned} k_{\pm 1} &= 2^{-\frac{1}{2}} k_{\perp} e^{\pm i\varphi} = 2^{-\frac{1}{2}} k \sin \vartheta e^{\pm i\varphi}, \\ k_0 &= k_z = k \cos \vartheta. \end{aligned} \quad (\text{A.21})$$

Vector and Tensor Algebra in P-W Space

The dot product of two vectors \underline{V} and \underline{B} is given by

$$\underline{V} \cdot \underline{B} = V_{-\nu} B_{\nu} \cdot$$

As usual, the summation convention is used with Greek indices ranging over the values +1, -1, 0. Similarly for dot products between vectors and tensors of arbitrary rank we define the dot product in P-W space as

$$\underline{B} \cdot \underline{\underline{R}} = B_{-\gamma} R_{\gamma\sigma} \dots \cdot \quad (\text{A.22})$$

Another form of the dot product frequently encountered is $\underline{k} \underline{V} \cdot \underline{R}$, which in P-W space is the tensor

$$k_{\sigma} V_{-\gamma} R_{\gamma\nu} \quad (A.23)$$

Using the transformation \underline{T} , the cross product $\underline{B} \times \underline{V}$ becomes

$$\underline{T} \cdot (\underline{B} \times \underline{V}) = i \begin{bmatrix} B_0 & 0 & -B_1 \\ 0 & -B_0 & B_{-1} \\ -B_{-1} & B_1 & 0 \end{bmatrix} \begin{bmatrix} V_1 \\ V_{-1} \\ V_0 \end{bmatrix} \quad (A.24)$$

also

$$\underline{T} \cdot (\underline{B} \times \underline{V}^*) = i \begin{bmatrix} B_0 & 0 & -B_1 \\ 0 & -B_0 & B_{-1} \\ -B_{-1} & B_1 & 0 \end{bmatrix} \begin{bmatrix} V_{-1}^* \\ V_1^* \\ V_0^* \end{bmatrix} \quad (A.25)$$

Note that if $\underline{B} = B_0 \hat{e}_z = B_0 \hat{e}_0$

$$\left[\underline{T} \cdot (\hat{e}_z \times \underline{V}) \right]_{\nu} = i \nu V_{\nu} \quad (\nu = +1, -1, \text{ or } 0). \quad (A.26)$$

When transforming vectors involving cross products, it is often convenient to express the cross product as a tensor. For example, in Cartesian coordinates $(\hat{e}_z \times \underline{x})$ is equivalent to

$$\begin{bmatrix} 0 & -1 & 0 \\ 1 & 0 & 0 \\ 0 & 0 & 0 \end{bmatrix} \quad (A.27)$$

Hence, in P-W space this tensor transforms to

$$\underline{\underline{T}} (\hat{e}_z \cdot \underline{x}) \underline{\underline{T}}^{-1} = i \begin{bmatrix} 1 & 0 & 0 \\ 0 & -1 & 0 \\ 0 & 0 & 0 \end{bmatrix} . \quad (\text{A.28})$$

The identity tensor $\underline{\underline{I}}$ keeps the same form in P-W space which it had in Cartesian space as do the related tensors $\underline{\underline{I}}_{\perp}$ and $\underline{\underline{I}}_{\parallel}$ defined by

$$\underline{\underline{I}}_{\perp} \equiv \begin{bmatrix} 1 & 0 & 0 \\ 0 & 1 & 0 \\ 0 & 0 & 0 \end{bmatrix} \quad \underline{\underline{I}}_{\parallel} = \begin{bmatrix} 0 & 0 & 0 \\ 0 & 0 & 0 \\ 0 & 0 & 1 \end{bmatrix} . \quad (\text{A.29})$$

When expressed in terms of Greek subscripts the tensor elements for $\underline{\underline{I}}$, $\underline{\underline{I}}_{\perp}$, and $\underline{\underline{I}}_{\parallel}$ become

$$I_{\mu\nu} = \delta_{\mu-\nu}, \quad I_{\perp\mu\nu} = \mu^2 \delta_{\mu-\nu}, \quad I_{\parallel\mu\nu} = (1 - \mu^2) \delta_{\mu-\nu}. \quad (\text{A.30})$$

Here $\delta_{\mu-\nu}$ has the usual meaning of the Kronecker delta, namely,

$$\delta_{\mu-\nu} = \begin{cases} 1, & \mu = -\nu \\ 0, & \mu \neq -\nu \end{cases} . \quad (\text{A.31})$$

The quantity $\delta_{\mu-\nu}$ is not to be taken in the sense of a component of a tensor even though we write it with subscripts similar to tensors.

Vector Analysis in P-W Space

The gradient, divergence and curl operations can also be transformed into the P-W space representation. In terms of cylindrical (ρ, z, ϕ) coordinates the gradient operator becomes

$$(\underline{\underline{T}}\nabla)_{\gamma} \equiv \left(\frac{\partial}{\partial \underline{r}} \right)_{\gamma} = [\gamma^2 2^{-\frac{1}{2}} \frac{\partial}{\partial \rho} + i\gamma 2^{-\frac{1}{2}} \rho^{-1} \frac{\partial}{\partial \phi} + (1-\gamma^2) \frac{\partial}{\partial z}] e^{i\gamma\phi}. \quad (\text{A.32})$$

The divergence is written

$$\nabla \cdot \underline{\underline{A}} = \left(\frac{\partial}{\partial \underline{\underline{r}}} \right)_{-\gamma} A_{\gamma} \cdot \quad (\text{A.33})$$

The curl is somewhat more complicated, taking the form

$$\begin{aligned} \left[\underline{\underline{T}} \cdot (\nabla \times \underline{\underline{A}}) \right]_{\gamma} = & i\gamma \left\{ \left(\frac{\partial}{\partial \underline{\underline{r}}} \right)_{\circ} A_{\gamma} - \left(\frac{\partial}{\partial \underline{\underline{r}}} \right)_{\gamma} A_{\circ} \right\} \\ & + i(1-\gamma^2) \left\{ \left(\frac{\partial}{\partial \underline{\underline{r}}} \right)_{+1} A_{-1} - \left(\frac{\partial}{\partial \underline{\underline{r}}} \right)_{-1} A_{+1} \right\} \cdot \quad (\text{A.34}) \end{aligned}$$

APPENDIX B

BASIC MAGNETO-IONIC THEORY

This appendix is intended as a brief description of those elements of basic magneto-ionic theory which are of use in making the remainder of the thesis more understandable. Also, since the notation used in this thesis may differ somewhat from that with which the reader is familiar, it seems reasonable to include this discussion of the simpler plasma concepts to supplement the more complex analyses. In this appendix collision effects are neglected.

Dispersion Relation

At the end of the second chapter we wrote down an expression for the dispersion relation, namely,

$$\det (n^2 I_{\sigma-\gamma} - K_{\sigma-\gamma} - n_{\sigma} n_{-\gamma}) = 0. \quad (\text{B.1})$$

which gives the functional dependence between frequency and wave propagation or refractive index vector. In this section we write the dispersion relation in a form which is more suitable for analysis. By writing the refractive index vector \underline{n} in spherical (n, ϑ, φ) coordinates and letting $S \equiv \sin \vartheta$, $C \equiv \cos \vartheta$, we can express the dispersion relation as

$$\Lambda(\omega) \equiv \begin{vmatrix} \frac{1}{2} n^2 (1+C^2) - K_{1-1} & -\frac{1}{2} n^2 S^2 e^{i\varphi} - K_{11} & -2^{-\frac{1}{2}} n^2 S C e^{i\varphi} - K_{10} \\ -\frac{1}{2} n^2 S^2 e^{-i\varphi} - K_{-1-1} & \frac{1}{2} n^2 (1+C^2) - K_{-11} & -2^{-\frac{1}{2}} n^2 S C e^{-i\varphi} - K_{-10} \\ -2^{-\frac{1}{2}} n^2 S C e^{-i\varphi} - K_{0-1} & -2^{-\frac{1}{2}} n^2 S C e^{i\varphi} - K_{01} & n^2 S^2 - K_{00} \end{vmatrix} = 0 \quad (\text{B.2})$$

where the parallel lines about the matrix indicate the determinant of the

matrix is to be taken. The angle ϑ is measured from the z-axis to \underline{k} or \underline{n} and the angle φ is measured from the x-axis to the projection of \underline{k} or \underline{n} on the (x-y) plane. The dispersion relation can now be written in the form of a polynomial in n^2 ,

$$A n^4 + B n^2 + C = 0 \quad (\text{B.3})$$

where

$$A = -\frac{1}{2} \sin^2 \vartheta \left[K_{1-1} + K_{-11} + e^{i2\varphi} K_{-1-1} + e^{-i2\varphi} K_{11} \right] - \cos^2 \vartheta K_{00} \\ - 2^{-\frac{1}{2}} \sin \vartheta \cos \vartheta \left[e^{-i\varphi} (K_{01} + K_{10}) + e^{i\varphi} (K_{-10} + K_{0-1}) \right] \quad (\text{B.4})$$

$$B = \sin^2 \vartheta \left[K_{1-1} K_{-11} - K_{11} K_{-1-1} + \frac{1}{2} K_{10} K_{0-1} + \frac{1}{2} K_{-10} K_{01} - \frac{1}{2} K_{00} K_{-11} \right. \\ \left. - \frac{1}{2} K_{00} K_{1-1} + \frac{1}{2} e^{-i2\varphi} (K_{00} K_{11} - K_{10} K_{01}) \right. \\ \left. + \frac{1}{2} e^{i2\varphi} (K_{00} K_{-1-1} - K_{-10} K_{0-1}) \right] + \\ 2^{-\frac{1}{2}} \sin \vartheta \cos \vartheta \left[e^{-i\varphi} (K_{10} K_{-11} + K_{1-1} K_{01} - K_{-10} K_{11} - K_{11} K_{0-1}) \right. \\ \left. + e^{i\varphi} (K_{-11} K_{0-1} + K_{-10} K_{1-1} - K_{-1-1} K_{01} - K_{10} K_{-1-1}) \right] \\ - K_{10} K_{0-1} - K_{-10} K_{01} + K_{00} K_{-11} + K_{00} K_{1-1} \quad (\text{B.5})$$

$$C = K_{1-1} K_{-10} K_{01} + K_{-1-1} K_{00} K_{11} - K_{-10} K_{0-1} K_{11} \\ + K_{10} K_{-11} K_{0-1} - K_{-1-1} K_{01} K_{10} - K_{1-1} K_{-11} K_{00} \quad (\text{B.6})$$

Similarly, in cylindrical $(n_{\perp}, \varphi, n_z)$ coordinates

$$\Lambda(\omega) = \begin{vmatrix} \frac{1}{2} n_{\perp}^2 + n_z^2 - K_{1-1} & -\frac{1}{2} n_{\perp}^2 e^{i2\varphi} - K_{11} & -2^{-\frac{1}{2}} n_{\perp} n_z e^{i\varphi} - K_{10} \\ -\frac{1}{2} n_{\perp}^2 e^{-i2\varphi} - K_{-1-1} & \frac{1}{2} n_{\perp}^2 + n_z^2 - K_{-11} & -2^{-\frac{1}{2}} n_{\perp} n_z e^{-i\varphi} - K_{-10} \\ -2^{-\frac{1}{2}} n_{\perp} n_z e^{-i\varphi} - K_{0-1} & -2^{-\frac{1}{2}} n_{\perp} n_z e^{i\varphi} - K_{01} & n_{\perp}^2 - K_{00} \end{vmatrix} \\ = 0, \quad (\text{B.7})$$

and we obtain a polynomial in n_{\perp}

$$\alpha n_{\perp}^4 + \alpha' n_{\perp}^3 + \beta n_{\perp}^2 + \beta' n_{\perp} + \mathcal{C} = 0 \quad (\text{B.8})$$

where

$$\alpha = -\frac{1}{2}(K_{1-1} + K_{-11}) - \frac{1}{2}(e^{-i2\varphi} K_{11} + e^{i2\varphi} K_{-1-1}) \quad (\text{B.9})$$

$$\alpha' = -n_{\perp}^2 2^{-\frac{1}{2}} [(K_{-10} + K_{0-1}) e^{i\varphi} + (K_{01} + K_{10}) e^{-i\varphi}] \quad (\text{B.10})$$

$$\begin{aligned} \beta = n_{\perp}^2 [-K_{00} - \frac{1}{2}(K_{1-1} + K_{-11}) + \frac{1}{2}(-e^{-i2\varphi} K_{11} - e^{i2\varphi} K_{-1-1})] + \\ \frac{1}{2}[K_{-11} K_{00} + K_{1-1} K_{00} - K_{-10} K_{01} - K_{0-1} K_{10} + 2K_{-11} K_{1-1} - 2K_{-1-1} K_{11} + \\ (K_{-1-1} K_{00} - K_{-10} K_{0-1}) e^{i2\varphi} + (K_{11} K_{00} - K_{01} K_{10}) e^{-i2\varphi}] \quad (\text{B.11}) \end{aligned}$$

$$\begin{aligned} \beta' = -n_{\perp}^3 2^{-\frac{1}{2}} [(K_{-10} + K_{0-1}) e^{i\varphi} + (K_{01} + K_{10}) e^{-i\varphi}] + \\ n_{\perp}^2 2^{-\frac{1}{2}} [(K_{01} K_{1-1} - K_{0-1} K_{11} - K_{-10} K_{11} + K_{-11} K_{10}) e^{-i\varphi} + \\ (K_{-10} K_{1-1} - K_{-1-1} K_{01} + K_{-11} K_{0-1} - K_{-1-1} K_{10}) e^{i\varphi}] \quad (\text{B.12}) \end{aligned}$$

$$\begin{aligned} \mathcal{C} = -n_{\perp}^4 K_{00} + n_{\perp}^2 [K_{-11} K_{00} + K_{1-1} K_{00} - K_{-10} K_{01} - K_{0-1} K_{10}] + \\ [K_{-11} K_{0-1} K_{10} - K_{-11} K_{00} K_{1-1} + K_{-10} K_{01} K_{1-1} + K_{11} K_{-1-1} K_{00} \\ - K_{11} K_{-10} K_{0-1} - K_{-1-1} K_{01} K_{10}] . \quad (\text{B.13}) \end{aligned}$$

Cold Plasma Dielectric Tensor

Assuming that $\nabla \cdot \underline{\underline{P}}_s \equiv 0$ and neglecting collision effects, the momentum equation (2.5 2) becomes

$$\partial \underline{V}_s / \partial t = q_s m_s^{-1} (\underline{E} + \underline{V}_s \times \underline{B}_0), \quad (\text{B.14})$$

or, if we are working with the Fourier-analyzed equation (2.55),

$$-i\omega \underline{\underline{\gamma}}_{s\nu} = q_s m_s^{-1} (\underline{\underline{\mathcal{E}}}_\nu - i\nu \omega_{bs} \underline{\underline{\gamma}}_{s\nu}). \quad (\text{B.15})$$

The mobility tensor $\underline{\underline{\mu}}_s$ follows straightforwardly by solving the force equation for $\underline{\underline{\gamma}}_s$ in terms of $\underline{\underline{\mathcal{E}}}$. This results in the following diagonal mobility tensor

$$\underline{\underline{\mu}}_s = i q_s (m_s \omega)^{-1} \begin{bmatrix} (1-Y_s)^{-1} & 0 & 0 \\ 0 & (1+Y_s)^{-1} & 0 \\ 0 & 0 & 1 \end{bmatrix} \quad (\text{B.16})$$

where

$$Y_s \equiv q_s B_0 / m_s \omega = \omega_{bs} / \omega. \quad (\text{B.17})$$

From our relation between the dielectric tensor $\underline{\underline{K}}$ and the mobility tensor $\underline{\underline{\mu}}_s$, i.e. eqn. (2.6 2), we find that

$$\underline{\underline{K}} = \begin{bmatrix} 1 - \sum_s X_s (1-Y_s)^{-1} & 0 & 0 \\ 0 & 1 - \sum_s X_s (1+Y_s)^{-1} & 0 \\ 0 & 0 & 1 - \sum_s X_s \end{bmatrix} \quad (\text{B.18})$$

where

$$X_s = N_{s0} q_s^2 / \epsilon_0 m_s \omega^2. \quad (\text{B.19})$$

It should be noted that the reason $\underline{\underline{K}}$ has the simple diagonal form shown is because we have chosen to express our equations in terms of Polarized-Wave space. We find that many of the equations relating to phenomena in anisotropic plasma are greatly simplified when expressed in terms of P-W space. We have expressed the dielectric tensor using the normalized gyro, Y_s , and normalized plasma, X_s , frequencies. In order to avoid confusion when comparing our equations to those given elsewhere, one should note that our definition of Y_s includes the sign of the charge of g_s . The dielectric tensor given here is usually referred to as the cold plasma dielectric tensor.

Cold Plasma Dispersion Relation

Having obtained the explicit expression for the cold plasma dielectric tensor in the previous section we can substitute this into (B.3) - (B.6). The result is

$$a n^4 + \beta n^2 + c = 0 \quad (\text{B.20})$$

with the coefficients a , β , and c simplifying to

$$a = -K_{\perp} \sin^2 \vartheta - K_{\text{O}} \cos^2 \vartheta \quad (\text{B.21})$$

$$\beta = (K_1 K_{-1} - K_{\text{O}} K_{\perp}) \sin^2 \vartheta + 2 K_{\text{O}} K_{\perp} \quad (\text{B.22})$$

$$c = -K_1 K_{-1} K_{\text{O}} \quad (\text{B.23})$$

where

$$K_{\nu} \equiv 1 - \sum_S X_S (1 - \nu Y_S)^{-1} \quad (\text{B.24})$$

and

$$K_{\perp} = \frac{1}{2} (K_1 + K_{-1}) \quad (\text{B.25})$$

This is usually referred to as the cold-plasma dispersion relation.

Now cutoffs are defined by $n^2 = 0$ while resonances are defined by $n^2 = \infty$. The principal cutoffs and resonances correspond to $\vartheta = 0$ and $\vartheta = \pi/2$. Setting $\vartheta = 0$ and $\pi/2$ and solving the resulting forms of the dispersion relation yields the following table of cutoffs and resonances.

TABLE 2
PRINCIPAL CUTOFFS AND RESONANCES FOR A COLD PLASMA

	CUTOFFS	RESONANCES
$\vartheta = 0$	$K_1 = 0, K_{-1} = 0, K_{\text{O}} = 0$	$K_1 = \infty, K_{-1} = \infty$
$\vartheta = \pi/2$	$K_1 = 0, K_{-1} = 0, K_{\text{O}} = 0$	$K_{\perp} = 0$

CMA Diagram

The CMA diagram is a convenient tool for presenting much of the information contained within the cold plasma dispersion relation of the previous section. The letters CMA refer to Clemmow, Mullaly and Allis who introduced the method of analyzing the dispersion relation which we are going to discuss in this section [11], [3].

The CMA diagram is a plot of the principal resonances and cutoffs in X_e, Y_e^2 coordinates. The result is that the X_e, Y_e^2 plane will be divided into a finite number of regions. Within each region the topology of the refractive index surface is the same [74].

For a two-component ion-electron cold plasma the subscript s takes on the values e , for electrons, and i , for ions. From our definition of Y_s , it follows that $Y_i = -Y_e m_e / m_i$. Hence, for a two species plasma the components of the dielectric tensor become

$$K_o = 1 - X_e (1 + m_e / m_i) \quad (\text{B.26})$$

$$K_1 = 1 - X_e \left[(1 - Y_e)^{-1} + m_e (m_i + Y_e m_e)^{-1} \right] \quad (\text{B.27})$$

$$K_{-1} = 1 - X_e \left[(1 + Y_e)^{-1} + m_e (m_i - Y_e m_e)^{-1} \right] \quad (\text{B.28})$$

and also

$$K_{\perp} = 1 - X_e \left[(1 - Y_e^2)^{-1} + m_i m_e (m_i^2 - Y_e^2 m_e^2)^{-1} \right]. \quad (\text{B.29})$$

For the range of the parameters shown in Figure 20, we can approximate K_o, K_1, K_{-1} , and K_{\perp} very well by

$$K_o \approx 1 - X_e \quad (\text{B.30})$$

$$K_1 \approx 1 - X_e (1 - Y_e)^{-1} \quad (\text{B.31})$$

$$K_{-1} \approx 1 - X_e (1 + Y_e)^{-1} \quad (\text{B.32})$$

$$K_{\perp} \approx 1 - X_e (1 - Y_e^2)^{-1} \quad (\text{B.33})$$

since $m_e \ll m_i$. Figure 20 shows the principal resonances and cutoffs in this high frequency regime. The various regions of the CMA diagram have arbitrarily been numbered for later reference.

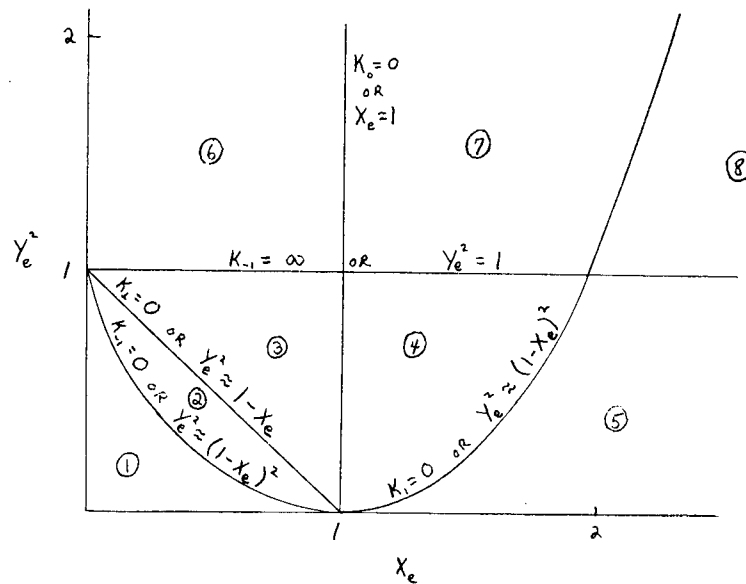


Fig. 20. Graph of principal cutoffs and resonances for high frequencies

At these high frequencies the curves for the principal cutoffs and resonances become nearly straight lines or parabolas.

Figure 21 is a plot of the principal cutoffs and resonances for the hydrogen-electron plasma for the frequencies $Y_e^2 \geq 1$, $X_e \geq 1$. The axes are log-log scale and the various regions have been arbitrarily numbered.

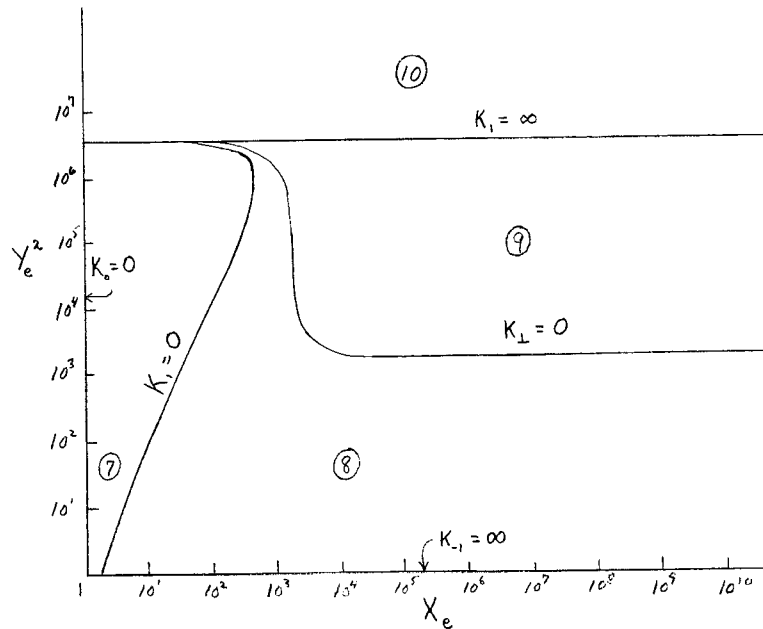


Fig. 21 . Graph of principal cutoffs and resonances
for $X_e \geq 1$ and $Y_e^2 \geq 1$.

The various principal resonances and cutoffs have names which are given in Table 3.

TABLE 3
NAMES OF PRINCIPAL CUTOFFS AND RESONANCES

Curve	Name
$K_1 = 0$	Ion cyclotron cutoff
$K_{-1} = 0$	Electron cyclotron cutoff
$K_0 = 0$	Plasma cutoff
$K_1 = \infty$	Ion gyro-resonance
$K_{-1} = \infty$	Electron gyro-resonance
$K_1 = 0 (Y_e^2 \leq 1)$	Upper hybrid resonance (UHR)
$K_1 = 0 (Y_e^2 > 1)$	Lower hybrid resonance (LHR)

We indicated earlier that within each of the numbered regions of the CMA diagram the topology of the wave phase velocity surface is unchanged. Table 4 lists sketches of the phase velocity surfaces along with the corresponding refractive index surfaces for the regions of the CMA diagram which we have shown. The magnitude of the refractive index is simply given by the reciprocal of the magnitude of the wave phase velocity times the velocity of light in a vacuum. The dashed circles represent reference surfaces for waves propagating in free space. In Table 4, the magnetic field \underline{B}_0 is assumed to be pointing vertically upwards. R and L refer to right and left circularly polarized waves while O and X refer to ordinary and extraordinary waves.

TABLE 4
 PHASE VELOCITY AND REFRACTIVE INDEX SURFACES
 FOR VARIOUS REGIONS OF THE CMA DIAGRAM

Region	Phase Velocity Surfaces	Refractive Index Surfaces
1		
2		
3		
4		
5		
6		
7		
8		
9		
10		

Ray Direction in Anisotropic Plasmas

For a cold lossless magnetoplasma the direction of energy flow associated with a given plane wave propagating at an angle ϑ with respect to the magnetic field is given by the perpendicular to the refractive index surface for that wave together with the requirement that the angle α between the group velocity and the phase velocity (or \underline{n}) be an acute angle [20]. However, for more complicated plasma models this may be an obtuse angle as is evidenced by the work by Bitoun et. al [8]. In such cases the ambiguity as to the sense of \underline{V}_g can be resolved by determining the sign of $(\partial\omega / \partial k)$.

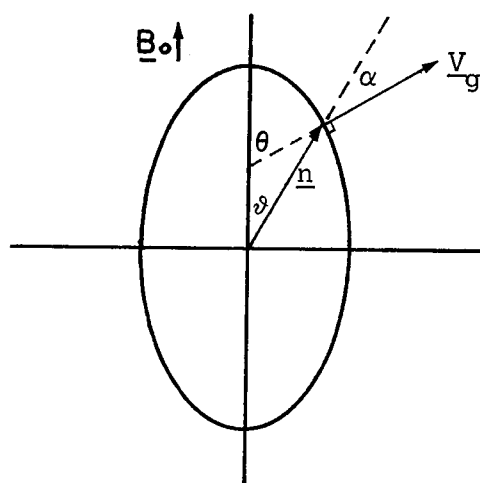


Fig. 32 . Geometrical relation between direction of the group velocity and the refractive index surface

The angles α and ϑ shown in Figure 32 are related by [74]

$$\tan \alpha = - \frac{1}{n} \frac{\partial n}{\partial \vartheta} \quad (\text{B.34})$$

where the angle α is taken to be positive if the vector \underline{n} lies between \underline{V}_g and \underline{B}_0 [75]. Therefore for a given propagating plane wave, the angle θ at which the ray propagates is given by

$$\theta = \vartheta + \alpha . \quad (\text{B.35})$$

For a cold plasma we showed in the previous section that the dispersion equation can be written

$$A n^4 + B n^2 + C = 0 \quad (\text{B.36})$$

where

$$A = -K_{\perp} \sin^2 \vartheta - K_{\text{O}} \cos^2 \vartheta \quad (\text{B.37})$$

$$B = K_{\perp} K_{-1} \sin^2 \vartheta + K_{\text{O}} K_{\perp} (1 + \cos^2 \vartheta) \quad (\text{B.38})$$

$$C = -K_{\perp} K_{-1} K_{\text{O}} . \quad (\text{B.39})$$

Using this dispersion equation we get after taking $\frac{\partial}{\partial \vartheta}$

$$\frac{\partial A}{\partial \vartheta} n^4 + 4 n^3 \frac{\partial n}{\partial \vartheta} A + \frac{\partial B}{\partial \vartheta} n^2 + 2n \frac{\partial n}{\partial \vartheta} B + \frac{\partial C}{\partial \vartheta} = 0 . \quad (\text{B.40})$$

Since $\frac{\partial C}{\partial \vartheta} = 0$, this simplifies, after dividing through by n^2 , to

$$\frac{\partial A}{\partial \vartheta} n^2 + 4 n^2 \frac{1}{n} \frac{\partial n}{\partial \vartheta} A + \frac{\partial B}{\partial \vartheta} + 2B \frac{1}{n} \frac{\partial n}{\partial \vartheta} = 0 . \quad (\text{B.41})$$

Solving for $\frac{1}{n} \frac{\partial n}{\partial \vartheta}$ gives

$$\frac{1}{n} \frac{\partial n}{\partial \vartheta} = - \frac{\frac{\partial A}{\partial \vartheta} n^2 + \frac{\partial B}{\partial \vartheta}}{4A n^2 + 2B} . \quad (\text{B.42})$$

From (B.37) and (B.38)

$$\frac{\partial A}{\partial \vartheta} = (K_{\text{O}} - K_{\perp}) 2 \sin \vartheta \cos \vartheta \quad (\text{B.43})$$

$$\frac{\partial B}{\partial \vartheta} = (K_{\perp} K_{-1} - K_{\text{O}} K_{\perp}) 2 \sin \vartheta \cos \vartheta \quad (\text{B.44})$$

Hence,

$$\tan \alpha = \left[(K_{\text{O}} - K_{\perp}) n^2 + K_{\perp} K_{-1} - K_{\text{O}} K_{\perp} \right] 2 \sin \vartheta \cos \vartheta$$

$$\left[-4 n^2 (K_{\perp} \sin^2 \vartheta + K_{\text{O}} \cos^2 \vartheta) + 2 K_{\perp} K_{-1} \sin^2 \vartheta \right.$$

$$\left. + 2 K_{\text{O}} K_{\perp} (1 + \cos^2 \vartheta) \right]^{-1} . \quad (\text{B.45})$$

Thus for a cold plasma we have a rather simple formula for determining group velocity direction as a function of ϑ when the components of the dielectric tensor are known. For our numerical studies we use a similar method to find the direction of \underline{V}_{g} for a warm plasma. For our warm plasma Models A and H, equation (B.36) is replaced by (G.17) and (G.5) respectively. As noted by Allis, et. al. [2], \underline{V}_{g} corresponds to the direction of the sum of the Poynting flux and the acoustic energy flux in a warm plasma.

APPENDIX C

ADJOINT MATRIX

The equation which relates the excitation current $\underline{j}^{(ex)}$ to the excited field $\underline{\delta}$ is the "wave equation"

$$\Lambda_{\nu-\sigma} \delta_{\sigma} = i(\epsilon_0 \omega)^{-1} j_{\nu}^{(ex)} \quad (C.1)$$

where the "wave matrix" $\underline{\Lambda}$ is given by

$$\Lambda_{\nu-\sigma} = n^2 L_{\nu-\sigma} - n_{\nu} n_{-\sigma} - K_{\nu-\sigma}. \quad (C.2)$$

Solving for the electric field, we have

$$\delta_{\sigma} = i(\epsilon_0 \omega \Lambda)^{-1} \alpha_{\sigma-\nu} j_{\nu}^{(ex)}. \quad (C.3)$$

Here $(\alpha_{\sigma-\nu})$ is the adjoint matrix of $(\Lambda_{\nu-\sigma})$ and Λ is the determinant of $(\Lambda_{\nu-\sigma})$.

The purpose of the present section is to analyze the explicit forms of the adjoint matrix for Models H and A. Note that these models differ only in the explicit expressions used for the dielectric tensor components $K_{\nu-\sigma}$.

Before we consider each model separately, we shall discuss some properties of the adjoint matrix which are common to both. Using cylindrical $(n_{\perp}, \varphi, n_z)$ coordinates, the φ dependence of $\Lambda_{\nu-\sigma}$ is simply given by $e^{i(\nu-\sigma)\varphi}$ for all models. Therefore the adjoint $\alpha_{\sigma-\nu}$ varies like $e^{i(\sigma-\nu)\varphi}$ while the determinant Λ is independent of φ . Separating the φ dependence, in the adjoint, we can write

$$\alpha_{\sigma-\nu}(n_{\perp}, \varphi, n_z) = \lambda_{\sigma-\nu}(n_{\perp}, n_z) e^{i(\sigma-\nu)\varphi}. \quad (C.4)$$

Hence, the electric field \mathcal{E}_ν can be written

$$\mathcal{E}_\nu = i(\epsilon_0 \omega \Lambda)^{-1} e^{i(\nu-\sigma)\varphi} \lambda_{\nu-\sigma} \mathcal{E}_\sigma^{(ex)}. \quad (C.5)$$

The matrix $(\lambda_{\sigma-\nu})$ is the adjoint of $(\Lambda'_{\nu-\sigma})$ where the latter matrix is defined by the equation

$$\Lambda_{\nu-\sigma} = \Lambda'_{\nu-\sigma} e^{i(\nu-\sigma)\varphi}. \quad (C.6)$$

That is, $\Lambda'_{\nu-\sigma}$ is $\Lambda_{\nu-\sigma}$ with the φ dependence removed. In many cases $(\Lambda'_{\nu-\sigma})$ is a symmetric matrix and in these cases $(\lambda_{\nu-\sigma})$ is also symmetric.

In addition, for each of our models the following symmetry holds $K_{\nu-\sigma}(\underline{n}, \omega) = K_{-\nu\sigma}^*(\underline{n}, -\omega)$. Therefore, it follows that we also have $\lambda_{\nu-\sigma}(\underline{n}, \omega) = \lambda_{-\nu\sigma}^*(\underline{n}, -\omega)$. If λ is written in terms of \underline{k} instead of \underline{n} , then \underline{k} must change sign also when using these symmetry relations. These symmetry properties of the matrix $(\lambda_{\nu-\sigma})$ reduce to only four or five the number of components of this matrix which must be worked out in detail. Consequently, there results an enormous savings of computational labor. For example, if we compute λ_{1-1} , λ_{11} , λ_{10} and λ_{00} explicitly and the adjoint matrix $\underline{\lambda}$ is symmetric, then the remaining components can be obtained from the relations $\lambda_{-1-1}(\underline{n}, \omega) = \lambda_{1-1}^*(\underline{n}, -\omega)$, $\lambda_{-1-1} = \lambda_{11}$, $\lambda_{0-1} = \lambda_{10}$, $\lambda_{-10}(\underline{n}, \omega) = \lambda_{10}^*(\underline{n}, -\omega)$ and $\lambda_{01} = \lambda_{-10}$.

The Adjoint Matrix for Model H

We are going to give here the explicit expressions for the components of the adjoint matrix using the dielectric tensor of Model H. More precisely, we are going to give the components of the matrix obtained by multiplying the adjoint matrix $(\lambda_{\nu-\sigma})$ by $D_e D_i$ where, you recall, we had (4.15)

$$D_s = 1 - \epsilon_s (n_1^2 g_{sx} + n_z^2), \quad (s = e \text{ or } i). \quad (C.7)$$

The reason for multiplying each adjoint element by $D_e D_i$ is to obtain simple polynomials in n_{\perp} , whereas the adjoint elements by themselves, are more complicated functions of n_{\perp} .

Using the definition of $\lambda_{\nu-\sigma}$ along with our expressions for the dielectric tensor \underline{K} for Model H (Chapter IV), and applying some matrix algebra we find that we can write

$$\begin{aligned} D_e D_i \lambda_{\nu-\sigma} &= \lambda_{\nu-\sigma}^0 + \sum \epsilon_s [-(n_{\perp}^2 g_{sx} + n_z^2) \lambda_{\nu-\sigma}^0 + \alpha_s^2 \lambda'_{s\nu-\sigma}] + \\ &\quad \epsilon_e \epsilon_i (n_{\perp}^2 g_{ex} + n_z^2) (n_{\perp}^2 g_{ix} + n_z^2) \lambda_{\nu-\sigma}^0 + \\ &\quad \{ \epsilon_e \epsilon_i \alpha_e^2 [\alpha_i^2 \lambda''_{e\nu-\sigma} - (n_{\perp}^2 g_{ix} + n_z^2) \lambda'_{e\nu-\sigma}] + \{e \leftrightarrow i\} \}. \quad (C.8) \end{aligned}$$

The quantity $(\lambda_{\nu-\sigma}^0)$ is the adjoint matrix one would obtain for a cold incompressible plasma. Explicitly, it is obtained from

$$\lambda_{1-1}^0 = \frac{1}{2} n_{\perp}^4 + n_{\perp}^2 \left[\frac{1}{2} n_z^2 - K_{-1} - \frac{1}{2} K_0 \right] - n_z^2 K_0 + K_{-1} K_0 \quad (C.9)$$

$$\lambda_{00}^0 = n_{\perp}^2 \left[n_z^2 - K_{\perp} \right] + n_{\perp}^4 - 2 n_z^2 K_{\perp} + K_{\perp} K_{-1} \quad (C.10)$$

$$\lambda_{11}^0 = \frac{1}{2} n_{\perp}^4 + \frac{1}{2} n_{\perp}^2 (n_z^2 - K_0) \quad (C.11)$$

$$\lambda_{10}^0 = 2^{-\frac{1}{2}} n_{\perp}^3 n_z + 2^{-\frac{1}{2}} n_{\perp} n_z (n_z^2 - K_{-1}) . \quad (C.12)$$

Note that $D_e D_i \lambda_{\nu-\sigma}$ is written in such a form that we can use it for dealing either with cold plasmas ($\epsilon_e = \epsilon_i = 0$) or single component warm plasmas ($\epsilon_e \neq 0, \epsilon_i = 0$) or two component warm plasmas ($\epsilon_e \neq 0, \epsilon_i \neq 0$).

For the temperature dependent part of $D_e D_i (\lambda_{\nu-\sigma})$ we have

$$\lambda'_{S1-1} = \frac{1}{2} n_{\perp}^4 g_{S+}^2 + \frac{1}{2} n_{\perp}^2 \left[n_Z^2 (1 + 2 g_{S+}) - K_0 g_{S+}^2 \right] + n_Z^2 (n_Z^2 - K_{-1}) \quad (C.13)$$

$$\lambda'_{S\infty} = n_{\perp}^4 g_{SX}^2 + \frac{1}{2} n_{\perp}^2 \left[n_Z^2 (g_{S+}^2 + g_{S-}^2) - K_1 g_{S+}^2 - K_{-1} g_{S-}^2 \right] \quad (C.14)$$

$$\lambda'_{S11} = -\frac{1}{2} n_{\perp}^4 g_{SX}^2 + \frac{1}{2} n_{\perp}^2 \left[n_Z^2 (1 - 2 g_{SX}) + K_0 g_{SX} \right] \quad (C.15)$$

$$\lambda'_{S10} = 2^{-3/2} n_{\perp}^3 n_Z (-3 g_{SX} + g_{S+}^2) - 2^{-\frac{1}{2}} n_{\perp} n_Z (n_Z^2 - K_{-1}) g_{S-}. \quad (C.16)$$

In addition,

$$\lambda''_{e1-1} = \frac{1}{2} n_{\perp}^2 n_Z^2 g_{e+} (g_{e+} - g_{i+}) \quad (C.17)$$

$$\lambda''_{e00} = \frac{1}{4} n_{\perp}^4 (g_{e-}^2 - g_{i+}^2 - g_{ex} g_{ix}) \quad (C.18)$$

$$\lambda''_{e11} = \frac{1}{2} n_{\perp}^2 n_Z^2 g_{e-} (g_{i+} - g_{e+}) \quad (C.19)$$

$$\lambda''_{e10} = 2^{-3/2} n_{\perp}^3 n_Z g_{i+} g_{e-} (g_{e+} - g_{i+}). \quad (C.20)$$

These expressions give us the explicit forms for $D_e D_i \lambda_{1-1}$, $D_e D_i \lambda_{00}$, $D_e D_i \lambda_{11}$, $D_e D_i \lambda_{10}$. The remaining components can be easily obtained by use of the symmetry properties of $\underline{\lambda}$. In particular note that $\underline{\lambda}$ is a symmetric matrix for Model H.

The Adjoint Matrix for Model A

The adjoint matrix for Model A is obtained by forming the adjoint of the matrix $\underline{\underline{A}}$ ' given by equations (C.6) and (C.2). The dielectric tensor to be used here in the expression for $\underline{\underline{A}}$ ' is the one derived for Model A, that is, equation (4.56).

Defining the quantities¹

$$\begin{aligned}
 a_{1-1} &= 2 \sum X_s g_{s-} g_{s-2} (d_{s\parallel} + d_{s\Delta}) \\
 c_{1-1} &= \sum X_s g_{s-}^2 (d_{s\parallel} g_{s-} + d_{s\Delta}) \\
 a_{00} &= \sum X_s g_{sx} d_{s\parallel}, \quad c_{00} = 3 \sum X_s d_{s\parallel} \\
 a_{11} &= \sum X_s g_{sx} (d_{s\parallel} + d_{s\Delta}) \\
 b_{10} &= \frac{1}{\sqrt{2}} \sum X_s g_{s-} \{ d_{s\parallel} (1 + g_{s-}) + d_{s\Delta} \}
 \end{aligned} \tag{C.21}$$

the explicit expressions for the components of the adjoint matrix $\underline{\underline{A}}$, for the case of a lossless plasma retaining only terms to first order in temperature, are the following

$$\begin{aligned}
 \lambda_{1-1} &= \lambda_{1-1}^0 + n_{\perp}^4 \left\{ \frac{1}{2} (a_{00} + a_{-11}) \right\} \\
 &\quad + n_{\perp}^2 \left\{ n_z^2 [(1-K_{-1}) a_{00} - K_0 a_{-11} + 2^{\frac{1}{2}} b_{-10} + \frac{1}{2} c_{00} + c_{-11}] \right\} \\
 &\quad + n_z^4 c_{00} - n_z^2 [K_0 c_{-11} + K_{-1} c_{00}]
 \end{aligned} \tag{C.22}$$

$$\begin{aligned}
 \lambda_{00} &= \lambda_{00}^0 + n_{\perp}^4 \left\{ \frac{1}{2} (a_{1-1} + a_{-11}) + a_{11} \right\} \\
 &\quad + n_{\perp}^2 \left\{ n_z^2 [(1-K_1) a_{-11} + (1-K_{-1}) a_{1-1} + \frac{1}{2} (c_{1-1} + c_{-11})] \right\} \\
 &\quad + n_z^4 [c_{1-1} + c_{-11}] - n_z^2 [K_1 c_{-11} + K_{-1} c_{1-1}]
 \end{aligned} \tag{C.23}$$

$$\begin{aligned}
 \lambda_{11} &= \lambda_{11}^0 + n_{\perp}^4 \left\{ \frac{1}{2} a_{00} - a_{11} \right\} \\
 &\quad + n_{\perp}^2 \left\{ n_z^2 \left[-2^{-\frac{1}{2}} (b_{10} + b_{-10}) + \frac{1}{2} c_{00} \right] \right\} + k_0 a_{11}
 \end{aligned} \tag{C.24}$$

$$\begin{aligned}
 \lambda_{10} &= \lambda_{10}^0 + n_{\perp}^3 \left\{ n_z \left[2^{-\frac{1}{2}} (a_{-11} - a_{11}) - \frac{1}{2} (b_{10} + b_{-10}) \right] \right\} \\
 &\quad + n_{\perp} \left\{ n_z^3 \left[-b_{10} + 2^{-\frac{1}{2}} c_{-11} \right] + n_z K_{-1} b_{10} \right\}
 \end{aligned} \tag{C.25}$$

The remaining components are obtained via the usual symmetry relations, noting also that for the lossless plasma $\underline{\underline{K}}$ and hence $\underline{\underline{\lambda}}$ is symmetric.

¹ These quantities obey the symmetry property $a_{\nu-\sigma}(\omega) = a_{-\nu\sigma}^*(-\omega)$ with similar relations for $b_{\nu-\sigma}$ and $c_{\nu-\sigma}$.

APPENDIX D

EVALUATION OF SELECTED INTEGRALS

A Useful Integral

$$\int_0^{\infty} dx x^{\ell+1} J_s(ax) J_t(ax) / \prod_m^n (x^2 - z_m^2) = \frac{1}{2} \pi i \sum_j^n z_j^{\ell} J_s(az_j) \left[\prod_{m \neq j}^n (z_j^2 - z_m^2) \right]^{-1} \times \begin{cases} H_t^{(1)}(az_j), \text{Im } z_j > 0 \\ (-)H_t^{(2)}(az_j), \text{Im } z_j < 0 \end{cases} \quad (\text{D.1})$$

provided $\ell+s-t$ is an even integer and $|t| - |s| - 2 < \ell < 2n-1$

and $|z_m|$ is bounded.

Proof. Following Watson [85, page 428], we first consider the integral

$$\int_c f(z) dz \text{ where } f(z) \equiv z^{\ell+1} J_s(az) H_t^{(1)}(az) / \prod_m^n (z^2 - z_m^2) \quad (\text{D.2})$$

and the integral is evaluated over the contour $c = c_+ + c_R + c_- + c_r$ shown in Figure 23.

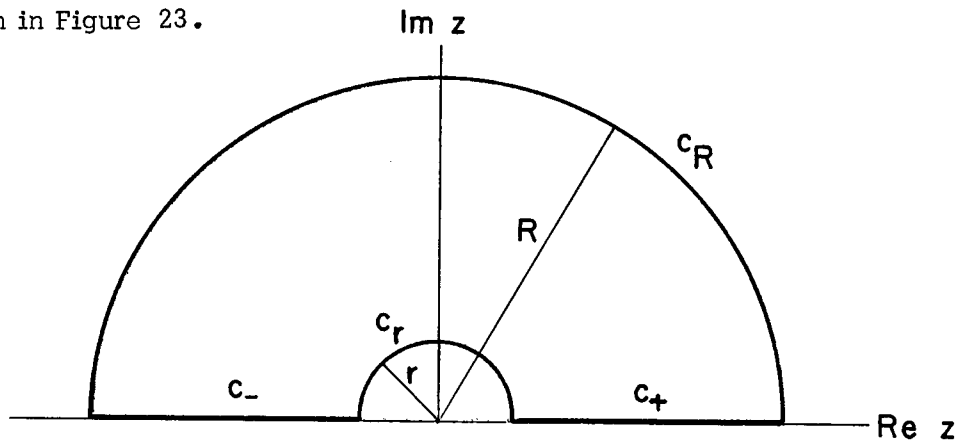


Fig. 23 . Integration Path for the Integral (D.2)

The advantage of choosing this particular contour lies in the property that, under certain conditions, the integral over the large semi-circle vanishes as $R \rightarrow \infty$ while the integral over the small semi-circle vanishes as $r \rightarrow 0$. In order to determine the range of parameters for which this occurs, we need the expansions of the Bessel functions for both small and large arguments. For integer s and $|w| \ll 1$, we have

$$J_s(w) \approx (w/2)^s / s! \quad , \quad s \geq 0 . \quad (D.3)$$

Since, for integer s ,

$$J_{-s}(w) = (-1)^s J_s(w) \quad , \quad s > 0 , \quad (D.4)$$

then for negative integer orders, the small argument expansion of $J_{-s}(w)$ is simply

$$J_{-s}(w) \approx (-1)^s (w/2)^s / s! \quad , \quad s > 0 . \quad (D.5)$$

The Hankel function $H_t^{(1)}$ is related to the ordinary Bessel function J_t and the Neumann function N_t by the equations

$$H_t^{(1)} = J_t + i N_t . \quad (D.6)$$

Since, for very small arguments, $H_t^{(1)}$ varies essentially like $i N_t$, we can use the small argument expansion of N_t , for t an integer, to write

$$H_t^{(1)}(w) \approx -i \pi^{-1} (t-1)! (2/w)^t \quad , \quad t > 0 \quad (D.7)$$

$$H_0^{(1)}(w) \approx i 2\pi^{-1} [\ln(w/2) + C] \quad (D.8)$$

where C here is the Euler-Mascheroni constant.

Using the relation

$$H_{-t}^{(1)} = e^{i t \pi} H_t^{(1)} \quad (\text{D.9})$$

allows us to write

$$H_{-t}^{(1)}(w) \approx -i \pi^{-1} (t-1)! e^{i t \pi} (2/w)^t, \quad t > 0. \quad (\text{D.10})$$

For $|w| \rightarrow \infty$, $|w| \gg |s|$, and $|\arg w| < \pi$ we can use the asymptotic expressions for the Bessel functions,

$$J_{\pm s}(w) \sim (2/\pi w)^{\frac{1}{2}} \cos(w \mp \pi s/2 - \pi/4), \quad s \geq 0 \quad (\text{D.11})$$

$$H_t^{(1)}(w) \sim (2/\pi w)^{\frac{1}{2}} \exp[i(w - \pi t/2 - \pi/4)], \quad t > -\frac{1}{2}. \quad (\text{D.12})$$

For negative integer orders, we have

$$H_{-t}^{(1)}(w) \sim (2/\pi w)^{\frac{1}{2}} \exp[i(w + \pi t/2 - \pi/4)], \quad t > -\frac{1}{2}. \quad (\text{D.13})$$

Note that

$$\lim_{R \rightarrow \infty} H_t^{(1)}(R e^{+i\vartheta}) = 0 \quad (\text{D.14})$$

if $0 \leq \vartheta < \pi$, that is, $H_t^{(1)}$ vanishes over the large semi-circle in the upper half plane.

Inserting the small argument expansions into the integral over c_r we find that

$$\begin{aligned} \left| \int_{c_r} f(z) dz \right| &\leq \int_{c_r} |f(z)| |dz| \\ &\leq \text{const} \begin{cases} r^{\ell+2+|s|-|t|}, & t \neq 0 \\ r^{\ell+2+|s|} \ll r, & t = 0. \end{cases} \end{aligned} \quad (\text{D.15})$$

Therefore

$$\lim_{r \rightarrow 0} \int_{C_r} f(z) dz = 0, \text{ if } \ell > |t| - |s| - 2. \quad (\text{D.16})$$

Similarly, for the integration over the contour using the asymptotic expansions, we get

$$\left| \int_{C_R} f(z) dz \right| \leq \text{const} * R^{\ell+1-2n} \quad (\text{D.17})$$

Therefore

$$\lim_{R \rightarrow \infty} \int_{C_R} f(z) dz = 0 \text{ if, } \ell < 2n - 1. \quad (\text{D.18})$$

We consider two cases corresponding to whether a particular root z_j has a positive or negative imaginary part. If z_j is pure real, we consider the contours passing either above or below the singularity z_j . If z_j lies in the upper half plane the integral (D.2) becomes

$$\pi i z_j^\ell J_s(a z_j) H_t^{(1)}(a z_j) / \prod_{m \neq j}^n (z_j^2 - z_m^2) + 2\pi i (\text{sum of residues at other poles}). \quad (\text{D.19})$$

When z_j lies in the lower half plane $-z_j$ falls in the upper half plane and (D.2) becomes

$$\pi i (-z_j)^\ell J_s(-a z_j) H_t^{(1)}(-a z_j) / \prod_{m \neq j}^n (z_j^2 - z_m^2) + 2\pi i (\text{sum of residues at other poles}). \quad (\text{D.20})$$

Making use of the symmetry relations (H.21) and (H.22) with s and t integers, (D.20) becomes

$$-\pi i (-)^{\ell+s+t} z_j^\ell J_s(a z_j) H_t^{(2)}(a z_j) / \prod_{m \neq j}^n (z_j^2 - z_m^2) + 2\pi i (\text{sum of other residues}). \quad (\text{D.21})$$

Finally, we can write

$$\int_{\mathcal{C}} dz z^{\ell+1} J_S(az) H_t^{(1)}(az) / \prod_m^n (z^2 - z_m^2) = \int_{\mathcal{C}} f(z) dz = \pi i \sum_j^{\ell} z_j^{\ell} J_S(az_j) \\ \times \left[\prod_{m \neq j}^n (z_j^2 - z_m^2) \right]^{-1} \begin{cases} H_t^{(1)}(az_j) & , \operatorname{Im} z_j > 0 \\ (-)^{\ell+s+t+1} H_t^{(2)}(az_j) & , \operatorname{Im} z_j < 0 \end{cases} . \quad (\text{D.22})$$

To relate this answer to the integral we are trying to solve, namely,

$$\int_0^{\infty} dx x^{\ell+1} J_S(ax) J_t(ax) / \prod_m^n (x^2 - z_m^2) , \text{ we write, for } r \rightarrow 0 \text{ and } R \rightarrow \infty , \quad (\text{D.23})$$

$$\int_{\mathcal{C}} f(z) dz = \int_{-\infty}^0 f(x) dx + \int_0^{\infty} f(x) dx . \quad (\text{D.24})$$

In the integration over $x < 0$ replace x by $-x$, then we get

$$\int_{\mathcal{C}} f(z) dz = \int_0^{\infty} dx x^{\ell+1} J_S(ax) \left[H_t^{(1)}(ax) + e^{i\pi(\ell+s-t)} H_t^{(2)}(ax) \right] / \prod_m^n (x^2 - z_m^2) . \quad (\text{D.25})$$

Replacing $H_t^{(1)}$ and $H_t^{(2)}$ by $J_t \pm i N_t$ we obtain the relation

$$\int_{\mathcal{C}} f(z) dz = \int_0^{\infty} dx x^{\ell+1} J_S(ax) e^{i\pi(\ell+s-t)/2} \left[\prod_m^n (x^2 - z_m^2) \right]^{-1} \\ \times 2 \left\{ J_t(ax) \cos \left[(\ell+s-t) \pi/2 \right] + N_t(ax) \sin \left[(\ell+s-t) \pi/2 \right] \right\} . \quad (\text{D.26})$$

If $\ell+s-t$ is an even integer, then this reduces to

$$\int_{\mathcal{C}} f(z) dz = 2 \int_0^{\infty} dx x^{\ell+1} J_S(ax) J_t(ax) / \prod_m^n (x^2 - z_m^2) . \quad (\text{D.27})$$

Therefore, we finally arrive at the solution we were seeking, namely,

$$\int_0^{\infty} dx x^{\ell+1} J_s(ax) J_t(ax) / \prod_m^n (x^2 - z_m^2) = \frac{1}{2} \pi i \sum_j^n z_j^{\ell} J_s(az_j) \times \left[\prod_{m \neq j}^n (z_j^2 - z_m^2) \right]^{-1} \begin{cases} H_t^{(1)}(az_j) & , \operatorname{Im} z_j > 0 \\ (-) H_t^{(2)}(az_j) & , \operatorname{Im} z_j < 0 \end{cases} \quad (\text{D.28})$$

provided $\ell + s - t$ is an even integer and, $|t| - |s| - 2 < \ell < 2n - 1$.

Integrals Related to Weber's Second Exponential Integral

Weber's Second Exponential Integral is defined as [85, p. 395]

$$\mathcal{J} \equiv \int_0^{\infty} e^{-qt^2} J_n^2(at) t dt = (2q)^{-1} e^{-a^2/2q} I_n(a^2/2q) . \quad (\text{D.29})$$

To cut down on the amount of relatively simple algebra presented, we indicate only the METHOD of evaluation used for each integral. Also, in this section the argument of the modified Bessel function is to be understood to be given by $\mu \equiv a^2/2q$.

$$\int_0^{\infty} e^{-qt^2} J_n(at) J_n'(at) t^2 dt = (a/4q^2) e^{-\mu} [-I_n + I_n'] \quad (\text{D.30})$$

METHOD: Take $\partial \mathcal{J} / \partial a$.

$$\int_0^{\infty} e^{-qt^2} J_n^2(at) t^3 dt = (2q^2)^{-1} e^{-\mu} [(1 - \mu) I_n + \mu I_n'] \quad (\text{D.31})$$

METHOD: Take $\partial \mathcal{J} / \partial q$.

$$\int_0^{\infty} e^{-qt^2} J_n(at) J_n''(at) t^3 dt = -(2q)^{-2} e^{-\mu} [(1 - 2\mu - n^2/\mu) I_n + (1 + 2\mu) I_n'] \quad (\text{D.32})$$

METHOD: Eliminate J_n'' using Bessel's equation (H.28), and use (b.) to obtain the result shown.

$$\int_0^{\infty} e^{-qt^2} J_n^2(at) t^3 dt = (2q^2)^{-1} e^{-\mu} \left[(-n^2/2\mu) I_n + (1-\mu) I_n' + \mu I_n'' \right] \quad (\text{D.33})$$

METHOD: Form $\partial^2 \mathcal{J} / \partial a^2$ and use c.

$$\int_0^{\infty} e^{-qt^2} J_n(at) J_{n\pm 1}(at) t^2 dt = (2aq)^{-1} e^{-\mu} \left[(n \pm \mu) I_n \mp \mu I_n' \right] \quad (\text{D.34})$$

METHOD: Replace $J_{n\pm 1}(at)$ by $\mp J_n'(at) + (n/at) J_n(at)$ and use (a) and \mathcal{J} to evaluate the resultant integrals.

$$\int_0^{\infty} e^{-qt^2} J_{n+1}(at) J_{n-1}(at) t^3 dt = (\mu/2q^2) e^{-\mu} \left[I_n' - I_n \right] \quad (\text{D.35})$$

METHOD: Solve $(J_{n-1} - J_{n+1})^2 = 4 J_n^2$ for $J_{n+1} J_{n-1}$, substitute this into the original integral, and use (b) and (d).

$$\int_0^{\infty} e^{-qt^2} J_{n\pm 1}^2(at) t^3 dt = (2q^2)^{-1} e^{-\mu} \left[\pm n I_n + (1-\mu \mp n) I_n' + \mu I_n'' \right] \quad (\text{D.36})$$

METHOD: Use (b) with $n \pm 1$ replacing n , and express all modified Bessel functions in terms of n^{th} order Bessel functions using the standard recurrence relation $\mu I_{n\pm 1} = \mu I_n' \mp n I_n$.

Integrals Related to the "Plasma Dispersion Function"

The "Plasma Dispersion Function" $Z(\zeta)$ is defined by

$$Z(\zeta) \equiv \pi^{-\frac{1}{2}} \int_{-\infty}^{\infty} \frac{e^{-x^2} dx}{x - \zeta} \quad (\text{D.37})$$

for $\text{Im } \zeta > 0$ and as the analytic continuation of this for $\text{Im } \zeta \leq 0$.

The "Plasma Dispersion Function" satisfies the differential equation [22].

$$Z' = -2(1 + \zeta Z). \quad (\text{D.38})$$

This property and the definition of Z are all we need to evaluate the following integrals. As in the preceding section, we shall only indicate the METHOD of solution.

$$\int_{-\infty}^{\infty} \frac{x e^{-x^2}}{x - \zeta} dx = -\frac{1}{2} \pi^{\frac{1}{2}} Z'(\zeta) \quad (\text{D.39})$$

METHOD: Take the derivative of Z , perform an integration by parts on (a.) and compare the two results.

$$\int_{-\infty}^{\infty} \frac{x^2 e^{-x^2}}{x - \zeta} dx = -\frac{1}{2} \pi^{\frac{1}{2}} \zeta Z'(\zeta) \quad (\text{D.40})$$

METHOD: First perform two successive partial integrations on (b.) and note that the remaining integral is proportional to Z'' as obtained from our definition for Z , then eliminate Z'' by using the differential equation satisfied by Z .

APPENDIX E

SPECIAL CASE

For the special case of a non-relativistic charge spiraling in a cold collisionless plasma our formula (5.79) for the power loss simplifies to

$$P = Q^2 (4\pi \epsilon_0 |V_z| c^2)^{-1} \sum_{j \neq m} \sum_{p=-\infty}^{\infty} \int_0^{\infty} d\omega \omega \times \left| \frac{1}{2} \lambda_{-\nu} \lambda_{\sigma} e^{i(\nu-\sigma)\pi} \lambda_{\nu-\sigma} J_{p+\nu} J_{p+\sigma} [K_{\perp}(n_{\perp j}^2 - n_{\perp m}^2)]^{-1} \right| \quad (E.1)$$

where j and m represent two various modes in a plasma and n_z is to be replaced by $\beta_z^{-1} (1 + pY)$ in the integrand. The purpose of this section is to show that this formula for the power loss is equivalent to that derived by Trulsen and Fejer [80], hereafter referred to as TF, as given in their formulas on pp. 833-834.

Letting

$$\iota = \text{sgn } \Omega \quad (E.2)$$

and writing out the summations over ν and σ using the fact that $(\lambda_{\nu-\sigma})$ is a symmetric matrix for the case of a cold collisionless plasma, we obtain

$$P = Q^2 (4\pi \epsilon_0 |V_z| c^2)^{-1} \sum_{j \neq m} \sum_{p=-\infty}^{\infty} \int_0^{\infty} d\omega \omega |K_{\perp}(n_{\perp j}^2 - n_{\perp m}^2)|^{-1} \times \left[\frac{1}{2} V_{\perp}^2 \lambda_{-1} J_{p+1}^2 + V_{\perp}^2 \lambda_{11} J_{p+1} J_{p-1} - 2^{\frac{1}{2}} V_{\perp} V_z \iota \lambda_{10} J_p J_{p+1} + \frac{1}{2} V_{\perp}^2 \lambda_{-11} J_{p-1}^2 - 2^{\frac{1}{2}} V_{\perp} V_z \iota \lambda_{01} J_p J_{p-1} + V_z^2 \lambda_{00} J_p^2 \right]. \quad (E.3)$$

Eliminating the Bessel functions of the form $J_{p\pm 1}$ using the identity

$$J_{p\pm 1}(u) = \frac{p}{u} J_p \mp J'_p \quad (\text{E.4})$$

results in the expression

$$\begin{aligned} P &= Q^2 (4\pi \epsilon_0 |V_z| c^2)^{-1} \sum_{j \neq m} \sum_{p=-\infty}^{\infty} \int_0^{\infty} d\omega \omega |K_{\perp}(n_{\perp j}^2 - n_{\perp m}^2)|^{-1} \\ &| J_p^2 \left\{ \frac{V_{\perp}^2 p^2}{u^2} \frac{1}{2} (\lambda_{1-1} + 2\lambda_{11} + \lambda_{-11}) - \iota \frac{2V_{\perp} V_z p}{u} 2^{-\frac{1}{2}} (\lambda_{10} + \lambda_{01}) + V_z^2 \lambda_{\infty} \right\} \\ &+ J_p J'_p \left\{ i \frac{2V_{\perp}^2 p}{u} \frac{1}{2} (\lambda_{1-1} - \lambda_{-11}) + i 2V_{\perp} V_z \iota 2^{-\frac{1}{2}} i (-\lambda_{10} + \lambda_{01}) \right\} \\ &+ J_p'^2 \left\{ V_{\perp}^2 \frac{1}{2} (\lambda_{1-1} - 2\lambda_{11} + \lambda_{-11}) \right\} | \quad . \quad (\text{E.5}) \end{aligned}$$

This can be expressed much more compactly by introducing the cartesian form for the adjoint matrix as given in Appendix A . Thus,

$$\begin{aligned} P &= Q^2 (4\pi \epsilon_0 |V_z| c^2)^{-1} \sum_{j \neq m} \sum_{p=-\infty}^{\infty} \int_0^{\infty} d\omega \omega |K_{\perp}(n_{\perp j}^2 - n_{\perp m}^2)|^{-1} \\ &| J_p^2 \left\{ \frac{V_{\perp}^2 p^2}{u^2} \lambda_{xx} - \iota \frac{2V_{\perp} V_z p}{u} \lambda_{xz} + V_z^2 \lambda_{zz} \right\} \\ &+ J_p J'_p \left\{ i \frac{2V_{\perp}^2 p}{u} \lambda_{xy} + i 2V_{\perp} V_z \iota \lambda_{yz} \right\} + J_p'^2 V_{\perp}^2 \lambda_{yy} | \quad . \quad (\text{E.6}) \end{aligned}$$

Since TF have expressed their results in terms of the wave propagation vector \underline{k} whereas we have used \underline{n} , we transform to their notation using the relation $\underline{n} = c\underline{k}/\omega$. Thus our adjoint matrix $\underline{\lambda}$ is related to their adjoint matrix $\underline{\Lambda}$ by

$$\underline{\lambda} = \frac{c^4}{\omega^4} \underline{\Lambda} \quad . \quad (\text{E.7})$$

Likewise, if we use their relation

$$k_{\perp j}^2 = (2 \epsilon_1)^{-1} (X \pm R), \quad (j=1,2), \quad (\text{E.8})$$

since our K_{\perp} equals ϵ_1 of TF, we have

$$|K_{\perp} (n_{\perp j}^2 - n_{\perp m}^2)| = R c^2 / \omega^2. \quad (\text{E.9})$$

Finally, we need to use $u = k_{\perp} V_{\perp} / |\Omega|$ which follows from (5.15) for a non-relativistic particle. Inserting these expressions into (E.6) we obtain

$$P = Q^2 (4\pi \epsilon_0 |V_z| c^2)^{-1} \sum_{\text{modes}} \sum_{p=-\infty}^{\infty} \int_0^{\infty} d\omega \omega |R \omega^2 / c^2|^{-1} \\ \left| \left\{ \frac{p^2 \Omega^2}{k_{\perp}^2} \Lambda_{xx} - \frac{2V_z p \Omega}{k_{\perp}} \Lambda_{xz} + V_z^2 \Lambda_{zz} \right\} J_p^2 \right. \\ \left. - i 2 V_{\perp} \left\{ -\frac{p \Omega}{k_{\perp}} \Lambda_{xy} - V_z \Lambda_{yz} \right\} J_p J_p' + V_{\perp}^2 \Lambda_{yy} J_p'^2 \right|. \quad (\text{E.10})$$

Recall that our quantity Ω contains the sign of the charge whereas in TF it is always a positive quantity. It is to be understood that in the integrand k_z is replaced by $(\omega + p \Omega) / V_z$ from the emission equation. This agrees with the expression which TF use for the emission equation only if we are considering a negative source charge. Hence for $Q < 0$ we get

$$P_{Q < 0} = Q^2 (4\pi \epsilon_0 |V_z| c^2)^{-1} \sum_{\text{modes}} \sum_{p=-\infty}^{\infty} \int_0^{\infty} d\omega \omega |R \omega^2 / c^2|^{-1} \\ \left| \left\{ \frac{p^2 \Omega^2}{k_{\perp}^2} \Lambda_{xx} + \frac{2V_z p |\Omega|}{k_{\perp}} \Lambda_{xz} + V_z^2 \Lambda_{zz} \right\} J_p^2 \right. \\ \left. + i 2 V_{\perp} \left\{ \frac{p |\Omega|}{k_{\perp}} \Lambda_{xy} - V_z \Lambda_{yz} \right\} J_p J_p' + V_{\perp}^2 \Lambda_{yy} J_p'^2 \right|. \quad (\text{E.11})$$

This agrees with the formula obtained by TF if one allows for differences in the physical units used by making the replacement $\epsilon_0 \rightarrow (4\pi)^{-1}$, which allows us to re-express our results, derived using MKS units, into the gaussian units used by TF. When $Q > 0$, we can put our emission equation into the same form as TF by making the replacement $p \rightarrow -p$. Doing this we obtain

$$\begin{aligned}
 P_{Q>0} = & Q^2 (4\pi \epsilon_0 |V_z| c^2)^{-1} \sum_{\text{modes}} \sum_{p=-\infty}^{\infty} \int_0^{\infty} d\omega \omega |R \omega^2/c^2|^{-1} \\
 & \left| \left\{ \frac{p^2 \Omega^2}{k_{\perp}^2} \Lambda_{xx} + \frac{2V_z p \Omega}{k_{\perp}} \Lambda_{xz} + V_z^2 \Lambda_{zz} \right\} J_p^2 \right. \\
 & \left. - i 2V_{\perp} \left\{ \frac{p \Omega}{k_{\perp}} \Lambda_{xy} - V_z \Lambda_{yz} \right\} J_p J_p' + V_{\perp}^2 \Lambda_{yy} J_p'^2 \right| \quad (\text{E.12})
 \end{aligned}$$

which also agrees with the expression obtained by TF after replacing ϵ_0 by $(4\pi)^{-1}$.

APPENDIX F

THE EMISSION EQUATION

From (5.79) we find that the condition which must be fulfilled in order for there to be radiation from a spiraling charge moving through a plasma is that

$$n_z = \beta_z^{-1} (1 + p Y/\gamma). \quad (F.1)$$

This is known as the "emission equation". If we write (F.1) in terms of the wave propagation vector instead of the refractive index and consider non-relativistic particles, then

$$k_z = \frac{\omega + p \Omega}{V_z} . \quad (F.2)$$

Now throughout this thesis we have assumed that all of the field quantities can be described by a sum of plane waves of the form

$$e^{ik_x x + ik_y y + ik_z z - i\omega t} . \quad (F.3)$$

Therefore equation (F.2) tells us that a spiraling charge in a magneto-plasma can only excite those plane waves whose propagation vector component along \hat{e}_z (the direction of the magnetic field in the magneto-plasma) satisfies the emission equation. In this appendix we will examine the meaning of this equation and explore some of its consequences.

In order to learn more about the meaning of this equation, we shall show alternate methods of obtaining it, first by studying Doppler effects, and second by using quantum mechanical considerations.

Doppler Effects and the Emission Equation

Consider the following situation. Suppose we have two coordinate systems, x, y, z and x', y', z' , and let us assume that the primed system is moving with respect to the unprimed system with the velocity V_z as shown in Figure 24.

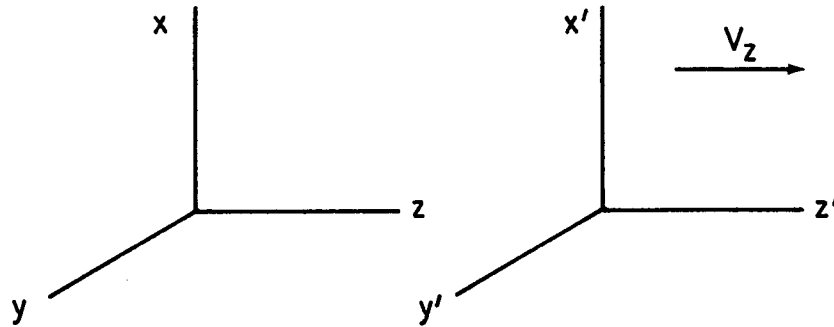


Fig. 24 . Geometry for obtaining the emission equation via Doppler effects

Then if we have a radiator of frequency ω' moving with the primed coordinates, it will emit radiation which can be understood by an observer fixed in the primed system as a superposition of plane waves of the form

$$e^{i\mathbf{k}' \cdot \mathbf{r}' - i\omega' t'} \quad . \quad (F.4)$$

The question arises as to what these plane waves will look like as viewed by an observer in the unprimed system. This is, of course, a straightforward problem involving Lorentz transformations.

Because the phase of a plane wave is the same in both the primed and unprimed system, it follows that since (\mathbf{r}, ct) is a four-vector then $(c\mathbf{k}, \omega)$ must also be a four-vector. The Lorentz transformation allows us to relate vectors in the primed and unprimed coordinate systems as follows:

$$\begin{bmatrix} ck'_x \\ ck'_y \\ ck'_z \\ \omega' \end{bmatrix} = \begin{bmatrix} 1 & 0 & 0 & 0 \\ 0 & 1 & 0 & 0 \\ \gamma_z & 0 & 0 & -\gamma_z \beta_z \\ 0 & 0 & -\gamma_z \beta_z & \gamma_z \end{bmatrix} \begin{bmatrix} ck_x \\ ck_y \\ ck_z \\ \omega \end{bmatrix} \quad (F.5)$$

or inversely,

$$\begin{bmatrix} ck_x \\ ck_y \\ ck_z \\ \omega \end{bmatrix} = \begin{bmatrix} 1 & 0 & 0 & 0 \\ 0 & 1 & 0 & 0 \\ \gamma_z & 0 & 0 & \gamma_z \beta_z \\ 0 & 0 & \gamma_z \beta_z & \gamma_z \end{bmatrix} \begin{bmatrix} ck'_x \\ ck'_y \\ ck'_z \\ \omega' \end{bmatrix} \quad (F.6)$$

where $\gamma_z \equiv (1 - \beta_z^2)^{-\frac{1}{2}}$ with $\beta_z = V_z/c$. From (F.5) we get the equation relating ω to ω' ,

$$\omega = k_z V_z + \omega' / \gamma_z . \quad (F.7)$$

This says that the frequencies ω' appear to be Doppler shifted to an observer at rest in the unprimed coordinate system. Neglecting relativistic effects and expressing (F.7) in the form of (F.2) gives

$$k_z = \frac{\omega - \omega'}{V_z} . \quad (F.8)$$

Identifying ω' with the frequency $-p\Omega$, we obtain the emission equation (F.2). Hence, the emission equation is another manifestation of the Doppler effect.

Quantum Mechanics and the Emission Equation

In this section we present another derivation of the emission equation. We shall use a quantum mechanical approach to analyze the radiation process. Suppose that the spiraling charge is in the state s specified by the energy E_s . From relativity theory we have the relation between total energy E_s and the momentum components,

$$E_s = (M^2 c^4 + p_z^2 c^2 + p_\perp^2 c^2)^{\frac{1}{2}}. \quad (\text{F.9})$$

Now the energy eigenvalues for a charged particle spiraling in a constant external magnetic field are well known [55], [43]. They can be written in the form of (F.9) with the transverse momentum, p_\perp , related to the quantum number s by

$$p_\perp^2 = M |\Omega| \hbar (2s+1), \quad s=0, 1, 2 \dots \quad (\text{F.10})$$

Here s is the quantum number associated with the state s and \hbar is 2π times Planck's constant h .

If the spiraling charge emits radiation spontaneously, then the particle will go from the state s , specified by the numbers

$$\{ p_z, s \} \quad (\text{F.11})$$

to the state s' specified by

$$\{ p'_z, s' \} = \{ p_z - \hbar k_z, s - \tilde{p} \}. \quad (\text{F.12})$$

By conservation of energy

$$\begin{aligned} \hbar \omega = E_s - E'_s &= E_s - [M^2 c^4 + c^2 (p_z - \hbar k_z)^2 + c^2 M |\Omega| \hbar (2s - 2\tilde{p} + 1)]^{\frac{1}{2}} \\ &= E_s - E_s [1 - 2 c^2 \hbar p_z k_z / E_s^2 + c^2 \hbar^2 k_z^2 / E_s^2 - \\ &\quad 2 \tilde{p} M |\Omega| \hbar c^2 / E_s^2]^{\frac{1}{2}}. \end{aligned} \quad (\text{F.13})$$

If the particle energy (E_s) is much greater than the photon energy $\hbar \omega$, we can write

$$\omega \approx c^2 p_z k_z / E_s - c^2 \hbar k_z^2 / 2E_s + \tilde{p} M |\Omega| c^2 / E_s . \quad (F.14)$$

Using the relativistic expressions for E_s and p_z

$$E_s = M \gamma c^2 , \quad (F.15)$$

$$p_z = M \gamma V_z \quad (F.16)$$

and taking the classical limit $\hbar \rightarrow 0$, the expression for the frequency of emitted radiation is

$$\omega \approx V_z k_z + \tilde{p} |\Omega| / \gamma . \quad (F.17)$$

For non-relativistic particle speeds this becomes

$$\omega \approx V_z k_z + \tilde{p} |\Omega| . \quad (F.18)$$

From (F.18) and (F.10) we find that $\tilde{p} > 0$ corresponds to a decrease in the perpendicular component of angular momentum while $\tilde{p} < 0$ means that the transverse momentum increases. $\tilde{p} > 0$ is called normal Doppler emission and $\tilde{p} < 0$ is called anomalous Doppler emission. If $\tilde{p} = 0$ the transverse momentum is unchanged. Comparing (F.18) with the emission equation (F.2), we see that for a positive charge (i.e. $\Omega > 0$), $p = \tilde{p}$, and for a negative charge (i.e. $\Omega < 0$), $p = -\tilde{p}$. Table 5 summarizes these conclusions.

TABLE 5

SUMMARY OF SIGNIFICANCE OF POSITIVE AND NEGATIVE HARMONICS
FOR SPIRALING CHARGED PARTICLES

	HARMONIC (p)	TRANSVERSE MOMENTUM	DESCRIPTION (DOPPLER)
Pos. charge	NEG. ZERO POS.	INCREASING UNCHANGED DECREASING	ANOMALOUS NORMAL NORMAL
Neg. charge	NEG. ZERO POS.	DECREASING UNCHANGED INCREASING	NORMAL NORMAL ANOMALOUS

Connection Between the Emission Equation and the Refractive Index Surfaces

The emission equation can be quite useful as an aid to understanding the frequency spectrum of radiation excited by a spiraling charge when it is used in conjunction with the refractive index surfaces. For our present purposes it is sufficient to consider the simple case of a cold plasma. The refractive index surfaces for a cold collisionless electron-proton plasma corresponding to the "operating line" $R^2 = 0.4$ shown in Figure 2 are given in Appendix G.

From the curves presented in the appendix, we see that for a cold plasma there are three topologically distinct refractive index surfaces which can occur. These three surfaces are sketched in Figure 25. The vertical direction in Figure 25 is the direction of the external magnetic field \underline{B}_0 ; the radius from the center of each figure to the surface is equal to the refractive index n . These diagrams are really cross-sections of the true surfaces which can be obtained by sweeping the curves 180° about the vertical axis.

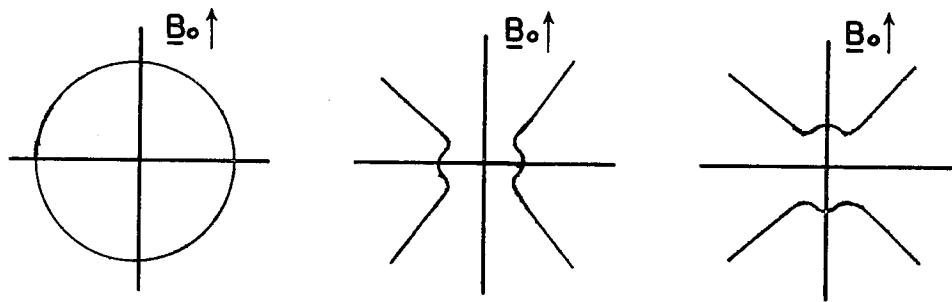


Fig. 25. The three topologically distinct refractive index surfaces which exist in a cold collisionless magnetoplasma. The external magnetic field is in the vertical direction. A radial from the origin to the surface represents the magnitude of the refractive index in the radial direction

The simplest surface to analyze is the closed surface shown in Figure 25 and shown enlarged in Figure 26.

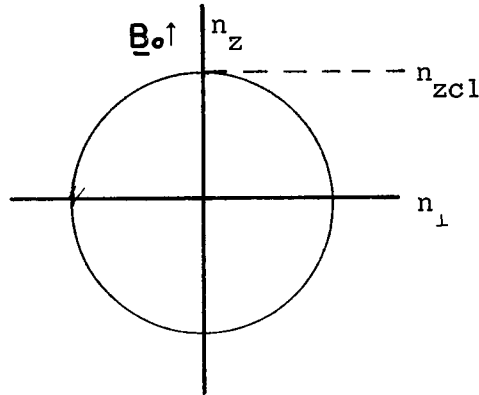


Fig. 26 . Typical shape for a closed refractive index surface with the critical index n_{zc1} indicated

This surface closely resembles the refractive index surfaces of ordinary solid dielectric materials. Hence we would expect Cerenkov radiation along those portions of the "operating line" where we have such surfaces, provided the particle speed is large enough.

For a given frequency, harmonic number and component of non-relativistic particle velocity along \underline{B}_0 , the emission equation specifies the allowed value of the z-component of the refractive index, namely,

$$n_z = (1 + p Y) / \beta_z . \quad (F.19)$$

In order to have radiation in these closed surface modes the inequality

$$|n_z| \leq n_{zc1} \quad (F.20)$$

must be satisfied where n_{zc1} is the largest positive value of n_z for our surface, as illustrated in Figure 26. Substituting for n_z from the emission equation, this inequality can be expressed as a bound on the allowable harmonics for which radiation is possible. When $\beta_z \geq 0$ this range is given by

$$-(1 + \beta_z n_{zc1}) < p Y < -(1 - \beta_z n_{zc1}) . \quad (F.21)$$

In many cases there do not exist any values of p which satisfy this inequality and in these cases no radiation is emitted.

The next surface we consider is shown in Figure 27, where we have also indicated two waves which might conceivably be excited by particles having different velocities. Note that wave 1 has a component of group velocity \underline{V}_{g1} in the direction in which the particle is moving, whereas wave 2 has a component of group velocity \underline{V}_{g2} antiparallel to the particle motion.

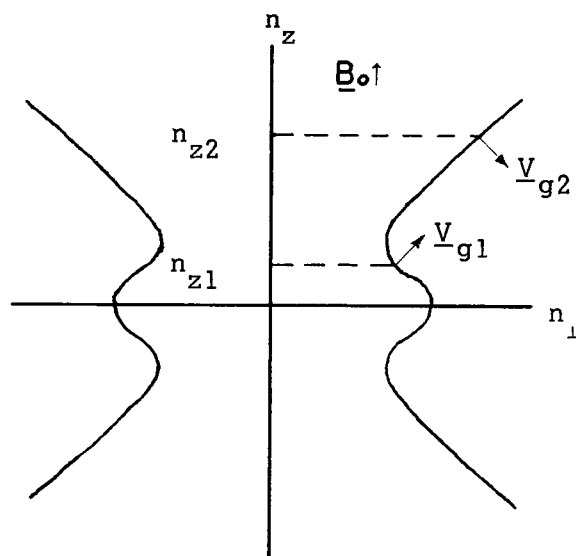


Fig. 27. Typical refractive index surface for modes which are evanescent in the direction of the magnetic field

Also note that in those regimes along the "operating line" where the surfaces are open along the magnetic field, Cerenkov or magnetobremstrahlung radiation will occur for any particle velocity β_z and for all harmonic numbers p , since n_{\perp} is real for every n_z which satisfies the emission equation.

The last surface we must examine is shown enlarged in Figure 28 with the critical indexes n_{zc2} and n_{zc3} illustrated. Such surfaces are open in the directions transverse to the magnetic field. In those regions

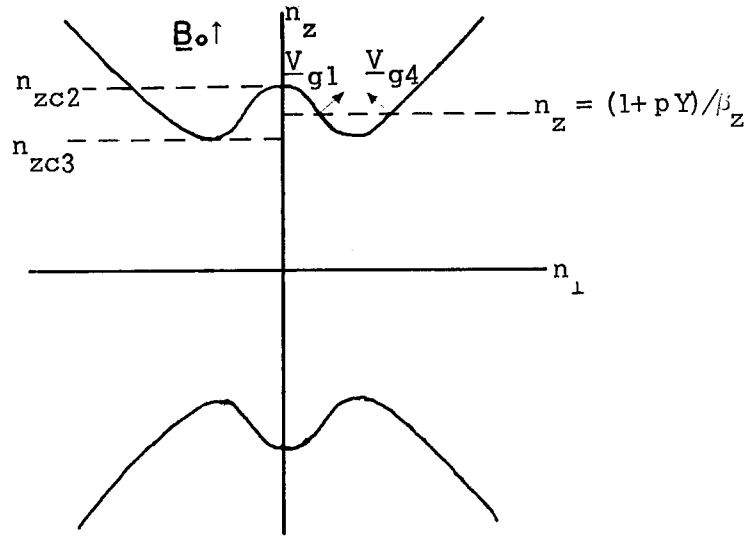


Fig.28 . Typical refractive index surface for modes which are evanescent in directions perpendicular to the magnetic field

of the "operating line" having this kind of surface, there are several possibilities for radiation. Consider the following cases.

Case 1. $|n_z| < n_{zc3}$ (F.22)

When Case 1 applies there is no radiation.

Case 2. $|n_z| > n_{zc2}$ (F.23)

In this case there is radiation, but only one wave is excited.

Case 3. $n_{zc3} < |n_z| \leq n_{zc2}$ (F.24)

When $|n_z|$ lies between n_{zc3} and n_{zc2} two waves may be excited at the same frequency. One of these waves will have the radial component of \underline{V}_g in the same direction as the radial component of the phase velocity vector while the other wave will have the radial component of \underline{V}_g antiparallel to the radial component of the phase velocity vector. The inequalities given in (F.22) - (F.24) can be used in a manner similar to that used in discussing closed surfaces, to generate allowed ranges for the harmonic p .

In the case of a cold plasma it is possible to express the critical indexes n_{zc1} , n_{xc2} , and n_{zc3} in terms of the magnetoionic variables X_e and Y_e^2 . Thus the locus of points corresponding to these critical indexes can be plotted on the CMA diagram. The intersection of these surfaces and the "operating line" determines the frequency spectrum of the radiation. The interested reader is referred to the paper by Sasiela and Friedberg [63] for details of this procedure.

APPENDIX G

REFRACTIVE INDEX DIAGRAMS

The following is an extensive listing of refractive index diagrams obtained using: 1) a cold plasma model, 2) Model H and 3) Model A. All surfaces are for a plasma having $R^2 \equiv f_{be}^2 / f_{pe}^2 = 0.4$ which corresponds to the operating line shown previously in the CMA diagram of Figure 2.

Cold Plasma Real Refractive Index Surfaces

The dispersion relation for a cold plasma is given by (see Appendix

B)

$$a n^4 + b n^2 + c = 0 \quad (G.1)$$

where

$$a = -K_{\perp} \sin^2 \vartheta - K_o \cos^2 \vartheta \quad (G.2)$$

$$b = (K_1 K_{-1} - K_o K_{\perp}) \sin^2 \vartheta + 2 K_o K_{\perp} \quad (G.3)$$

$$c = -K_1 K_{-1} K_o \quad (G.4)$$

The surfaces shown in this section were obtained using this form for the dispersion equation.

The plasma is assumed to be composed of electrons and protons. Collision effects have been neglected. All Index Surfaces have cylindrical symmetry about the magnetic field direction; only cross sections of these surfaces are shown.

The figures are in order of decreasing frequencies which are indicated on the graphs by the values of X_e . At any given frequency there are at most two real refractive surfaces for this model. The surfaces are somewhat arbitrarily numbered by subscripts on the value of X_e so as to assist in the identification of modes.

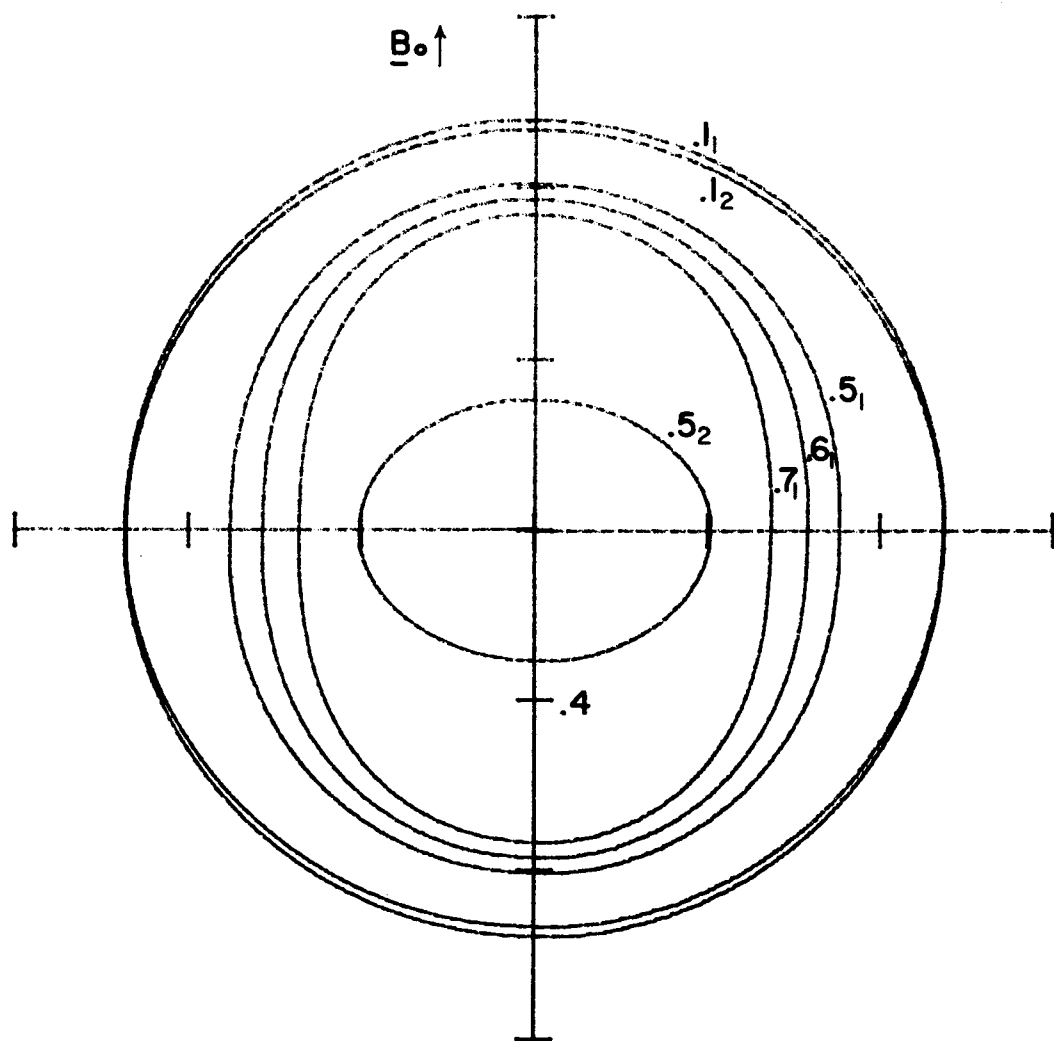


Fig. 29. Cold plasma refractive index surfaces for frequencies above the upper hybrid resonance. Curves are labeled according to values of X_e with $R^2 = 0.4$.

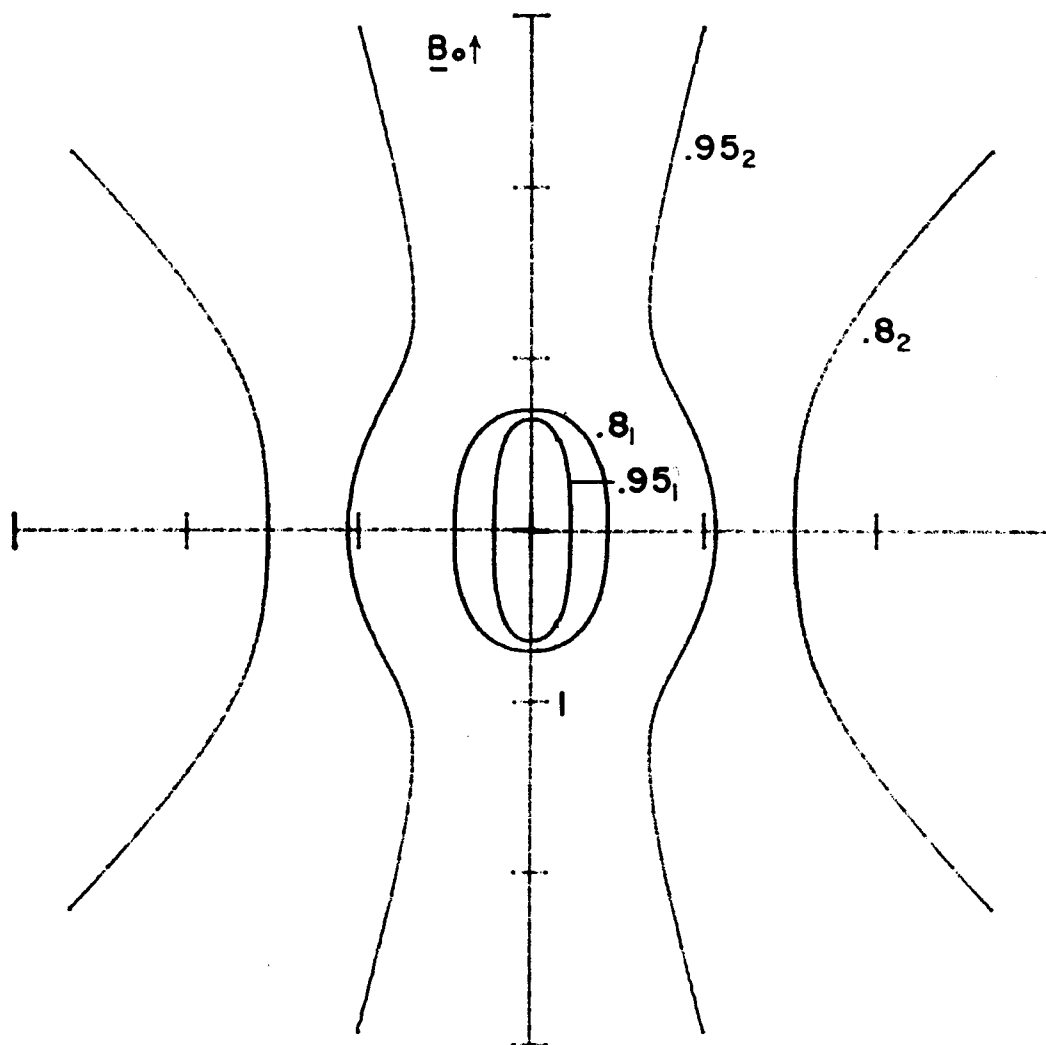


Fig.30. Cold plasma refractive index surfaces for frequencies between the upper hybrid resonance and the electron plasma frequency. Curves are labeled according to values of X_e with $R^2 = 0.4$.

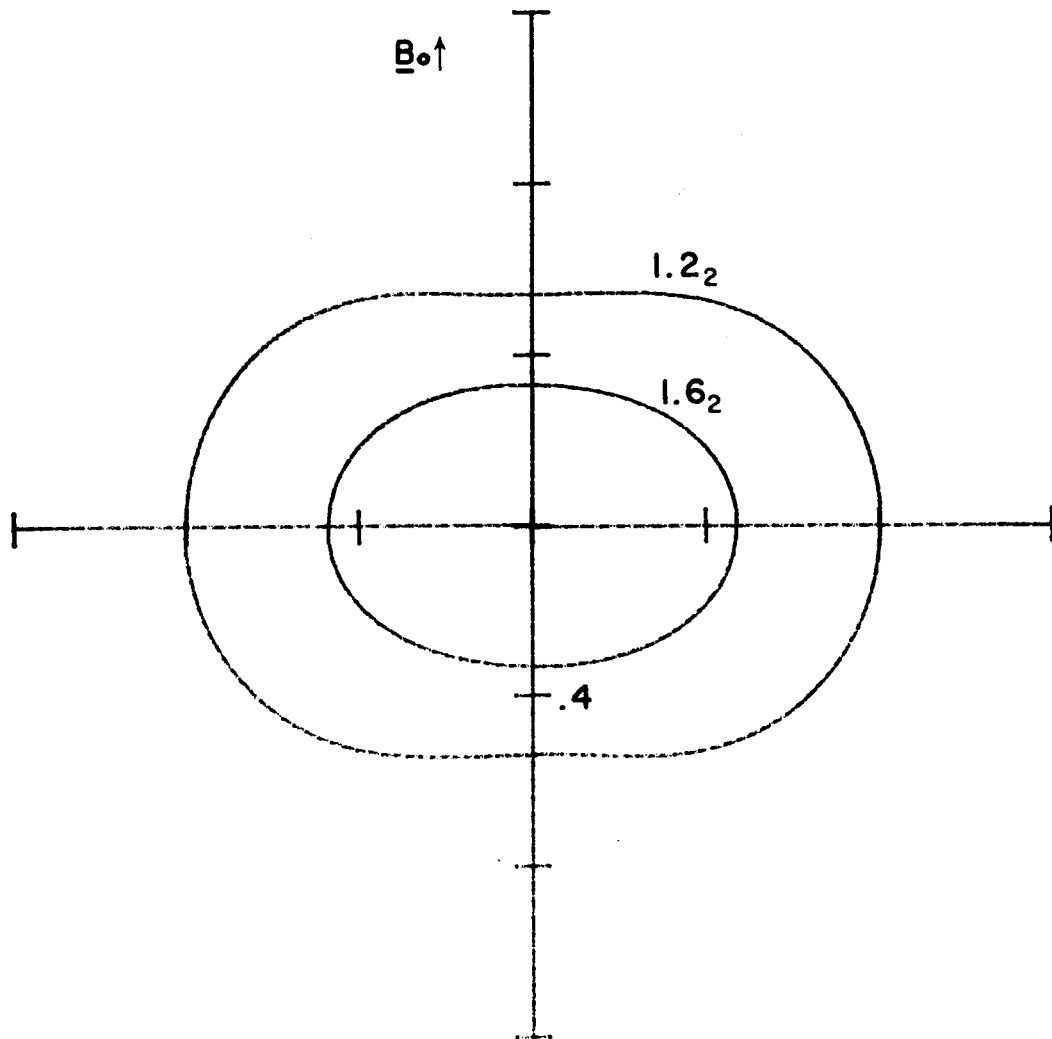


Fig. 31. Cold plasma refractive index surfaces for frequencies between the electron plasma frequency and the ion cyclotron cutoff frequency. Curves are labeled by values of X_e with $R^2 = 0.4$.

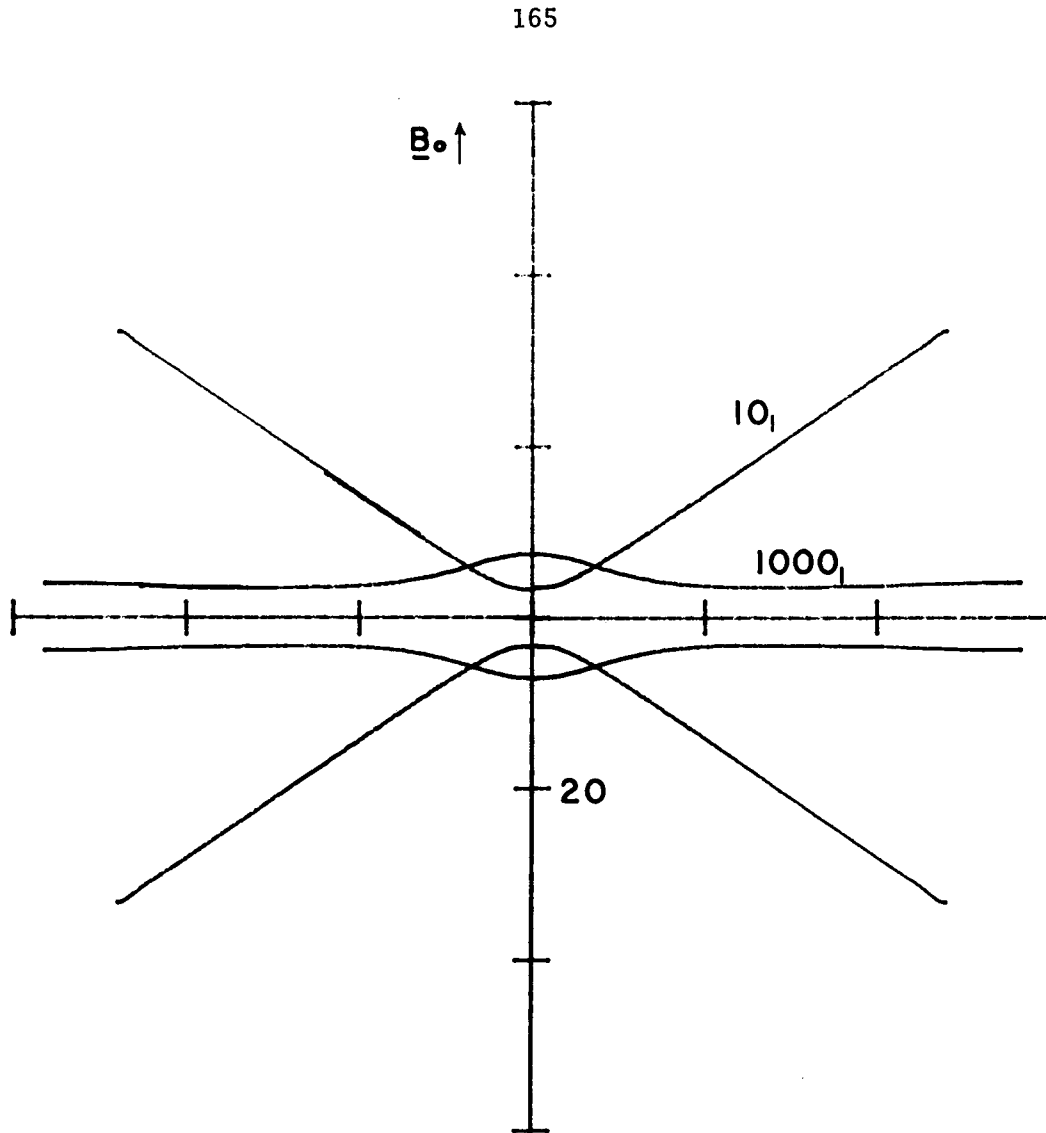


Fig. 32. Cold plasma refractive index curves for frequencies between the electron gyro-resonance and the lower hybrid resonance. Curves are labeled by values of X_e with $R^2 = 0.4$.

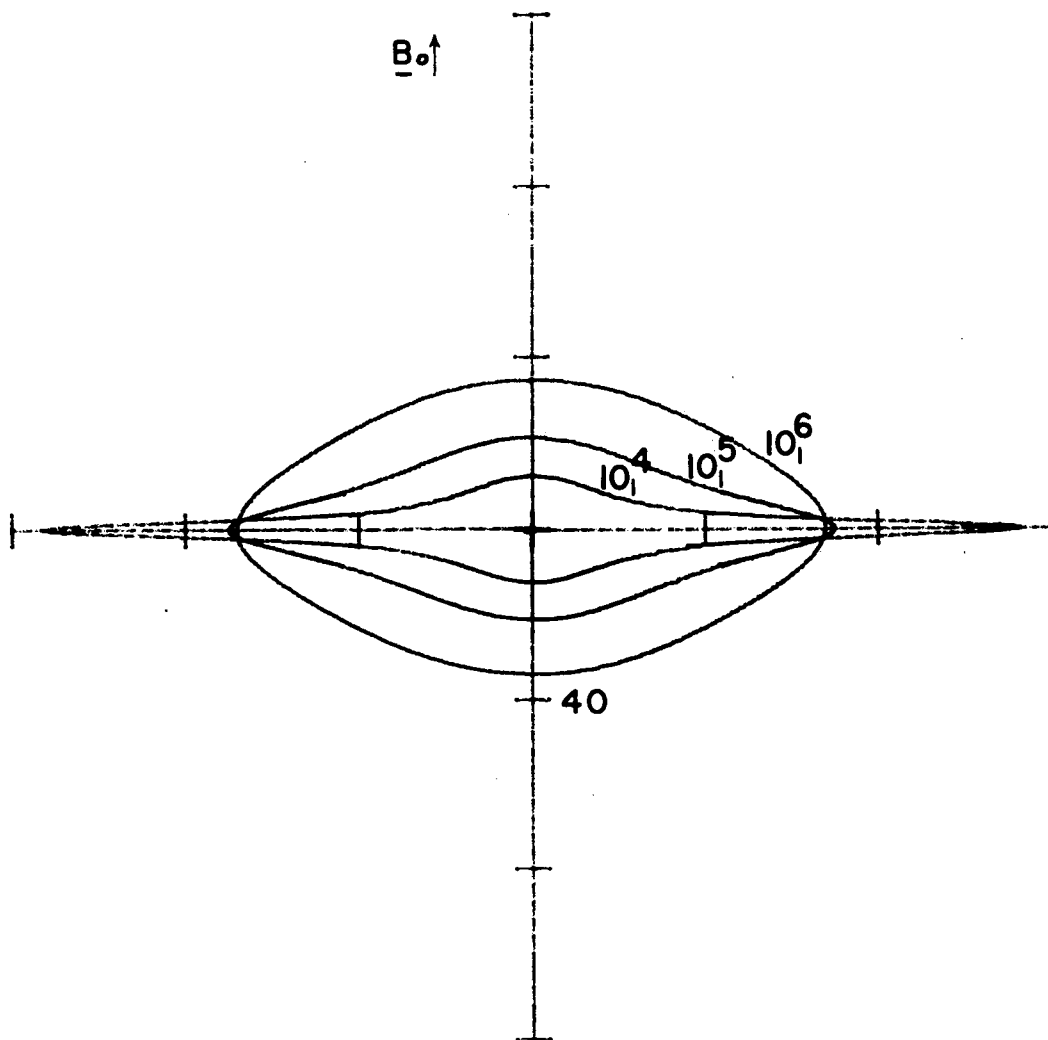


Fig. 33. Cold plasma refractive index surfaces for frequencies between the lower hybrid resonance and the ion gyro-resonance. Curves are labeled by values of X_e with $R^2 = 0.4$.

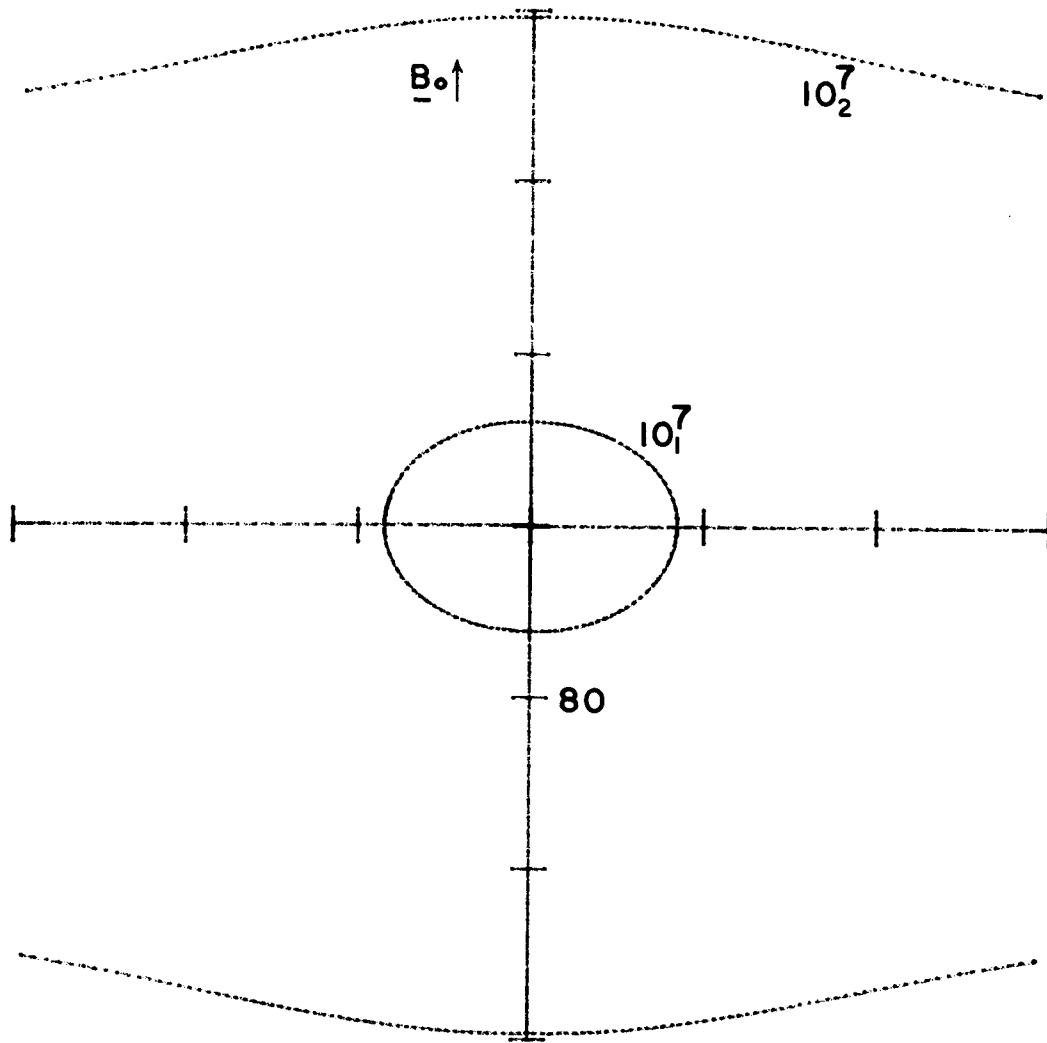


Fig.34. Cold plasma refractive index surfaces for a frequency below the ion gyro-resonance. Curves are labeled by values of X_e with $R^2 = 0.4$.

Refractive Index Curves for Model H

We shall assume a plasma containing only two charged species, namely, electrons ($s = e$) and one type of ions ($s = i$).

The dispersion relation for Model H in both spherical (n, ϑ, φ) and cylindrical (n_{\perp}, φ, n_z) coordinates is given in the form of polynomials

$$S_5 n^8 + S_4 n^6 + S_3 n^4 + S_2 n^2 + S_1 = 0 \quad (\text{G.5})$$

and

$$C_5 n_{\perp}^8 + C_4 n_{\perp}^6 + C_3 n_{\perp}^4 + C_2 n_{\perp}^2 + C_1 = 0 \quad (\text{G.6})$$

Multiplying equation (B.3) by $\prod_s D_s$, inserting for \underline{K} the appropriate expressions for Model H and abbreviating $\sin \vartheta$ by S and $\cos \vartheta$ by C we find after extremely tedious algebraic manipulations that

$$S_1 = -K_1 K_{-1} K_0 \quad (\text{G.7})$$

$$S_2 = +K_1 K_{-1} S^2 + K_0 K_1 (1+C^2) + \sum_s \epsilon_s \left\{ K_1 K_{-1} K_0 (g_{sx} S^2 + C^2) + \alpha_s^2 \left[\frac{1}{2} K_0 S^2 (K_1 g_{s+}^2 + K_{-1} g_{s-}^2) + K_1 K_{-1} C^2 \right] \right\} \quad (\text{G.8})$$

$$\begin{aligned} S_3 = & -K_{\perp} S^2 - K_0 C^2 - \sum_s \epsilon_s \left\{ (g_{sx} S^2 + C^2) \left[K_1 K_{-1} S^2 + K_0 K_1 (1+C^2) \right] \right. \\ & + \alpha_s^2 \left[\frac{1}{2} K_1 (g_{s+} S^2 + C^2)^2 + \frac{1}{2} K_{-1} (g_{s-} S^2 + C^2)^2 + K_1 C^2 \right] \\ & + \alpha_s^2 \frac{1}{2} K_0 S^2 \left[g_{sx} S^2 + (g_{s+}^2 + g_{s-}^2) (1 - \frac{1}{2} S^2) \right] \left. \right\} \\ & - \epsilon_e \epsilon_i \left\{ K_1 K_{-1} K_0 (g_{ex} S^2 + C^2) (g_{ix} S^2 + C^2) \right. \\ & + \sum_{s \neq t} \alpha_s^2 (g_{tx} S^2 + C^2) \left[\frac{1}{2} K_0 S^2 (K_1 g_{s+}^2 + K_{-1} g_{s-}^2) + K_1 K_{-1} C^2 \right] \\ & + \frac{1}{2} \alpha_e^2 \alpha_i^2 S^2 \sum_{s \neq t} \left[K_1 C^2 g_{s+} (g_{s+} - g_{t+}) + K_{-1} C^2 g_{t-} (g_{t-} - g_{s-}) \right. \\ & \left. \left. + \frac{1}{2} K_0 S^2 (g_{s-}^2 - g_{t+}^2 - g_{sx} g_{tx}) \right] \right\} \quad (\text{G.9}) \end{aligned}$$

$$\begin{aligned}
S_4 = & \sum_S \epsilon_s (g_{sx} S^2 + C^2) \left[(K_{\perp} + \alpha_s^2 g_{sx}) S^2 + (K_0 + \alpha_s^2) C^2 \right] \\
& - \epsilon_e \epsilon_i \left\{ (g_{ex} S^2 + C^2) (g_{ix} S^2 + C^2) \left[-K_{\perp} K_{\perp} S^2 - K_0 K_{\perp} (1 + C^2) \right] \right. \\
& - \sum_{s \neq t} \alpha_s^2 (g_{tx} S^2 + C^2) \left[\frac{1}{2} K_{\perp} (g_{s+} S^2 + C^2)^2 + \frac{1}{2} K_{\perp} (g_{s-} S^2 + C^2)^2 + \right. \\
& \left. K_{\perp} C^2 + \frac{1}{2} K_0 S^4 g_{sx} + \frac{1}{2} K_0 S^2 (1 - \frac{1}{2} S^2) (g_{s+}^2 + g_{s-}^2) \right] \\
& + \alpha_e^2 \alpha_i^2 S^2 \sum_{s \neq t} \left[\frac{1}{2} S^2 C^2 (g_{s-} g_{t+} - \frac{1}{2} g_{s-} g_{t-} - \frac{1}{2} g_{s+} g_{t+} + \frac{1}{2} g_{s-}^2 \right. \\
& \left. + \frac{1}{2} g_{s+}^2 - g_{sx} - g_{s-} g_{t+}^2 - g_{s+} g_{t-}^2 + 2 g_{sx} g_{tx} \right) + \\
& \left. \frac{1}{4} S^4 (-g_{s-}^2 g_{t+}^2 + g_{sx} g_{tx}) + \frac{1}{2} C^2 (g_{s+} g_{t+} + g_{s-} g_{t-} - g_{s-}^2 - g_{s+}^2) \right] \left. \right\} \\
\end{aligned} \tag{G.10}$$

$$\begin{aligned}
S_6 = & -\epsilon_e \epsilon_i \left\{ (g_{ex} S^2 + C^2) (g_{ix} S^2 + C^2) (K_{\perp} S^2 + K_0 C^2) \right. \\
& \left. + \sum_{s \neq t} \alpha_s^2 (g_{sx} S^2 + C^2)^2 (g_{tx} S^2 + C^2) \right\} \\
\end{aligned} \tag{G.11}$$

Similarly, for cylindrical coordinates, using $\prod_s D_s$ times equation (B.8), we have

$$\begin{aligned}
C_1 = & -K_0 (n_z^2 - K_{\perp}) (n_z^2 - K_{\perp}) + \sum_S \epsilon_s n_z^2 (n_z^2 - K_{\perp}) (n_z^2 - K_{\perp}) (K_0 + \alpha_s^2) - \\
& \epsilon_e \epsilon_i n_z^4 (n_z^2 - K_{\perp}) (n_z^2 - K_{\perp}) \\
\end{aligned} \tag{G.12}$$

$$\begin{aligned}
C_2 = & -n_z^2 (K_0 + K_{\perp}) + K_{\perp} K_{\perp} + K_0 K_{\perp} + \sum_S \epsilon_s \left\{ n_z^4 (2 \alpha_s^2 g_{sx} + K_{\perp} + K_0 + \right. \\
& \left. \alpha_s^2 + K_0 g_{sx}) - n_z^2 (K_0 K_{\perp} + K_{\perp} \alpha_s^2 + K_{\perp} \alpha_s^2 g_{s-} + K_{\perp} \alpha_s^2 g_{s+} \right. \\
& \left. + K_{\perp} K_{\perp} + \frac{1}{2} K_0 \alpha_s^2 g_{s-}^2 + \frac{1}{2} K_0 \alpha_s^2 g_{s+}^2 + 2 K_0 K_{\perp} g_{sx}) + \right. \\
& \left. \frac{1}{2} K_0 K_{\perp} \alpha_s^2 g_{s-}^2 + \frac{1}{2} K_0 K_{\perp} \alpha_s^2 g_{s+}^2 + K_{\perp} K_{\perp} K_0 g_{sx} \right\} \\
& + \epsilon_e \epsilon_i \left\{ -n_z^6 \left[1 + K_{\perp} + \sum_{s \neq t} (K_0 g_{sx} + \alpha_s^2 g_{tx} + 2 \alpha_s^2 g_{sx}) \right] + \right. \\
& \left. n_z^4 \left[K_{\perp} K_{\perp} + K_0 K_{\perp} - \alpha_e^2 \alpha_i^2 (g_{e-} g_{i-} + g_{e+} g_{i+}) + \right. \right. \\
\end{aligned}$$

$$\begin{aligned}
& \sum_{s \neq t} \left(\frac{1}{2} K_0 \alpha_s^2 g_{s-}^2 + \frac{1}{2} K_0 \alpha_s^2 g_{s+}^2 + K_{-1} \alpha_s^2 g_{s-} + \right. \\
& K_1 \alpha_s^2 g_{s+} + \frac{1}{2} \alpha_e^2 \alpha_i^2 g_{s-}^2 + \frac{1}{2} \alpha_e^2 \alpha_i^2 g_{s+}^2 + \\
& \left. K_{-1} \alpha_s^2 + K_0 K_{-1} g_{sx} + 2 K_{-1} g_{tx} \alpha_s^2 \right) + \\
& n_z^2 \left[\alpha_e^2 \alpha_i^2 (K_{-1} g_{e-} g_{i-} + K_1 g_{e+} g_{i+}) - \right. \\
& \left. \sum_{s \neq t} \left(\frac{1}{2} K_0 K_{-1} \alpha_s^2 g_{s-}^2 + \frac{1}{2} K_0 K_1 \alpha_s^2 g_{s+}^2 + \frac{1}{2} K_{-1} \alpha_e^2 \alpha_i^2 g_{s-}^2 + \right. \right. \\
& \left. \left. \frac{1}{2} K_1 \alpha_e^2 \alpha_i^2 g_{s+}^2 + K_1 K_{-1} K_0 g_{sx} + K_1 K_{-1} g_{tx} \alpha_s^2 \right) \right] \quad (G.13)
\end{aligned}$$

$$\begin{aligned}
C_3 = & -K_1 + \sum_s \epsilon_s \left\{ n_z^2 (K_1 + \alpha_s^2 g_{sx}^2 + 2 \alpha_s^2 g_{sx} + K_{-1} g_{sx} + K_0 g_{sx}) - \right. \\
& \left. \left(\frac{1}{2} K_{-1} \alpha_s^2 g_{s-}^2 + \frac{1}{2} K_1 \alpha_s^2 g_{s+}^2 + K_0 \alpha_s^2 g_{sx}^2 + K_1 K_{-1} g_{sx} + K_0 K_{-1} g_{sx} \right) \right\} + \\
& \epsilon_e \epsilon_i \left\{ -n_z^4 \left[K_{-1} + K_0 g_{ex} g_{ix} + \sum_{s \neq t} \left(\alpha_s^2 g_{sx}^2 + 2 \alpha_s^2 g_{sx} + \right. \right. \right. \\
& \left. \left. \left. 2 g_{ex} g_{ix} \alpha_s^2 + g_{tx} \alpha_s^2 + K_0 g_{sx} + K_{-1} g_{sx} \right) \right] + \right. \\
& n_z^2 \left[2 K_0 K_{-1} g_{ix} g_{ex} - \alpha_e^2 \alpha_i^2 2 g_{ex} g_{ix} + \right. \\
& \left. \sum_{s \neq t} \left(-\frac{1}{2} \alpha_e^2 \alpha_i^2 g_{s+} g_{t-} + \frac{1}{2} \alpha_e^2 \alpha_i^2 g_{s+}^2 g_{t-} - \alpha_e^2 \alpha_i^2 g_{s-} g_{t-} / 4 + \right. \right. \\
& \left. \frac{1}{2} \alpha_e^2 \alpha_i^2 g_{s-} g_{t+} - \alpha_e^2 \alpha_i^2 g_{s+} g_{t+} / 4 + \frac{1}{2} K_{-1} \alpha_s^2 g_{s-}^2 + \right. \\
& \left. \frac{1}{2} K_1 \alpha_s^2 g_{s+}^2 + K_0 \alpha_s^2 g_{sx}^2 + \alpha_e^2 \alpha_i^2 g_{sx}^2 + K_1 K_{-1} g_{sx} + \right. \\
& \left. K_0 K_{-1} g_{sx} + K_{-1} g_{tx} \alpha_s^2 g_{s-} + K_1 g_{tx} \alpha_s^2 g_{s+} + \right. \\
& \left. K_{-1} g_{tx} \alpha_s^2 + \frac{1}{2} K_0 g_{tx} \alpha_s^2 g_{s-}^2 + \frac{1}{2} K_0 g_{tx} \alpha_s^2 g_{s+}^2 \right) \right] + \\
& \frac{1}{2} \alpha_e^2 \alpha_i^2 K_0 g_{ex} g_{ix} - K_1 K_{-1} K_0 g_{ex} g_{ix} - \\
& \left. \sum_{s \neq t} \left(\alpha_e^2 \alpha_i^2 K_0 g_{s-}^2 g_{t+} / 4 + \frac{1}{2} K_0 K_{-1} g_{tx} \alpha_s^2 g_{s-}^2 + \right. \right. \\
& \left. \left. \frac{1}{2} K_0 K_1 g_{tx} \alpha_s^2 g_{s+}^2 \right) \right\} \quad (G.14)
\end{aligned}$$

$$\begin{aligned}
C_4 = & \sum_s \epsilon_s \left\{ \alpha_s^2 g_{sx}^2 + K_{\perp} g_{sx} \right\} + \\
& \epsilon_e \epsilon_i \left\{ n_z^2 \left[-g_{ex} g_{ix} (K_0 + K_{\perp}) + \sum_{s \neq t} (-\alpha_s^2 g_{sx}^2 - K_{\perp} g_{sx} - \right. \right. \\
& \left. \left. g_{tx} \alpha_s^2 g_{sx}^2 + 2 g_{tx} \alpha_s^2 g_{sx}) \right] + \right. \\
& \left. g_{ex} g_{ix} \left(-\frac{1}{2} \alpha_e^2 \alpha_i^2 + K_{\perp} K_{\perp} + K_0 K_{\perp} \right) + \right. \\
& \left. \sum_{s \neq t} \left(\alpha_e^2 \alpha_i^2 g_{s-}^2 g_{t+}^2 / 4 + \frac{1}{2} K_{\perp} g_{tx} \alpha_s^2 g_{s-}^2 \right. \right. \\
& \left. \left. + \frac{1}{2} K_{\perp} g_{tx} \alpha_s^2 g_{s+}^2 + K_0 \alpha_s^2 g_{tx} g_{sx}^2 \right) \right\} \quad (G.15)
\end{aligned}$$

$$C_5 = -\epsilon_e \epsilon_i \left\{ g_{ex} g_{ix} K_{\perp} + \sum_{s \neq t} g_{tx} g_{sx}^2 \alpha_s^2 \right\} \quad (G.16)$$

Real refractive index surfaces for the case where only first order temperature effects are retained (i.e. terms containing $\epsilon_i \epsilon_e$ are neglected) in eqn. (G.5) follow. These surfaces are for a lossless, electron-proton plasma with $T_e = T_i = 2000^{\circ}\text{K}$.

Refractive index surfaces are presented in order of decreasing frequencies which are indicated on the graphs by the values of X_e . At any given frequency there are at most three refractive index surfaces for this model. The real refractive index surfaces are somewhat arbitrarily numbered by subscripts on the value of X_e so as to assist in the identification of modes.

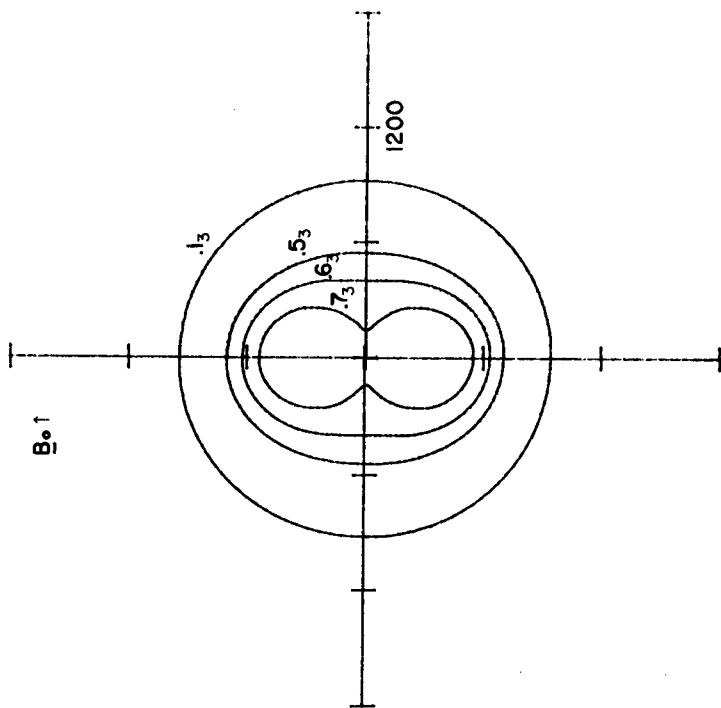


Fig. 35 . Refractive index surfaces obtained with Model H (first order in temperature) for frequencies above the upper hybrid resonance. (Expanded scale shown) . Curves are labeled according to values of X_e with $R^2 = 0.4$.

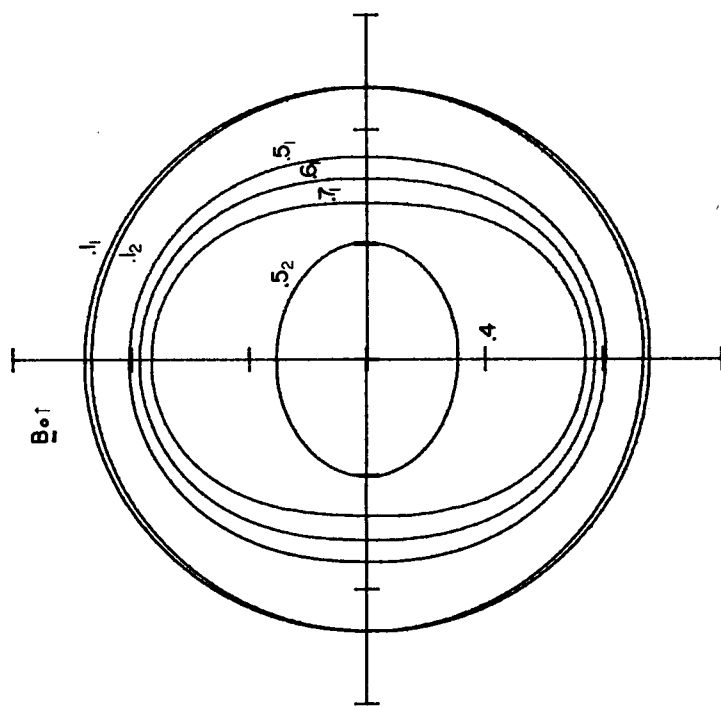


Fig. 36 . Refractive index surfaces obtained with Model H (first order in temperature) for frequencies above the upper hybrid resonance. (Compressed scale shown) . Curves are labeled according to values of X_e with $R^2 = 0.4$.

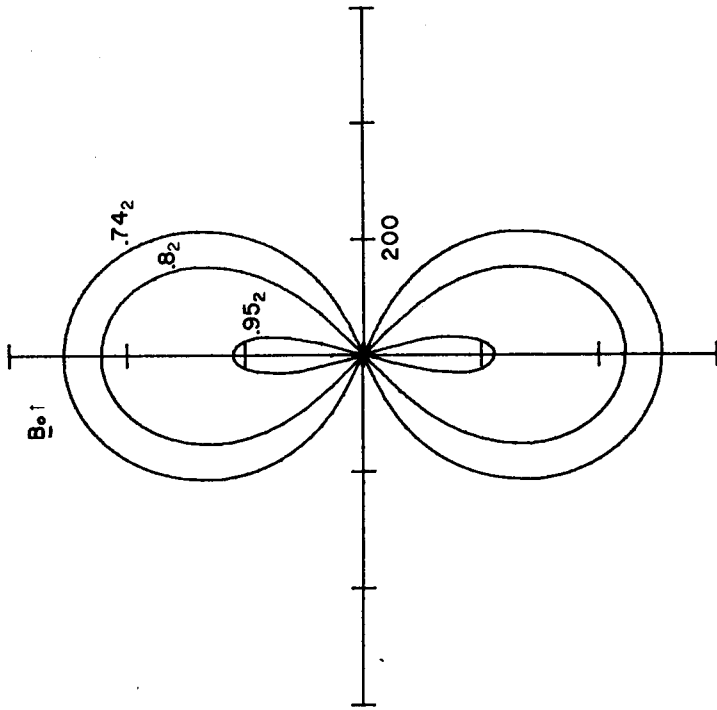


Fig. 37 . Refractive index surfaces obtained with Model H (first order in temperature) for frequencies between the UHR and the plasma cutoff. (Expanded scale shown). Curves are labeled according to values of X_e with $R^2 = 0.4$.

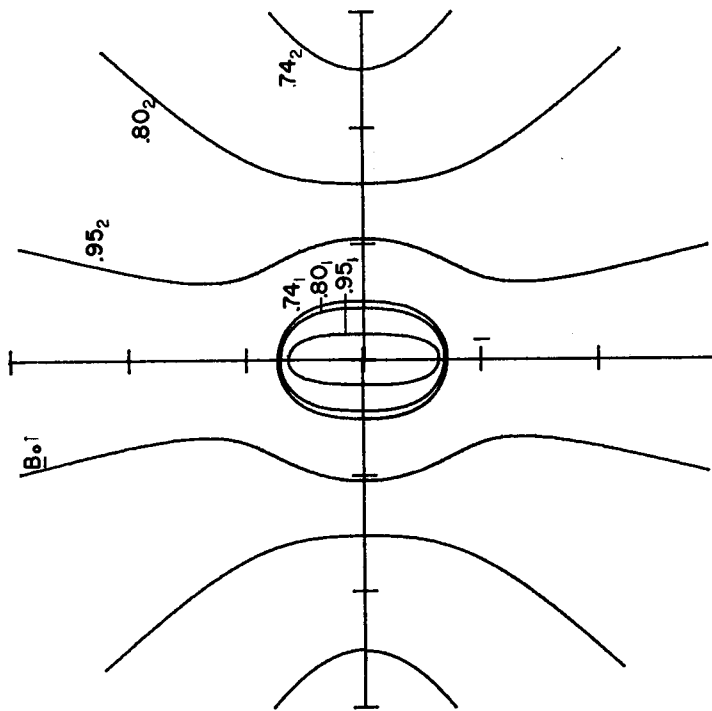


Fig. 38 . Refractive index surfaces obtained with Model H (first order in temperature) for frequencies between the UHR and the plasma cutoff. (Compressed scale shown). Curves are labeled according to values of X_e with $R^2 = 0.4$.

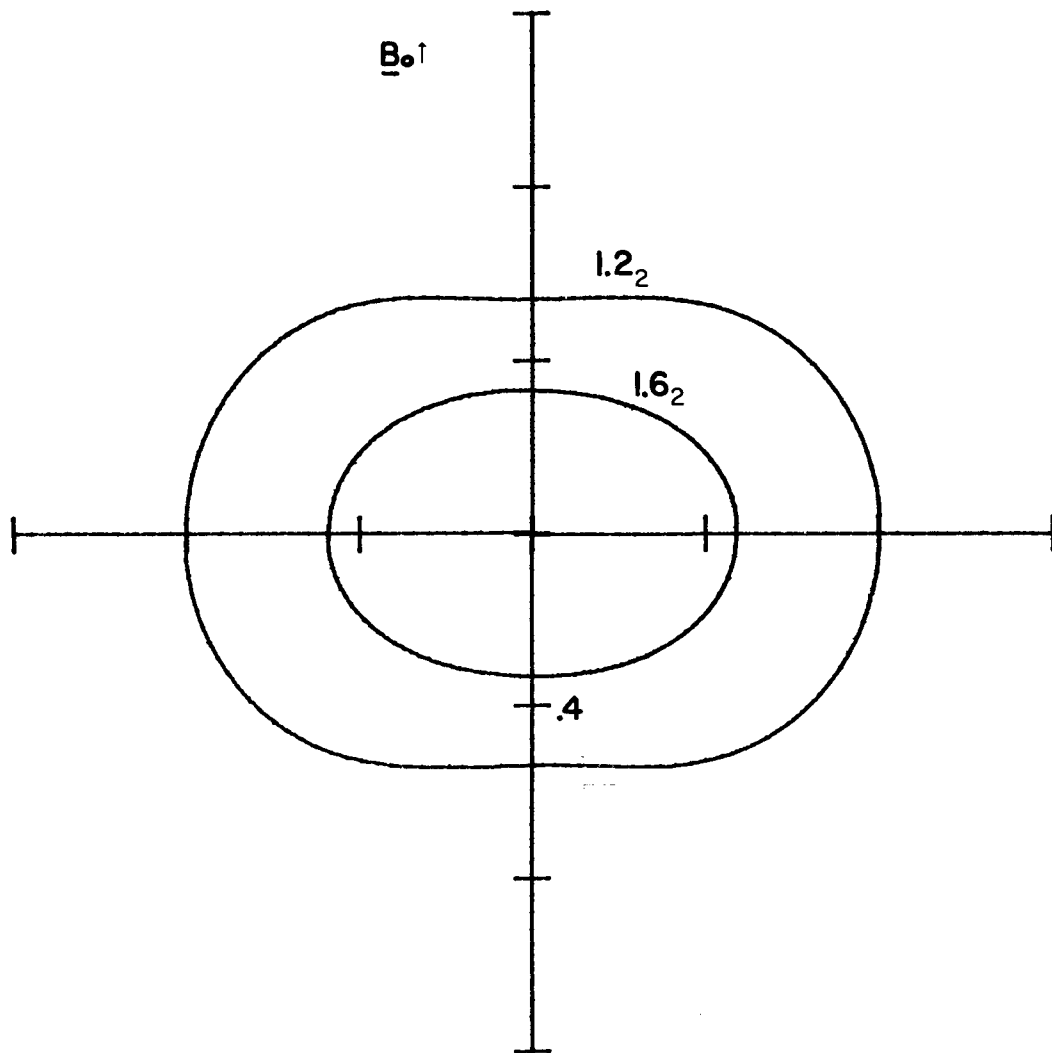


Fig. 39 Refractive index surfaces obtained with Model H (first order in temperature) for frequencies between the plasma cutoff and the ion cyclotron cutoff. Curves are labeled according to values of X_e with $R^2 = 0.4$.

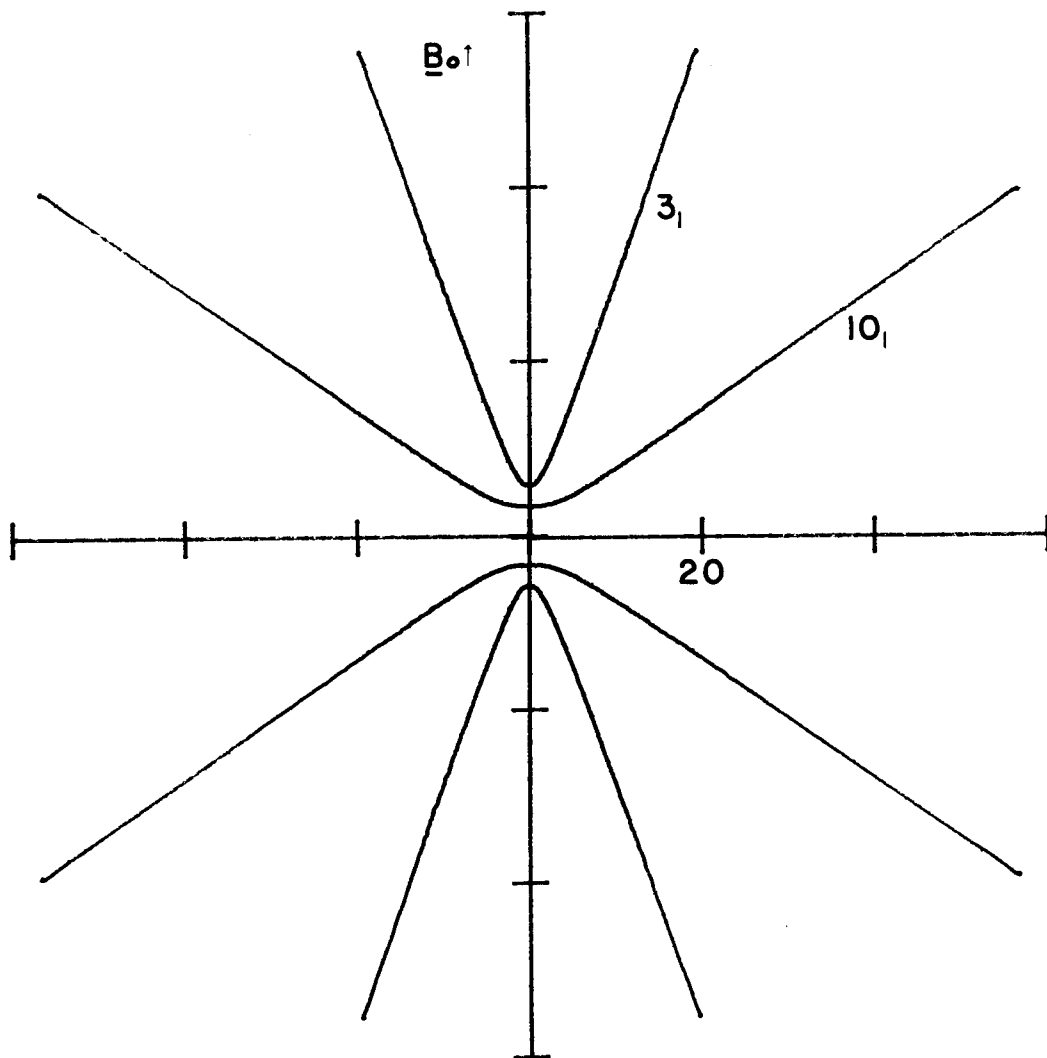


Fig. 40 Refractive index surfaces obtained with Model H (first order in temperature) for the higher frequency portion of the band between the electron gyro-resonance and the LHR. Curves are labeled according to the value of X_e with $R^2 = 0.4$.

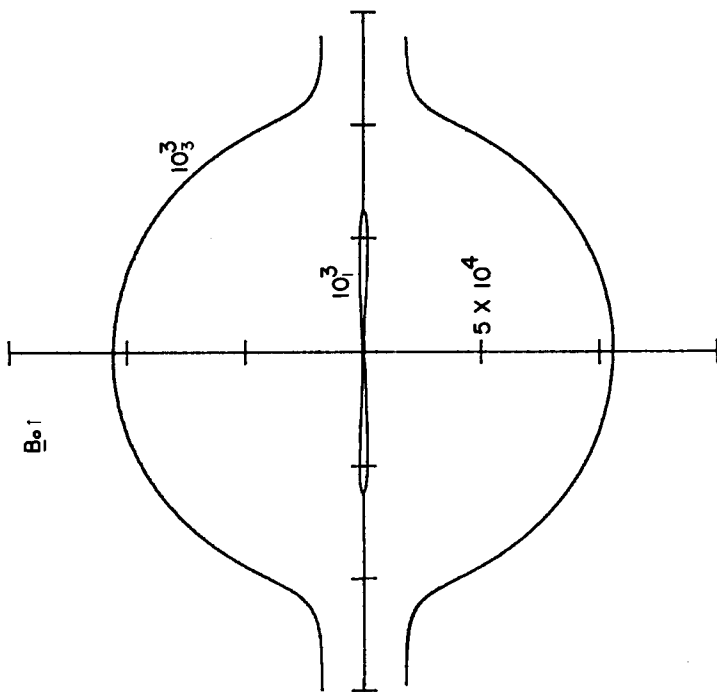


Fig. 41 . Refractive index surface obtained with Model H (first order in temperature) for a frequency in the lower frequency portion of the band between the electron gyro-resonance and the LHR. (Expanded scale shown). The curve is labeled according to the value of X_e with $R^2 = 0.4$.

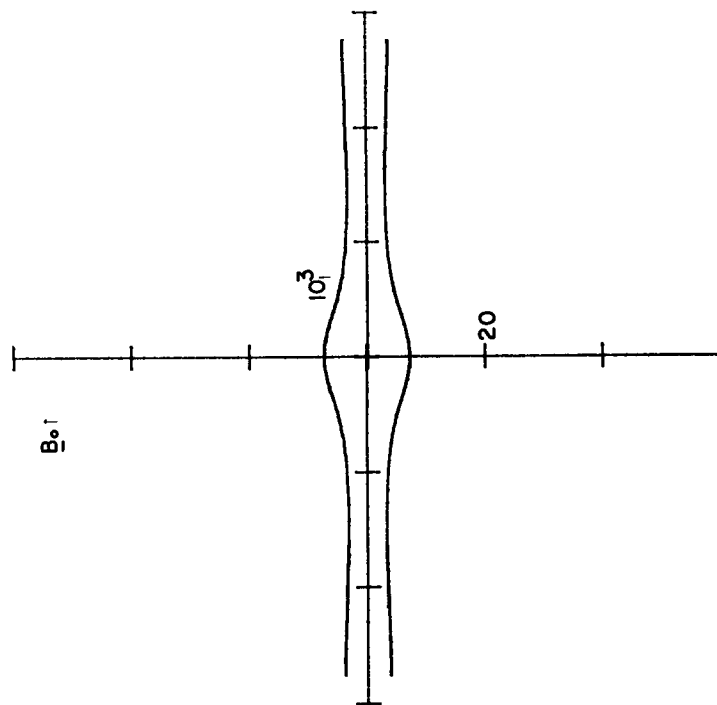


Fig. 42 . Refractive index surfaces obtained with Model H (first order in temperature) for a frequency in the lower frequency portion of the band between the electron gyro-resonance and the LHR. (Compressed scale shown). The curves are labeled according to the value of X_e with $R^2 = 0.4$.

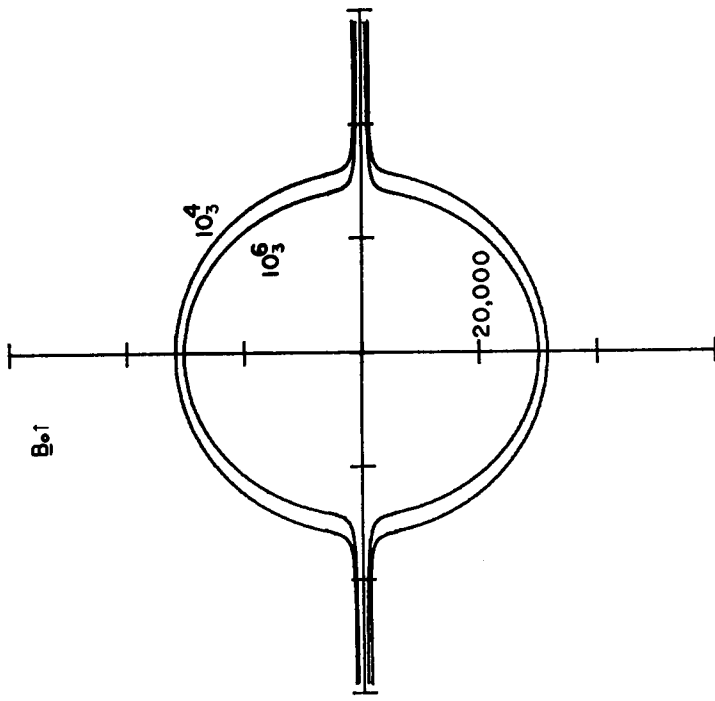


Fig. 43 . Refractive index surfaces obtained with Model H (first order in temperature) for frequencies between the LHR and the ion gyroresonance. (Expanded scale shown). Curves are labeled according to values of X_e with $R^2 = 0.4$.

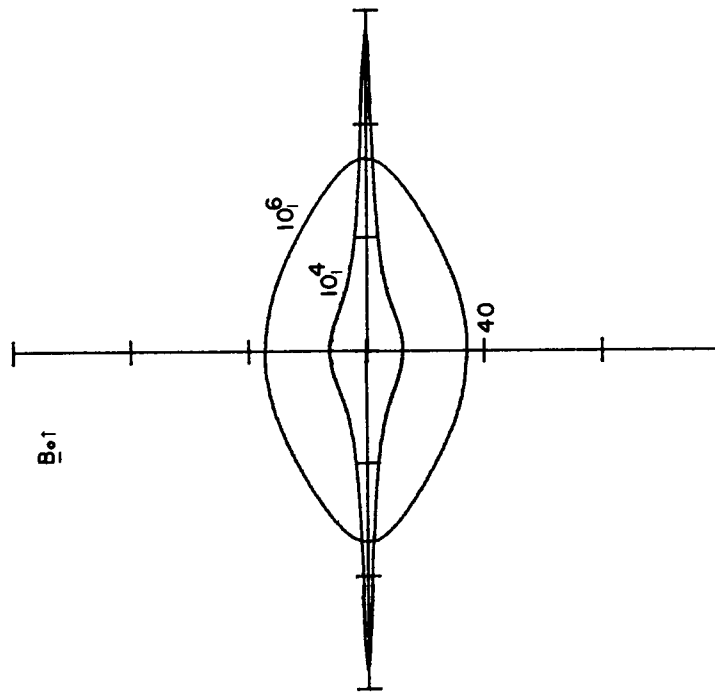


Fig. 44 . Refractive index surfaces obtained with Model H (first order in temperature) for frequencies between the LHR and the ion gyroresonance. (Compressed scale shown). Curves are labeled according to values of X_e with $R^2 = 0.4$.

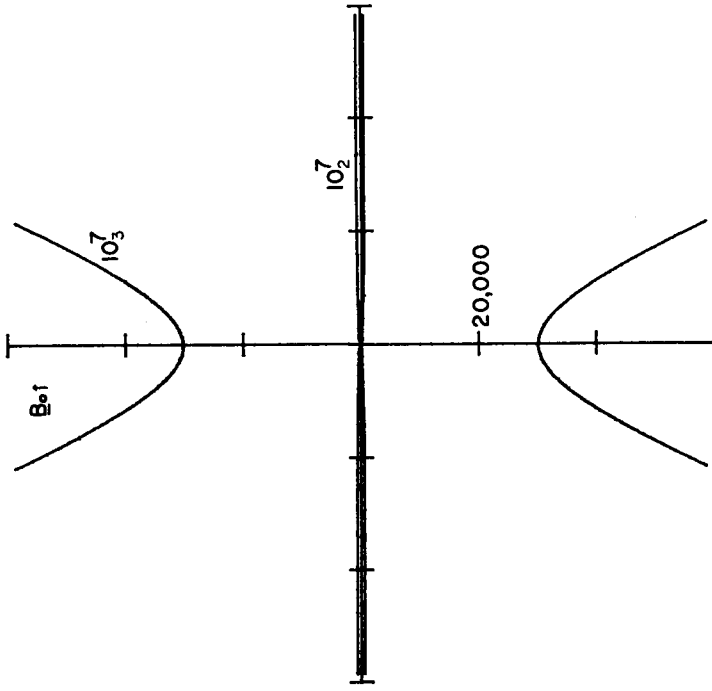


Fig. 45. Refractive index surfaces obtained with Model H (first order in temperature) for a frequency below the ion gyro-resonance. (Expanded scale shown). Curves are labeled according to values of X_e with $R^2 = 0.4$.

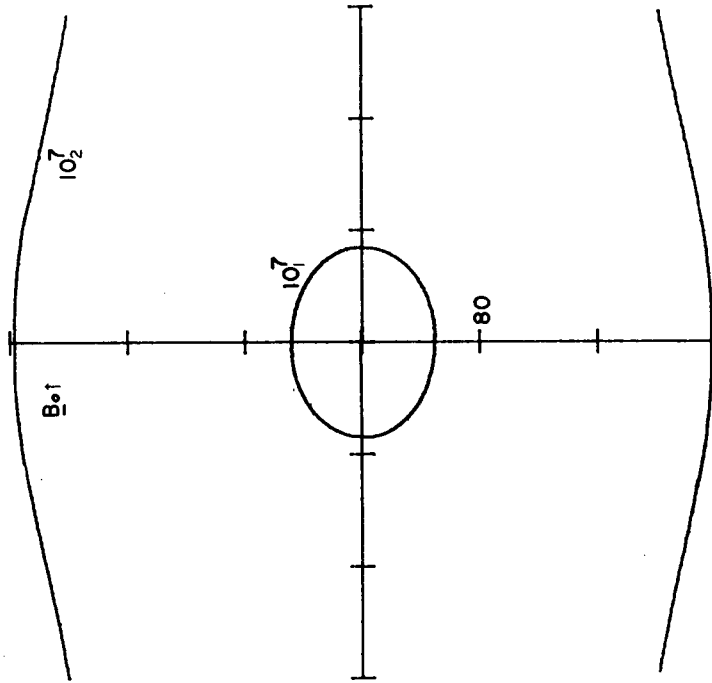


Fig. 46. Refractive index surfaces obtained with Model H (first order in temperature) for a frequency below the ion gyro-resonance. (Compressed scale shown). Curves are labeled according to values of X_e with $R^2 = 0.4$.

Refractive Index Surfaces for Model A

By substituting our expressions (4.82) - (4.87) and (4.77) - (4.81) for the dielectric tensor elements into equations (B.3) - (B.6) and (B.8) - (B.13), respectively, we obtain the dispersion relations for Model A. In spherical (n, ϑ, φ) coordinates this dispersion relation can be written

$$S_4 n^6 + S_3 n^4 + S_2 n^2 + S_1 = 0 \quad (\text{G.17})$$

where*

$$\begin{aligned} S_4 = & -\frac{1}{2} \sin^2 \vartheta [K'_{1-1} + K'_{-11} + e^{i2\varphi} K'_{-1-1} + e^{-i2\varphi} K'_{11}] \\ & - \cos^2 \vartheta K'_{00} - 2^{-\frac{1}{2}} \sin \vartheta \cos \vartheta [e^{-i\varphi} (K'_{01} + K_{10}) \\ & + e^{i\varphi} (K'_{-10} + K'_{0-1})] \end{aligned} \quad (\text{G.18})$$

$$\begin{aligned} S_3 = & -K_1 \sin^2 \vartheta - K_0 \cos^2 \vartheta + \sin^2 \vartheta [K_1 K'_{-11} + K'_{1-1} K_{-1} \\ & - \frac{1}{2} K_0 K'_{-11} - \frac{1}{2} K'_{00} K_{-1} - \frac{1}{2} K_0 K'_{1-1} - \frac{1}{2} K'_{00} K_1 \\ & + \frac{1}{2} e^{-i2\varphi} K_0 K'_{11} + \frac{1}{2} e^{i2\varphi} K_0 K'_{-1-1}] \\ & + 2^{-\frac{1}{2}} \sin \vartheta \cos \vartheta [e^{-i\varphi} (K'_{10} K_{-1} + K_1 K'_{01}) \\ & + e^{i\varphi} (K_{-1} K'_{0-1} + K'_{-10} K_1)] + K_0 K'_{-11} + K'_{00} K_{-1} \\ & + K_0 K'_{1-1} + K'_{00} K_1 \end{aligned} \quad (\text{G.19})$$

$$\begin{aligned} S_2 = & \sin^2 \vartheta [K_1 K_{-1} - K_0 K_1] + 2 K_0 K_1 \\ & - K'_{1-1} K_{-1} K_0 - K_1 K'_{-11} K_0 - K_1 K_{-1} K'_{00} \end{aligned} \quad (\text{G.20})$$

$$S_1 = -K_1 K_{-1} K_0 . \quad (\text{G.21})$$

In cylindrical (n_\perp, n_z, φ) coordinates, the dispersion equation (with no collisions) can be written

$$C_4 n_\perp^6 + C_3 n_\perp^4 + C_2 n_\perp^2 + C_1 = 0 \quad (\text{G.22})$$

where

* Only terms linear in temperature are retained ; this is consistent with the derivation of the corresponding dielectric tensor elements (see especially p.42).

$$C_1 = n_z^6 c_{oo} - n_z^4 [K_o + K_o (c_{-11} + c_{1-1}) + 2K_{\perp} c_{oo}] \\ + n_z^2 [2K_{\perp} K_o + K_{-1} K_o c_{1-1} + K_1 K_o c_{-11} + K_1 K_{-1} c_{oo}] - K_1 K_{-1} K_o \quad (G.23)$$

$$C_2 = n_z^4 [a_{oo} + 2^{-\frac{1}{2}} (b_{10} + b_{-10}) + \frac{1}{2} (c_{1-1} + c_{-11}) + c_{oo}] \\ - n_z^2 [K_o + K_{\perp} + 2K_{\perp} a_{oo} + K_o (a_{1-1} + a_{-11}) + 2^{\frac{1}{2}} \\ \cdot (K_1 b_{10} + K_{-1} b_{-10}) + \frac{1}{2} K_o (c_{1-1} + c_{-11}) + K_{-1} c_{1-1} + K_1 c_{-11} \\ + K_{\perp} c_{oo}] + K_o K_{\perp} + K_1 K_{-1} + \frac{1}{2} K_{-1} K_o a_{1-1} + \frac{1}{2} K_1 K_o a_{-11} \\ + K_1 K_{-1} a_{oo} \quad (G.24)$$

$$C_3 = n_z^2 [a_{11} + a_{oo} + 2^{\frac{1}{2}} (b_{10} + b_{-10}) + \frac{1}{2} (c_{1-1} + c_{-11})] \\ - K_{\perp} - \frac{1}{2} (K_o + K_1) a_{-11} - \frac{1}{2} (K_o + K_{-1}) a_{1-1} - K_o a_{11} - K_{\perp} a_{oo} \quad (G.25)$$

$$C_4 = \frac{1}{2} (a_{-11} + a_{1-1}) + a_{11} \quad (G.26)$$

where we have used the definitions (C.21).

The following real refractive index surfaces shown in this section were obtained from (G.17), for the case where collisions are neglected. The plasma is taken to be composed of electrons and protons at a uniform temperature of 6000°K. Refractive index surfaces are presented in order of decreasing frequencies which are indicated on the graphs by the values of X_e . At any given frequency there are at most three refractive index surfaces for this model. The real refractive index surfaces are somewhat arbitrarily numbered by subscripts on the value of X_e so as to assist in the identification of modes.

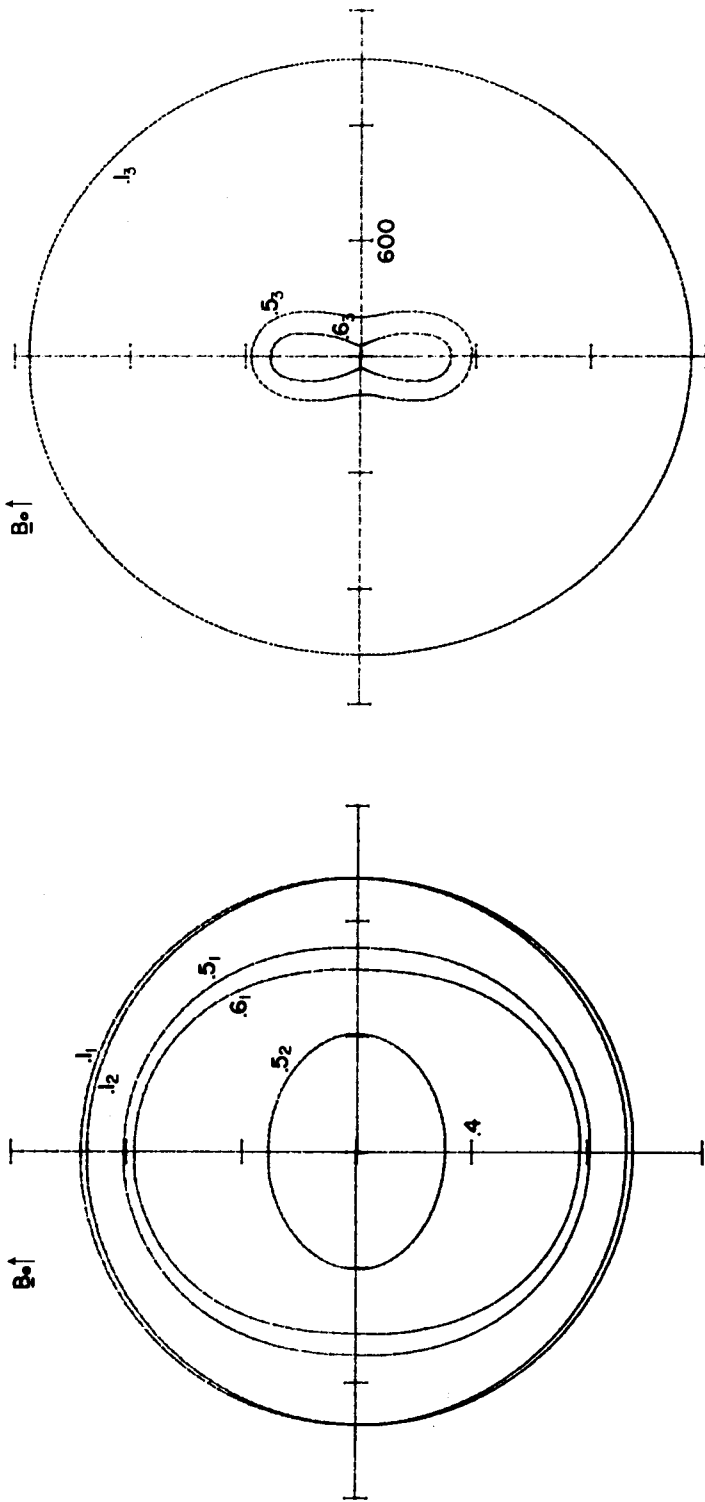


Fig.47 . Refractive index surfaces obtained with Model A for frequencies above $X_e = 0.625$. (Expanded scale shown). Curves are labeled according to values of X_e with $R^2 = 0.4$.

Fig. 48 . Refractive index surfaces obtained with Model A for frequencies above $X_e = 0.625$. (Compressed scale shown). Curves are labeled according to values of X_e with $R^2 = 0.4$.

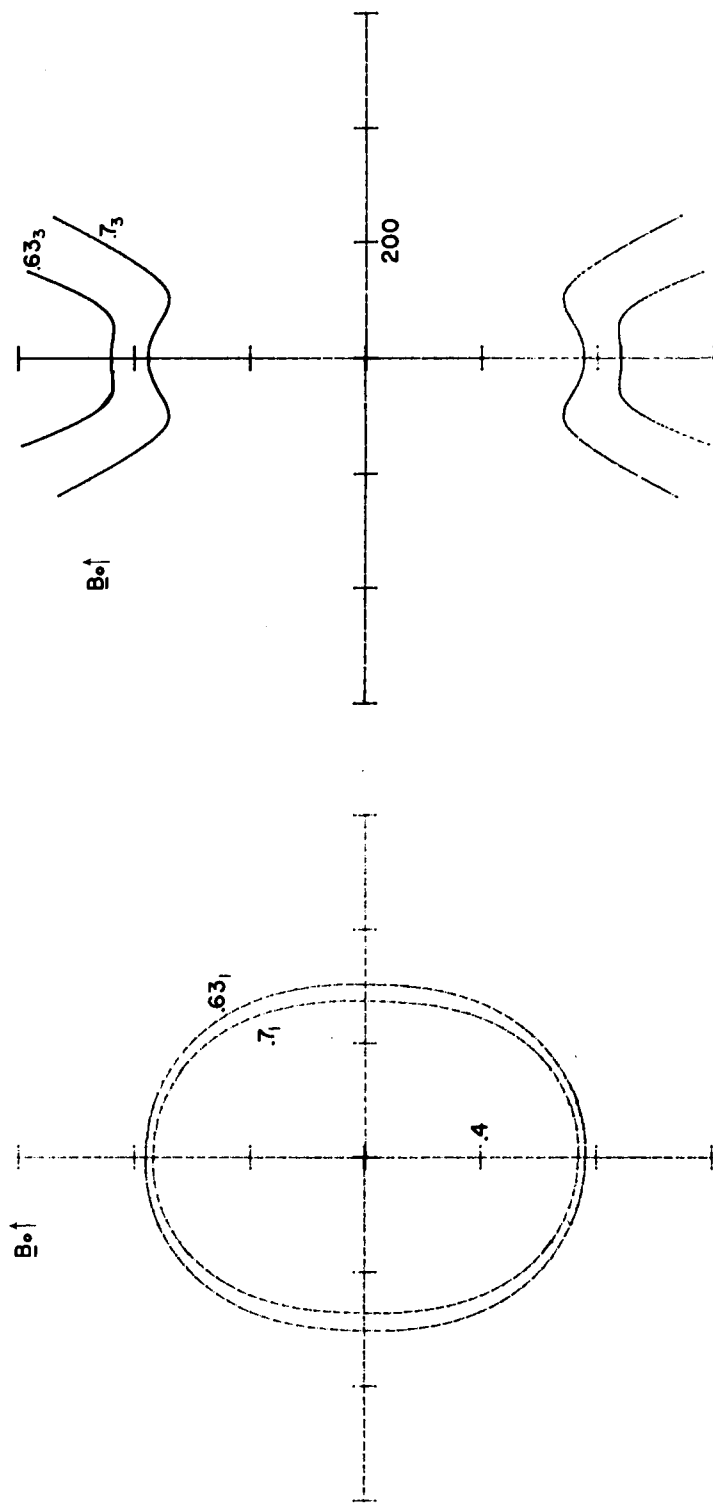


Fig. 49 . Refractive index surfaces obtained with Model A for frequencies between $X_e = 0.625$ and the upper hybrid resonance. (Expanded scale shown). Curves are labeled according to values of X_e with $R^2 = 0.4$.

Fig. 50 . Refractive index surfaces obtained with Model A for frequencies between $X_e = 0.625$ and the upper hybrid resonance. (Compressed scale shown). Curves are labeled according to values of X_e with $R^2 = 0.4$.

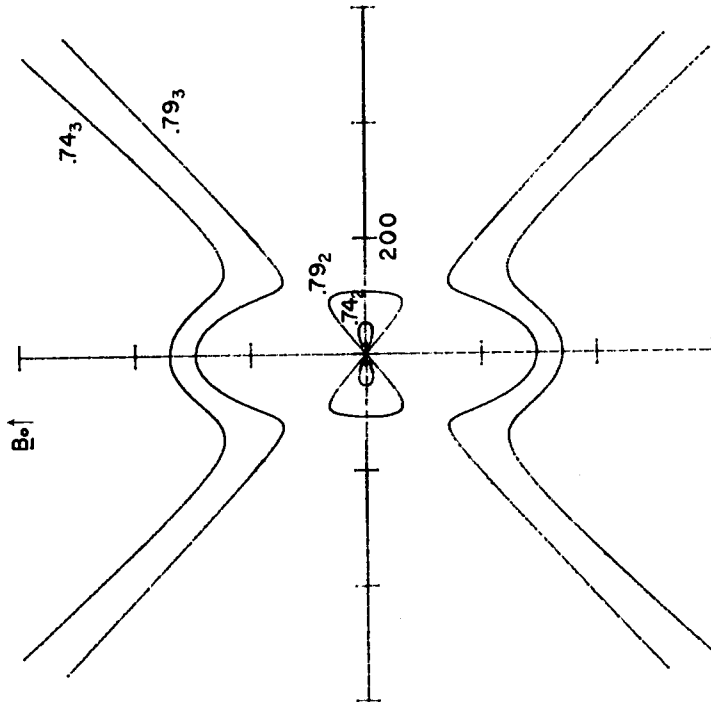


Fig. 51. Refractive index surfaces obtained with Model A for the higher frequency portion of the band between the UHR and the plasma cutoff. (Expanded scale shown). Curves are labeled according to values of X_e with $R^2 = 0.4$.

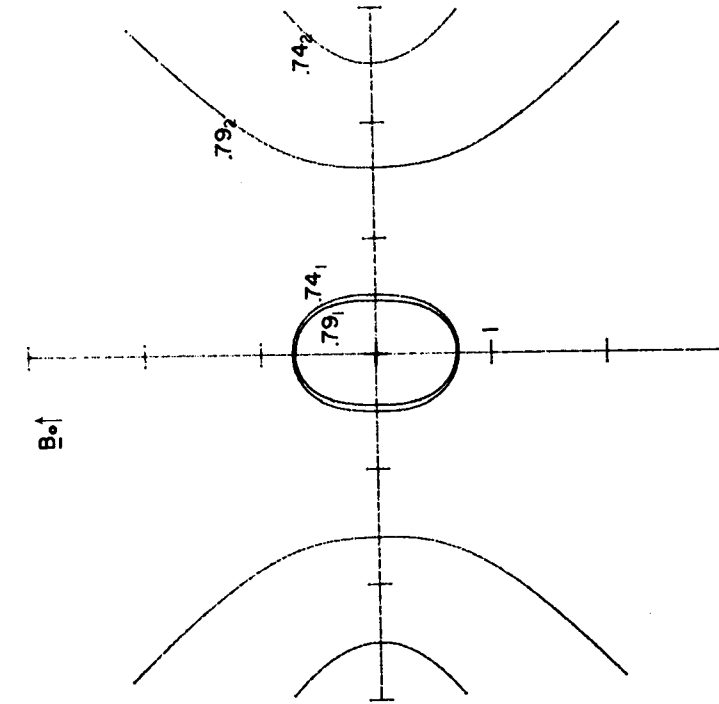


Fig. 52. Refractive index surfaces obtained with Model A for the higher frequency portion of the band between the UHR and the plasma cutoff. (Compressed scale shown). Curves are labeled according to values of X_e with $R^2 = 0.4$.

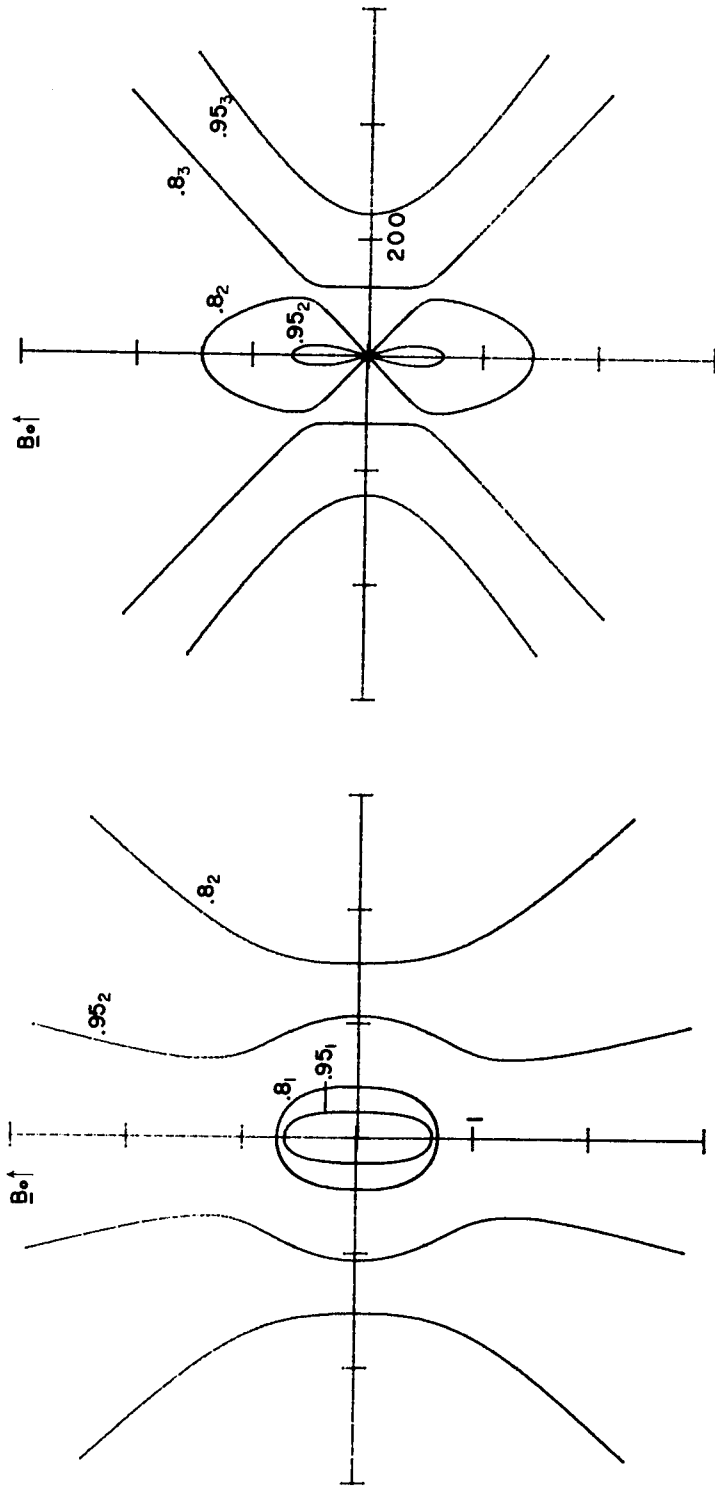


Fig. 53 . Refractive index surfaces obtained with Model A for the lower frequency portion of the band between the UHR and the plasma cutoff. (Expanded scale shown). Curves are labeled according to values of X_e with $R^2 = 0.4$.

Fig. 54 . Refractive index surfaces obtained with Model A for the lower frequency portion of the band between the UHR and the plasma cutoff. (Compressed scale shown). Curves are labeled according to values of X_e with $R^2 = 0.4$.

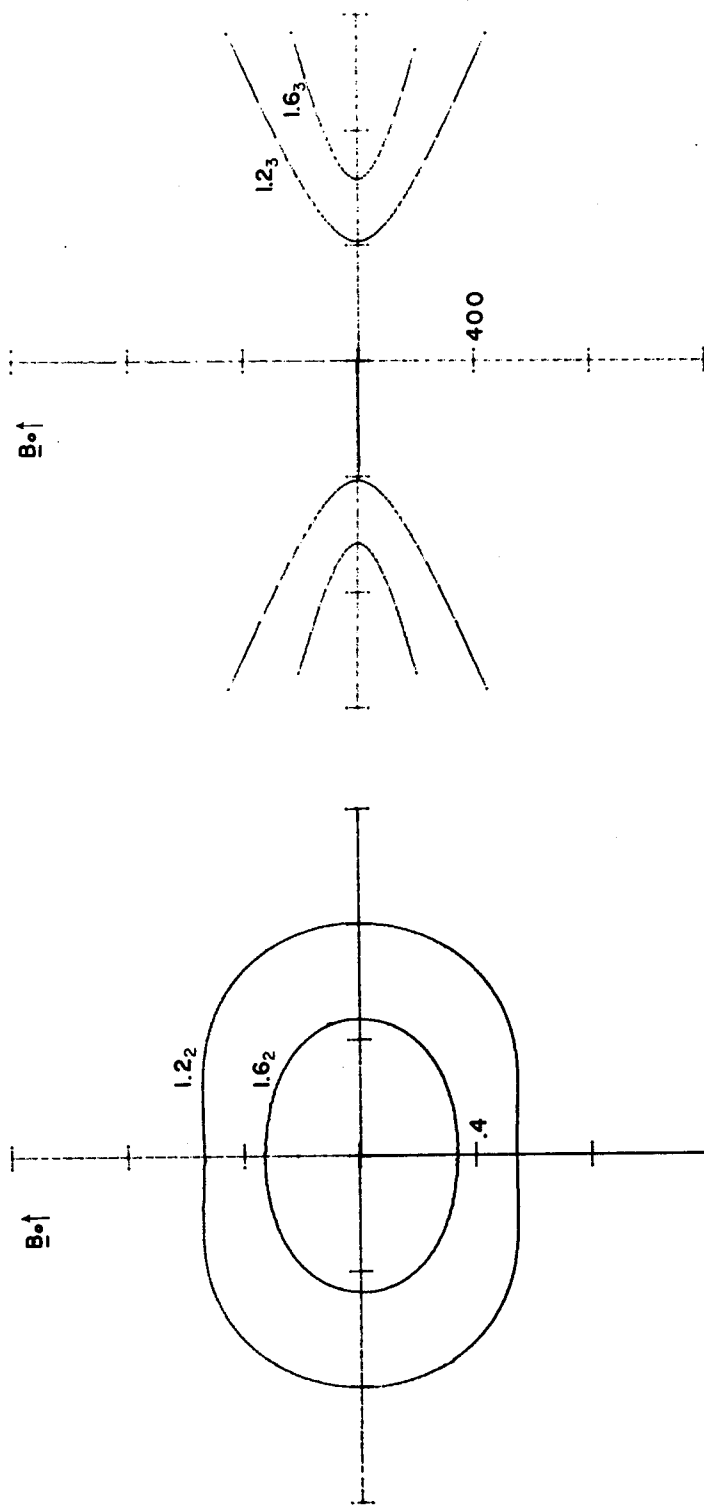


Fig. 55 . Refractive index surfaces obtained with Model A for frequencies between the plasma cutoff and the ion cyclotron cutoff. (Expanded scale shown). Curves are labeled according to values of X_e with $R^2 = 0.4$.

Fig. 56 . Refractive index surfaces obtained with Model A for frequencies between the plasma cutoff and the ion cyclotron cutoff. (Compressed scale shown). Curves are labeled according to values of X_e with $R^2 = 0.4$.

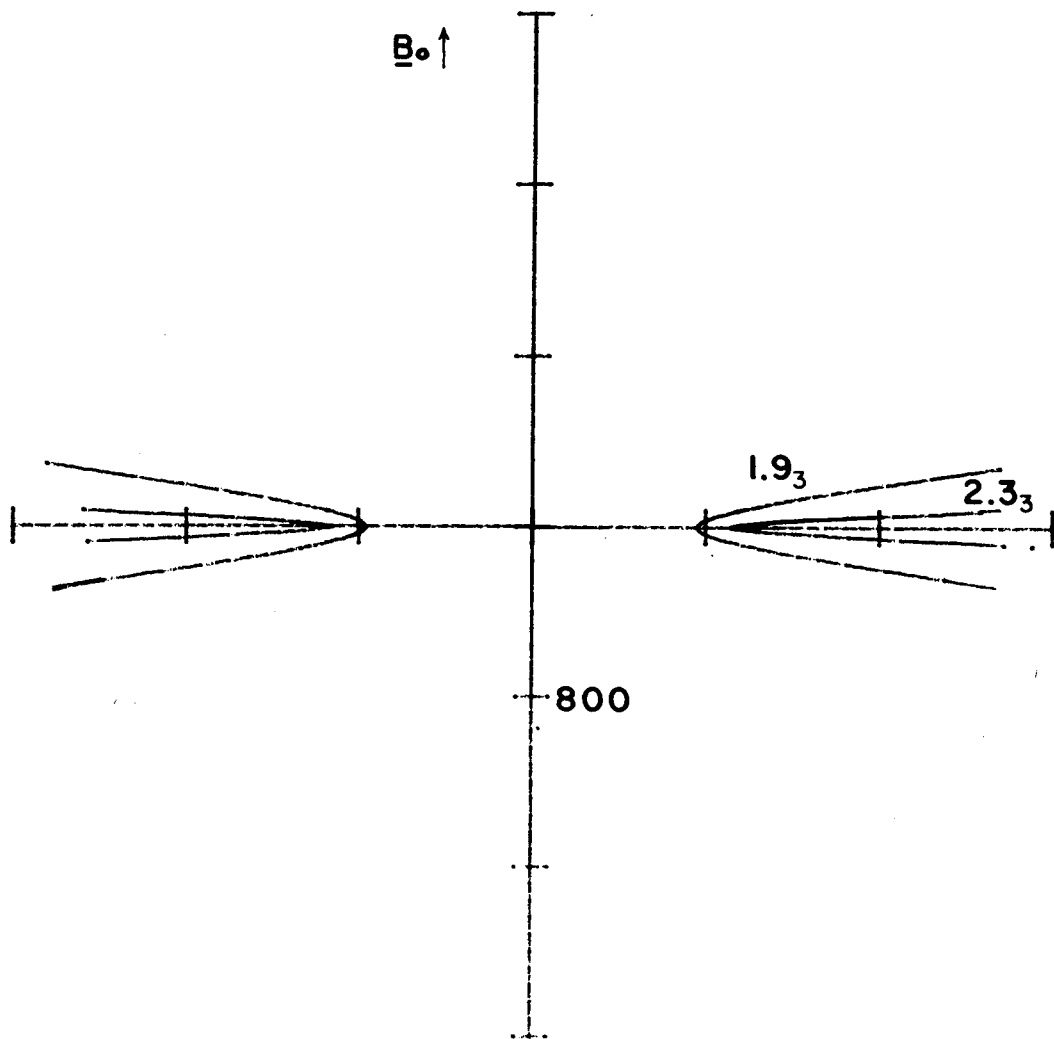


Fig. 57 Refractive index surfaces obtained with Model A for frequencies between the ion cyclotron cutoff and the electron gyro-resonance. Curves are labeled according to values of X_e with $R^2 = 0.4$.

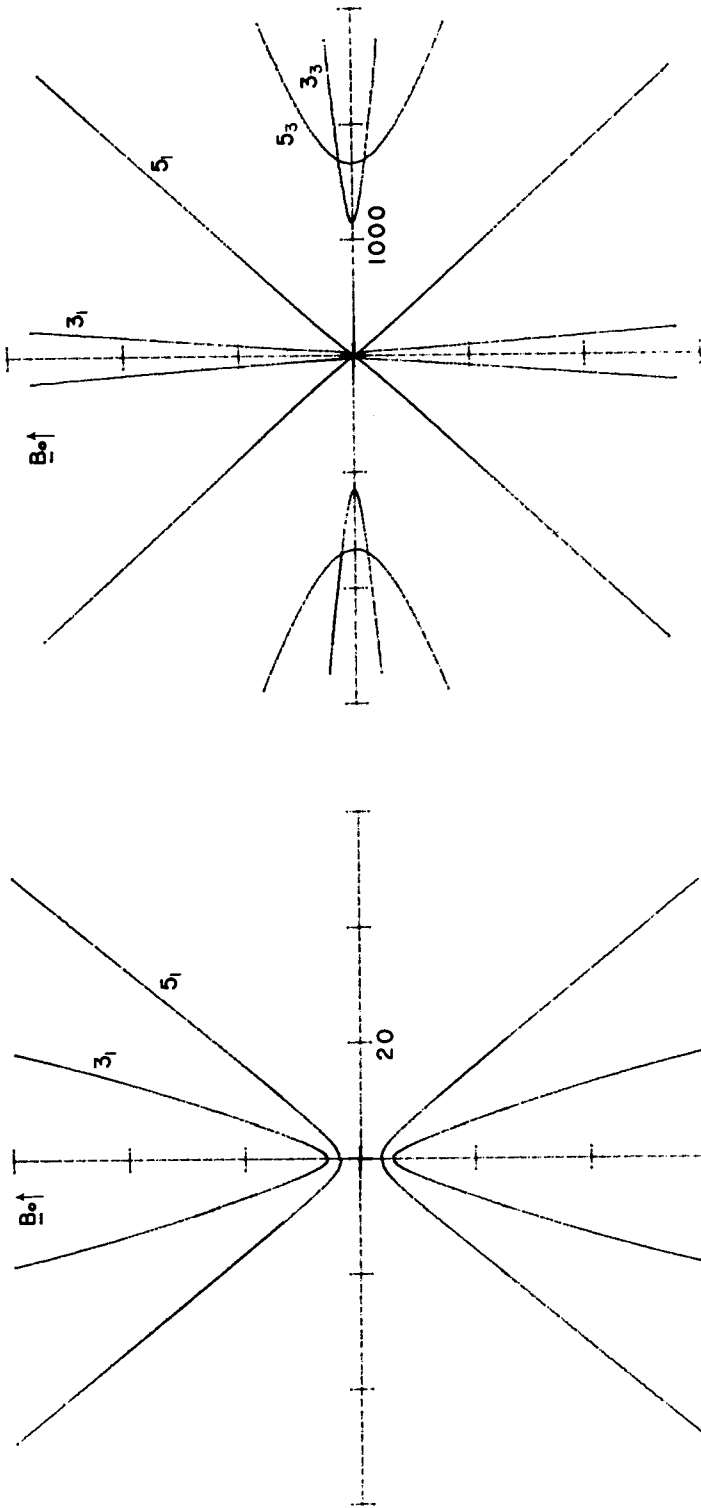


Fig. 58 . Refractive index surfaces obtained with Model A for frequencies just below the electron gyro-resonance. (Expanded scale shown). Curves are labeled according to values of X_e with $R^2 = 0.4$.

Fig. 59 . Refractive index surfaces obtained with Model A for frequencies just below the electron gyro-resonance. (Compressed scale shown). Curves are labeled according to values of X_e with $R^2 = 0.4$.

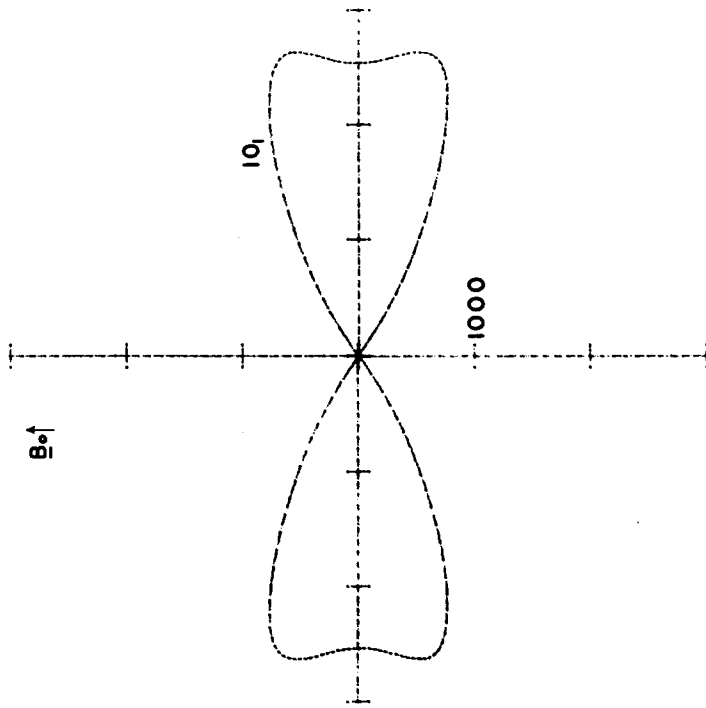


Fig. 60 . Refractive index surface obtained with Model A for the higher frequency portion of the band between the LHR and the electron gyro-resonance. (Expanded scale shown). Curve is labeled according to value of X_e with $R^2 = 0.4$.

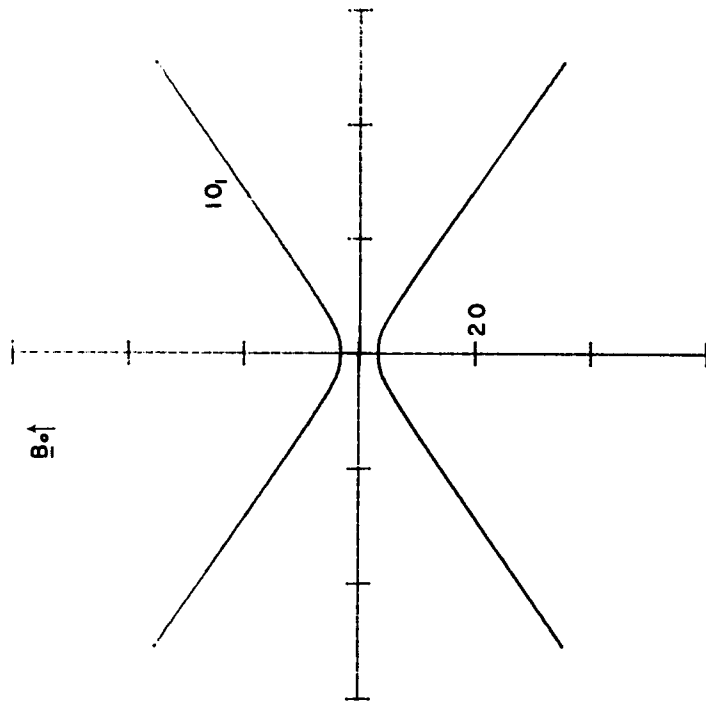


Fig. 61 . Refractive index surface obtained with Model A for the higher frequency portion of the band between the LHR and the electron gyro-resonance. (Compressed scale shown). Curve is labeled according to value of X_e with $R^2 = 0.4$.

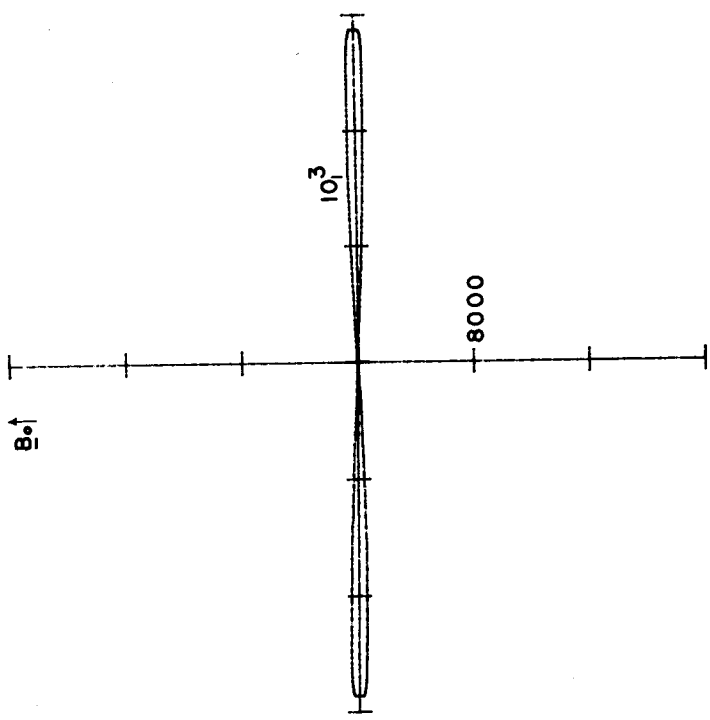


Fig. 63 . Refractive index surface obtained with Model A for the lower frequency portion of the band between the LHR and the electron gyro-resonance. (Compressed scale shown). Curve is labeled according to value of X_e with $R^2 = 0.4$.

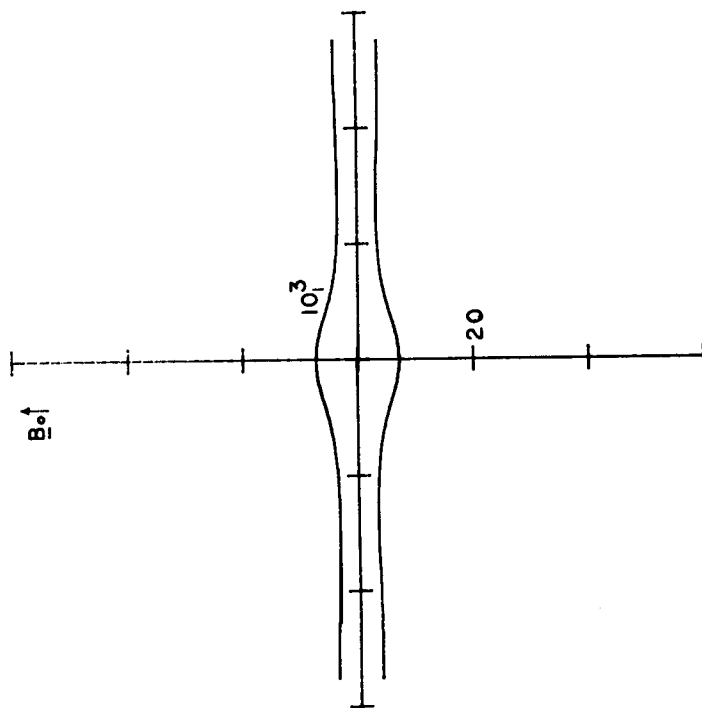


Fig. 62 . Refractive index surface obtained with Model A for the lower frequency portion of the band between the LHR and the electron gyro-resonance. (Expanded scale shown). Curve is labeled according to value of X_e with $R^2 = 0.4$.

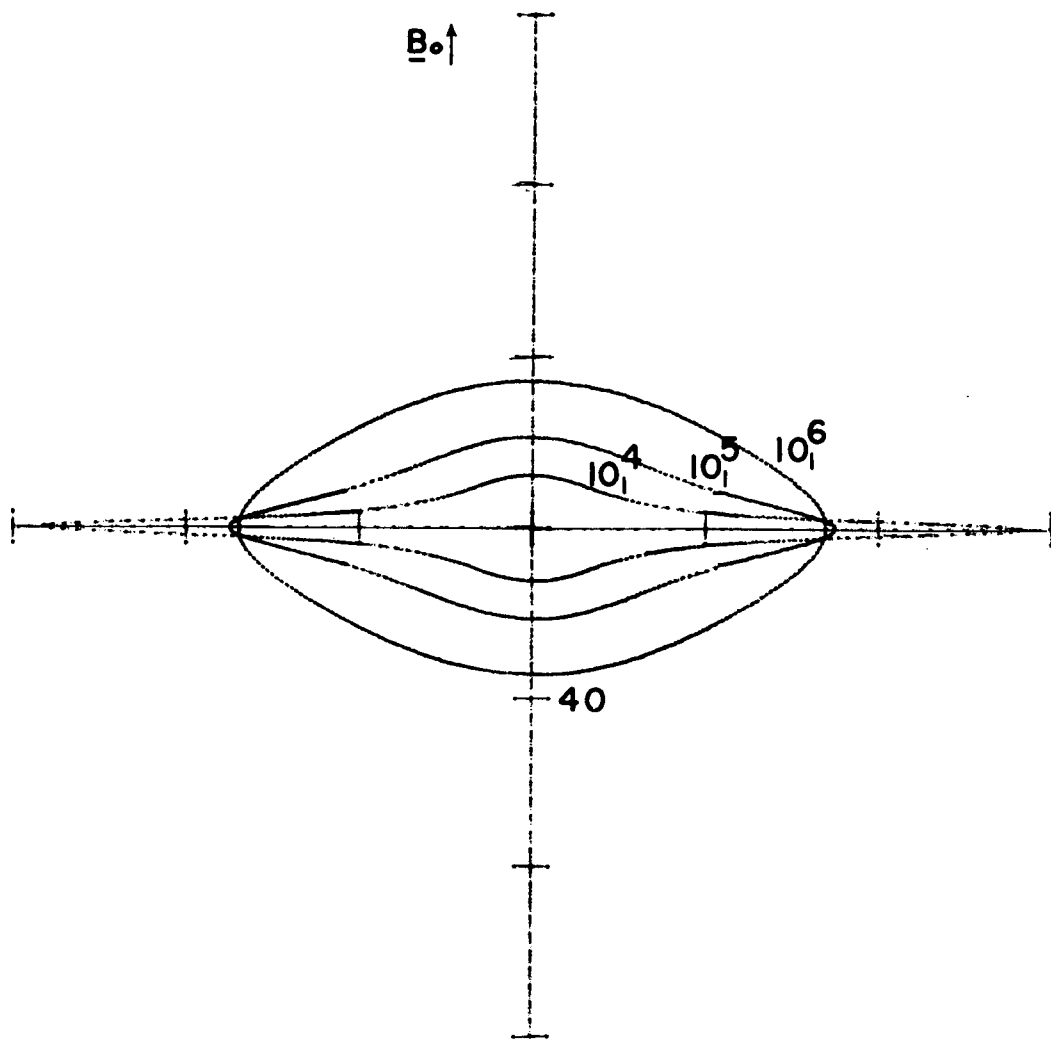


Fig. 64. Refractive index surfaces obtained with Model A for frequencies between the LHR and the ion gyro-resonance. Curves are labeled according to values of X_e with $R^2 = 0.4$.

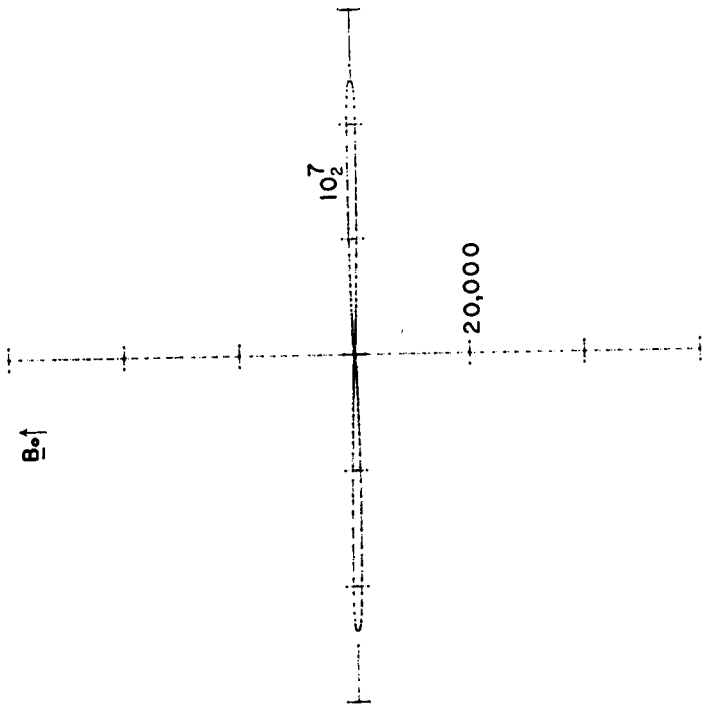


Fig. 66 . Refractive index surface obtained with Model A for a frequency below the ion gyro-resonance. (Compressed scale shown). Curve is labeled according to value of X_e with $R^2 = 0.4$.

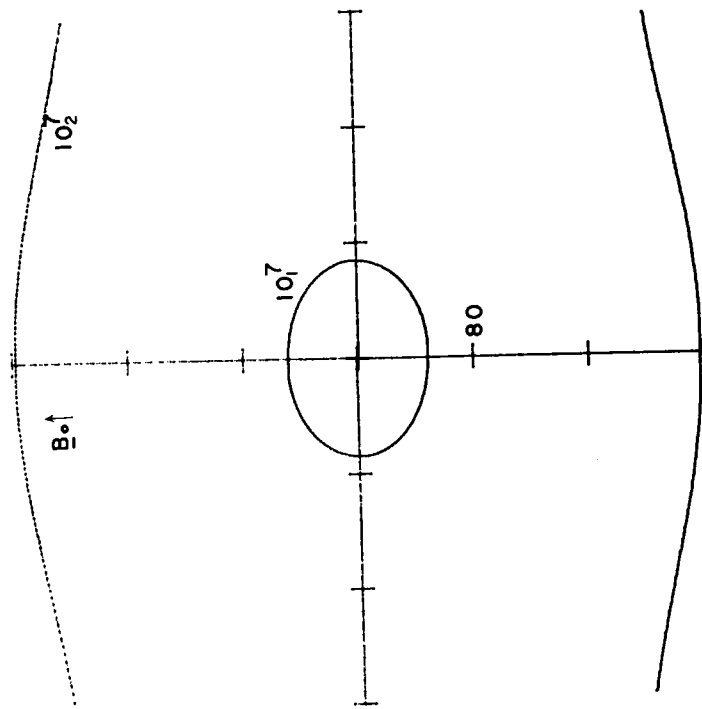


Fig. 65 . Refractive index surfaces obtained with Model A for a frequency below the ion gyro-resonance. (Expanded scale shown). Curves are labeled according to values of X_e with $R^2 = 0.4$.

APPENDIX H

RELEVANT FORMULAS, DEFINITIONS, AND PHYSICAL CONSTANTS

Physical Constants (MKS units, degrees Kelvin)

Charge of a proton, q	1.602×10^{-19}
Mass of an electron, m_e	9.109×10^{-31}
Mass of a proton, m_p	1.673×10^{-27}
Boltzmann's constant, K	1.380×10^{-23}
Speed of light in vacuum, $c = (\mu_o \epsilon_o)^{-\frac{1}{2}}$	2.998×10^8
Planck's constant, h	6.625×10^{-34}
Planck's constant divided by 2π , \hbar	1.054×10^{-34}
Permittivity of free space, ϵ_o	8.854×10^{-12}
Permeability of free space, μ_o	$4 \pi \times 10^{-7}$
Electron to proton mass ratio, m_e/m_p	5.445×10^{-4}
Proton to electron mass ratio, m_p/m_e	1837
Electron charge to mass ratio, q/m_e	1.759×10^{11}
Free space wave impedance, $Z_o = (\mu_o/\epsilon_o)^{\frac{1}{2}}$	377

Conversion Factors

- 1 weber/m² = 1 tesla = 10⁴ gauss
- 1 gamma = 1 nano-weber/m²
- 1 joule = 10⁷ ergs
- 1 eV = 1.6 x 10⁻¹⁹ joules

Plasma Parameters (MKS units and degrees Kelvin
unless otherwise indicated)

$$\text{Electron cyclotron frequency, } |\omega_{ce}| = q B/m_e \quad (\text{H.1})$$

$$|\omega_{ce}| = 1.76 \times 10^{11} B \text{ rad/sec} \quad (\text{H.2})$$

$$f_{ce} = |\omega_{ce}|/2\pi = 2.80 \times 10^{10} B \text{ Hz.} \quad (\text{H.3})$$

$$\text{Electron plasma frequency, } \omega_{pe} = (N_e q^2/m_e \epsilon_0)^{\frac{1}{2}} \quad (\text{H.4})$$

$$\omega_{pe} = 56.5 N_e^{\frac{1}{2}} \quad (\text{H.5})$$

$$f_{pe} = 8.99 N_e^{\frac{1}{2}} \quad (\text{H.6})$$

$$\text{Electron Debye length, } \lambda_{De} = (KT_e/m_e)^{\frac{1}{2}}/\omega_{pe} \quad (\text{H.7})$$

$$\lambda_{De} = 69.0 (T_e/N_e)^{\frac{1}{2}} \quad (\text{H.8})$$

$$\text{Electron thermal speed, } V_{the} = \lambda_{De} \omega_{pe} = (KT_e/m_e)^{\frac{1}{2}} \quad (\text{H.9})$$

$$\text{Electron kinetic energy, } E_{kin} = m_e c^2 (\gamma - 1) \quad (\text{H.10})$$

where $\gamma \equiv (1 - v^2/c^2)^{-\frac{1}{2}}$ is the Lorentz factor for a particle moving at the speed v .

$$E_{kin} = 8.187 \times 10^{-14} (\gamma - 1) \text{ joules} = 0.5117 (\gamma - 1) \text{ Mev} \quad (\text{H.11})$$

Formulas Involving Bessel Functions (Integer s)

This section contains those formulas involving Bessel functions which are pertinent to this thesis. We use the notation that J_s and N_s are Bessel functions of the first and second kind, respectively, $H_s^{(1)}$ and $H_s^{(2)}$ are Hankel functions of the first and second kind and I_s is the modified Bessel function.

a. Interrelationships:

$$J_s(z) = \frac{1}{2} \left[H_s^{(1)}(z) + H_s^{(2)}(z) \right] \quad (\text{H.12})$$

$$H_s^{(\frac{1}{2})}(z) = J_s(z) \pm i N_s(z) \quad (\text{H.13})$$

$$I_s(z) = i^{-s} J_s(iz) \quad (-\pi < \arg z \leq \frac{1}{2}\pi) \quad (\text{H.14})$$

b. Recurrence relations for J_s^{-1}

$$J_s(z) = \frac{z}{2s} \left[J_{s-1}(z) + J_{s+1}(z) \right] \quad (\text{H.15})$$

$$J'_s(z) = \frac{1}{2} \left[J_{s-1}(z) - J_{s+1}(z) \right] \quad (\text{H.16})$$

$$J_{s\pm 1}(z) = \frac{s}{z} J_s(z) \mp J'_s(z) \quad (\text{H.17})$$

c. Recurrence relations for I_s

$$I_s(z) = \frac{z}{2s} \left[I_{s-1}(z) - I_{s+1}(z) \right] \quad (\text{H.18})$$

$$I'_s(z) = \frac{1}{2} \left[I_{s-1}(z) + I_{s+1}(z) \right] \quad (\text{H.19})$$

$$I_{s\pm 1}(z) = I'_s(z) \mp \frac{s}{z} I_s(z) \quad (\text{H.20})$$

¹ The same recurrence relations apply to J_s , N_s , $H_s^{(1)}$, and $H_s^{(2)}$.

d. Symmetry properties

$$J_s(-z) = (-1)^s J_s(z) \quad (\text{H.21})$$

$$H_s^{(1)}(e^{i\pi} z) = -e^{-i\pi s} H_s^{(2)}(z) \quad (\text{H.22})$$

$$H_s^{(2)}(e^{-i\pi} z) = -e^{i\pi s} H_s^{(1)}(z) \quad (\text{H.23})$$

$$I_s(-z) = (-1)^s I_s(z) \quad (\text{H.24})$$

$$J_{-s}(z) = (-1)^s J_s(z) \quad (\text{H.25})$$

$$H_{-s}^{(\pm)}(z) = (-1)^{\pm s} H_s^{(\pm)}(z) \quad (\text{H.26})$$

$$I_{-s}(z) = I_s(z) \quad (\text{H.27})$$

e. Differential equation satisfied by J_s

$$z^2 J_s'' + z J_s' + (z^2 - s^2) J_s = 0 \quad (\text{H.28})$$

f. Differential equation satisfied by I_s

$$z^2 I_s'' + z I_s' - (z^2 + s^2) I_s = 0 \quad (\text{H.29})$$

g. Relations involving fractional orders

$$J_{3/2}(z) = \sqrt{\frac{2}{\pi z}} \left[\frac{\sin z}{z} - \cos z \right] \quad (\text{H.30})$$

h. Sums of Bessel functions

$$e^{iL \sin M} = \sum_{s=-\infty}^{\infty} J_s(L) e^{isM} \quad (\text{H.31})$$

$$e^{-iL \sin M} = \sum_{s=-\infty}^{\infty} J_s(L) e^{-isM} \quad (\text{H.32})$$

$$e^{iL \cos M} = \sum_{s=-\infty}^{\infty} J_s(L) e^{is(M+\pi/2)} \quad (\text{H.33})$$

$$e^{-iL \cos M} = \sum_{s=-\infty}^{\infty} J_s(L) e^{-is(M+\pi/2)} \quad (\text{H.34})$$

i. Integrals related to Bessel functions

$$\int_0^{2\pi} e^{i(\ell\varphi - a \sin \varphi)} d\varphi = 2\pi J_\ell(a) \quad (\text{H.35})$$

$$\int_0^{2\pi} \cos \varphi e^{i(\ell\varphi - a \sin \varphi)} d\varphi = (2\pi \ell/a) J_\ell(a) \quad (\text{H.36})$$

j. Small argument expansions

$$J_s(z) = \left(\frac{1}{2}z\right)^s \sum_{k=0}^{\infty} \frac{(-\frac{1}{4}z^2)^k}{k! (s+k)!}, \quad s \geq 0 \quad (\text{H.37})$$

$$I_s(z) = \left(\frac{1}{2}z\right)^s \sum_{k=0}^{\infty} \frac{(\frac{1}{4}z^2)^k}{k! (s+k)!}, \quad s \geq 0 \quad (\text{H.38})$$

In particular, for $|z| \ll 1$

$$I_0(z) \approx 1 + z^2/4 + z^4/64$$

$$I'_0(z) \approx z/2$$

$$I''_0(z) \approx \frac{1}{2}$$

$$I_1(z) = I_{-1}(z) \approx z/2 + z^3/16$$

$$I'_1(z) = I'_{-1}(z) \approx \frac{1}{2} \quad (\text{H.39})$$

$$I''_1(z) = I''_{-1}(z) \approx 3z/8$$

$$I_2(z) = I_{-2}(z) \approx z^2/8$$

$$I'_2(z) = I'_{-2}(z) \approx z/4$$

$$I''_2(z) = I''_{-2}(z) \approx \frac{1}{4}$$

$$I_3(z) = I_{-3}(z) \approx z^3/48$$

$$I'_3(z) = I'_{-3}(z) \approx z^2/16$$

$$I''_3(z) = I''_{-3}(z) \approx z/8$$

Formulas Involving the Plasma Dispersion Function $Z(\zeta)$

a. Definition: The plasma dispersion function $Z(\zeta)$ is defined by

$$Z(\zeta) = \pi^{-\frac{1}{2}} \int_{-\infty}^{\infty} dx \frac{e^{-x^2}}{x - \zeta} = i \pi^{\frac{1}{2}} e^{-\zeta^2} [1 + \operatorname{erf}(i \zeta)] \quad (\text{H.40})$$

for $\operatorname{Im} \zeta > 0$ and as the analytic continuation of this for $\operatorname{Im} \zeta \leq 0$.

b. Symmetry properties:

$$Z(\zeta^*) = - [Z(-\zeta)]^* \quad (\text{H.41})$$

c. Differential equation characterization

$$\begin{aligned} Z' &= -2(1 + \zeta Z) \\ Z(0) &= i \pi^{\frac{1}{2}} \end{aligned} \quad (\text{H.42})$$

d. Power series

$$Z(\zeta) = i \pi^{\frac{1}{2}} e^{-\zeta^2} - 2 \zeta \left[1 - 2 \zeta^2/3 + 4 \zeta^4/15 - \dots \right] \quad (\text{H.43})$$

e. Asymptotic expansion

$$Z(\zeta) \approx i \pi^{\frac{1}{2}} \sigma e^{-\zeta^2} - \zeta^{-1} \left[1 + 1/2 \zeta^2 + 3/4 \zeta^4 + \dots \right] \quad (\text{H.44})$$

where

$$\sigma = \begin{cases} 0, & \operatorname{Im} \zeta > 0 \\ 1, & \operatorname{Im} \zeta = 0 \\ 2, & \operatorname{Im} \zeta < 0 \end{cases}$$

Vector and Tensor Identities

$$\underline{A} \times (\underline{B} \times \underline{C}) = (\underline{A} \cdot \underline{C}) \underline{B} - (\underline{A} \cdot \underline{B}) \underline{C} \quad (\text{H.45})$$

$$(\underline{A} \times \underline{B}) \times \underline{P} = \underline{B} \underline{A} \cdot \underline{P} - \underline{A} \underline{B} \cdot \underline{P} \quad (\text{H.46})$$

Formulas Involving the Dirac Delta Functions

$$\int_{-\infty}^{\infty} e^{ikx} dk = 2\pi \delta(x) \quad (\text{H.47})$$

$$\int e^{i\mathbf{k} \cdot \mathbf{r}} d^3k = (2\pi)^3 \delta(\mathbf{r}) \quad (\text{H.48})$$

LIST OF REFERENCES

Reference

- 1 Alexander, J.K. and R.G. Stone (1965), Rocket Measurements of Cosmic Radio Noise Intensities Below Five Mc/s, Rep. NASA-TM-X-55216, Greenbelt, Maryland.
- 2 Allis, W.P., S.J. Buchsbaum, and A. Bers (1963), Waves in Anisotropic Plasmas, M.I.T. Press, Cambridge, Mass.
- 3 Allis, W.P. (1959), Waves in a Plasma, Quart. Prog. Rpt. 54(5), Mass. Inst. Technol. Research Lab.
- 4 Aubry, M.P., J. Bitoun, and Ph. Graff (1970), Propagation and Group Velocity in a Warm Magnetoplasma, Radio Sci., 5(3), 635-645.
- 5 Baker, D.J., H. Weil, and L.S. Bearce (1973), Impedance and Large Signal Excitation of Satellite-Borne Antennas in the Ionosphere, IEEE Trans. Antennas Propagat., AP-21, 672-679.
- 6 Beghin, C. and R. Debie (1972), Characteristics of the Electric Field Far from and Close to a Radiating Antenna Around the Lower Hybrid Resonance in the Ionospheric Plasma, J. Plasma Phys., 8(3), 287.
- 7 Bernstein, I.B. (1958), Waves in a Plasma in a Magnetic Field, Phys. Rev., 109(1), 10-21.
- 8 Bitoun, J., Ph. Graff and M. Aubry (1970), Ray Tracing in a Warm Magnetoplasma and Applications to Topside Resonances, Radio Sci., 5(11), 1341-1349.
- 9 Blair, W.E. (1968), Ionospheric Diagnostics Using Resonances of an Electric Dipole Impedance, Radio Sci., 3(2), 155-161.

- 10 Buneman, O. (1961), Gas Law and Conductivity of a Collision-Free Plasma, *Phys. Fluids*, 4, 669-680.
- 11 Clemmow, P.C. and R.F. Mullaly (1955), The Dependence of the Refractive Index in Magneto-Ionic Theory on the Direction of the Wave Normal, "The Physics of the Ionosphere: Report of the Phys. Soc. Conf...Cavendish Lab.", Physical Society, London, 340.
- 12 Cohen, M.H. (1961), Radiation in a Plasma. I. Čerenkov Effect, *Phys. Rev. (second ser.)*, 123(3), 711-721.
- 13 Cook, K.R. and B.C. Edgar (1966), Current Distribution and Impedance of a Cylindrical Antenna in an Isotropic Compressible Plasma, *Radio Sci.*, 1(1), 13-19.
- 14 Delcroix, J.L. (1965), Plasma Physics, John Wiley, New York.
- 15 DeWolf, D.A. (1966), Impedance of a Small VLF Dipole in the Ionosphere, *Radio Sci.*, 1(5), 571-575.
- 16 Dowden, R.L. (1973), Use of Electron and Proton Beams for Production of Very Low Frequency and Hydromagnetic Emissions, *J. Geophys. Res.*, 78(4), 684-696.
- 17 Duncan, A.J. and J.R. Forrest (1970), Low Frequency Axisymmetric Waves in a Weakly Ionized Magnetoplasma Column, Rep. 366, Stanford U. Institute for Plasma Research (SUIPR), Stanford, California.
- 18 Ellis, G.R.A. and P.M. McCulloch (1963), The Decametric Radio Emissions of Jupiter, *Aust. J. Phys.*, 16, 380-397.
- 19 Ellis, G.R. (1957), Low-Frequency Radio Emission from Aurorae, *J. Atmos. Terr. Phys.*, 10, 302-306.

- 20 Felsen, L.B. (1965), On the Use of Refractive Index Diagrams for Source-Excited Anisotropic Regions, *Radio Sci. J. Res.*, NBS, 69D(2), 155-169.
- 21 Frank, I.M. and I. Tamm (1937), *Doklady Akad. Nauk (S.S.S.R.)* 14(3), 109.
- 22 Fried, B.D. and S.D. Conte (1961), The Plasma Dispersion Function, Academic Press, New York.
- 23 Galejs, J. (1967), Effective Radiation Resistance of a Short Antenna in a Lossy Uniaxial Medium, Rpt. 522, Applied Res. Lab., Sylvania Electronic Systems, Waltham, Mass.
- 24 Galejs, J. (1967), Power Flow From a Short Antenna in a Lossy Uniaxial Medium, *Radio Sci.*, 2(12), 1419-1430.
- 25 Gallet, R.M. (1959), The Very Low-Frequency Emissions Generated in the Earth's Exosphere, *Proc. IRE*, 47, 211-231.
- 26 Gradshteyn, I.S. and I.M. Ryzhik (1965), Table of Integrals, Series, and Products, 4th ed., Academic Press, New York.
- 27 Gregory, P.C. (1971), Satellite Observations of Magnetospheric Radio Noise - I. Emissions Between the Plasma and Upper Hybrid Resonance Frequencies, *Planet. Space Sci.*, 10, 813-820.
- 28 Gurnett, D.A. and B.J. O'Brien (1964), High-Latitude Geophysical Studies with Satellite Injun 3. 5. Very-Low-Frequency Electromagnetic Radiation, *J. Geophys. Res.*, 69(1), 65-89.
- 29 Harvey, C.C. (1965), Results from the UK-2 Satellite, *Annales d'Astrophys.* 28, 248-254.

- 30 Helliwell, R.A. (1965), Whistlers and Related Ionospheric Phenomena, Stanford University Press., Stanford, Calif.
- 31 Huguenin, G.R., A.E. Lilley, W.H. McDonough, and M.D. Papagiannis (1964), Measurements of Radio Noise at 0.700 Mc and 2.200 Mc from a High-Altitude Rocket Probe, *Planetary Space Sci.*, 12, 1157-1167.
- 32 John, F. (1971), Partial Differential Equations, Springer-Verlag.
- 33 Johnston, T.W. (1970), Anisotropic Plasma Pressure and the Dielectric Tensor, *J. Plasma Phys.*, 4(2), 283-295.
- 34 Jorgensen, T.S. (1968), Interpretation of Auroral Hiss Measured on OGO 2 and at Byrd Station in Terms of Incoherent Cerenkov Radiation, *J. Geophys. Res.*, 73(3), 1055-1069.
- 35 Kasha, M.A. (1969), The Ionosphere and Its Interaction with Satellites, Gordon and Breach, New York.
- 36 Kiepenheuer, K.O. (1946), Origin of Solar Radiation in the 1-6 Metre Radio Wave-length Band, *Nature* 158, 340.
- 37 Kikuchi, H. (1968), General Features and Satellite Observations of Magnetoionic and Magnetohydrodynamic Waves in the Outer Ionosphere, in Low-Frequency Waves and Irregularities in the Ionosphere - ed. by N.D' Angelo, *Astrophysics and Space Sci. Library*, 12-60.
- 38 Kikuchi, H. (1964), Cerenkov Radiation in a Plasma, *Proc. of the Symposium on Quasi-Optics*, 14, Polytechnic Press, Brooklyn, 235-272.
- 39 Klimontovich, Yu. L. (1967), The Statistical Theory of Non-Equilibrium Processes in a Plasma, The M.I.T. Press, Cambridge, Mass.

- 40 Kogelnik , H. (1960), On Electromagnetic Radiation in Magneto-Ionic Media, *Radio Sci. J. Res. NBS*, 64D(5), 515-523.
- 41 Kolomenskii, A.A. (1953), *J. Exptl. Theoret. Phys.(U.S.S.R.)*, 24, 167.
- 42 Lacombe, C. (1968), Les Bandes de Bruit de l'ionosphère: Rayonnement Gyromagnétique Incohérent d'électrons Supra-thermiques, *Ann. Géophys.*, 24, 81.
- 43 Landau, L.D. and E.M. Lifshitz (1958), Quantum Mechanics: Non-Relativistic Theory, Pergamon Press Ltd., New York.
- 44 Lee, K.S.H. and C.H. Papas (1965), A Further Explanation of the New Theory of Antenna Radiation with Particular Reference to Uniaxial Media, *Radio Sci.*, 1(9), 1020-1023.
- 45 Lee, K.S.H. and C.H. Papas (1966), On Walsh and Weil's Defense of the Conventional Method, *Radio Sci.*, 1(9), 1027.
- 46 Lee, K.S.H. and C.H. Papas (1965), Irreversible Power and Radiation Resistance of Antennas in Anisotropic Ionized Gases, *Radio Sci.*, 69D(10), 1313-1320.
- 47 Liemohn, H.B. (1965), Radiation from Electrons in Magneto-plasma , *Radio Sci. J. Res. NBS*, 69D(5), 741-766.
- 48 Lim, T.L. and T. Laaspere (1972), An Evaluation of the Intensity of Cerenkov Radiation from Auroral Electrons with Energies down to 100 ev, *J. Geophys. Res.*, 77, 4145-4157.
- 49 Lin, Sing-Hsiung and K.K. Mei (1968), Numerical Solution of Dipole Radiation in a Compressible Plasma, *IEEE Trans. Antennas Propagat.*, AP-16 (2), 235-241.

- 50 Mansfield, V.N. (1967), Radiation from a Charged Particle Spiraling in a Cold Magnetoplasma, *Astrophys.J.*, 147, 672-680.
- 51 McIlwain, C.E. (1961), Coordinates for Mapping the Distribution of Magnetically Trapped Particles, *J. Geophys. Res.*, 66, 3681-3691.
- 52 McKenzie, J.F. (1967), Radiation Losses from a Test Particle in a Plasma, *Phys. of Fluids*, 10(12), 2680-2694.
- 53 McKenzie, J.F. (1967), Dipole Radiation in Moving Media, *Proc. Phys. Soc.*, 91, 537-551.
- 54 McPherson, D.A., W.B. Harbridge, and H.C. Koons (1972) "Nonlinear Impedance and Near Fields of VLF Dipole Antenna Measured in the Magnetosphere", paper presented at URSI Spring Meeting 13-15 April, Wash., D.C.
- 55 Melrose, D.B. (1968), The Emission and Absorption of Waves by Charged Particles in Magnetized Plasmas, *Astrophys. Space Sci.*, 2, 171-235.
- 56 Oraevskii, V., R. Chodura, and W. Feneberg (1968), Hydrodynamic Equations for Plasmas in Strong Magnetic Fields - I. Collisionless Approximation, *Plasma Phys.*, 10, 819-828.
- 57 Osborne, F.J.F. and M.A. Kasha (1967), The $\underline{V} \times \underline{B}$ Interaction of a Satellite with Its Environment, *Can.J.Phys.*, 45, 263-277.
- 58 Oster, L. (1960), Linearized Theory of Plasma Oscillations, *Rev. Mod. Phys.*, 32 (1), 141-168.
- 59 Pavkovich, J. and G.S. Kino (1964), RF Behavior of the Plasma Sheath, Rpt. ARL-15, Aerospace Research Laboratories, Los Angeles, Calif.

- 60 Reber, G. and G.R. Ellis (1956), Cosmic Radio-Frequency Radiation Near One Megacycle, *J. Geophys. Res.*, 61 (1), 1-10.
- 61 Rishbeth, H. and O.K. Garriott (1969), Introduction to Ionospheric Physics, Academic Press, New York.
- 62 Sakurai, K. and T. Ogawa (1969), Radiation Fields of Energetic Electrons in Helical Orbits within a Magneto-Active Plasma, *Planet. Space Sci.*, 17, 1449-1458.
- 63 Sasiela, R. and J.P. Freidberg (1967), Utilization of the Refractive Index Surfaces to Evaluate Cerenkov Radiation in Magnetoplasma, *Radio Sci.* 2(7), 703-710.
- 64 Schwinger, J. (1949), On the Classical Radiation of Accelerated Electrons, *Phys. Rev.*, 75(12), 1912-1925.
- 65 Seshadri, S.R. (1968), Spectrum of Cerenkov Radiation in a Warm Anisotropic Plasma, *Int. J. Electr.*, 25 (5), 401-416.
- 66 Sharma, S.R. (1968), Effect of Collisions on Wave Motions in a Plasma with Anisotropic Pressure, *J. Phys. A. (Proc. Phys. Soc.)*, 1, 367-375.
- 67 Sharma, S.R. (1967), Wave Propagation in a Plasma with Anisotropic Pressure, *Can. J. Phys.*, 45 (10), 3189-3198.
- 68 Shkarofsky, I.P. (1972), Non Sheath Admittance, Currents, and Charges Associated with High Peak Voltage Drive on a VLF/ELF Dipole Antenna Moving in the Ionosphere, *Radio Sci.*, 7(4), 503-523.
- 69 Shkarofsky, I.P., T.W. Johnston, and M.P. Bachynski (1966), The Particle Kinetics of the Plasmas, Addison-Wesley, Reading, Mass.

- 70 Singh, N. (1973), Radiation Resistance of a Dipole in a Drifting Magnetoplasma, IEEE Trans. Antennas Propagat., AP-21 (3), 399-400.
- 71 Snyder, M.A. and H. Weitzner (1968), VLF Electromagnetic Radiation in a Magnetoionic Medium, Radio Sci., 3(9), 943-954.
- 72 Staras, H. (1966), The "Infinity Catastrophe" Associated with Radiation in Magnetoionic Media, Radio Sci., 1(9), 1013-1020.
- 73 Staras, H. (1964), The Impedance of an Electric Dipole in a Magneto-ionic Medium, IEEE Trans. Antennas Propagat., AP-12 (6), 695-702.
- 74 Stix, T.H. (1962), The Theory of Plasma Waves, McGraw-Hill, New York.
- 75 Storey, L.R.O. (1953), An Investigation of Whistling Atmospherics, Royal Soc. London, Phil. Trans., 246A (908), 113-141.
- 76 Stratton, J.A. (1941), Electromagnetic Theory, McGraw-Hill, New York.
- 77 Swift, J.D. and M.J.R. Schwar (1969), Electrical Probes for Plasma Diagnostics, American Elsevier, New York.
- 78 Tanenbaum, B.S. (1967), Plasma Physics, McGraw-Hill, New York.
- 79 Toll, J.S. (1956), Causality and the Dispersion Relation: Logical Foundations, Phy. Rev., 104 (6), 1760-1770.

- 80 Trulsen, J. and J.A. Fejer (1970), Radiation From a Charged Particle in a Magnetoplasma, *J. Plasma Phys.*, 4 (4), 825-841.
- 81 Tuan, H.S. and S.R. Seshadri (1963), *IEEE Trans. Microw. Theory Tech.*, 11, 462.
- 82 Verheest, F.G. (1967), Waves in Multicomponent Vlasov Plasmas with Anisotropic Pressure, *Z. Naturforschg*, 22 a, 1927-1935.
- 83 Walsh, D. and H. Weil (1966), Irreversible Power and Radiation Resistance of Antennas in Magnetoionic Media, *Radio Sci.*, 1(9), 1025-1027.
- 84 Walsh, D., F.T. Haddock, and H.F. Schulte (1964), Cosmic Radio Intensities at 1.225 and 2.0 Mc Measured up to an Altitude of 1700 km, *Space Research IV*, 935-959.
- 85 Watson, G.N. (1966), A Treatise on the Theory of Bessel Functions, Cambridge U. Press, London, England.
- 86 Weil, H. (1972), Effects of Satellite Motion on Antenna Radiation, paper given at Proceedings of Conf. on Sub-LF Downlink Satellite Communications, 6-9 June 1972, NRL, Wash., D.C.
- 87 Weil, H. and D. Walsh (1965), Radiation Resistance of an Elementary Loop Antenna in a Magnetoionic Medium, *IEEE Trans. Antennas Propagat.*, AP-13 (1), 21-27.
- 88 Whale, H.A. (1963), The Excitation of Electroacoustic Waves by Antennas in the Ionosphere, *J. Geophys. Res.*, 68 (2), 415-422.
- 89 Zheleznyakov, V.V. (1970), Radio Emission of the Sun and Planets, Pergamon Press, New York.